Compilation and Applications of Glacier Inventories using Satellite Data and Digital Terrain Information

---

Dissertation
zur
Erlangung der Naturwissenschaftlichen Doktorwürde
(Dr. sc. nat.)

vorgelegt der
Mathematisch-naturwissenschaftlichen Fakultät
der
Universität Zürich

von

Holger Frey
von
Richterswil ZH

Promotionskomitee
Prof. Dr. Wilfried Haeberli (Vorsitz)
Dr. Frank Paul (Leitung der Dissertation)
Dr. Christian Huggel

Zürich 2011

Summary

Glacier variations are considered a very reliable and easily understandable, natural indicator of climate change. With few exceptions, there has been a global trend toward glacier retreat since the beginning of the 20th century, with this retreat becoming more rapid and more uniform since the 1980s. This process has been accompanied by significant changes in the entire high-mountain environment, sometimes leading to new, potentially hazardous situations with no historical precedent.

The goal of a detailed, accurate, and complete global inventory of glaciers and ice caps has been pursued for more than five decades. Nevertheless, the resulting picture of the world's glaciers is still not complete, although the data produced have proven to be a great asset to the improved calculations of sea-level rise or to the modeling of further changes. There is also an increasing demand for regional applications to aid in the assessment of climate change impacts on the landscape, the water cycle, and on natural hazards.

Spaceborne satellite imagery provide a useful means to map glaciers and ice caps efficiently over large areas, even in remote regions that are difficult to access for topographical or political reasons. In combination with digital elevation models (DEMs), remote sensing data and methods offer the possibility to generate standardized glacier inventory data and to detect and analyze glacier lakes. In view of rapidly melting glacier tongues and the potential hazards, but also benefits, associated with glacier lakes, such applications have become increasingly important in recent years.

Methods for semi-automated mapping of glaciers and lakes based on remote sensing data have been well established for several years, and model approaches to assess the hazard potential of glacier lakes have been developed and successfully tested as well. With the free availability of pre-processed satellite imagery and DEM datasets having a near-global coverage, new possibilities have emerged to integrate these methods and approaches into a comprehensive framework that allows the situation of glaciers and glacier lakes in larger regions to be assessed and scenarios of their potential future evolution to be developed.

Clean-ice glacier parts can be mapped in a straightforward manner by applying a threshold to a band ratio of multispectral remote sensing data. Using these techniques, a glacier inventory has been compiled for the western Himalayas, a region that exhibits

challenging conditions for glacier mapping due to extensive debris cover and frequent cloudiness. This region has not to date been represented either in the World Glacier Inventory or in the glacier database of the Global Land Ice Measurements from Space (GLIMS) initiative. In addition to the established mapping methods, coherence images from radar image pairs were used to facilitate the manual delineation of debris-covered glacier parts. This glacier inventory contains more than 10,000 glaciers covering about 9,300 km^2 and largely closes one of the gaps in the available global glacier datasets.

Topographic parameters are core components of glacier inventories as they provide crucial information for characterizing glaciers. The global elevation datasets of the Shuttle Radar Topography Mission (SRTM) and the ASTER global DEM (GDEM) offer the possibility to derive such topographic parameters for glaciers in most regions of the world. For the first time, the suitability for this purpose of these two near-global DEMs has been investigated systematically based on the example of the Swiss Alps. The analysis reveals that the InSAR acquisition technique of SRTM is superior to the photogrammetric ASTER GDEM over glaciers, but both datasets were found to be suitable for the compilation of topographic glacier inventory parameters.

The formation of new glacier lakes in the course of glacier retreat is a phenomenon that can be observed in most mountain regions of the world. Such lakes constitute attractive new elements in the high-mountain landscape, but they are also a potential source of far-reaching natural disasters. As glacier lakes and their surrounding can undergo rapid changes, frequent assessments of the situation for larger regions are required. To facilitate this task, tools have been developed for Geographic Information Systems (GIS) for the detection and analysis of glacier lakes. They integrate existing mapping approaches as well as flow-routing models for the simulation of potential outbursts of such lakes.

In order to anticipate already today critical situations in the future, a multi-level strategy for the identification of sites with potential future lake formation has been developed. The design of the strategy allows a rough overview of a large region to be acquired quickly, and then to focus on smaller regions by applying more detailed methods and modeling approaches. Applications of this strategy to test sites in the Swiss Alps indicate that the formation of numerous new glacier lakes has to be expected in the near future. Some of these might represent unprecedented hazard situations, while others may offer the potential for hydro-power production.

The approaches presented here integrate existing and newly developed methodologies in a comprehensive and harmonized framework. In combination with freely available satellite imagery and DEM datasets, they offer integrative approaches for observing and assessing the current situation of glaciers, glacier lakes, and associated hazard potentials, as well as the means to develop scenarios of potential future evolutions.

Zusammenfassung

Gletscheränderungen gelten als sehr verlässliche und leicht verständliche, natürliche Indikatoren für Klimaänderungen. Gletscher zeigen seit dem 20. Jahrhundert einen globalen Rückzugstrend, der seit den 1980er Jahren besonders schnell und eindeutig geworden ist; ein Prozess der von schnellen Veränderungen der gesamten Umwelt im Hochgebirge begleitet wird, was zu neuen, eventuell auch gefährlichen Situationen führen kann, die jenseits des historischen Erfahrungshorizonts liegen.

Bereits seit mehr als fünfzig Jahren wird das Ziel eines detaillierten, genauen und global kompletten Inventars der Gletscher und Eiskappen verfolgt. Obwohl es dringend benötigt würde um zum Beispiel Vorhersagen des Meeresspiegelanstiegs zu verbessern oder die Erfassung von Gletscheränderungen zu ermöglichen, konnte eine globale Abdeckung noch nicht erreicht werden. Mehr und mehr gefragt werden auch Anwendungen zur regionalen Abschätzungen der Auswirkungen des Klimawandels auf die Landschaft, den Wasserkreislauf und Naturgefahren.

Weltraumgestützte Satellitendaten bieten die Möglichkeit, Gletscher und Eiskappen über grössere Regionen zu kartieren, selbst in Regionen die aus topographischen oder politischen Gründen nur schwer zugänglich sind. In Kombination mit digitalen Geländemodellen ermöglichen Fernerkundungsdaten und -methoden die Generierung standardisierter Gletscherinventardaten. Zudem können auch Gletscherseen erfasst und deren Situation analysiert werden, was in Anbetracht rapide schmelzender Gletscherzungen und der potentiellen Gefährlichkeit aber auch möglichen Nutzungspotentiale solcher neuer Seen in den letzten Jahren zunehmend wichtig geworden ist.

Methoden zur teilautomatisierten Kartierung von Gletschern und Seen aus Fernerkundungsdaten wurden schon vor mehreren Jahren entwickelt und Modelle zur Abschätzung der Gefahrenpotentiale von Gletscherseen existieren ebenfalls. Die kostenlose Verfügbarkeit von vorverarbeiteten Satellitenszenen und Geländemodellen mit beinahe globaler Abdeckung eröffnet nun die Möglichkeit, diese Methoden und Ansätze in einem konsistenten Rahmen zu integrieren, und so die Situation der Gletscher und Seen über ein grösseres Gebiet abzuschätzen und mögliche Zukunftsszenarien zu entwickeln.

Mit der Anwendung eines Schwellenwertes auf Verhältnisbilder von multispektralen Satellitendaten können schuttfreie Gletscherpartien einfach und direkt kartiert werden.

Mit dieser Technik wurde ein Gletscherinventar für den westlichen Himalaya erstellt, eine Region in der die Gletscherkartierung durch ausgedehnte Schuttbedeckung und häufige Bewölkung erschwert ist. Zusätzlich zu den bewährten Kartierungsmethoden wurden auch Kohärenzbilder aus Radarbildpaaren beigezogen, um die manuelle Abgrenzung der schuttbedeckten Gletscherpartien zu erleichtern. Dieses Gletscherinventar umfasst mehr als 10'000 Gletscher, welche eine Gesamtfläche von 9'300 km^2 haben. Eine der grossen Lücken in den globalen Gletscherinventaren wird dadurch teilweise geschlossen.

Topographische Parameter sind Kernkomponenten von Gletscherinventaren weil sie entscheidende Informationen zur Charakterisierung der Gletscher enthalten. Die globalen Geländemodelle der Shuttle Radar Topography Mission (SRTM) und des globalen ASTER DHMs (ASTER GDEM) ermöglichen es, solche topographischen Parameter für Gletscher in den meisten Regionen der Welt zu berechnen. Erstmals wurde die Eignung dieser beiden Datensätze für eine solche Anwendung systematisch untersucht. Es zeigte sich, dass das mit SAR-Interferometrie erstellte Geländemodell (SRTM) dem photogrammetrischen ASTER GDEM über Gletschern zwar leicht überlegen ist, dass aber beide Datensätze geeignet sind, um topographische Gletscherparameter abzuleiten.

Die Bildung neuer Gletscherseen im Zuge des Gletscherrückzugs ist ein Phänomen das in den meisten Gebirgsregionen der Welt beobachtet wird. Solche Seen sind einerseits attraktive neue Landschaftselemente, können aber auch eine potentielle Quelle für weit reichende Naturkatastrophen darstellen. Aufgrund der möglichen raschen Veränderungen von Gletscherseen und ihrer Umgebung muss die Situation insbesondere in grösseren Gebieten regelmässig überwacht werden. Um dies zu vereinfachen wurden GIS-basierte Werkzeuge entwickelt die bestehende Kartierungsansätze sowie Modelle zur Simulation möglicher Seeausbrüche verbinden.

Damit bereits heute kritische zukünftige Situationen antizipiert werden können, wurde zudem eine mehrstufige Strategie entwickelt, die es erlaubt Regionen zu identifizieren, wo sich in der Zukunft neue Gletscherseen bilden könnten. Der Aufbau der Strategie ermöglicht es, sich rasch einen groben Überblick über ein grosses Gebiet zu verschaffen und dann kleinere Gebiete mit aufwändigeren Ansätzen zu untersuchen. Eine Anwendung der Strategie auf Testgebiete in der Schweiz zeigte, dass in näherer Zukunft mit der Bildung von zahlreichen neuen Gletscherseen zu rechnen ist.

In die vorliegende Arbeit sind sowohl bestehende als auch neue Methoden in einem umfassenden Rahmen integriert. In Kombination mit frei zugänglichen Satellitendaten und Geländeinformationen ermöglichen diese Ansätze Gletscher und Gletscherseen zu beobachten, ihre aktuelle Situation und mögliche Gefahrenpotentiale zu analysieren, sowie mögliche Entwicklungsszenarien zu berechnen.

Contents

Part I Synopsis

Part II Research papers

Part III Appendix

List of Figures

List of Tables

X

Abbreviations

ALOS	Advanced Land Observation Satellite
ASTER	Advanced Spaceborne Thermal Emission and Reflection Radiometer
ASTER GDEM	ASTER Global DEM
CGIAR	Consultative Group on International Agricultural Research
DCW	Digital Chart of the World
DEM	Digital Elevation Model
DLR	Deutsches Zentrum für Luft- und Raumfahrt
DSM	Digital Surface Model
DTM	Digital Terrain Model
DHM25	Digital Height Model of Switzerland (25 m resolution)
DN	Digital Number
ECV	Essential Climate Variable
EM	Electromagnetic
EO	Earth Observation
ERSDAC	Earth Remote Sensing Data and Analysis Center
ESA	European Space Agency
ESRI	Environmental Systems Research Institute, Inc.
ETM+	Enhanced Thematic Mapper Plus
FCC	False Color Composite
GAPHAZ	(Working group on) Glacier and Permafrost Hazards in Mountains
GCM	Global Circulation Model
GCOS	Global Climate Observing System
GCP	Ground Control Point
GGHYDRO	Global Hydrographic Data
GHOST	Global Hierarchical Observing Strategy
GIS	Geographic Information System / Geographic Information Science
GLIMS	Global Land Ice Measurements from Space
GLOVIS	Global Visualization Viewer
GLS	Global Land Survey

GTN-G	Global Terrestrial Network for Glaciers
GTOS	Global Terrestrial Observing System
IACS	International Association of Cryospheric Sciences
ICESat	Ice, Cloud, and land Elevation Satellite
InSAR	Interferometric SAR / SAR Interferometry
IPA	International Permafrost Association
LDCM	Landsat Data Continuity Mission
LIA	Little Ice Age
MF	Multiple Flow Direction
MSF	Modified Single Flow Direction
MSS	Multispectral scanner
NASA	National Aeronautics and Space Administration
NED	National Elevation Dataset (USGS)
NDSI	Normalized Difference Snow Index
NDVI	Normalized Difference Vegetation Index
NDWI	Normalized Difference Water Index
NIR	Near Infrared
NSIDC	National Snow and Ice Data Center
PALSAR	Phased Array type L-band SAR
PSFG	Permanent Service on the Fluctuations of Glaciers
RAMMS	Rapid Mass Movement Model
RCM	Regional Climate Model
RMSE	Root Mean Square Error
SAR	Synthetic Aperture Radar
SPIRIT	SPOT 5 stereoscopic survey of Polar Ice: Reference Images and Topographies
SPOT	Satellite Pour l'Observation de la Terre
SRTM	Shuttle Radar Topography Mission
SWIR	Short Wave Infrared
TM	Thematic Mapper
TIN	Triangular Irregular Network
TTS/WGI	Temporary Technical Secretariat of the World Glacier Inventory
USGS	United States Geological Survey
UTM	Universal Transverse Mercator (coordinate system)
VIS	Visible
WGI	World Glacier Inventory
WGI-XF	World Glacier Inventory - Extended Format
WGMS	World Glacier Monitoring Service

Part I

Synopsis

1 Introduction

1.1 Motivation

Today, no doubt remains that global temperatures are increasing and that current levels already exceed pre-industrial conditions (*IPCC*, 2007). Glaciers and ice caps are considered as very reliable and unequivocal terrestrial indicators of climate change (e.g. *Oerlemans*, 1994, *Haeberli et al.*, 1999, *Haeberli*, 2005) due to their sensitive response to changes in temperature and precipitation (*Haeberli and Beniston*, 1998). They have been selected for this reason as an Essential Climate Variable (ECV) by the Global Climate Observing System (GCOS) (*GCOS*, 2003). In addition, glacier retreat has a strong impact on the perception of the landscape, as firn and ice areas are a symbol of an intact high-mountain environment and represent a cultural component for people living in their vicinity (*Carey*, 2007, *Haeberli*, 2005, *Haeberli and Hohmann*, 2008, *WGMS*, 2008b).

In the European Alps, glaciers lost about half of their total volume between 1850 and approx. 1975; roughly 25% of the remaining amount between 1975 and 2000; and an additional 10 to 15% in the first 5 years of the 21st century (*Paul et al.*, 2004b, *Zemp et al.*, 2006, *Haeberli et al.*, 2007). Most recent area loss estimations from satellite data show a reduction in the glacier surface in the entire Alps of about 30% since the mid 1970s (*Paul et al.*, 2011). Such increasing retreat rates since the second half of the 19th century, with an accelerating trend, can be observed over the entire globe (*Haeberli et al.*, 1999,

Dyurgerov and Meier, 2000, *Hoelzle et al.*, 2003, *WGMS*, 2008b). The vanishing of glaciers has impacts on different scale levels: Locally they affect the landscape, the hydrologic regime, and in many cases also the natural hazard situation. On a regional to continental scale, the hydrological cycle is influenced by glaciers and their changes (*Huss et al.*, 2008, *Kaser et al.*, 2010); whereas on a global scale, questions and predictions related to sea-level changes are of high interest (*Raper and Braithwaite*, 2006, *Meier et al.*, 2007, *Radić and Hock*, 2011).

A fundamental requirement for investigating all kinds of different phenomena, processes and consequences of such glacier changes are datasets containing information about the spatial distribution of glaciers and their topographic characteristics, i.e. glacier inventories (*Kääb et al.*, 2002). Remote sensing data from satellites are very helpful for mapping and monitoring glaciers and their changes over large areas, repeatedly, and by covering large regions with sufficient spatial detail at the same time (*Aniya et al.*, 1996, *Jacobs et al.*, 1997, *Kääb et al.*, 2002). Methods for a semi-automated mapping of glaciers based on multispectral, optical satellite images are well established (*Paul et al.*, 2002, *Andreassen et al.*, 2008, *Bolch et al.*, 2010) and offer a powerful tool for completing and updating the global glacier databases (*Kääb et al.*, 2003a, *Kargel et al.*, 2005, *Raup et al.*, 2007a). Despite the demand for a global snapshot of glaciers and ice caps and technical possibilities to complete this task, the global glacier databases are still far from being complete at the required level of detail (*Dyurgerov and Meier*, 2005, *Cogley*, 2009, *Ohmura*, 2009).

As mentioned earlier, glacier fluctuations directly affect the hazard situation in the respective mountain regions (*Evans and Clague*, 1994, *Haeberli and Beniston*, 1998, *Clague and Evans*, 2000, *Richardson and Reynolds*, 2000, *Huggel et al.*, 2004a). Remote sensing methods in combination with geographic information systems (GIS) provide useful means to detect potentially hazardous situations and to perform a preliminary assessment of related hazard potentials (e.g. *Huggel et al.*, 2002, *Kääb et al.*, 2005a). The most far-reaching hazardous processes in glacial and periglacial regions are related to drainages of glacier lakes, which often result from a combination of different processes (*Costa and Schuster*, 1988, *Clague and Evans*, 1994, *Walder and Costa*, 1996, *Huggel et al.*, 2003b, *Reynolds Geo-Science*, 2003, *Kääb et al.*, 2005b). Reliable and robust approaches are required in order to detect potentially critical lake sites in advance. The combination of remote sensing data and Digital Elevation Models (DEMs) in a GIS provides suitable tools to monitor precarious situations and to estimate maximum runout distances of involved processes, particular in remote regions where not much local information is available (*Kääb et al.*, 2003b, *Huggel et al.*, 2003b).

Due to the observed rapid changes in the high-mountain cryosphere, projections about future developments of different components of the environmental system are of grow-

ing importance (*Haeberli and Hohmann*, 2008). However, so far only a few studies exist that deal with projections of future hazard situations (e.g. *Clague and Evans*, 2000, *Reynolds*, 2000, *Quincey et al.*, 2007). Nevertheless, information about future scenarios would allow stakeholders and policymakers to prepare already today for potentially adverse situations in the future.

Research related to the the issues discussed above (i.e., detailed glacier inventory and hazard analyses) bears two main challenges: on the one hand, methodological developments are required to address technical challenges, and on the other, large quantities of data need to be generated and analyzed by applying existing and newly developed methods. Remote sensing data in combination with freely available elevation datasets with (nearly) global coverage enables different aspects of these challenges to be addressed. The present thesis develops and applies such approaches to study the current situation of glaciers in different mountain ranges, their characteristics, related hazard potentials and possible future developments.

1.2 Objectives and research questions

Glacier inventories and elevation datasets are the core topics of this thesis. All objectives and research questions have a relation to glacier inventories and DEMs and treat theoretical and methodological issues, data compilation in a specific region, and further applications of such datasets, for investigating glacier hazards.

Methodological aspects of compiling glacier inventories. Methods and procedures for glacier mapping based on optical, multispectral remote sensing data are well established (e.g. *Rott*, 1994, *Paul et al.*, 2002, *Paul and Kääb*, 2005; cf. Section 2.2.2). Besides the mapping of glaciers, further steps are needed for the compilation of a glacier inventory, including the separation of individual glaciers and the establishment of topographic parameters, both requiring a DEM (*Paul et al.*, 2002, *Paul and Kääb*, 2005, *Andreassen et al.*, 2008, *Bolch et al.*, 2010). Since no local or national DEM of sufficient quality is available for many glacierized regions in the world, the DEM datasets of SRTM and ASTER GDEM (cf. Sections 2.3.3 and 2.3.4) with their (nearly) global coverage provide a valuable alternative. However, there do not yet exist systematic investigations of whether SRTM and ASTER GDEM are suitable for the compilation of topographic parameters. This topic is addressed by the first research question:

> *Are the SRTM DEM and the ASTER GDEM suitable for the compilation of topographic glacier parameters?*

Based on the findings of this investigation and the knowledge from previous studies, a glacier inventory has been compiled for the western Himalayas. In this region is found one of the largest gaps in the global glacier databases of WGI and GLIMS (cf. Section 2.1.2) (*Cogley*, 2009, *Ohmura*, 2009). The vast extent of the region and the challenging conditions for glacier mapping (extensive debris cover on glacier tongues and frequent cloud and snow cover) may be reasons why these glaciers have still not been accurately mapped. The second research question is thus:

> *What are the current state and character of glaciers in the western Himalayas?*

Detection and analysis of existing and future glacier lakes. Glacier fluctuations imply continuous changes in the hazard situation. Glacier retreat is often accompanied by the formation of new glacier lakes, whose hazard situation in turn is influenced by other glacial and periglacial processes. Remote sensing provides helpful means to detect critical situations and to monitor specific sites on a regular basis (e.g. *Kääb et al.*, 2003b, *Kääb et al.*, 2005a). *Haeberli et al.* (1991), *Alean* (1985), *Huggel et al.* (2002, 2003b, 2004a) and *Salzmann et al.* (2004) presented methods for lake detection as well as empirical investigations and modeling approaches of mass-movement processes for a first-order assessment of glacier hazards. To be able to efficiently detect and analyze glacier lakes in a larger region, comprehensive approaches are required that integrate the different methodologies developed in these studies. This issue is addressed by the third research question:

> *How can glacier lakes automatically be detected in large regions and how can they be analyzed with regard to their hazard potential?*

Rapid changes in glaciers and the surrounding landscape can lead to situations with no historical precedent. Information about future conditions, in particular regarding the hazard situation, would be very helpful to decisionmakers and stakeholders for anticipating potential future scenarios already in the present. Little research has been conducted to date regarding future developments of glacier hazards, exceptions being *Reynolds* (2000) and *Quincey et al.* (2007). As glacier inventories in combination with DEMs contain information about the current surface geometry of glaciers, they could be used as a key means for anticipating future lake formation and related hazard potentials. Research question four, hence, is:

> *Is it possible to anticipate future glacier lake formation and related hazard potentials based on glacier inventory data and digital terrain information?*

1.3 Organization of the thesis

The thesis is divided into three parts:

Part I provides a synopsis of the entire thesis. After the Introduction, the thematic and scientific background is reviewed in Chapter 2, where the current state of research is described. In Chapter 3, the research papers that form the core of this thesis are summarized. A general discussion of the applied methods and findings is given in Chapter 4, relating the outcomes of the research papers to the scientific context described previously. Chapter 5 concludes the synopsis and provides an outlook on potential future research.

Part II contains full versions of the research papers which constitute the main part of the thesis.

Part III consists of the appended material (CV, personal bibliography, and the acknowledgements).

2

Thematic and scientific background

2.1 International glacier monitoring

2.1.1 Historical overview and strategy

In 1894, at the 6th International Geological Congress in Zurich, François-Alphonse Forel, a professor of medicine from Lausanne, initiated the founding of the International Glacier Commission (*Haeberli*, 1998). It was hoped that a coordinated observation of glaciers would help provide insights into the mechanisms and dynamics of glacier and climate variations and reveal the reasons and processes that brought about the ice ages (*Forel*, 1895). Between 1895 and 1913, the commission published annual reports on glacier variations. During and between the two world wars, fewer glacier measurements were performed and the reports, now published by the Commission of Snow and Ice, were issued less frequently. Since 1967, the Permanent Service on the Fluctuations of Glaciers (PSFG) has published the "Fluctuations of Glaciers" series in 5-year intervals (*Haeberli*, 1998). For the International Hydrological Decade (1965-1974), it was planned to assess the amount, distribution and variation of all snow and ice masses as part of the World Glacier Inventory (WGI) (*Ohmura*, 2009). In 1986, the World Glacier Monitoring Service (WGMS) was established by merging the PSFG and the Temporary Technical Secretariat of the World Glacier Inventory (TTS/WGI).

At present, together with the Global Land Ice Measurements from Space (GLIMS) initiative and the National Snow and Ice Data Center (NSIDC), the WGMS is in charge of the Global Terrestrial Network for Glaciers (GTN-G) within the Global Climate/Terrestrial Observing Systems (GCOS/GTOS). Glacier observation by GCOS/GTOS follows a tiered Global Hierarchical Observing Strategy (GHOST), which is designed to retain adequate spatial and temporal resolution: On the one end a few variables are measured regularly at a large number of places, and at the other end a large number of variables are measured at a few locations for a limited period (*GCOS*, 1997). This strategy is designed to be applied to all variables observed by GCOS/GTOS, but for many observation networks it has not yet been considered.

Applied to glacier monitoring, the GHOST tiers are implemented as follows (after *Haeberli et al.*, 2000 and *WGMS*, 2008a):

- *Tier 1: multicomponent system observations across environmental gradients*. The observations should have a broad spatial diversity and the focus is on uninterrupted, long-term measurements, e.g., a transect of observation sites ranging from Svalbard via Scandinavia and through the Alps to the Pyrenees.
- *Tier 2: extensive glacier mass balance and flow studies within major climatic zones for improved process understanding and calibration of numerical models*. Study sites selected for Tier 2 should represent the characteristic environmental conditions of the respective climatic zone.
- *Tier 3: determination of regional glacier volume change within major mountain systems using cost-saving methodologies*. At this tier, the intention is to sample the range of environmental conditions within climatic zones, without spatial representativeness.
- *Tier 4: long-term observations of numerous glacier length, area and thickness changes within major mountain ranges for assessing the representativeness of continuous mass balance and volume change measurements on single glaciers*. Here, spatial representativeness is of highest priority, a minimum of about ten sites should be selected within each mountain range. Glaciers where only length changes are recorded belong to this tier.
- *Tier 5: glacier inventories repeated at time intervals of a few decades by using remote sensing*. This includes the acquisition of data from airborne or – in most cases – spaceborne remote sensing products in yet uncovered regions to complete the global picture of the world's glaciers, the upgrading and repetition of existing glacier inventories at time intervals of a few decades, and the analysis of such datasets.

Activities related to Tier 5 require coordinated efforts and strategies for the acquisition, management and archiving of the large amount of data, and to ensure data quality. The GLIMS initiative maintains a database of glacier inventories at the NSIDC in Boulder, Colorado. Originally, the GLIMS glacier database was designed to archive glacier inventory data obtained from ASTER images and other multispectral remote sensing data, but during the last decade it evolved to a database that holds 2- and 3-dimensional digital glacier inventory data of various sources and fulfills the aims of GHOST-Tier 5 (*Raup et al.*, 2007b). Regarding the global picture of the world's glaciers, the GLIMS glacier database can be seen as a continuation of the WGI task and is therefore a complement to the point data as stored by the WGI.

2.1.2 Current state of the global glacier inventory

The global inventory of all glaciers in the world is currently still far from comprehensive. However, efforts are continuing towards the ultimate goal of a globally complete glacier inventory, as there is a high demand for such a dataset for various reasons. For one, answers could be found to both the more simple and the more complex questions, which at present can scarcely be attempted (*Cogley*, 2009). Such questions address, for instance, global sea-level rise projections, river runoff at various scales, mechanisms of glacier-climate interactions, and more. Examples of studies which investigate these questions are given in Chapter 2.4.2.

WGI and GLIMS. *Dyurgerov and Meier* (2005) estimated the total area of glaciers and ice caps outside Greenland and Antarctica to be 540 ± 30 x 10^3 km^2. According to *Ohmura* (2009), the WGI in 2009 covered 46% of this estimated total glacier surface area, the GLIMS database 34%, but 26% is covered by both datasets, resulting in 54% of the global glacier area that is represented by the combination of the two datasets. The status of the WGI and the GLIMS glacier database as of 2010 are shown in Figs. 2.1 and 2.2.

The most obvious data gaps are located in the Arctic and the Antarctica Peninsula, where a large number of glaciers and ice caps without connection to the ice sheets are located, potentially storing huge amounts of ice (*Ohmura*, 2009, *Cogley*, 2009, *Gardner et al.*, 2011, *Radić and Hock*, 2011). Outside the polar regions, the GLIMS database is still incomplete in northern Alaska, large parts of South America, Asia and New Zealand. It is also important to note that the GLIMS coverage in China currently consists only of data from the first Chinese glacier inventory, which is the same data that is also represented in the WGI, i.e., the glacier outlines in the GLIMS glacier database are digitized from maps and orthophotos from the 1960s and 1970s. Due to the small scale of the map in Fig. 2.1 it appears like the Himalayas are completely covered in the datasets. However, data for large parts of India and Pakistan, in the Karakoram and Pamir mountains,

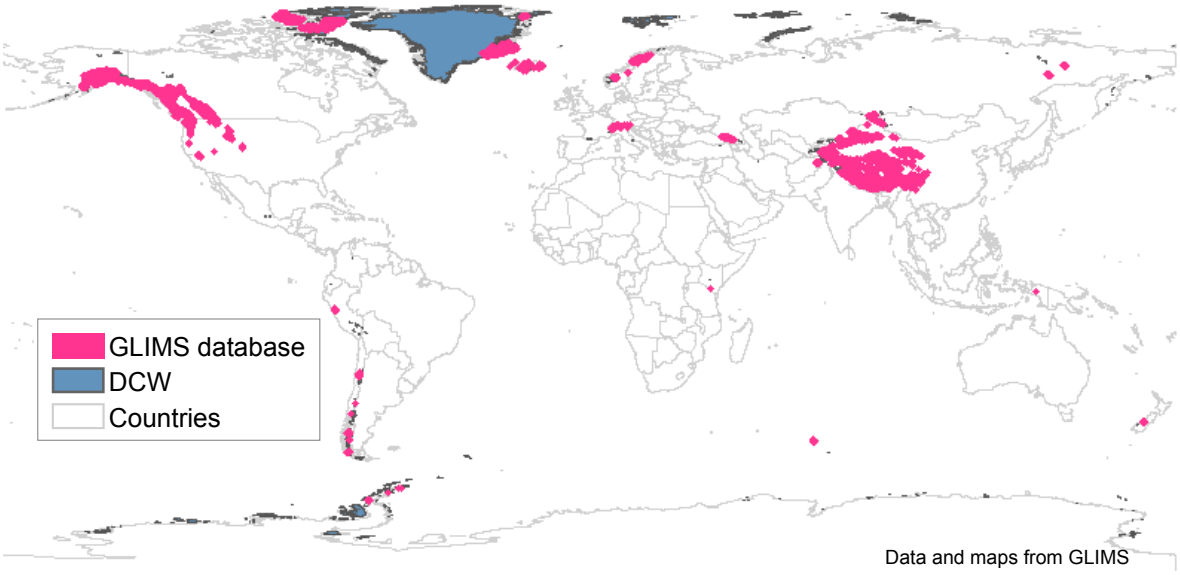

Figure 2.1: *State of the GLIMS glacier database as of December 2010. DCW is shown in the background to indicate data gaps. Compare with the status of WGI (Fig. 2.2).*

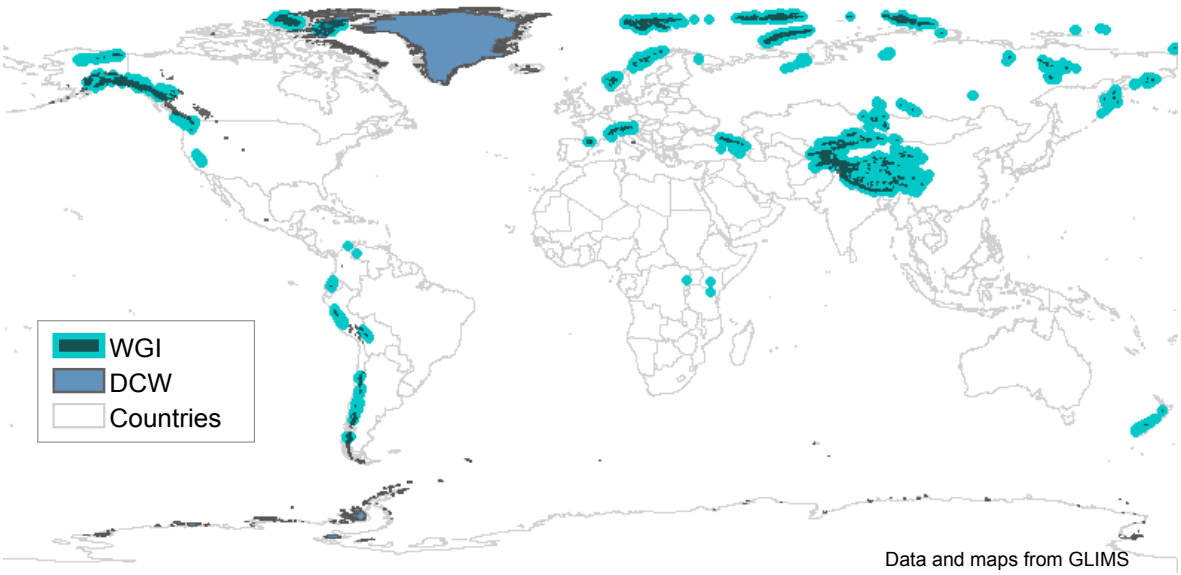

Figure 2.2: *State of the WGI as of December 2010. DCW is shown in the background to indicate data gaps. Compare with the status of the GLIMS glacier databse (Fig. 2.1).*

are still missing. This gap is addressed in *Paper II*, where the compilation of a glacier inventory for the western Himalayas is presented.

Format. Besides the different regions covered by the WGI and the GLIMS database, the datasets differ in regard to their formats. The WGI has a tabular form and holds up to 40 parameters for each glacier, including geographic location, area and extents, glacier type, topographic parameters, morphological classification, date, source material, and accuracy estimations. This design allows an efficient storage of large datasets and an application of the data for various purposes, such as statistical analyses or glaciological parameterization schemes (e.g. *Haeberli and Hoelzle*, 1995). The drawbacks are that the accuracy of the data is hardly traceable and corrections are almost impossible because the outlines of the glaciers are not represented in the dataset. This is also due to the fact that the WGI was conceived as a snapshot of the late 20th century rather than a tool for change analysis (*Cogley*, 2009).

The GLIMS glacier database, on the other hand, stores the mapped glacier outlines as polygons in a digital vector format, which allows a comparison of the data with any other geocoded information in a GIS, such as other glacier outlines, digital maps, orthophotos or satellite imagery (*Raup et al.*, 2007a). Without access to the glacier polygons, a change assessment with another glacier dataset is hardly possible (e.g. *Andreassen et al.*, 2008).

Other datasets. Besides the WGI and the GLIMS glacier database, a number of other global glacier datasets exists. Probably the most complete, albeit not the most accurate, dataset is the glacier layer of the Digital Chart of the World (DCW), a project by the Environmental Systems Research Institute, Inc. (ESRI) (*Danko*, 1992). This dataset comprises the global distribution of more than 20 themes with raster and vector data, amongst many others also a layer about the 'glaciated regions' of the world. The data quality differs strongly from region to region and is generally low, the scale is, at best, 1:1,000,000. *Raup et al.* (2000) completed this dataset in regions which are not covered in the original DCW. To do so, data from the WGMS (WGI), NSIDC data, and miscellaneous maps and atlases were used. As some of this auxiliary databases have no polygonal glacier outlines but only tabular information, some of the data of this extended DCW version is represented by approximately circular polygons of correct area at the respective location. Although the quality is limited, difficult to assess, and insufficient for answering most scientific glaciological queries, this extended DCW version is the only dataset that covers all glacierized regions of the world in a vector format (cf. Figs. 2.1 and 2.2). The latitude-longitude polygons for the ASTER data acquisition request of the GLIMS initiative were defined based on this data (*Raup et al.*, 2000). Figure 2.3 shows glacier data from GLIMS, WGI and DCW for a valley in the Tibet, PR China, illustrating the different properties of these datasets.

There are other datasets such as the extended version of the WGI, the WGI-XF (*Cogley*, 2009, XF stands for 'extended format') or the Global Hydrographic Data (GGHYDRO), a 1° by 1° grid, storing the relative amount of different kinds of terrain relevant for hydrology, including glaciers (*Cogley*, 2003) (Fig. 2.4). The data source for this dataset consisted of 1:1,000,000 scale maps and the glacier layer was then crosschecked with existing glacier inventories. The GGHYDRO glacier layer covers the entire globe as well, but the coarse spatial resolution is far too low for many applications and not comparable with the other datasets described above. An overview of all the described datasets is given in Table 2.1.

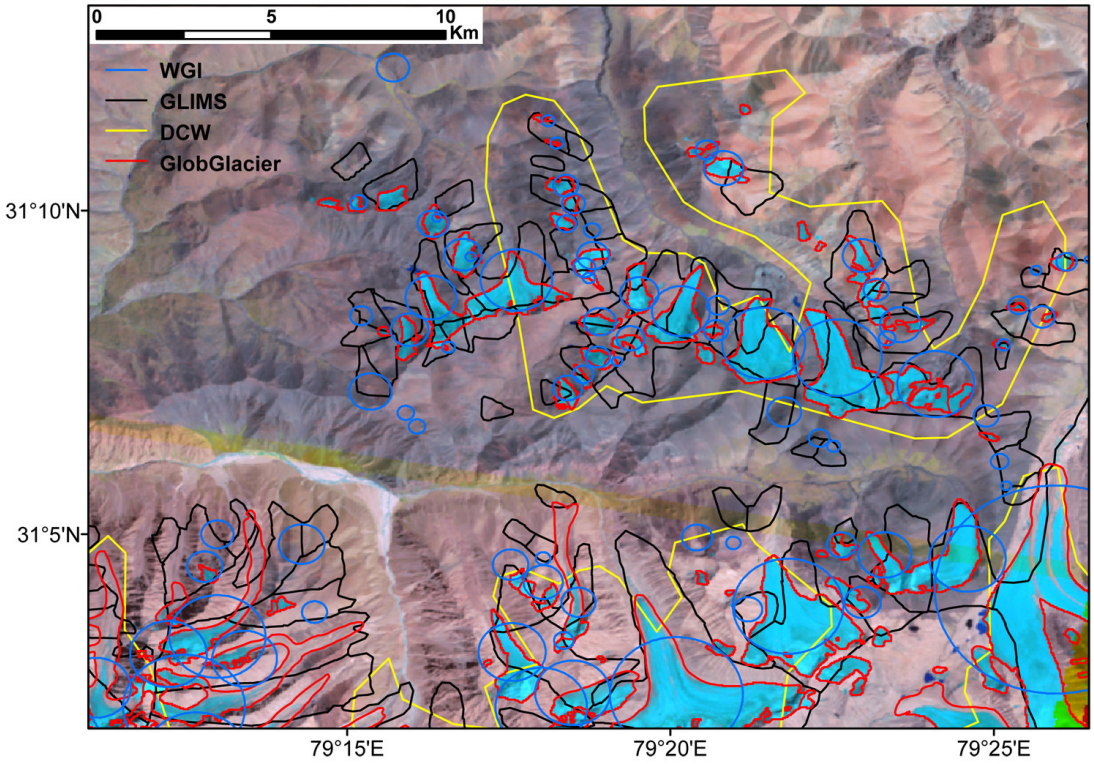

Figure 2.3: *Glacier data from WGI (blue circles), GLIMS (black lines), DCW (yellow lines), and an inventory from the GlobGlacier project (red lines, cf. below and* Paper II*) in a region in Tibet, PR China. Background image is an ETM+ scene from 2001, on the basis of which the GlobGlacier outlines were compiled. Note the different levels of detail of GLIMS outlines (from around the 1950s) and DCW. The tabular information from the WGI was visualized by constructing circles at the location of the glaciers coordinates, and with area equal to the glacier area.*

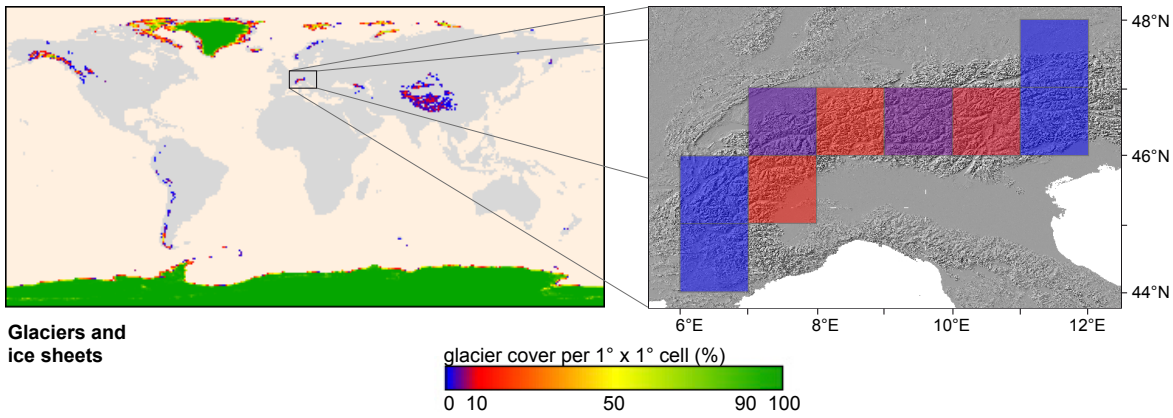

Figure 2.4: *The glacier layer (gghglac) of the GGHYDRO dataset, showing the percentage of glacier and ice-sheet cover per 1° by 1° grid cell. Left: global overview of the dataset (source: `http://people.trentu.ca/~gcogley/glaciology/index.htm`). Right: the Alps in GGHYDRO, hillshade view of the SRTM DEM in the background.*

To address the need for a detailed global inventory of glaciers, the European Space Agency (ESA) initiated the GlobGlacier project back in 2007. Major aims of this project include to complete the WGI and GLIMS databases in selected key regions which were still uncovered at that time, to update the point information of the WGI by 2D vector outlines, and to document the processing workflows by which these products were compiled (*Paul et al.*, 2009b). The present thesis was to a large extent funded by the GlobGlacier project.

2.2 Remote sensing

2.2.1 Concepts and sensors

Remote sensing consists of instruments and methodologies to measure the physical properties of an object without direct contact. In a narrower sense as used in a geoscientific context, this includes sensors and techniques to measure emitted or reflected radiation of the earth, and methods to analyze such data. Remote sensing offers powerful tools to study the spatial and temporal distribution and characteristics of objects or landscape elements such as glaciers. In the following, a brief overview and some historical aspects are given for sensors, which were relevant for the work of this thesis. Methodological aspects of glacier and lake mapping based on remote sensing are outlined in the next sections (2.2.2 and 2.2.3).

Table 2.1: *Overview of the described global glacier datasets*

	WGI[1]	**GLIMS**[2]	**DCW**[3]	**WGI-XF**[4]	**GGHYDRO**[5]
format	tabular	outlines	outlines	tabular	tabular (containg % of 1 deg grid cells)
topographic parameters	yes	partly	no	partly	no
coverage (of estimatet total glacier area)	46%	34%	about 90%	60%	almost 100%
hosted by	WGMS / NSIDC	GLIMS NSIDC	Penn State University / GLIMS	Trent University (J. Cogley)	Trent University (J. Cogley)

[1] `http://nsidc.org/data/glacier_inventory`
[2] `http://www.glims.org`
[3] `http://www.maproom.psu.edu/dcw`
[4] `http://people.trentu.ca/~gcogley/glaciology/index.htm`, *Cogley*, 2009
[5] `http://people.trentu.ca/~gcogley/glaciology/index.htm`, *Cogley*, 2003

Sensors. Remote sensing data and sensors can be classified according to a number of aspects like location of the platform (ground-based, airborne, spaceborne), flight track or orbit, section of the electromagnetic spectrum that is used, active or passive systems, different types of resolution (spatial, temporal (i.e., the revisiting time), and spectral (i.e., the number of different bands and the widths of the individual bands)), and other special features such as a stereo channel, interferometric and polarimetric capabilities; possibility to rotate the sensor, and data availability (costs, time in operation, accessibility of archives). In this thesis the focus is on spaceborne optical sensors with sun-synchronous near-polar orbits and medium-to-high spatial resolution (10 m – 50 m).

Spaceborne multispectral sensors of medium-to-high resolution have proved to be suitable for glacier mapping (see Section 2.2.2). These Earth Observation (EO) sensors like the Landsat MultiSpectral Scanner (MSS) and the Thematic Mapper (TM); the Advanced Spaceborne Thermal Emission and Reflection Radiometer (ASTER) onboard the Terra platform and the SPOT (Satellite Pour l'Observation de la Terre) satellites have been used in the context of glacier inventory production. Besides having bands and resolutions suitable for glacier mapping (e.g., *Williams Jr*, 1987, *Paul et al.*, 2002, *Paul and Kääb*, 2005, *Berthier et al.*, 2007, *Bolch et al.*, 2007, *Racoviteanu et al.*, 2008a, *Jiskoot et al.*, 2009). ASTER and SPOT both have stereo mapping capabilities, offering the possibil-

ity to produce digital elevation models (DEMs) (cf. *Toutin* (2008) for ASTER and *Korona et al.* (2009) for the SPOT SPIRIT (SPOT 5 stereoscopic survey of Polar Ice: Reference Images and Topographies) DEM). As the first efforts of the GLIMS initiative started as an ASTER science team, GLIMS is still closely related to the ASTER sensor (*Kargel et al.*, 2005) and fostered the use of its data. *Raup et al.* (2000), *Kääb et al.* (2003a), *Khalsa et al.* (2004), *Ranzi et al.* (2004) or *Svoboda and Paul* (2009) are examples of studies using ASTER for glacier mapping. There are also many publications related to other applications of ASTER in a glaciological context such as assessments of volumetric changes, flow studies and glacier hazards (e.g., *Wessels et al.*, 2002, *Kääb et al.*, 2003b, *Kääb*, 2005a). Many of these works are also related to the application of DEMs derived from ASTER data and their utilization for glaciological research (e.g., *Bolch and Kamp*, 2005, *Kääb et al.*, 2005a, *Fujita et al.*, 2008, *Racoviteanu et al.*, 2008b).

Landsat history and availability. Due to their free availability in an orthorectified format since 2008, imagery from NASA's Landsat program became the most frequently used remote sensing data for glacier mapping. Unless otherwise cited, the contents of the following two paragraphs comes from the Landsat history webpage (`http://landsat.gsfc.nasa.gov/about/history.html`, accessed April 2011). Satellites of the Landsat mission have been in operation since the launch of Landsat 1 in 1972 with the first MSS on board. Landsat 4, launched in 1982, had the first TM sensor onboard. Compared to MSS, TM had an improved spectral and spatial resolution, including a blue-channel, which allows the compilation of true-color composites at 30 m resolution and bands in the short-wave infrared (SWIR) spectrum that, in turn, allow snow and clouds to be separated. The latest Landsat sensor is the Enhanced Thematic Mapper Plus (ETM+), onboard of Landsat 7 (launched 1999). Landsat 5 and 7 are still in operation; the TM of Landsat 5 is now operating for almost 25 years longer than its designated lifetime (MSS onboard of Landsat 5 was turned off in 1995). The EO data of the Landsat mission thus constitutes a unique time series of earth observation, covering almost four decades to date. This fact makes the Landsat data archive a powerful tool for studying landscape features such as glaciers, their distribution over the planet, and their changes over time. In order to provide continuity with the Landsat imaging dataset, NASA in collaboration with the U.S. Geological Survey (USGS) initiated the Landsat Data Continuity Mission (LDCM), which should be launched by the end of 2012. An overview of technical details, methodological aspects and various potential applications of EO satellites, with a special concentration on Landsat can be found in *Sabins* (1997); or, with a focus on remote sensing of glaciers, in *Paul* (2007).

Availability of EO data strongly depends on the economic perspective of the operator. On the one hand, there are satellites with high data costs run by private companies, and on the other, governmental organizations responsible for satellites and their archives,

offering data at low or no cost, in particular for scientific applications. Another difference is related to the strategy for data acquisition: commercial programs often acquire only on request or only if a potential customer for the data exists, whereas scientific missions tend to collect and archive as much data as possible for potential future studies. The Landsat program was originally run by a private agency (with governmental subsidies). During the first decade, the image prices rose by more than 600% to a height of $ 4,400 in the 1980s, due in part to the monopoly on this kind of data, which made it impossible for many data users to continue to afford it. As a consequence, many observations from 1984 to 1999 were not carried out because there was no obvious and immediate client. Only the launch of SPOT1 in 1986 broke through this monopoly situation. In 2001, the operational control was officially returned to the US Government. Today, Landsat data is managed and distributed by the USGS. Since 2008, all Landsat data is freely available from the USGS data portal Global Visualization Viewer (GLOVIS, `http://glovis.usgs.org`, accessed April 2011) (*USGS*, 2005) or EarthExplorer (`http://edcsns17.cr.usgs.gov/NewEarthExplorer/`, accessed April 2011). Depending on the availability of the necessary ground control data, the best possible level is offered: If sufficient ground-control data is available, the scenes are processed to Standard Terrain Correction (Level 1T), which includes the employment of a DEM to remove topographic distortions. This is the case for most scenes. The lowest processing level is Systematic Correction (Level 1G), which is derived from data collected by the sensor and spacecraft only (cf. Landsat processing details, `http://landsat.usgs.gov/Landsat_Processing_Details.php`, accessed April 2011). Level 1T data is very efficient to use, as the laborious task of orthorectification falls away and a very high relative spatial accuracy to adjacent scenes and images of another date is given. In the meantime, all Landsat scenes (including MSS) are offered in L1T quality (i.e. orthorectified). The open access policy will possibly pressure other EO data suppliers to open their archives as well.

Other data. For particular applications data and products from other sensors were also used within this thesis, such as the PALSAR (Phased Array type L-band Synthetic Aperture Radar) sensor onboard of ALOS (Advanced Land Observation Satellite) for the production of coherence images to map debris-covered glaciers (cf. *Paper II*). Also the DEM of the Shuttle Radar Topography Mission (SRTM) and the ASTER Global DEM (GDEM) (cf. Sections 2.3.3 and 2.3.4) are remote sensing data in a broader sense.

2.2.2 Remote sensing of glaciers

The spectral signature, i.e., the proportion of the incoming electromagnetic (EM) radiation that is reflected by an object at different wavelengths, can either be measured (e.g.

Zeng et al., 1984, for glacier ice) or modeled numerically (e.g. *Dozier*, 1989, for snow). If the spectral signature of an object is known, data from multispectral sensors can be used to classify the object automatically. Most objects (including glaciers), however, do not have homogeneous surface properties with a specific spectral signature, they are composites. Glaciers consist of snow with different grain sizes and ice with different degrees of contamination with dust or soot, debris, and water on the surface. An algorithm for mapping of (debris-free) glaciers therefore needs to consider the spectral properties of ice and snow.

Spectral properties of ice and snow. Optical EO sensors typically operate in the visible (VIS), the Near Infrared (NIR), and the thermal range of the electromagnetic spectrum. All Landsat TM, ETM+, ASTER, and SPOT have their bands in similar EM ranges (except the blue channel, which exists only on a few sensors, e.g., on TM and ETM+). In Fig. 2.5 the spectral properties of ice and snow in combination with the bands 1 to 5 of Landsat TM are shown. Snow reflection is very high in the visible part of the spectrum (TM1, TM2, and TM3), attaining almost 100% (cf. Fig. 2.5 and 2.6a). This can cause a saturation of the channel if the surface is tilted toward the sensor (*Dozier*, 1989); otherwise, if the snow is contaminated with particles, the reflectivity decreases strongly. Glacier ice on the other hand is always polluted to a certain degree and thus appears much darker than snow in the VIS range. In the NIR part, around 0.75 μm – 0.9 μm (i.e. TM4), the reflectivity of snow decreases and shows a higher sensitivity to grain size. Clean glacier ice decreases as well to about 40%, probably due to the presence of liquid water at the surface, which strongly absorbs radiation at such wavelengths (*Paul*, 2007). In the SWIR range of TM5 (1.55 μm – 1.75 μm), the reflection of snow is much lower and more strongly determined by grain size. Since glacier ice can be considered as metamorphosed snow with relatively large grain sizes, it becomes obvious that the reflectivity of clean glacier ice is even lower in this part of the EM spectrum (cf. Fig. 2.6b). This strong difference in the reflectance characteristics of ice and snow in the VIS compared to the SWIR range allows rather simple classification techniques to be applied.

Algorithms for glacier mapping. A variety of algorithms for glacier mapping have been developed. For instance, a ratio of TM4 and TM5 has been used to distinguish between ice- and snow-covered glacier surfaces (*Hall et al.*, 1987), and for glacier delineation (*Jacobs et al.*, 1997, *Sidjak and Wheate*, 1999); the Normalized Difference Snow Index (NDSI), developed by *Dozier* (1989), was applied for both snow mapping *Hall et al.* (1995) and glacier mapping (*Sidjak and Wheate*, 1999). The latter also included a supervised maximum likelihood classification in their mapping algorithm. Comprehensive overviews of these approaches can be found in *Gao and Liu* (2001), *Paul et al.* (2002) and *Paul* (2007).

Besides the drawback that debris-covered glacier parts are not captured correctly by any of these methods, it proved difficult to apply these algorithms to map glaciers in

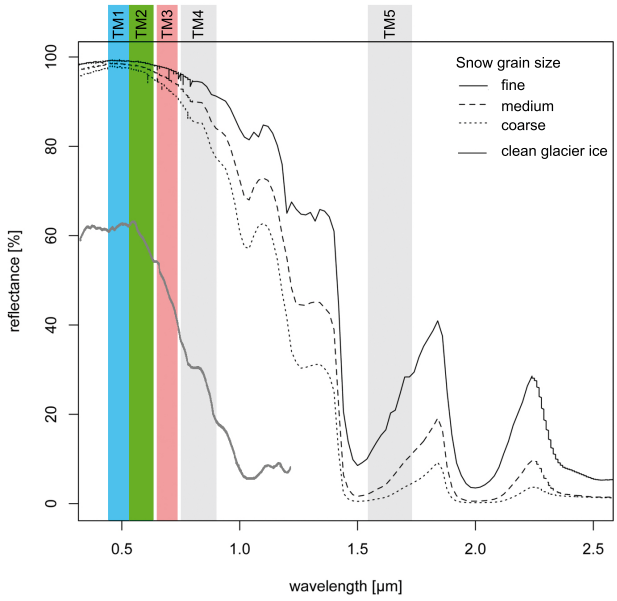

Figure 2.5: *Spectral signatures of snow with different grain sizes and clean glacier ice. Snow reflectance values taken from the ASTER spectral library (*Baldridge et al.*, 2009); reflectance of clean glacier ice is taken from* Zeng et al. *(1984) (field measurement).*

cast shadow, which is common in rough mountain topography. Although band ratio techniques proved workable in shadowed areas as well (*Hall et al.*, 1987), mapping inaccuracies could not be avoided. Using a DEM to compensate for the effect of illumination differences can help to overcome the problem (*Gao and Liu*, 2001). *Rott* (1994) for example, created a glacier map by thresholding the ratio of the atmospherically corrected channels TM3 and TM5. *Paul et al.* (2002) found that the TM4/TM5 ratio applied to the raw digital numbers (DN) (i.e., without atmospheric correction) yields the best results, also in shadowed areas. They also applied a 3 by 3 kernel-size low pass filter to eliminate isolated pixels (i.e., single glacier pixels as well as isolated "holes" in glacier areas). *Paul and Kääb* (2005) compared the performance of ETM3/ETM5, ETM4/ETM5 and NDSI ((ETM2 – ETM5)/(ETM2 + ETM5)) for glacier mapping on Baffin Island in Arctic Canada and found ETM3/ETM5 and NDSI to work best. Due to the higher efficiency, band ratio techniques can be applied faster and are widely used today (*Paul et al.*, 2009a). By applying an additional threshold to a VIS channel, the mapping result in shadowed areas can be further improved (*Paul and Kääb*, 2005). For the mapping activities performed in the framework of the GlobGlacier project, and therefore also for the work related to this thesis, this technique was used for glacier mapping (Fig. 2.6).

Mapping of debris-covered glacier parts. In Figs. 2.6c and 2.6d the shortcomings of these methods can be seen: (1) debris-covered glacier parts are not captured with the algorithm, and (2) other classification errors such as turbid water surfaces require further processing. Several approaches to the mapping of debris-covered glacier parts exist, including the application of artificial neural networks (*Bishop et al.*, 1999), ice detection using thermal channels (*Taschner and Ranzi*, 2002), geomorphometric DEM analyses (e.g. *Bishop et al.*, 2001, *Paul et al.*, 2004a), and combinations thereof (*Bolch et al.*, 2007, *Racoviteanu et al.*, 2008b). However, all the approaches require either a major computational effort, or time-consuming preparations, and often entail subsequent manual corrections as well. Therefore, the most efficient way is still a manual adjustment of the automatically mapped glacier outlines based on the satellite image, but this procedure requires sound glaciological and remote sensing knowledge on the part of the analyst.

Scene selection. Due to the fact that (1) the optical signal is not able to penetrate clouds, and (2) glaciers are mapped by discriminating ice and snow from the surrounding rock, debris, vegetation, and water surfaces, it is crucial for the mapping quality that only those scenes are chosen that have (1) no cloud cover (at least over the glaciers), and (2) as little snow cover as possible beyond the edge of the glaciers as of the end of the ablation period. The following section describes the recommended workflow for glacier mapping as it is also used in this thesis (*Paper II*, cf. Fig. 2.7).

Pre-, main-, and post-processing. First, some pre-processing steps are required. For satellite scenes other than the USGS L1T products, this includes the georeferencing and orthorectification of the scene. Pre-processing requires a DEM, a set of ground control points (GCPs) with known coordinates that can be identified in the satellite image, and specific image processing software to perform the related calculations (cf. Section 2.3.1). Landsat TM and ETM+ scenes that are freely available from the USGS, however, come already in an orthorectified format (Level 1T) and make the time-consuming task of geocoding and orthorectification redundant, which is a great advantage. For further use on the main- and post-processing level, contrast-stretched RGB images, so-called false color composites (FCCs) with different band combinations (e.g. RGB321 and RGB543), are produced. To do so, red, green and blue layers are overlaid and contrast stretched, and saturation is chosen according to the digital numbers (DNs) of the respective channels (0 = black, 255 = full saturation).

Depending on the purpose, different band combinations enhance the visible content of the image: Displaying the bands TM3, TM2, and TM1 in red, green and blue (RGB321) gives a (pseudo) true-color image, similar to a normal (digital) photo, which is therefore easy to interpret by a human analyst (Fig. 2.8a). This is, however, possible only for data from a sensor that has a blue channel (e.g. TM and ETM+). Other combinations are used to enhance particular aspects of interest, using the information of the different

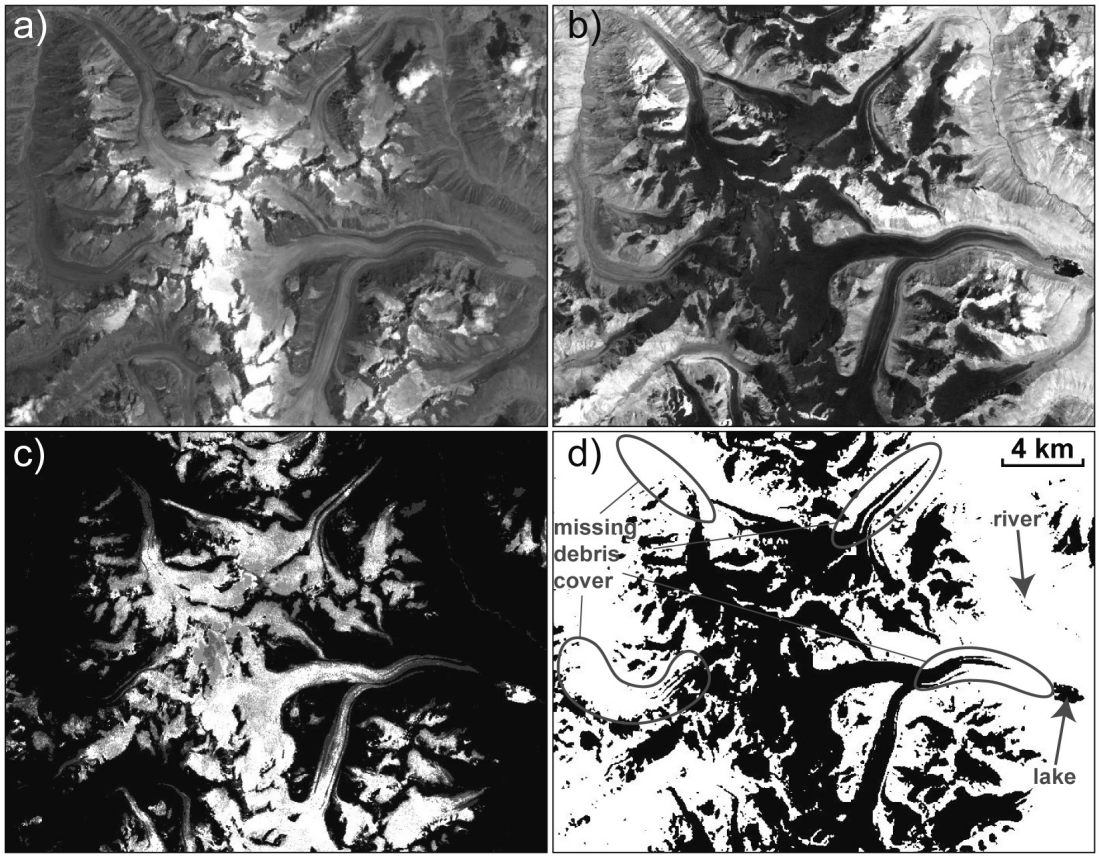

Figure 2.6: *Glacier mapping with band ratioing at the Samudra Tapu glacier in the Indian Himalaya. a) TM3, b) TM5, c) TM3/TM5 ratio, d) Raw glacier map after thresholding the ratio image (c) and applying a 3 by 3 kernel-size low pass filter. Note that debris-covered glacier parts are not mapped and the lake in front of the glacier and parts of the river are misclassified as being glaciers. (Fig. 2.8 shows false color composites of this region.)*

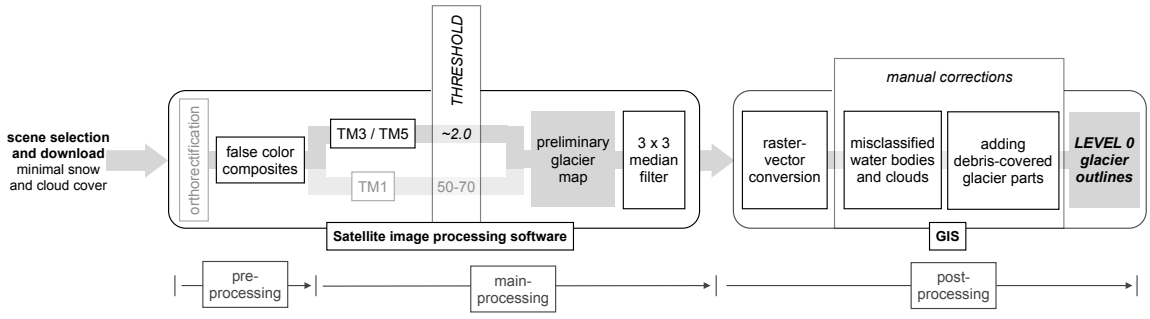

Figure 2.7: *Schematic workflow of procedures for glacier mapping from satellite imagery. Processing steps displayed in grey are not required in some cases.*

spectral bands. A widely known band combination is, for instance, RGB432, which is used to analyze the health state of vegetation, since the reflection in the spectral range of TM4 (NIR) is strongly dependent on the chlorophyll content of leaves. A combination of RGB543, on the other hand, results in glacier ice and snow displayed in blue, rock and debris in purple to red, vegetation in yellow, and clouds in white (Fig. 2.8b). An overview of suitable band combinations for different purposes is given in Table 2.2.

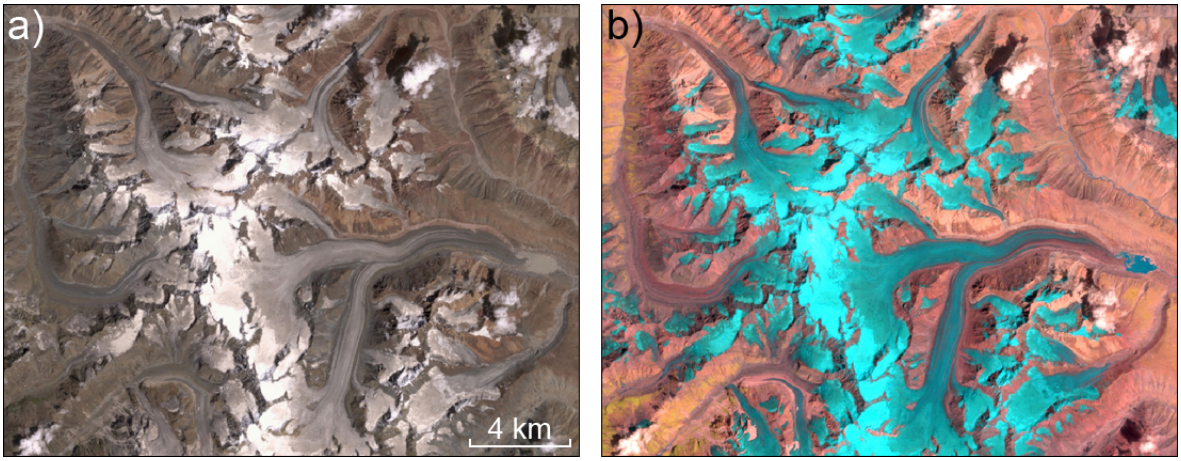

Figure 2.8: *False color composites of an ETM+ scene, same region as in Fig. 2.6. a) RGB321, a quasi true-color image. b) RGB543, a suitable combination for glacier mapping. Note the different colors of glaciers and clouds.*

Table 2.2: *Suitable band combinations (false color composites) for different purposes. Numbering is related to Landsat TM bands (1=blue, 2=red, 3=green, 4=NIR, 5=SWIR)*

	RGB321	**RGB432**	**RGB543**
purpose	(pseudo) true-color separation of snow and ice	enhanced contrast over snow areas, vegetation health state, lake identification	separation of ice and rock / debris, snow / ice and clouds
typically applied in	all regions	arctic regions	regions with debris-covered glaciers
Landsat	✓	✓	✓
ASTER	–	✓	✓
SPOT HRV	–	✓	✓

The actual glacier mapping is performed on the main processing stage. This includes the selection of the threshold applied to the TM3/TM5 band ratio and, if required, the

threshold applied to TM1 (cf. *Paul et al.*, 2002, *Paul and Kääb*, 2005). As described above, the mapping result in shadowed regions is most sensitive to the selected thresholds. Therefore, the most efficient way to find a suitable threshold is to test different thresholds in a shadowed area and compare the results in an iterative procedure. Normally, the threshold for the band ratio is around 2.0 ± 0.2 and the threshold for the blue band (TM1) in the range of 40 – 70 of the uncorrected DNs. Once the thresholds for a satisfying classification are found, the described low-pass filter (e.g., a median filter) can be applied to the glacier map.

For the post-processing stage, the binary glacier map is transferred to a geographic information system (GIS) and converted from raster to vector format, enabling manual editing of the outlines (e.g., *Burrough and McDonnell*, 1998, *Longley et al.*, 2011). Then, in a first step, the misclassified water bodies, sea, lake, or river ice, and clouds with ice content are removed. In a second step, the debris-covered glacier parts are added. This is done using the information from the false color composites, and, if available, from any other source of information such as a hillshade view of the DEM, detailed maps, high-resolution images from aerial photography (e.g. from GoogleEarth^{TM}), older glacier inventories, or similar datasets. The post-processing is normally the most time-consuming part of the mapping procedure, in particular the manual digitizing of glacier extents under thick debris cover (*Paul and Hendriks*, 2010). *Paul and Kääb* (2005) estimated an average working time of about 5 min per glacier, i.e., about 100 8-hr work days are required for mapping and accurately correcting 10,000 glaciers.

2.2.3 Remote sensing of lakes

Spectral properties of water and mapping of lakes. Similar methods as described above for glacier mapping can be used to detect water surfaces in multispectral remote sensing data. The spectral signature of water (Fig. 2.9) is characterized by a strong absorption in the NIR and SWIR wavelengths (0.8 μm – 2.5 μm, e.g. *Pietroniro and Leconte*, 2000). *Huggel et al.* (2002) developed a normalized difference water index (NDWI), similar to the well-known normalize difference vegetation index (NDVI) (e.g. *Goward et al.*, 1985, *Hardy and Burgan*, 1999) and the NDSI (*Dozier*, 1989, cf. Section 2.2.2). As for all these normalized difference indices, two bands with high and low reflectances, respectively, are chosen (i.e., for water the blue channel (TM1, high reflectance) and the NIR channel (TM4, low reflectance)), and the difference in the DNs of these two channels is divided by their sum, i.e.,

$$\mathrm{NDWI} = \frac{(\mathrm{TM4} - \mathrm{TM1})}{(\mathrm{TM4} + \mathrm{TM1})}$$

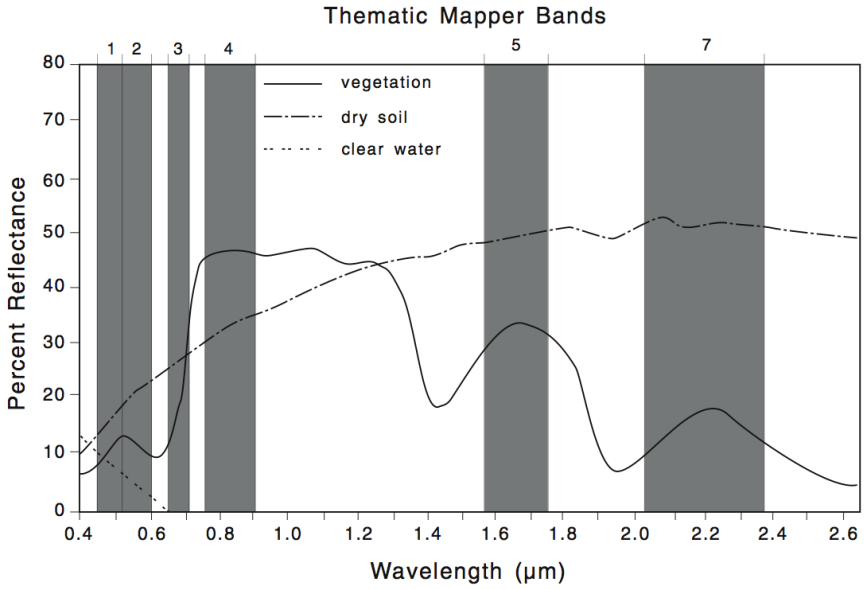

Figure 2.9: *Spectral signatures of clear water, vegetation, and dry soil, taken from* Lusch *(1999). Grey bars indicate the spectral bands of Landsat. Note that the reflectivity of water is very low above 0.65 μm.*

After calculating the NDWI, the processing is very similar to the mapping procedure for glaciers (Section 2.2.2): a threshold is defined, and, after applying a kernel-shaped median filter for elimination of isolated pixels, the resulting lake mask is manually corrected if necessary. The NDVI, which also uses the NIR band (TM4, but as the high-reflectance channel) and a band from the VIS range (e.g., the green channel, TM3), gives results similar to those of the NDWI, also for lakes; or even a simple ratio (TM4 / TM1) could be used for the mapping of water surfaces. However, the NDWI proved to have a better contrast to the surrounding terrain, and the resulting numerical range is normalized. Lake surfaces typically have NDWI values of -0.60 to -0.85 (*Huggel et al.*, 2002).

A major problem of all methods of lake mapping is related to water in shadowed areas (*Huggel et al.*, 2002): Shadowed areas have comparably high reflectances in the short-wave part of the VIS range (i.e. the blue channel) due to reflections at air molecules (*Crippen*, 1988). Therefore, shadowed areas are often misclassified as lakes. A cast shadow mask, calculated on the basis of a DEM and using the sun elevation angle and azimuth at the time of the image acquisition, can be used to identify such misclassified cast-shadow regions (*Huggel et al.*, 2002, *Frey*, 2007). However, besides requiring a high-quality DEM, this implies that lake surfaces in shadow cannot be mapped. Using slope information from a DEM would theoretically allow further classification criteria to be added in order to improve the lake mask. For instance, lakes could be identified by

extracting flat surfaces (slope < 0.1°), or slope gradients of more than 5° could be used to eliminate misclassifications. This, however, only works if the DEM and the satellite image are acquired at the same time. If the DEM is older than the satellite image, which is often the case, the DEM still represents pre-lake formation surface conditions with potentially steep slopes at the location of new lakes.

Turbidity of glacier lakes. Water bodies in general and glacier lakes in particular exhibit a wide range of spectral properties, depending on the concentration of suspended material (Fig. 2.10). Humus particles, for instance, strongly enhance the absorption of water in all wavelengths (*Fraser*, 1998). For this reason, tests using a supervised and an unsupervised classification algorithm applied to multispectral data both failed: in the unsupervised classification an individual class was built for each lake, and the supervised classification would require a training sample for each lake (*Frey*, 2007). More details about supervised and unsupervised classification can be found in *Richards* (1999), *Schowengerdt* (2007) or *Lillesand et al.* (2008).

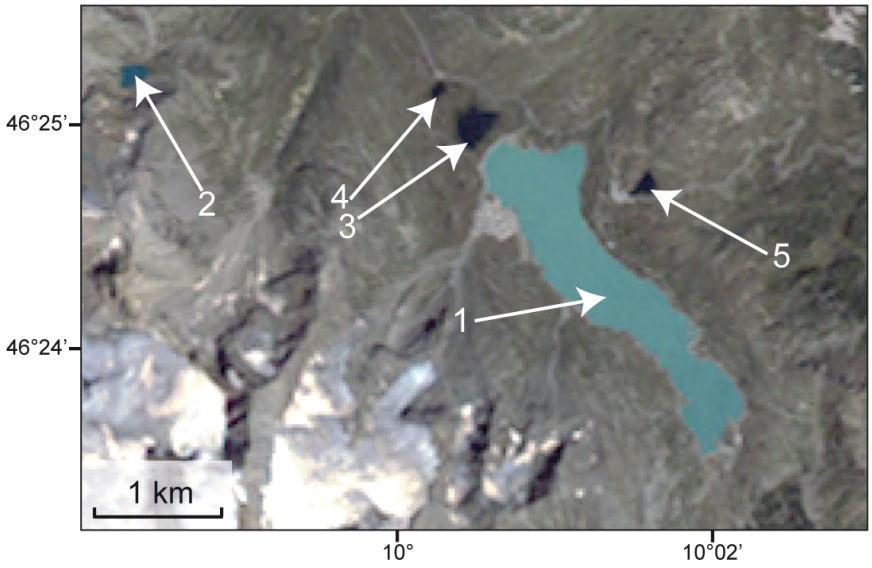

Figure 2.10: *Landsat TM 5 image of the Bernina pass, Swiss Alps, and surrounding lakes, exhibiting a large variety of different colors, depending on the concentration of suspended material. Lago Bianco (1) is turquoise, the smaller Lej d'Arlas (2) is in between, whereas Lej Nair (3), Lej Pitschen (4) and Lagh da la Cruseta (5) appear very dark, although (1), (3), and (4) are directly connected.*

2.3 Digital elevation models

2.3.1 Principles and applications

Characteristics and classification of DEMs. Information about the Earth's surface is of key importance to geoscientific research. Digital elevation models, hence, are a basic pre-requisite for understanding the link between processes and forms and vice versa for the modeling of many geospatial processes. Every surface point in such a dataset consists of three coordinate values representing its location in the x, y, and z direction. To discretize the continuous face of the earth, either triangular irregular networks (TIN), or equally spaced raster datasets with an elevation value for each grid cell can be used. A TIN has the ability to represent the landscape in different levels of detail by varying the mesh size according to the complexity of the respective landforms. Gridded datasets, on the other hand, are more suitable to be implemented in a GIS and to be combined with other raster data.

In disciplines such as geographic information sciences and photogrammetry, a distinction is sometimes made between digital surface models (DSM) and digital terrain models (DTM). A DSM includes the objects on the surface with temporal variation such as trees, vegetation and snow as well as constructed objects, i.e. buildings. A DTM, on the other hand, represents only the bare ground surface. The abbreviation 'DEM' is often used as a generic term, but there is no common usage for these expressions. To avoid confusion, 'DEM' is used here for all datasets representing the Earth's surface in a gridded data format.

DEM datasets can be classified according to different criteria:

- *spatial resolution (cell size):* Very low resolution (1 km up to > 250 km, e.g. in general circulation models (GCMs)), low resolution (250 m up to > 1 km, e.g. GTOPO30, GLOBE), medium resolution (50 m to 250 m, e.g. SRTM), high resolution (10 m to 50 m) as many other datasets used in this thesis (ASTER GDEM, DHM25), and very high resolution (< 1 m to 10 m, laser DEMs). It is important to note that a higher spatial resolution does not necessarily imply a more detailed representation of the terrain.

- *spatial extent:* Determined by the purpose or the producer: local (a specific landform or object, such as a geomorphologic feature or a catchment), regional (an administrative or organizational unit), national (for countries), or global.

- *acquistion technique:* Ground-based: topographic survey (optical leveling, triangulation, GPS, terrestrial laser scanning). Air- or space-borne: photogrammetry,

interferometric synthetic aperture radar (InSAR). Some DEMs are obtained by the digitization of contour lines, however, this cannot be considered as an actual acquisition technique, as the underlying contour lines themselves were obtained by one of the techniques mentioned above.

- *acquisition date:* Acquired at a specific date or within a short time span (such as SRTM, cf. section 2.3.3), different acquisition dates within the dataset, however, the acquisition date is known at each location (such as DHM25, cf. Section 2.3.2), acquisition is spread over a longer time span and is undefined for a specific point (such as the ASTER GDEM, cf. Section 2.3.4).
- *availability:* Determined by data costs, distribution restrictions, or know-how and software requirements for data preparation and processing.

Applications of DEMs in remote sensing and glaciology. A proper alignment of the different layers is a prerequisite for any GIS analysis, therefore all data needs to be in the same map projection and free of geometric distortions (e.g., *Burrough and McDonnell*, 1998, *Longley et al.*, 2011). *Nuth and Kääb* (2011) presented a method to detect and number shifts, thus co-registering two different DEM datasets. Besides a proper geolocation, a DEM is also required for the orthorectification of satellite scenes, i.e., to remove image distortions caused by topography (e.g. *Lillesand et al.*, 2008). Mountain topography causes major location shifts in the satellite image: a point at 3000 m elevation, 70 km from the nadir point of a Landsat TM image is shifted by about 300 m from its real position (*Paul*, 2007). Georeferencing and orthorectification of a satellite scene is a laborious and time-consuming task that includes the collection of suitable GCPs, (e.g. *Richards*, 1999), which should be on stable ground, evenly distributed in space and elevation and identifiable in the satellite scene. Furthermore, an image processing software is required to calculate the unknown transformation coefficients between the image coordinates and the reference geometry (e.g. *Schowengerdt*, 2007, *Richards*, 1999). However, the procedures for georeferencing and orthorectification were of minor importance for this thesis since USGS offers Landsat data in a georeferenced form for free and, for the most part, with sufficient accuracy (< 1 pixel RMSE) (cf. section 2.2.2).

When investigating glaciers using remote sensing and GIS, DEMs are a necessity for the data processing, and there are a great number of applications and methods which use DEM information in combination with digital glacier outlines. Estimations of glacier volume changes by DEM subtractions are a frequent application in glaciology. Examples of such studies are *Paul and Haeberli* (2008), who analyzed the spatial distribution of elevation changes in the Swiss Alps by DEM subtraction, or *Möller and Schneider* (2010) who estimated volume changes of an ice cap in Patagonia. *Larsen et al.* (2007), *Schiefer et al.* (2007) and *Berthier et al.* (2010) (re-)assessed the contribution of Alaskan glaciers

to sea-level rise by DEM differencing. To detect and remove systematic errors in the mass balance series obtained by the direct glaciological method (*Østrem and Brugman*, 1991), such measurements need to be calibrated with geodetic measurements (e.g. *Haeberli et al.*, 2007) at a repetition rate of about 10 years (*Haeberli*, 2006). An example for such a harmonization of a long-term mass balance series can be found in *Huss et al.* (2009). *Huss et al.* (2010) estimated glacier volume changes and mass balances based on differencing of different DEMs and *Zemp et al.* (2010) compared the mass balance of Storglaciären in Sweden obtained by the direct glaciological method with volumetric mass changes obtained from five photogrammetric DEMs (*Koblet et al.*, 2010).

Further DEM applications include modeling of mass movements in glacial and periglacial environments on different levels of detail (e.g., *Huggel et al.*, 2003b, *Allen et al.*, 2009), modeling of the ice thickness distribution of glaciers (e.g., *Linsbauer et al.*, 2009, *Farinotti et al.*, 2009), and numerical modeling of future glacier evolution (e.g., *Le Meur et al.*, 2007, *Jouvet et al.*, 2009).

Table 2.3 gives an overview of the three DEM datasets used in this thesis, and they are described in more detail in the following sections (2.3.2 to 2.3.4). In this thesis, DEMs are used for various purposes: to calculate topographic parameters by merging the DEM with the glacier outlines (*Paper I* and *Paper II*); to identify hydrological drainage divides for separation of individual glaciers (*Paper II*); to model potential glacier lake outburst floods and related processes (*Papers III and IV*); and to analyze current glacier surface topography in order to identify sites with potential future glacier lake formation (*Paper IV*).

2.3.2 DHM25

The Digital Height Model of Switzerland (DHM25) is the Swiss national DEM produced by the Federal Office of Topography, swisstopo. It is derived from the elevation information from the Swiss national topographic map on a scale of 1:25,000. First, a so-called basis model was produced, which is essentially the digital form of the elevation information in the topographic maps. It includes digitized contour lines, lake perimeters and selected spot heights. Based on this basis model, the DHM25 Level 1 was produced by interpolating the elevation values at the grid point locations using in-house software developed for this purpose. Since 2001, an improved version of this dataset has been available, the DHM25 Level 2. It is based on the same basis model, but includes additional terrain information from photogrammetrically derived breaklines in the Alps. Furthermore, the contour lines of glaciers were revised in the lower parts and the interpolation algorithm was improved for this version (*Swisstopo*, 2004). The Level 2 version of DHM25 was used in *Papers I*, *III*, and *IV*.

Table 2.3: *Overview of DEM datasets used in the thesis*

	SRTM	**ASTER GDEM**	**DHM25**
acquisition technique	single-pass InSAR (C-Band)	automated photogrammetry applied to the entire ASTER scene archive	digitized contour lines, spot heights, main breaklines, and lake perimeters from the Swiss national map (1:25,000)
spatial resolution	3 arc seconds ($\sim$ 90 m)	1 arc second ($\sim$ 30 m)	25 m
acquisition date / period	February 2000	2000 to 2007 (information stems from multiple scenes, exact dating is not possible)	1985-1997 (depending on the map sheet)
coverage	60°N - 56°S	83°N - 83°S	Switzerland
problems / errors	data voids in rough terrain; radar penetration into snow	artificial pits and bumps, particularly in accumulation regions; acquisition date undetermined; missing co-registration of underlying sat. scenes (*Nuth and Kääb*, 2011)	accumulation regions not updated
price	free	free	$>$ 1000 CHF

Swisstopo estimates the horizontal (x and y direction) accuracy at 2.5 m - 7.5 m, and the mean vertical difference to be less than 10 m in the Alps (*Swisstopo*, 2004). The product description includes maps showing the status of the data and accuracy estimations of the DHM25 for every 1:25,000 map sheet.

There are several studies relating to glaciology and glacier hazards which used the DHM25. The automated mapping approach for debris-covered glacier tongues by *Paul et al.* (2004a) used the DHM25, and *Bolch and Kamp* (2005), developed a glacier mapping method using DEM data. Mass balance studies employing the DHM25 were presented by *Huss et al.* (2010) and *Paul and Kotlarski* (2010). *Paul and Haeberli* (2008) subtracted SRTM data from the DHM25 to derive surface elevation changes in glaciers. Modeling of mass movements in high mountains based on the DHM25 were presented by several authors: for debris flows by *Huggel et al.* (2003b, 2004c) and *Gruber et al.* (2008);

Huggel et al. (2004a) for reconstruction of glacier lake outbursts; *Huggel et al.* (2004c) and *Salzmann et al.* (2004) for ice avalanches, and *Noetzli et al.* (2006) for rockfalls.

2.3.3 SRTM

From 11 February to 22 February 2000 a DEM covering all land masses of the Earth between 60°N and 56°S was acquired by the Shuttle Radar Topography Mission (SRTM), a joint project of NASA and the German Aerospace Center (Deutsches Zentrum für Luft- und Raumfahrt (DLR)). The DEM was computed by SAR interferometry (InSAR), using a C-band (5.6 cm wavelength) radar system on board the Endeavour Space Shuttle (*Van Zyl*, 2001, *Rabus et al.*, 2003). In contrast to repeat-pass InSAR, SRTM used a single-pass observation system in order to avoid temporal decorrelation at the surface and to remove uncertainties related to the measurement of the baseline between the different acquisitions. To allow this single-pass measurement, in addition to the main transmitting and receiving antenna situated in the Shuttle's payload bay, a second receive-only antenna was attached to a 60-m long, retractable mast (*Rabus et al.*, 2003, *Farr et al.*, 2007). Parallel to this C-band system, an X-band system was onboard the space shuttle that acquired data at discrete 50 km swaths. This X-band data was processed independently by DLR. Primarily, experiences gained from this mission were used for the planning of the TanDEM-X mission (cf. 5.3). This SRTM X-band data became freely available in May 2011 (*DLR*, 2011), but is not further used nor discussed here.

During the eleven-day mission, nearly one trillion paired pulse-echoes were obtained, and then processed over a period of nine months to attain a seamless, near-global dataset (*Farr et al.*, 2007). SRTM is available from NASA in three different formats: a 1 arc second version (SRTM-1), available for US territory only, and a version with 3 arc seconds resolution (SRTM-3) and 30 arc seconds resolution (SRTM30), both available also for non-US territory. All datasets are distributed by 1° x 1° tiles and freely downloadable at `http://edcsns17.cr.usgs.gov/NewEarthExplorer/` (accessed April 2011). Post-mission accuracy assessments revealed a horizontal accuracy of ± 3 m to ± 7 m for 90% of the data and a relative and absolute vertical accuracy of ± 16 m (90%) (*Rabus et al.*, 2003). Thus all of the accuracy values surpassed the pre-mission specifications.

Radar shadow and layover effects are often associated with radar data in high-mountain topography, and result in numerous data voids of various sizes (e.g., *Eineder and Holzner*, 2001). In Switzerland, such data voids cover a total area of about 1000 km^2, and more than 50% of all glaciers are partially covered by such no-data areas in SRTM (Fig. 2.11). To overcome these data gaps, the Consultative Group on International Agricultural Research (CGIAR), offers a void-filled version, where data gaps have been filled using auxiliary DEM information from other elevation datasets or maps if available or

at least void-free data from the SRTM30 dataset. Details about the applied methodology and the interpolation algorithms used are described in *Reuter et al.* (2007) and at `http://srtm.csi.cgiar.org/` (accessed April 2011), where the data also can be downloaded in 5° x 5° tiles. CGIAR reports the vertical error of the void-filled DEM to be less than 16 m (*Rabus et al.*, 2003), and also other studies found differences of meters up to several decameters (*Rignot et al.*, 2003, *Stevens et al.*, 2002), in particular in high-mountain terrain (*Kääb et al.*, 2005a).

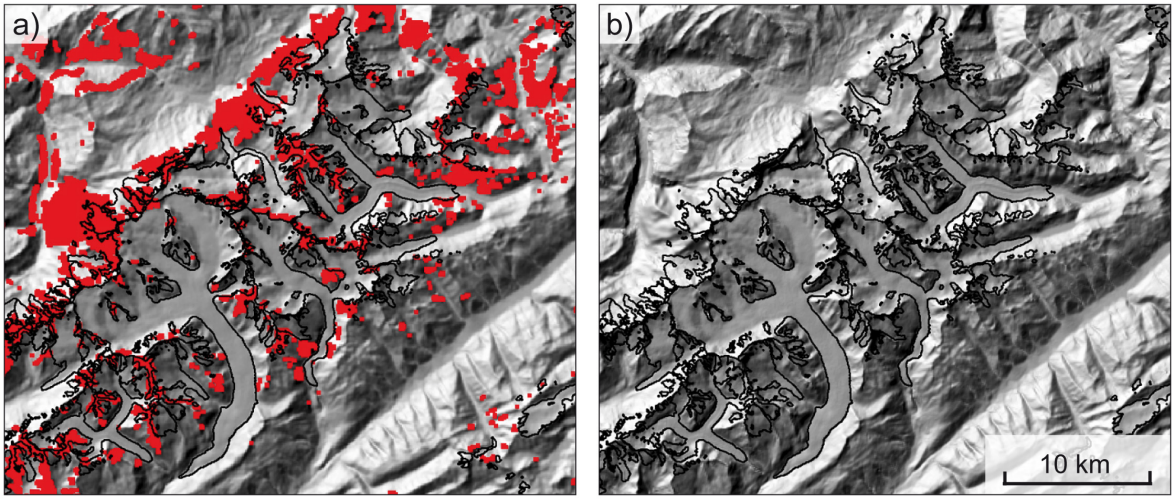

Figure 2.11: *Hillshade views of SRTM in the region of Aletsch and Rhone glaciers. Black lines represent glacier outlines. a) 'Raw' version with data voids highlighted in red. b) void-filled SRTM version from CGIAR.*

Berthier et al. (2006) found an elevation-dependent bias in SRTM of -7 m/1000 m to -9 m/1000 m and thus an overestimation of the surface elevations below 1700 m a.s.l. - 1800 m a.s.l. and an underestimation of the elevation above this elevation band. *Larsen et al.* (2007) on the other hand did not find this bias in Alaska and British Columbia, and *Möller et al.* (2007) even found an inverse bias for an ice cap in southern Patagonia. *Paul* (2008) investigated whether this bias is an SRTM artifact, and found that the reason for this trend is related to the more frequent occurrence of steep ridges and pronounced crests at higher elevations, which normally are underestimated due to the coarse resolution of SRTM. This also explains the inverse bias found by (*Möller et al.*, 2007) on a Patagonian ice cap where steep slopes are found at low elevations and gentle slopes dominate the highest elevations (*Möller and Schneider*, 2010). *Nuth and Kääb* (2011) found as well an elevation dependent error in SRTM for test sites in New Zealand and Svalbard, and systematic aspect-dependent differences to reference datasets. In this study they also propose a workflow to identify and eliminate such errors.

2.3.4 ASTER GDEM

The along-track stereo capability of the back-looking band 3 of the ASTER sensor allows for the production of DEMs (*Kääb*, 2002, *Fujisada et al.*, 2005, *Toutin*, 2008). Such ASTER DEMs based on individual scenes were used in many studies, examples are *Kääb* (2002), *Sing Khalsa et al.* (2004), *Kääb* (2005a), *Rivera et al.* (2005) or *Schneider et al.* (2008).

In June 2009 the Japanese Ministry of Economy, Trade and Industry (METI), in collaboration with NASA, released the ASTER Global DEM (ASTER GDEM). It was compiled using automated photogrammetry applied to the complete ASTER scene archive, containing more than 1.65 million scenes acquired between 2000 and 2007 (*METI*, 2009). It covers all land surfaces of the Earth at 1 arc second ($\sim$ 30 m) spatial resolution between 83°N and 83°S; i.e. compared to SRTM, arctic regions are included as well. In contrast to single-scene based ASTER DEMs, the ASTER GDEM was compiled by stacking of 1,264,118 individual ASTER scenes. Outliers were removed and the remaining elevation values were averaged to create the final pixel values (*METI/NASA/USGS*, 2009). This brings assets and drawbacks: on the one hand, a high number of scenes reduces the probability of large errors and artifacts, but on the other hand the surface as represented in the GDEM cannot be dated exactly.

ASTER GDEM data can be freely downloaded freely in 1° x 1° tiles from the Earth Remote Sensing Data Analysis Center (ERSDAC) portal at `http://www.gdem.aster.ersdac.or.jp` (accessed April 2011). Along with the DEM information in GeoTIFF format a so-called NUM-file is provided, indicating the number of ASTER scenes that were used for the DEM compilation. This is an indirect quality indicator, as the quality of the DEM can be expected to be poor if only one or two suitable scenes were available for the DEM generation.

The standard deviation of vertical elevation errors is expected to be 7 m to 14 m, in the validation summary report (*METI/NASA/USGS*, 2009), a root mean square error (RMSE) of 10.87 m was found between the ASTER GDEM and the USGS National Elevation Dataset (NED) (*Gesch et al.*, 2002). Over ice and snow however, the RMSE between these two datasets is 21.19 m, probably due to the low optical contrast of these land cover types. Even if such low-contrast land cover types (ice/snow, shadow, and water) are excluded from the comparison, the RMSE is still 10.48 m, resulting in a DEM accuracy slightly below 20 m at a 95% confidence interval (*Slater et al.*, 2011). As a result of this validation, "METI and NASA acknowledge that Version 1 of the ASTER GDEM should be viewed as 'experimental' or 'research grade'. However, they have decided to release the ASTER GDEM, because they believe its potential benefits outweigh its flaws and because they hope the work of the user community can help lead to an improved ASTER GDEM in the future" (*METI/NASA/USGS*, 2009).

Besides these overall comparisons and differences, typical small-scale errors and artifacts occur in the ASTER GDEM. Negative (pits) and positive (bumps) anomalies (Fig. 2.12b) are frequently observed in all GDEM tiles. As these artifacts often occur at the boundaries between different stack number zones, the reason for their occurence is probably related to the changes in the number of stacked scenes used for the compilation (*Slater et al.*, 2011). The size of these artifacts normally ranges from a few meters to decameters and they are often located in accumulation regions of glaciers with low optical contrast or in steep, north-oriented slopes, which are distorted or even hidden from the back-looking ASTER telescope on its descending orbit (*Kääb et al.*, 2005a). Fig. 2.12 shows such false effects in the region of Eiger, Mönch, and Jungfrau in the Bernese Alps.

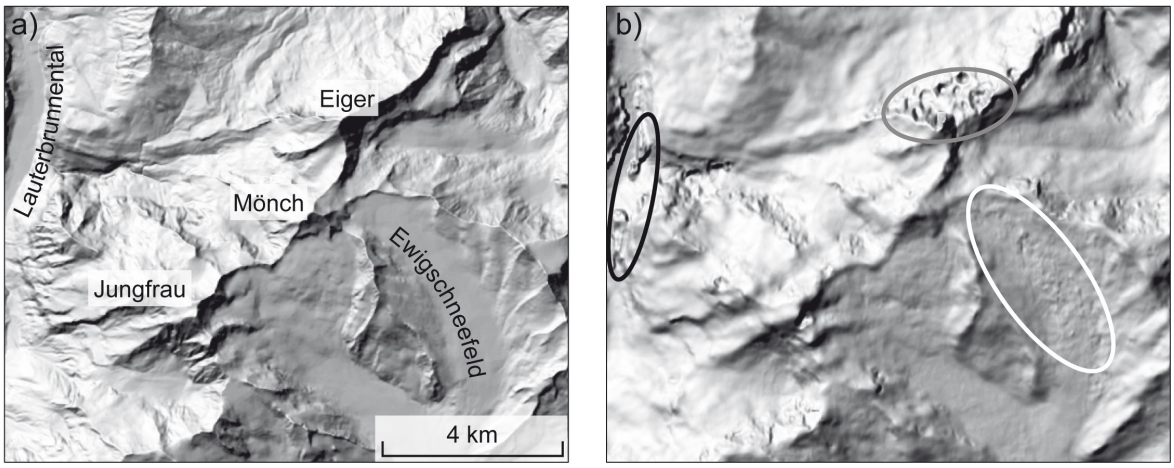

Figure 2.12: *Small-scale errors in the ASTER GDEM shown for the region of Eiger, Mönch, and Jungfrau. a) Hillshade view of the DHM25; b) Hillshade view of the ASTER GDEM. Typical artifacts are bumps (e.g., in the Lauterbrunnental, black oval), pits (e.g., at the north face of Eiger, grey oval), and combinations thereof (e.g., on the Ewigschneefeld, probably due to the low optical contrast of snow, white circle).*

By comparing the hillshade view images of the ASTER GDEM and the DHM25, it also becomes apparent that the effective resolution of ASTER is less then 30 m, although the dataset has a grid cell size of 30 m. Probably the applied correction algorithms and the DEM-stacking have a terrain-smoothing effect. This observation is confirmed by *de Ferranti*, the author and operator of the 'viewfinder panoramas' homepage (`http://www.viewfinderpanoramas.org`, accessed April 2011), who states that the "detail of topographic expression resolvable in the ASTER GDEM appears to be between 100 m and 120 m" (`http://www.viewfinderpanoramas.org/reviews.html#aster`, accessed April 2011). In addition, in the validation summary report it is stated that the spatial detail

resolvable by the ASTER GDEM is only slightly better than 120 m (*METI/NASA/USGS*, 2009).

Nuth and Kääb (2011) compared the SRTM, the ASTER GDEM, and data from NASA's Ice, Cloud, and land Elevation Satellite (ICESat, *Zwally et al.*, 2002), assessed their quality and developed a methodological framework for the comparison and correction of DEM datasets with different spatial resolutions and acquisition techniques. Besides aspect-dependent differences between SRTM and the ASTER GDEM, they detected biases along and cross track biases at two different frequencies, associated with the satellite acquisition geometry. They hypothesized that the higher frequency bias (10 - 12 cyles per ASTER scene and an amplitude of about 2 m) is caused by unrecorded pitch variations of the satellite (jitter), causing slight variations in the looking angle of the back-looking telescope and thus affecting the parallax estimates. The cause of the lower frequency pattern (2 - 3 cycles per scene, up to 5 m amplitude) remains uncertain. The fact that these biases are present in the ASTER GDEM indicates that the underlying ASTER scenes have not been co-registered before processing. Such a co-registration would clearly improve the quality of a new ASTER GDEM version.

2.3.5 Further datasets

A multitude of other elevation datasets exists in addition to the three DEMs described above. The NED and the SPIRIT project were already mentioned, as well as examples of single-scene based ASTER DEMs. Another widely used technique is the DEM acquisition by aerial photography (e.g., *Rivera et al.*, 2005, *Koblet et al.*, 2010). Airborne and terrestrial laser scanning and light detection and ranging (LiDAR) are used to compile high-resolution DEMs (e.g. *Baltsavias et al.*, 2001, *Geist et al.*, 2003, *Ruiz et al.*, 2004, *Abermann et al.*, 2010, *Fischer et al.*, 2011).

However, many of the methods for DEM compilation cannot be applied in some mountain regions due to remoteness, political reasons, and/or high costs. In such cases, information from the global datasets of SRTM and the ASTER GDEM, or topographic maps, remain the only alternatives to obtaining elevation data with a spatial resolution of 100 m or better. The website 'viewfinder panoramas' mentioned above contains a collection of datasets with a focus on mountain regions (`http://www.viewfinderpanoramas.org`, accessed April 2011). It is based mainly on SRTM-3 data but uses information from topographic maps and local DEMs to fill the data voids and to detect and correct erroneous regions.

2.4 Glacier inventories

2.4.1 Compiling remotely sensed glacier inventories

In Section 2.1.2 the status of the global glacier inventories was described and in Section 2.2.2 glacier mapping using multispectral remote sensing data and methods was discussed. In this section the steps required to produce a glacier inventory are described.

Compiling a glacier inventory builds on these foundations, but includes further processing steps and requires a DEM (cf. Section 2.3). *Paul et al.* (2009a) give a comprehensive description and recommendations regarding the compilation of glacier inventories; this subsection is widely based on this article and explains the workflow and nomenclature that was used for the production of the GlobGlacier products (Fig. 2.13).

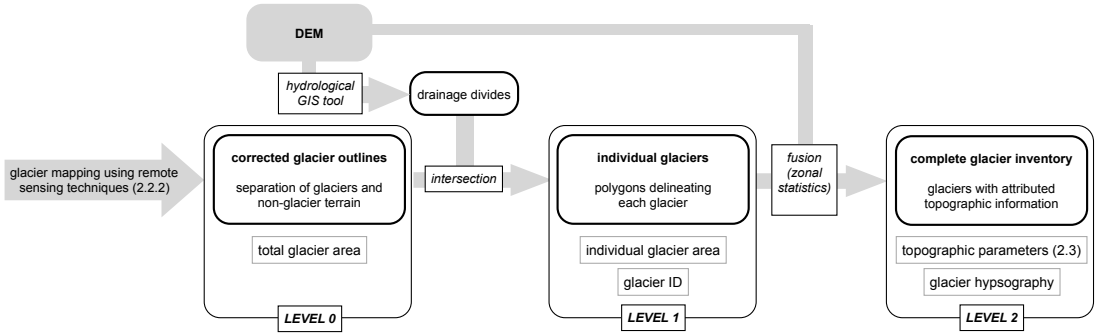

Figure 2.13: *Workflow for the compilation of remotely sensed glacier inventories according to the recommendations given in* Paul et al. *(2009a).*

The result of the glacier mapping procedure (cf. 2.2.2) is a binary classification of the satellite scene into glacier area and non-glacier area. Such a binary map consists of the outlines of contiguous ice masses, i.e., glacier to non-glacier boundaries only (Level 0, L0). On this level, the total glacier area of a region, and, in combination with a DEM, overall hypsographies, can be derived. The specific geomorphometric features of glacier and non-glacier terrain can also be assessed based on such a dataset. This includes the quantification of DEM cell-size related effects of the terrain (*Paul*, 2008) as well as some preliminary assessments of glacier-related hazards.

For the analysis of individual glaciers, internal ice-ice divides are required to calculate glacier specific parameters. In other words, glacier parts providing ice to a glacier tongue need to be separated from parts of the same accumulation region belonging to another glacier tongue (Level 1, L1). This is done by cutting the L0 glaciers along the hydrological drainage divides that are obtained from a DEM (*Paul et al.*, 2002). *Bolch*

et al. (2010) presented a methodology that allows a certain automation of this process by generating a buffer around the L0 glacier outlines, clipping the DEM with this buffer, and calculating the basins with hydrologic GIS tools. On the basis of individual glaciers it is now possible to calculate several parameters for each glacier, such as the area or a glacier ID, that has an inventory-specific format. Such L1 outlines offer the possibility for a change assessment on the level of individual glaciers. However, assessing the area changes between two or more points in time is related to uncertainties, inaccuracies and differences in the mapping purpose, applied methodologies, as well as knowledge and skills of the analyst (*Andreassen et al.*, 2008). In any case, all L1 glacier outlines that are compared must be derived using identical drainage divides (*Paul and Andreassen*, 2009).

To create Level 2 (L2) outlines, the L1 outlines are fused with a DEM to obtain topographic parameters for each glacier (*Paul et al.*, 2002). On this stage, the information stored in the attribute tables of the glacier inventory is comparable to the WGI information. The quality and accuracy of L1 and L2 information is of course not only related to the mapping accuracy, but also to the DEM quality. *Paper I* of this thesis is dedicated to the influence of the DEM quality on the resulting topographic inventory parameters.

Area calculations in UTM. Area calculations of polygons are straightforward in a GIS and can be used to calculate the glacier areas. However, it must be considered that geographic data normally is represented by a projection of a sphere to a plane. Within this thesis, mainly the Universal Transverse Mercator coordinate system (UTM) was used, which is suitable for maps of a few degrees east-west extent. Each of the 60 zones of the UTM projection zone system is based on the Transverse mercator projection, a cylindrical projection with the axis in the equator plane and a cylinder diameter slightly smaller than the pole-to-pole distance. This results in a secant projection with two lines of true scale, located approximately 180 km on both sides of the central meridian (*Snyder*, 1987). Projected shapes are therefore not exactly equal-distance and, hence, are also not equal-area: a north-south line at the central meridian is scaled by the factor of 0.9996 (i.e. 40 cm/km). At 180 km east or west of the central meridian the scaling factor is 1 (i.e. true scale), and further east or west it exceeds 1 (i.e. areas are overestimated, Fig. 2.14a). However, regarding the uncertainties related to the mapping of the glaciers itself or even only the raster-vector and vice-versa conversions, these uncertainties are much greater than the planar distortions caused by the Transverse Mercator projection. Reprojection to a neighboring UTM zone causes an area distortion of 0.1% to 0.4%, depending on the location within the zone (Fig. 2.14b). A reprojection over plus or minus two UTM zones introduces an overestimation of the area by 1.7% to 2.1%, this corresponds approximately to the mapping uncertainty. Thus three neighboring UTM zones can be merged by reprojecting the data to the central zone, but a reprojection over three zones or more must be avoided since an areas would be overestimated by 5% or more.

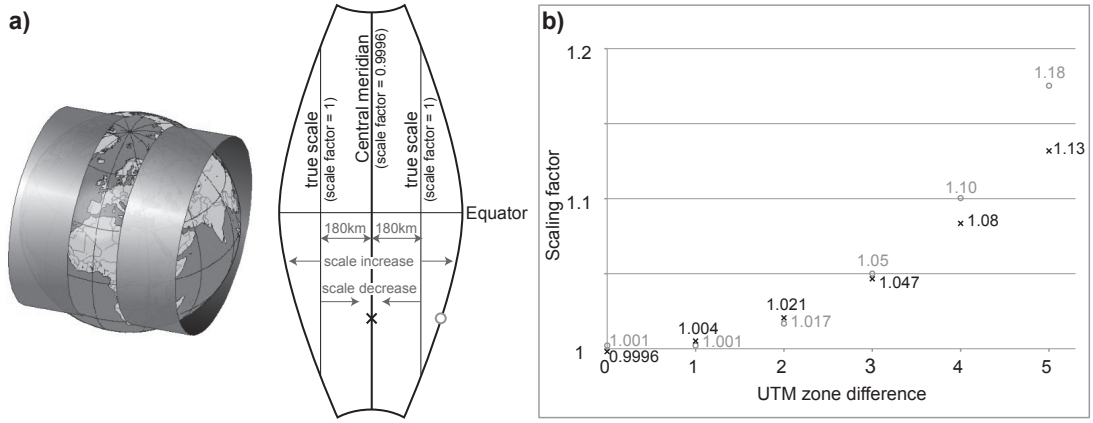

Figure 2.14: *Scaling issues in the UTM system. a) left: Scale-exaggerated schematic sketch of the projection cylinder for the UTM zone 30 (Greenwich meridian as central meridian). Taken from wiki commons (*`http://commons.wikimedia.org/wiki/File:Utmzylinderrp.jpg`*, accessed April 2011). a) right: resulting scalings in the projection of the sphere on the cylinder. The two lines of true scale correspond to the intersection circles of the cylinder and the terrestrial sphere. b) scaling factors introduced by reprojections over serveral UTM zones. Black crosses: a polygon located at the central meridian of the original UTM zone, grey circles: a polygon located at the borderline between two zones (see a)).*

2.4.2 Applications of glacier inventory data

One of the most prominent questions related to the urgently required global overview of the world's glaciers and ice caps is their potential contribution to sea-level rise (*IPCC*, 2007). Estimates of the sea-level equivalent of glaciers still rely on extrapolations that are associated with high uncertainties (e.g. *Radić and Hock*, 2011; *Paul*, 2011), mainly due to the large gaps in the global glacier inventory (e.g. *Raper and Braithwaite*, 2006; cf. Section 2.1.2). Other studies estimated the contribution of glaciers and ice caps to sea-level rise by using a simple glacier mass or energy balance model (e.g., *Kaser et al.*, 2006) or calculate the runoff resulting from estimated future glacier volume changes by coupling such a model to an atmospheric warming scenario (e.g. *Meier et al.*, 2007). Another approach was presented by *Oerlemans* (2005) who extracted a temperature reconstruction based on length-change records of 169 glaciers, or by *Oerlemans et al.* (2007), who used lengthchange records of 197 glaciers together with a mass balance and ice flow model to determine the sea-level rise contribution of glaciers and ice caps from 1850 to 2000. In all these studies the contributions from the two ice sheets in Greenland and Antarctica are not considered.

On smaller scales (regional to continental), the influence and contribution of glacier melt to river runoff is of great interest. Many studies using different methods exist, in particular on a regional to local scale; recent examples can be found in *Huss et al.* (2008) or *Koboltschnig et al.* (2008). On a larger scale, *Kaser et al.* (2010) presented a study about the contribution of glaciers to the total discharge of large rivers using WGI and WGI-XF data.

Detailed glacier data is becoming more and more important for climate modeling as well. Ice sheets are represented dynamically in GCMs by bi-directional coupling of the ice sheets and climatic forcing (e.g., *Ridley et al.*, 2005). Glaciers and ice caps, however, are too small to be represented in the grid spacing of such models, even in RCMs with higher resolutions of several hundred meters. *Kotlarski et al.* (2010) developed a new approach to replace the binary static glacier mask by representing the glacier as a fraction of the total gridcell area and combined this with an interactive energy and mass balance parameterization scheme to include the dynamic adjustment of the glacierized area. This approach was applied successfully to the RCM REMO, which includes the European Alps in their entirety. However, an application in RCMs covering other regions of the world requires not only a glacier inventory of sufficient detail, accuracy and timeliness, but also of a high degree of completeness and, if possible, a distinction between clean-ice and debris-covered glacier surfaces (*Paul and Kotlarski*, 2010).

Haeberli and Hoelzle (1995) developed a parameterization scheme based on geometric parameters as stored in tabular glacier inventories. It allows a detailed assessment of glacier characteristics, and also projections of future glacier reactions induced by climate change. *Hoelzle et al.* (2007) used the same methodology to compare the glacier characteristics of the southern Alps of New Zealand with the glaciers in the European Alps. Although the approach was developed and tested with WGI data, the principles are also applicable to modern 2D glacier inventory data in most other regions of the world. *Huggel et al.* (2003a) used this scheme to assess future projections of glacier area, volume, and runoff using a remotely sensed glacier inventory of the Cordillera Vilcanota and Carabaya in Peru. *Paul and Svoboda* (2009) applied the parameterization scheme to a remotely sensed glacier inventory to characterize the glaciers of Baffin Island in Arctic Canada. Most of the required topographic parameters can be easily and accurately obtained by combining the digital glacier outlines with a DEM. However, there is still a potential to further improve the scheme of *Haeberli and Hoelzle* (1995) by adapting it to the possibilities of modern 2D glacier inventory data. One of the major challenges remaining is to develop a methodology to automatically obtain the glacier length or the central flowline, one of the basic parameters required in the scheme of *Haeberli and Hoelzle* (1995).

Linsbauer et al. (2009) developed a GIS-based approach to estimate the ice thickness distribution. This model calculates a DEM of the glacier bed topography based on digital glacier outlines (e.g. a glacier inventory), a DEM, and (manually digitized) central flowlines for each glacier branche. The approach allows the ice thickness distribution to be modeled (*Linsbauer et al.*, subm.), and predictions to be made of sites with potential lake formation (cf. *Paper IV*) in the course of glacier retreat. Such glacier bed topographies can be useful input data for glacier retreat models (e.g. *Jouvet et al.*, 2009).

2.5 Assessing glacier hazards by remote sensing and GIS

Glacier and permafrost hazards originate from remote regions that are often difficult to access for topographical or political reasons (*Kääb et al.*, 2005a). Related processes have the potential to be far-reaching, can be a result of rapid changes, frequently include different processes and chain reactions, and often lack any historical precedence. Due to these reasons, remote sensing techniques and DEMs of sufficient quality are required to effectively assess such hazards (e.g. *Kääb et al.*, 2003b). Detailed overviews of air and spaceborne remote sensing techniques for early detection and analysis of glacier and permafrost related hazards are provided for instance by *Huggel* (2004), *Kääb* (2005b) and *Kääb et al.* (2005a). In the following section the focus is on the detection and analysis of glacier hazards using spaceborne remote sensing techniques in combination with a GIS.

To improve and foster the scientific communication related to glacier and permafrost related hazards, the Glacier and Permafrost Hazards in Mountains (GAPHAZ) working group was founded as a working group of the International Association of Cryospheric Sciences (IACS) and the International Permafrost Association (IPA). Besides providing a network of international scientists, GAPHAZ also aims at compiling a state of knowledge relating to glacier and permafrost hazards in high mountains, it gives recommendations and guidelines for the assessment of such hazards, and it also helps to improve the communication between scientific and governmental communities. Furthermore, a database of glacier and permafrost related disasters is maintained.

2.5.1 Processes

Glaciers continuously react to changes of the atmospheric forcing by adjusting their size to achieve a balanced mass budget. Resulting length and geometry changes are often associated with glacier hazards: Advancing glaciers can destroy infrastructure and indirectly cause new hazard potentials by damming rivers or resulting in new situations for ice avalanches. Such advances can be either stable (e.g. *Paul et al.*, 2004a), or take place

in the form of surges (e.g. *Kamb et al.*, 1994, *Post and Lachapelle*, 2000, *Fowler et al.*, 2001, *Copland et al.*, 2003), or other surge-like movements (e.g. *Haeberli et al.*, 2002). Glacier retreat can also alter the ice avalanche situation and trigger secondary hazards such as slope destabilizations due to debuttressing, even millennia after the glacier retreat (*Augustinus*, 1995, *Ballantyne*, 2002). The resulting changes in the stress field of deglaciated slopes can provoke landslides (e.g. *Matsuoka and Masahiro*, 2002, *Casson et al.*, 2003) or rockfalls due to glacier retreat since the Little Ice Age (LIA) or even since the last ice age (*Matthews and Shakesby*, 2004, *Korup and Tweed*, 2007, *Oppikofer et al.*, 2008, *Fischer et al.*, 2010). Another effect of glacier retreat is the exposition of unconsolidated material and loose sediments such as till and debris (*Paul et al.*, 2004b, *Egli et al.*, 2006, *Haeberli and Hohmann*, 2008, *Oerlemans et al.*, 2009), which enlarges the potential starting zones and volumes of debris flows (e.g. *Huggel et al.*, 2004b).

Ice avalanches are another source of glacier hazards. Compared to the debuttressing of steep rock slopes after glacier retreat, the hazard situation of ice avalanches changes more rapidly as it is directly influenced by glacier geometry. Besides the direct threat from the kinetic energy of the mass movement itself, there are also secondary hazards related to ice avalanches such as the damming of rivers or impact waves on lakes, which in turn can cause a lake outburst (*Clague and Evans*, 2000, *Kääb et al.*, 2003b, *Haeberli et al.*, 2004, *Kershaw et al.*, 2005). Basically, two different situations of starting zones for ice avalanches can be differentiated: a ramp-type and a cliff-type situation (*Alean*, 1985, *Pralong and Funk*, 2006, Fig. 2.15). Avalanches from cliff-type starting situations tend to be of smaller volumes but occur repeatedly, whereas ramp-type ice avalanches can potentially include larger ice volumes. Nevertheless, glaciers or glacier parts that were detached from a ramp-type situation can recover and build up their ice mass again after a collapse. *Fischer et al.* (2011) showed an example of a hanging glacier in the Monte Rosa east face that regained mass again after it was detached almost completely. In the extreme case of the Kolka / Karmadon event in September 2002 in the Russian Caucasus, complete erosion and detachment of an entire glacier has been observed (*Haeberli et al.*, 2004, *Huggel et al.*, 2005).

The most far-reaching glacier hazard is related to floods resulting from glacier lake outbursts (e.g. *Richardson and Reynolds*, 2000, *Huggel et al.*, 2002, *Kääb et al.*, 2005a). Glacier lake formation is a frequent phenomenon associated with glacier retreat. Such glacier lakes form at the front or at the margins of a glacier (*Clague and Evans*, 1994, 2000, *Paul et al.*, 2007), or as supraglacial lakes on flat, debris-covered glacier tongues, which grow by the coalescence of small ponds that merge to a lake which can cover the entire glacier width (*Watanabe et al.*, 1994, *Benn et al.*, 2000, *Komori*, 2008). Similar cases occurred also on debris-covered glaciers in the Alps, for instance on Belvedere Glacier at the foot of the Monte Rosa east face (*Haeberli et al.*, 2002, *Kääb et al.*, 2004, *Tamburini and Mortara*,

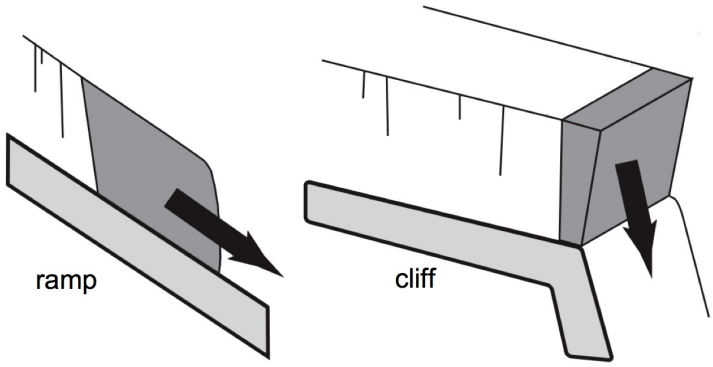

Figure 2.15: *Schematic sketches of ramp- and cliff-type starting situations of ice avalanches. Modified from* Huggel et al. *(2004a), based on* Alean *(1985).*

2005) or on the tongue of the Lower Grindelwald Glacier (*Werder et al.*, 2010). As mentioned before, lakes can also form through a river blockage caused by an advancing glacier or deposits of a mass movement. *Costa and Schuster* (1988) provide an overview of different kinds of natural dams. Hazards originating from glacier lakes often include the interaction of various processes, i.e., a rock or ice avalanche, which reaches a lake and causes an overtopping of water or even damage to the dam, which in turn causes an outburst flood or debris flow, which can reach a lower lake or dam a river in the valley (e.g. *Huggel et al.*, 2004c, Fig. 2.16). Hazard-related case studies focusing on single lakes are presented for instance by *Watanabe et al.* (1994) (investigating the formation of Imja Lake in the Everest region in Nepal and evaluating lake outburst scenarios), *Hubbard et al.* (2005) (a post-event analysis of a rock avalanche triggering a large displacement wave at Laguna Safuna Alta in the Cordillera Blanca, Peru), *Fujita et al.* (2008) (evaluation the development of three glacier lakes in the Lunana region, Bhutan, and re-assessing the volume of a past lake outburst), and *Werder et al.* (2010) (assessing potential future outbursts of a supraglacial lake on the Lower Grindelwald Glacier in the Bernese Alps, Switzerland, by analyzing past events).

The Kolka / Karmadon event is a prominent example of such a chain reaction: a rock failure initiated a rock-ice avalanche, which sheared off the entire tongue of Kolka glacier – an incident that had been unknown so far. After a 18 km trajectory, the mass of rock, ice, firn, snow, and water was blocked at the entrance to a gorge. From this point, a debris flow continued for another 15 km through the subjacent valley, and the compressed mass at the entrance to the gorge dammed a river, causing large inundations and resulting in a number of lakes *Haeberli et al.* (2004), *Huggel et al.* (2005).

Such interactions of processes point to the importance of considering the entire system of involved factors and processes for hazard assessments. Atmospheric warming can

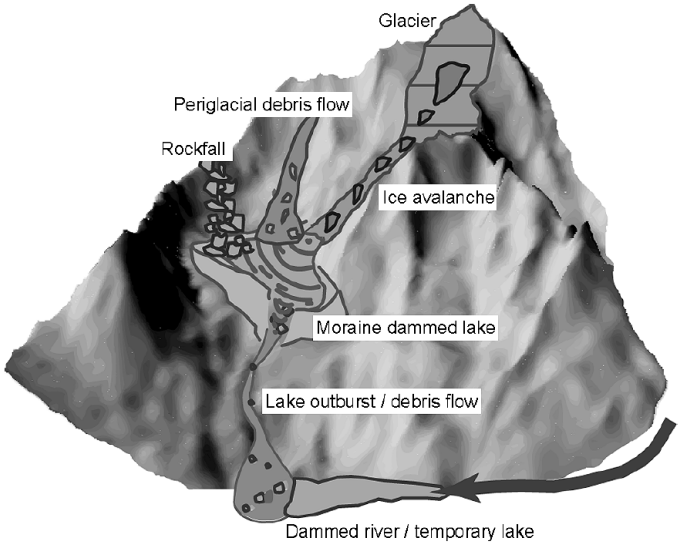

Figure 2.16: *Schematic overview of potential hazardous interactions of glacial and periglacial processes. Taken from* Huggel et al. *(2004c).*

for instance cause a glacier to retreat to a new cliff-type ice avalanche disposition, lead to the formation of a new lake, reveal loose material that can be entrained during a lake outburst, change the stability of a 40° steep, formerly cold-based hanging glacier due to basal warming, and so on (e.g. *Vilimek et al.*, 2005). *Reynolds Geo-Science* (2003) provide guidelines for an integrative assessment of glacier hazards in the field and by using geophysical methods.

In terms of predictions about potential future evolution of hazard situations, not much scientific literature exists. *Reynolds* (2000) presented an approach to identify sites on debris-covered glaciers with potential future lake formation. To do so, he used a surface-gradient threshold of 2° as an indicator to identify glacier parts with low flow velocities. Findings from this study were confirmed by *Quincey et al.* (2007), who additionally used InSAR data to derive flow velocities.

2.5.2 Detection, analysis, and assessment of hazards

A detailed and comprehensive assessment of a particular hazard situation includes sophisticated modeling, in-situ field investigations, and a thorough analysis of uncertainties. Examples of detailed post-event analyses are provided for instance by *Fischer et al.* (2010) for a rock avalanche, *Faillettaz et al.* (2008) for the collapse of a part of a hanging glacier, or *Hubbard et al.* (2005) for a lake outburst triggered by a rock avalanche.

However, simpler and faster approaches are required to investigate hazard potentials on a coarser scale. DEMs and GIS tools provide powerful means for analyses of larger regions. *Salzmann et al.* (2004) for instance implemented the empirical information from *Alean* (1985) in a GIS to select steep glacier parts which have the potential to produce ice avalanches. An integrative assessment procedure for glacier hazards on such larger scales, combining remote sensing and empirical relationships, is presented by *Huggel et al.* (2004a) for the Swiss Alps and by *Richardson* (2010) for the assessment of glacier lakes in the Hindu Kush Himalaya.

Regarding the modeling of mass movements such as debris flows, rock falls, ice or snow avalanches, a number of physically based numerical models such as the rapid mass movement model (RAMMS, *Christen et al.*, 2008) do exist, which include mass conservation and can compute velocities and flow heights by solving the shallow water equations for granular flows. By choosing reasonable values for the dry Coulomb friction μ and the turbulent friction ξ of the Voellmy approach (*Bartelt et al.*, 1999), different mass movements such as rock/ice avalances (*Allen et al.*, 2009, *Schneider et al.*, 2010) or debris flows can be modeled (*Scheuner et al.*, 2009). A much simpler approach was presented by *O'Callaghan and Mark* (1984), who developed a hydrological flow-routing approach for the extraction of drainage networks from a DEM by selecting the steepest gradient from each DEM cell to its eight neighbors, thus called the D8 approach. *Huggel et al.* (2003b) adapted and modified this methodology - that was initially not developed for modeling mass movements - to a so-called modified single flow (MSF) model and a multiple flow (MF) model by introducing the possibility of the flowing mass to deviate to up to 45° from the steepest gradient. These models consider neither the mass nor the velocity of the moving mass, rather they assign a probability to which a particular DEM cell is affected by the mass movement. Finally, average slope values from empirical studies are used to determine maximum runout distances. For debris flows in the Alps, a probable maximum runout distance corresponding to overall trajectory slope of 11° (or 20%) was used (*Haeberli et al.*, 1991, *Huggel et al.*, 2003b), and for ice avalanches an average slope of 17° (33%) can be used, according to the findings of *Alean* (1985). This approach proved to provide reasonable results for debris flows (*Huggel et al.*, 2003b), ice avalanches (*Salzmann et al.*, 2004), rockfalls (*Noetzli et al.*, 2006) and floods (*Allen et al.*, 2009). However, it has to be noted that the average slope values for the maximum runout distances are based on emprical studies, mainly from the European Alps. For applications to other regions or different processes, these values might be exceeded (e.g. *Haeberli et al.*, 2004, *Huggel et al.*, 2005, *Schneider et al.*, in press).

2.5.3 Glacier inventories for assessing glacier hazards

The combination of glacier inventory information with simple but robust models has a vast potential for the assessment of natural hazards on a local to regional scale. Using glacier inventories as a support for glacier hazard assessment is, for instance, among the main aims of the GLIMS initiative (*Kargel et al.*, 2005). A couple of studies exist which used such glacier inventory data in the context of glacier hazard assessment. For example *Bajracharya and Mool* (2009) related the growth of glacier lakes with glacier retreat in the Nepalese Himalayas by using a national glacier invnetory; *Salzmann et al.* (2004) used inventory information for their modeling of potential ice avalanches; and *Fischer et al.* (2010) assessed the debuttressing of an oversteepened rock wall due to glacier retreat since the Little Ice Age (LIA). Another application of glacier inventory data in glacier hazard predictions is presented in *Paper IV* of this thesis, where an approach is presented to detect sites with potential future glacier lake formation based on the current surface geometry and characteristics.

3
Summary of research papers

This thesis consists of four research papers that are published in or submitted to peer-reviewed scientific journals and a proceedings volume of a conference. They are grouped around the core topics of remote sensing of glaciers and lakes, glacier inventories, and glacier hazards. Methodological aspects of the compilation of glacier inventory data are covered in both *Papers I* and *II*, an example of data acquisition and analysis is presented in *Paper II*. Furthermore, integrative frameworks are developed for the detection and preliminary hazard analysis of existing glacier lakes (*Paper III*), as well as an application of glacier inventory data in the context of glacier hazard development, i.e., the anticipation of future glacier lake formation in *Paper IV*. In the following the papers are briefly summarized; the full versions can be found in Part II.

Paper I: Compiling topographic parameters with SRTM and the ASTER GDEM

Frey, H. and Paul, F. (in press). On the suitability of the SRTM DEM and ASTER GDEM for the compilation of topographic parameters in glacier inventories. *International Journal of Applied Earth Observation and Geoinformation*. doi: 10.1016/j.jag.2011.09.020

This paper investigates the influence of DEM data on topographic parameters in glacier inventories. At present, satellite imagery suitable for glacier mapping is easily available for all glacierized regions of the world. Glacier-specific topographic parameters are of vital importance for many further applications of glacier inventories, such as volume estimations, and the modeling of runoff and potential future glacier evolution. However, many entries in the GLIMS glacier database still currently lack such topographic information, as local or national DEMs of sufficient resolution and quality are not available for many regions. The SRTM DEM and ASTER GDEM represent valuable alternatives for providing the required elevation information.

Data of the void-filled SRTM version and the ASTER GDEM were downloaded and resampled to both 25 m and 100 m resolution. Seven topographic parameters (minimum, maximum, mean, and median elevation, mean slope, mean aspect, and mean aspect sector) were calculated for 1,786 glaciers in Switzerland based on these four DEM datasets. The parameter values were then compared to reference values calculated with the DHM25. To separate the influence of resolution from other DEM specific influences, the topographic glacier parameters were also calculated for a 50 m and a 100 m version of the DHM25 and compared to the DHM25 reference value.

In addition to the differences for each individual glacier to the reference values obtained the DHM25, standard deviations for different size classes were also calculated. Although the differences from the reference values featured a large scatter for some parameters of individual glaciers, the standard deviations were in an acceptable range, i.e., in the same range as for the comparison with only the DHM25 in different resolutions. Obviously, parameters depending on a single DEM-cell value (minimum and maximum elevation) are more error-prone than parameters that are averaged over the entire glacier area. The latter tend to average out errors caused by DEM artifacts and show a decreasing scatter for increasing glacier size. The InSAR acquisition technique of SRTM seems to be superior to the photogrammetry of the ASTER GDEM over the typically low-contrast glacier areas with a comparably smooth surface geometry.

Thus, both the SRTM and the ASTER GDEM can be considered as suitable for the compilation of topographic information, and used to update the missing topographic information in many existing inventories.

Paper II: A glacier inventory for the western Himalayas

Frey, H., Paul, F., and Strozzi, T. (in rev.). Compilation of a glacier inventory for the western Himalayas from satellite data: Methods, challenges and results. *Remote Sensing of Environment*

In this study, a glacier inventory of the western Himalayas, namely the northwestern part of India, was compiled. In this region, the global datasets still revealed a large data gap. The inventory is based on seven Landsat ETM+ scenes acquired between August 2000 and August 2002.

The main challenges were related to difficult mapping conditions caused by cloud cover in the southwestern part of the study region, varying snow-cover conditions within the scenes, extensive debris cover, and difficult interpretation of debris-covered glacier extents in the cold-dry northwestern part of the study region, where glacier tongues are likely situated in the zone of continuous permafrost.

Using coherence images from ALOS PALSAR image pairs acquired in summer proved to be a very helpful and promising tool for the determination of the extent of debris-covered glacier parts. In the snow-free summer months and in regions without vegetation, glacier flow is the main cause for the loss of coherence, hence, debris-covered glacier extents are clearly defined in such coherence images due to their movement.

For the delineation of drainage divides and for the calculation of topographic inventory parameters, the SRTM and ASTER GDEM were compared to each other. Although SRTM was expected to be more suitable for this task, gross errors were found in the void-filled version: The void-filling algorithms seem to have failed in this region, as the terrain in the data voids of the SRTM3 is underestimated by several hundred meters up to more than a kilometer. Therefore, the ASTER GDEM was chosen for this study.

In total, 11,783 glaciers larger than 0.02 km^2 were mapped, covering a total area of 9,372 km^2, and of which 14% were under debris cover. Clear gradients across the mountain range from southeast to northwest of increasing mean glacier elevation and at the same time decreasing amount of debris cover could be observed. Furthermore, glacier parts below the mean elevation have a significantly smaller surface slope (16.8°) than glacier parts above the mean glacier elevation (25.8°). As ice thicknesses are larger in flat glacier parts, this indicates that large ice volumes are stored at relatively low elevations.

This study showed how region-specific challenges for glacier mapping can be addressed by combining different datasets and methods. Furthermore, the potential of analyses of the glacier inventory parameters could be demonstrated. And finally, the inventory provides a consistent baseline for future research and closes a prominent gap in the global glacier map.

Paper III: Detection and analysis of glacier lakes

Frey, H., Huggel, C., Paul, F., and Haeberli, W. (2010b). Automated detection of glacier lakes based on remote sensing in view of assessing associated hazard potentials. In: *Grazer Schriften der Geographie und Raumfoschung 45: Proceedings of the 10th Internatinal Symposium on High Mountain Remote Sensing Cartography, 8.-11.9.2008, Kathmandu, Nepal.*, (edited by Kaufmann, V. and Sulzer, W.), pp. 261–272

This study is dedicated to the development of a semi-automated approach for the detection and analysis of existing glacier lakes and a preliminary analysis of their hazard potentials. The goal was to integrate different existing approaches for glacier and lake mapping, and simple models to investigate flow paths and runout distances of mass movements into one comprehensive framework.

As a first step, a GIS tool was created to automatically compile a glacier and a lake layer using three Landsat bands and a DEM. Glacier parts without debris cover were mapped using a band ratio, lakes were mapped based on the NDWI and a shadow mask. The tools work automatically; the only required user interaction is the selection of the mapping thresholds. For the preliminary analysis of the hazard potentials, potential ice avalanches and lake-outburst floods were modeled using simple flow-routing approaches.

Problems of glacier lake detection are related to inaccuracies in the cast-shadow mask and misclassifications over glacier areas due to channel saturation or water near the glacier surface. Regarding the analysis of the hazard potential, many potential triggers are neglected in this study. Nevertheless, MSF proved able to provide valuable information about the potential reach of ice avalanches and lake outburst, based on very limited input information; also potential chain reactions could be identified by this approach.

The strength of the presented approach is the very limited amount of required input parameters. Satellite data and digital terrain information is basically available for all parts of the world and the applied tools and methodologies allow large regions to be investigated all at one time. By applying some adjustments, in particular to the empirical thresholds for runout distances of ice avalanches and debris flows, the approach can also be applied to other mountain regions.

Paper IV: Anticipating future glacier lake formation

Frey, H., Haeberli, W., Linsbauer, A., Huggel, C., and Paul, F. (2010a). A multi-level strategy for anticipating future glacier lake formation and associated hazard potentials. *Natural Hazards and Earth System Sciences*, 10: 339–352

In this work, a strategy for the identification of sites with potential lake formation in the future is presented. Combinations of existing and newly developed methodologies are applied on four different levels. The design of the strategy aims at covering large regions efficiently with low effort and then to subsequently focus on regions of particular interest by applying more sophisticated and detailed approaches.

At all levels of detail the principal idea is the detection of overdeepened parts of the glacier bed, based on the geometry and characteristics of the current glacier topography. Such overdeepenings have the potential to form a proglacial lake in the course of glacier retreat.

On the first level, a simple slope threshold is applied, as the glacier surface over an overdeepening is expected to be flat. On the second level, three criteria concerning the changes in the surface slope, glacier width and crevasse pattern are evaluated. On Level 3, more quantitative information is gained by applying more detailed and labor-intensive models to estimate ice-thickness distribution and, hence, the topography of the entire glacier bed. Finally, in-situ field measurements are proposed at Level 4 in order to obtain detailed, site-specific information.

As this study analyzes future conditions, validation is difficult. Nevertheless, the criteria of the Levels 1 and 2 were found on historic maps at locations of recent glacier lake formation. In addition to the Swiss DHM25, the SRTM DEM and the ASTER GDEM were also tested for use in this strategy with promising results. This indicates that the approach could also be applied in other parts of the world.

Finally, potential outbursts of expected future lakes were simulated using the MSF model. This cannot be considered as a complete hazard assessment; nevertheless such scenario calculations provide important information for stakeholders and authorities to prepare for potential future situations, already in the present.

4 General discussion

In this chapter, the findings of the research papers (Chapter 3) are put in context and discussed in view of previous studies and the current state of the art as presented in Chapter 2. First, in Section 4.1 general aspects regarding the used DEM datasets are discussed, as they play an important role in all parts of the thesis. Section 4.2 analyzes remotely sensed glacier inventories, including glacier mapping and the subsequent steps for the compilation of glacier inventories. In Section 4.3 the focus is on detection and first-order hazard assessment approaches for existing and potential future glacier lakes.

The issues discussed in this chapter are all related to the research papers. Furthermore, more general matters and points already addressed in Chapter 2 are revisited here as well, even if they are not directly linked to analyses or findings of a specific research paper. Finally, a number of practical recommendations based on experiences gained during the data processing steps are also given.

4.1 Digital elevation models

The SRTM and the ASTER GDEM elevation datasets are unique due to their (near) global coverage. Thus, these two datasets were of key importance for various aspects of the present thesis. Technical details like acquisition techniques, estimated accuracy, and known artifacts and errors have already been described in Sections 2.3.3 and 2.3.4.

In this part, some further insights and considerations based on experiences with these datasets, especially during the preparations of *Papers I* and *II*, are presented.

Errors and their implications. Based on findings from the Alps (*Paper I*), the void-filled SRTM version from CGIAR was expected to be the most suitable DEM for the compilation of the glacier inventory for the western Himalayas (*Paper II*). However, the respective SRTM tile (srtm_52_06) revealed large underestimations of the surface elevation in certain regions (Fig. 4.1). Differences of up to 1000 m compared to the ASTER GDEM were observed. An evaluation of the SRTM-3 data (with data voids) showed, that the areas with underestimated elevation values are congruent to the data voids in the original SRTM data. Hence, the reason for these errors is probably a problem with the void-filling algorithms applied by CGIAR (*Reuter et al.*, 2007).

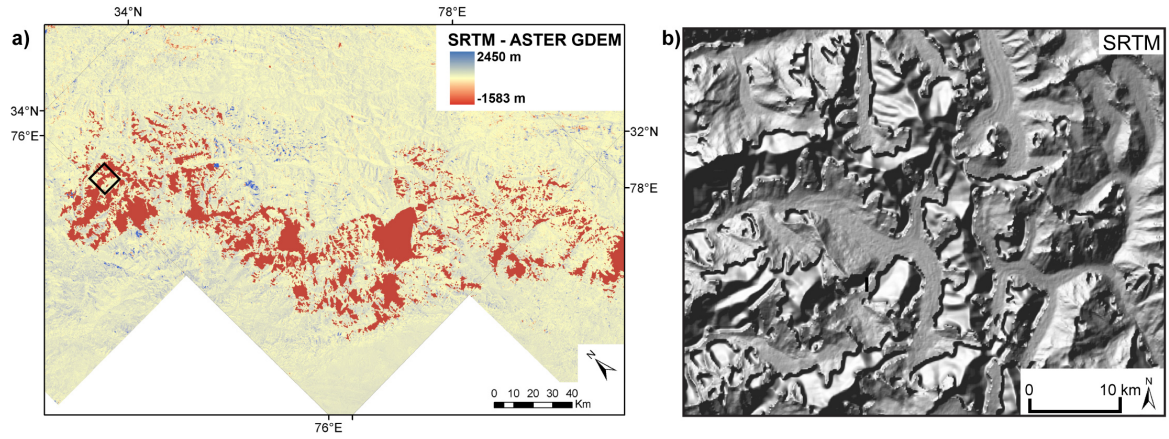

Figure 4.1: *In the western Himalayas, the surface elevation is significantly underestimated by the void-filled SRTM version in regions with data interpolation. a) Differences of SRTM compared to the ASTER GDEM. Red areas (i.e., regions where SRTM elevation values are more than 1 km lower than in the ASTER GDEM), are congruent to the data voids in SRTM-3. b) Hillshade view of a zoom of the void-filled SRTM. Regions with interpolated terrain are clearly indicated due to the smoothed topography, but also the steep drops in the terrain at the margins of these interpolated data voids are visible. Location of b) is indicated by the rectangle in a).*

Comparing the original SRTM-3 to the void-filled SRTM further uncovers a slight relative shift in the datasets: The version from CGIAR is shifted by about 60 m to 70 m in a southeastern direction. These shifts are potentially due to an assignment problem during the void-filling processes, when for instance elevation values were assigned to the cell center instead of to a corner of the grid cell. In the 90 m SRTM DEM such a shift from the upper left corner to the cell center results in a southeastern shift of 63.34 m

($90\,m * \sqrt{2}/2$), which corresponds well with the observed shift of about 65 m. More details and formulas relating to analytical detection of DEM shifts and their dependency on slope and aspect can be found in *Kääb* (2005b) and *Nuth and Kääb* (2011).

In addition, the ASTER GDEM at certain places revealed differences relative to the reference DEMs of several hundred meters in addition to the specific small-scale artifacts described in Section 2.3.4. One reason for this might be related to orographic clouds, which are not detected by the cloud-masking algorithm, as the clouds are surrounded by glacier and snow areas with similar high reflectance values in the visible spectral range. One of the largest differences between ASTER GDEM and the DHM25 in Switzerland occurs at the location of the famous Matterhorn (Fig. 4.2). The highest elevation in the vincinity of the mountain is given as only 3,837 m a.s.l. in the ASTER GDEM and the elevation value at the location of the peak as only 3,632 m a.s.l., instead of 4,484 m a.s.l.

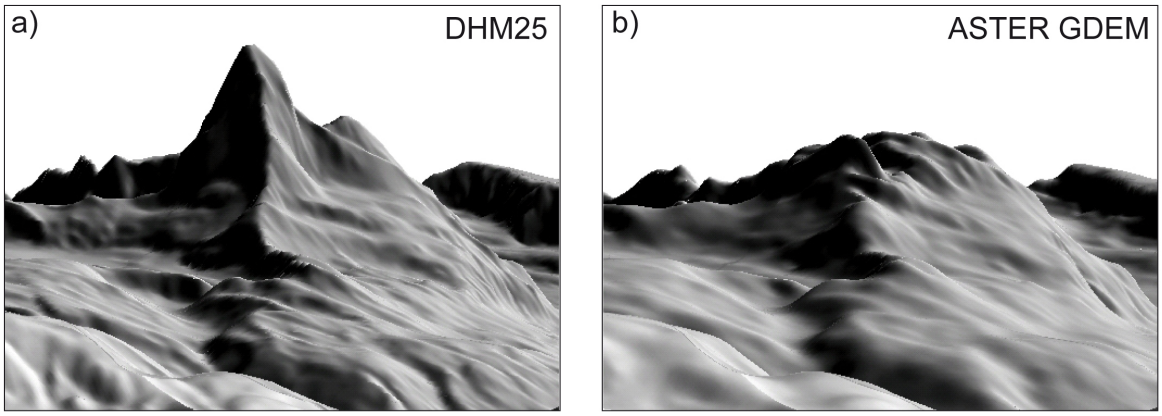

Figure 4.2: *Oblique views of the Matterhorn, Valais, Switzerland: a) with the DHM25 from swisstopo, b) with the ASTER GDEM from the same observation point as a). In the ASTER GDEM the mountain peak is missing completely; the elevation at the peak is underestimated by 852 m.*

Such errors in DEMs – as well as the typical artifacts on a smaller scale – have different implications, depending on the purpose and context of the application. Elevation differences of several hundred meters in DEMs with a spatial resolution of several decameters, however, render these datasets useless in the vincinity of such errors. This emphasizes the importance of a rough qualitative data check, such as a comparison to another DEM and the derivation of a hillshade view, before using the data. The partly erroneous void-filled SRTM DEM is used in several studies in this region (e.g. *Gardelle et al.*, 2011, *Scherler et al.*, 2011), without mentioning these gross errors.

The mentioned errors in SRTM also affect the spatial accuracy of the Landsat scenes orthorectified by the USGS. The GLSDEM, the DEM of the Global Land Survey (GLS), which is used by the USGS for the orthorectification of satellite scenes (*Tucker et al.*, 2004), consists of CGIAR SRTM data for Africa and Eurasia south of 60°N (`http://www.glcf.umd.edu/data/glsdem/description.shtml`, accessed April 2011). Depending on the distance from the Nadir line, an elevation error of several hundred meters causes a significant location error in the orthorectified satellite scene, and, hence, also for instance in the mapped glacier outlines (*Paper II*). As these DEMs with (near-) global coverage are widely used for countless further applications, it is impossible to estimate all potential implications of such errors.

Hayakawa et al. (2008) compared a pre-released part of the ASTER GDEM for western Japan to SRTM-3 data and concluded that ASTER GDEM will become the standard dataset for geoscientific applications due to its completeness and the higher spatial resolution. This, however, has not happened so far: in most cases SRTM is still preferred if available, which is in agreement with the findings from *Paper I*. Besides the lower resolution of the effectively resolved topographic detail, its impracticality for any change detection applications due to the undetermined acquisition date and the characteristic small-scale artifacts might be a further reason for this. The latter is a severe drawback in particular for any application related to hydrological flow modeling. In regions outside the coverage of SRTM, the ASTER GDEM nevertheless provides a valuable alternative (*Slater et al.*, 2011).

Comparing different DEMs. It is important to take the acquisition techniques into account when comparing different DEMs. For glaciers, in particular in the typically snow-covered accumulation regions, the acquisition technique has a major impact on the derived elevation values, in general resulting in a higher uncertainty. First of all, the surface has a much higher temporal variability and changes over short time periods. Optical systems have problems with the low optical contrast in snow-covered regions, whereas radar systems to a certain extent penetrate the snow pack. The penetration depth again depends on the used wavelength and the dielectric properties of the snowpack, i.e., the temperature or the amount of liquid water, respectively (*Drinkwater et al.*, 2001, *Rignot et al.*, 2001). Similar effects occur for vegetated terrain, where the radar signal penetrates the canopy to a certain extent, depending on the wavelength and the properties of the vegetation (e.g. *Carabajal and Harding*, 2005, 2006), but in the optical systems the vegetation mantle is considered as the surface (i.e., a DTM versus a DSM, respectively).

Ready-to-use datasets. Typical artifacts associated with the different datasets are known (cf. Sections 2.3.3 and 2.3.4), and different procedures for corrections are proposed, e.g. by *Nuth and Kääb* (2011). However, only a few studies take such findings into account

and apply the corrections to the original data (e.g., *Möller et al.*, 2007, *Möller and Schneider*, 2010). In most cases, the data is used one-to-one as it is downloaded from the web. It is unclear whether this is due to ignorance of such internal errors, technical difficulties, lack of know-how and/or lack of access to the required software to apply such corrections. In any case, there is evidence that ready-to-use data, such as orthorectified satellite imagery from USGS or the void-filled SRTM version from CGIAR, are very popular. Hence, it would be a great asset if established correction algorithms were applied to the entire existing 'raw' data and made available to the general scientific public as ready-to-use datasets.

4.2 Compiling remotely sensed glacier inventories

Glacier mapping based on remote sensing data and the compilation of digital glacier inventories are the core issues of *Paper I* and *Paper II*. In this section, first the findings related to the remote sensing procedures are discussed, followed by a discussion about the steps of glacier inventory compilation that include a DEM, i.e., the digitization of drainage divides and the calculation of topographic parameters.

4.2.1 Glacier mapping

Automated mapping of clean ice and snow. Suitable mapping results for clean ice and snow are obtained normally by choosing a threshold of 2.0 ± 0.2 for the TM3/TM5 ratio. The specific values are determined in principle by the gain-settings of the channels and the atmospheric conditions in each individual scene. For successive scenes of the same path, the same threshold could be used often. Nevertheless, the search for the best threshold is crucial since the mapping accuracy of the main processing determines, to a large extent, the efforts required for manual corrections on the post-processing stage. Mapping results in shadowed glacier parts are most sensitive to changes in the threshold, therefore, the threshold should be selected in such regions with glacier parts in terrain shadow (e.g. *Sidjak and Wheate*, 1999, *Paul et al.*, 2002, *Andreassen et al.*, 2008).

In most regions, an additional threshold applied to TM1 as proposed by *Paul and Kääb* (2005) proved to be useful to reduce misclassifications in cast-shadow regions. But in the comparably low latitudes of the western Himalayas, the sun elevation during the scene acquisition in August and September was relatively high, between 55° and 63°. This results (a) in a reduction of shadowed area, and (b) in reduced illumination differences caused by the topography, which are helpful for recognizing debris-covered

glacier parts. The additional threshold in TM1 might therefore be necessary only in higher latitudes.

Challanges and related manual corrections. Debris cover, icebergs in front of calving glaciers, clouds (with or without ice content), frozen lakes, other atmospheric contamination such as dust or smoke from forest fires, and water bodies are the main sources for misclassifications and require manual corrections.

Most prominent, also in the scientific literature (cf. Section 2.2.2), is the problem of the determination of glacier extent under debris cover. For glacier mapping in the western Himalayas, coherence images from ALOS PALSAR image pairs with a 46-day time interval were used to support the manual correction of the glacier outlines (*Paper II*, Fig. 4.3). *Atwood et al.* (2010) already mapped glaciers in a basin of the Wrangell Mountains, Alaska, solely based on coherence images and a DEM. The PALSAR coherence images proved to be very helpful, in particular in the Himalayas with extensive debris cover on the glacier tongues and the high sun elevations mentioned above. Although the use of this scenes includes the costs of the SAR images and the specific know-how and software required for the calculation of the coherence images, it has the potential to be used widely in the future, also in other regions.

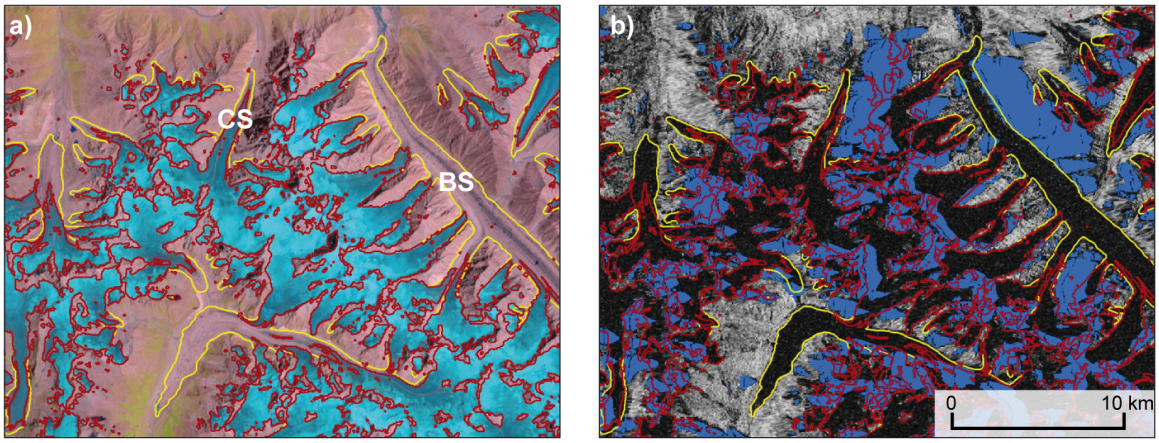

Figure 4.3: *Mapping of debris-covered glacier parts based on coherence images shown for the regions of Chhota Shigri (CS), and Bara Shigri (BS). Results from the automated mapping of clean ice are shown in red, manually corrected glacier outlines in yellow. a) RGB543 false-color composite of a Landsat ETM+ scene. b) Coherence image of an ALOS PALSAR image pair. Bright pixels indicate high coherence between the two SAR images, dark pixels a loss of coherence, i.e., due to glacier flow; blue regions indicate no-data regions. The extents of the (moving) glaciers are clearly visible.*

Glacier parts that are hidden by clouds or snow cover cannot be mapped based on the respective scene (cf. *Paper II*). If only a small portion of the glacier margin is invisible, the extent can be interpolated by drawing a straight line connecting the two ends of the visible outline. Another solution is to consult a different scene, e.g., from another date, from an adjacent path, or even from another sensor, where omitted glacier parts are visible. In such cases it is important to keep records of the used source scene and date, especially if they were acquired in a different year.

Another solution, if no additional satellite scene is available, is to check for additional data sources such as GoogleEarth™, (digital) maps, or other existing glacier inventories. In particular GoogleEarth™ offers a growing coverage of high-resolution imagery from satellite data (Ikonos, Quickbird) and aerial photography. In combination with the terrain data that is also available, some uncertain cases can be resolved with this information. The same is true for digital maps; however, it has to be considered that glaciers often have a lower mapping accuracy and longer updating intervals than other features on the map. In most cases, the underlying information source (e.g. aerial photography) has an acquisition date other than the date of the map issue and has been acquired in July or August instead of September, therefore seasonal snow is often misinterpreted. Information from other glacier inventory datasets is only useful in regions with a clear trend of the glacier evolution, and serves only as additional information to another, primary data source: For instance, in regions where a strong glacier retreat has been observed for many years, it can be assumed that outlines from an older glacier inventory determine the maximum possible extent of current glaciers.

4.2.2 Glacier inventory compilation

Defining drainage divides. After the glacier mapping procedure, the DEM comes into play in order to compile glacier inventory data. The first step is the definition of drainage divides, which are required to separate individual glaciers. The application of automated and semi-automated approaches as presented, for instance, by *Bolch et al.* (2010) to SRTM and the ASTER GDEM needed a lot of manual corrections. This is due to the fact that most of the errors and inaccuracies of these datasets occur in the accumulation regions of glaciers, but these are exactly the regions of drainage divides. Therefore, in the western Himalayas the automatically calculated drainage divides served only as a reference, but the ultimately used glacier separations were manually digitized based on illumination differences in the satellite scenes and the flow-direction grid of the DEM (*Paper II*).

Calculating topographic glacier inventory parameters. The quality and accuracy of the used DEM of course influences the values of topographic glacier inventory param-

eters (minimum, maximum, mean and median elevation; mean slope, mean aspect, and mean aspect sector, cf. *Paul et al.*, 2009a and *Paper I*). Gross DEM errors like those described in Section 4.1, make the elevation dataset useless in the affected regions, but the typical small-scale artifacts have only a minor influence on most topographic parameters. Further, many of them are not very sensitive to glacier changes over time: maximum elevation is determined mainly by the topography and rather constant even in periods of glacier fluctuations. The same is true for mean aspect. Even mean slope is not very sensitive to glacier changes, although in general a slight increase in mean elevation has to be expected in the course of glacier retreat, as the surface lowering normally is more pronounced at lower elevations.

Changes in topographic parameters over time are determined by changes in the glacier outlines and changes in the glacier surface elevation. For an accurate calculation of the topographic parameters it is thus important to use a DEM and glacier outlines acquired at a similar point in time. *Paul et al.* (2009a) recommend avoiding differences of more than a decade between the acquisition date of the DEM and the glacier outlines. As in most cases the DEM and the glacier outlines will not have an identical date, this has a variety of influences on the topographic parameters: maximum elevation is considered to be stable over time and is thus less affected by differences in the acquisition data. Minimum elevation, on the other hand, is the most rapidly changing parameter; however, if a more recent DEM is combined with older glacier outlines, representing larger glaciers (e.g., DHM25 combined with outlines from the LIA), minimum elevation can be calculated accurately, as the parameter value is measured in the glacier forefield.

Other differences emerge from the algorithms used to calculate the topographic parameters. If for instance mean elevation is calculated by averaging minimum and maximum elevation, as is traditionally done with tabular glacier inventories, large differences can occur relative to the mean elevation value calculated by averaging all the DEM values of a glacier: Lowering of the glacier surface is neglected in the first case but considered in the second approach. Similar effects occur for the calculation of mean slope and aspect.

Glacier inventory for the western Himalayas. In the study on the glacier inventory for the western Himalayas (*Paper II*), a large amount of glacier inventory data was compiled for a region that was so far not covered in the global glacier databases. The analysis of the inventory data demonstrated the possibility to extract complex information from a dataset that goes beyond descriptive statistics. The spatial distribution of mean elevation, for instance, clearly reflected the precipitation gradients across the mountain range (see also *Le Bris et al.* (2011)). Even more complex conclusions could be drawn from the combination of different parameters: by combining mean elevation with surface slope it was found that lower-lying glacier parts have significantly gentler slopes (16.8°) than

glacier parts above mean elevation (25.8°), hence suggesting that a large part of the total glacier volume is located at lower elevations.

Due to the applied mapping procedure, a separation of debris-covered and clean ice is a straightforward process. The separate analysis of these two types of glacier surfaces in combination with other topographic parameters also provides interesting information about the glacier characteristics: debris cover is, as expected, predominantly located at relatively low elevations and on flat glacier parts. The average slope gradient of debris-covered glacier parts is 15.4°, compared to the 22.5° average slope of clean-ice parts. Furthermore is was found that in the elevation band between 3200 m a.s.l. and 4400 m a.s.l. more than 50% of the glacier area is debris-covered, between 3500 m a.s.l. and 4100 m a.s.l. even more than 75%.

Compared to other studies in that region (e.g. *Berthier et al.*, 2007, *Scherler et al.*, 2011), our inventory covers a large region and is complete (in total over 10,000 glaciers covering an area of more than 9,300 km^2 are included in the inventory, i.e., about ten times the glacier area of Switzerland). This allows statements to be made about the entire glaciation of the region, such as number and area distributions per size class or aspect. Furthermore, it also guarantees that every different aspect of the entire region is covered, including all the different local conditions and peculiarities, which is one of the weak points if only a few selected test sites are analyzed.

Change assessments. A separation into individual glaciers is required not only for the calculation of glacier-specific parameters (see above), but also for glacier-specific change assessments. If glacier inventory data from two different points in time are compared, it is essential to assure that identical drainage divides are used in both datasets (*Paul and Andreassen*, 2009). Otherwise, the detected changes in glacier area will be caused by differences in the glacier margins in the accumulation regions (i.e., the drainage divides) rather than real glacier changes.

Nevertheless, even if identical basin separations are used for the two datasets being compared, the definition of a glacier entity has a vital influence on the feasbility and accuracy of the change assessment. For instance, it has to be defined whether or not the steep flanks above the accumulation regions - that are often snow- and ice-covered - are part of the glacier. On the one hand, the bergschrund determines the upper margin of a glacier, as it defines the limits of the moving ice body that compensates ice loss in the ablation region by ice flow from the accumulation region (*Post and Lachapelle*, 2000). On the other hand, according to the GLIMS analysis tutorial (*Raup and Singh Khalsa*, 2010) "bodies of ice above the bergschrund that are connected to the glacier shall be considered part of the glacier, because they contribute snow (through avalanches) and ice (through creep flow) to the glacier". The latter is clearly more suitable for glacier inventories compiled from satellite images, since (a) the bergschrund is normally not

visible in satellite images with a spatial resolution of 15 m to 30 m, and (b) snow and ice (above the bergschrund) are mapped anyway by the automated mapping procedure. This, however, implies that differing snow conditions in high-elevation slopes have a direct and strong influence on the change assessment, and that each individual glacier needs to be visually inspected and, if necessary, corrected before it can be considered for the change assessment.

4.3 Detection and analysis of existing and potential future glacier lakes

Both studies dealing with existing and potential future glacier lakes (*Papers III* and *IV*) focus on the regional scale. They are intended for application in a preliminary phase, i.e., to gain an initial overview of larger regions where only sparse information and data are available. Both studies integrate existing and newly developed methods into a comprehensive tool or strategy, respectively. Specific points of the individual studies are discussed in the related publications (cf. Part II); here, more general aspects of such regional scale approaches are discussed.

Lake detection. The GIS tool for semi-automated lake detection based on multispectral satellite imagery and a DEM as presented in *Paper III* can be applied to an entire satellite scene, i.e., covering several thousand square kilometers. Therefore, the tool addresses the demand for frequent monitoring of the potentially rapidly changing conditions of glacier lakes and related hazard situations (e.g. *Kääb et al.*, 2003a, *Kääb et al.*, 2005a). Despite the fact that lakes or parts of lakes in cast shadow cannot be detected, the tool yields reliable results on a regional-scale level and can be used to guide subsequent and more detailed investigations of individual glacier lakes by focusing on critical situations, as done for instance by *Bajracharya and Mool* (2009) or *Gardelle et al.* (2011). In brief, the approach is a good trade-off between required working effort, quality, and completeness. All the raster calculations required for the image classification are performed in a GIS environment, which is more common than special image processing software. In particular since orthorectified remote sensing data is freely available today, this expands the circle of potential users significantly.

In *Paper IV*, different scale levels are covered by the multi-level strategy for the detection of future lakes. Although the focus is again more on the regional scale (i.e., Levels 1 to 3 of the strategy), the strategy demonstrates how the quick and qualitative approaches, as well as the more detailed methodologies, can be integrated into a consistent framework. A major problem of predictions of future situations is the limited possibility for validation. If historic data is available that can be used as input for the approach, one option is

to apply the methodology to such data and compare the result to the current situation, as done in *Paper IV*. The only fully reliable validation is, perhaps, the comparison of the results to observations in reality. Therefore, it is of vital importance to precisely evaluate the proposed procedure from a conceptual point of view during the development, and to critically assess the results for their plausibility. This may also be a reason for the fact that only very few studies exist that deal with potential future evolutions of glacier lakes and related hazards (e.g. *Reynolds*, 2000, *Quincey et al.*, 2007).

Analysis of glacier lake related hazard potentials. In both studies (*Papers III* and *IV*), mass movements related to glacier lake outburst are assessed by applying the MF and MSF GIS-models from *Huggel et al.* (2003b) (cf. Section 2.5.2). These regional-scale hydrologic flow routing models are suitable to be employed with the available input data. They are appropriate for implementing different estimation values from empirical studies of different processes such as in *Alean* (1985), *Haeberli et al.* (1991), *Walder and Costa* (1996) or *Huggel et al.* (2004a). Compared to more sophisticated and detailed models (cf. Section 2.5.2), they require only a DEM, defined stopping zones for the respective mass movement (i.e., glacier lakes or steep glacier parts), and an abort criterion represented by an average slope value for the maximum expected runout distance. Compared to other models, the volume and therefore the kinetic energy, flow velocity, flow depth, mass entrainment and deposition are not considered. This is appropriate for implementation in a framework where large uncertainties are already associated with the input data. Therefore the results of these models should not be compared to other modeling approaches, but rather seen as a preliminary guide for further, more detailed investigations that focus on single lakes (cf. Section 2.5.1).

Furthermore, the applied models can also detect potential chain reactions for instance of ice avalanches falling into glacier lakes or outburst floods or debris flow from a glacier lake reaching a subjacent lake or river. This is a fundamental aspect of an integrated hazard assessment (*Huggel et al.*, 2004a,c, *Salzmann et al.*, 2004). From a modeling perspective it is nearly impossible to numerically simulate such process interactions with one model, but with the applied flow routing models, such connections can be qualitatively identified. In the context of such highly complex combinations of different processes, it is thus important to anticipate the development not only of the process or object in question (i.e., a glacier lake), but also for all other involved processes, such as glacier fluctuations (geometry changes influencing ice-avalanche dispositions), thermal conditions on the bed of steep hanging glaciers (influencing the stability), permafrost conditions in rock walls, and so on.

Since volume is neglected and the result of the applied flow-routing models is a probability for each DEM cell to be affected by the respective process, the DEM resolution can have unexpected effects on the modeling results: (a) The affected area is determined

only by the topography and the location of the starting situation. As the model considers only the eight directly adjacent cells, small-scale DEM artifacts – as observed for instance in the ASTER GDEM – have a strong impact on the model results. (b) Depending on the topography of the subjacent terrain, even a very small starting zone (i.e., lake or steep glacier part) can affect large areas, depending on the volume released or entrained on the flow-path. On the other hand, if the channel of a river is represented in the DEM, the runout path will be restricted to this channel and not cause inundation of the surrounding terrain as would likely occur in reality. Thus, depending on the local situation, the flow-channel characteristics, and the volume, the modeling results based on a high-resolution DEM may in some cases become less realistic than with a DEM of a more moderate resolution (*Stolz and Huggel*, 2008, *Huggel et al.*, 2008).

Integrating glacier inventories into glacier hazard analyses. Both studies are examples of potential applications of digital glacier inventory data. In the strategy for future glacier lake detection (*Paper IV*), glacier inventories are used explicitly as input data. The semi-automated approach for detecting existing glacier lakes (*Paper III*) basically includes a tool for the compilation of a rough glacier mask, but is only able to map glacier parts with clean ice; debris-covered glacier parts are not identified by the approach. However, in regions where digital glacier inventory information is available, this data can be combined in order to get a more accurate picture of the glacier situation in proximity to the glacier lakes. Besides the numerous applications of glacier inventory data for hydrological purposes on different scales (cf. Section 2.4.2), the approaches presented here focus on glacier hazards. From this point of view, *Papers III* and *IV* can be regarded as applications of glacier inventory data in the context of natural hazards, and therefore link the research of the different papers in this thesis.

5 Conclusions and perspectives

In the first section of this chapter the major findings of the research questions and papers are summarized. Overall conclusions are drawn in Section 5.2; and finally an outlook on potential future research is given in Section 5.3.

5.1 Major findings

Here, the major findings are condensed and organized according to the research question formulated in Section 1.2. More details can be found in the full versions of the research papers in *Part II*.

Paper I: Are the SRTM DEM and the ASTER GDEM suitable for the compilation of topographic glacier parameters?

- Both SRTM and ASTER GDEM are suitable for the compilation of topographic glacier inventory parameters.
- Broader differences occur for some topographic parameters of individual glaciers, but averaged for larger samples, the differences are minor.
- Over glaciers, DEMs compiled using InSAR (SRTM) seem to be superior to photogrammetric DEMs (ASTER GDEM). This is due to the relatively smooth geome-

try of glaciers compared to the surrounding terrain and because of the low optical contrast in accumulation regions.

Paper II: What are the current state and character of glaciers in the western Himalayas?

- More than 10,000 glaciers larger than 0.02 km^2 were mapped in the study region by applying semi-automated mapping techniques to seven Landsat ETM+ scenes. They cover an area of almost 10,000 km^2, which is about five times the present glacier area of the European Alps.
- Mean glacier elevation and the relative amount of debris-covered surface area per glacier have a pronounced gradient from southwest to northeast across the mountain range. Mean elevation increases by about 1500 m (from less than 4300 m a.s.l. to more than 5700 m a.s.l.), whereas the amount of debris cover decreases from 22% to 6%, probably due to the plateau-type glaciers in the north with less debris accumulation from surrounding head walls than the southbound glaciers (cf. *Kääb*, 2005a).
- Ablation areas have significantly gentler slope gradients (16.8°) than accumulation areas (25.8°). As the ice thickness is generally greater where the surface slope is small, this indicates that most of the ice is located at lower elevations.
- The extensive debris cover (about 15% of the entire glacier surface area) posed the main challenge to glacier mapping. Coherence images from SAR image pairs proved to be very helpful to detect the glacier margins under debris cover based on glacier movement.

Paper III: How can glacier lakes automatically be detected in large regions and how can they be analyzed with regard to their hazard potential?

- A GIS tool was developed that allows a semi-automated detection of lakes and clean-ice glacier parts in an entire satellite scene based only on a VIS and NIR band and a DEM.
- It has to be accepted that water surfaces in cast shadow as well as debris-covered glacier parts are not detected by the tools. However, the asset of the limited manual interaction and effort prevails. In combination with an existing glacier inventory, the deficits in the glacier map can be compensated for.

- The applied flow-routing models allow a preliminary assessment over larger regions of ice avalanches (potential lake outburst triggers) and debris flows and flood waves originating from glacier lake outbursts. This is valuable in particular for detecting potential process interactions.

Paper IV: Is it possible to anticipate future glacier lake formation and related hazard potentials based on glacier inventory data and digital terrain information?

- A multi-level strategy to identify sites with potential future lake formation has been developed. It allows large regions to be covered efficiently with a minimum of effort and then to subsequently focus on regions of interest in more detail.
- An application in most regions of the world is possible, since the required input data (glacier outlines and a DEM) are available for many mountain regions (through the GLIMS glacier database and the SRTM and ASTER GDEM).
- The applied flow-routing models proved to be suitable for assessing potential future lake outburst scenarios based on the limited data available.

5.2 Conclusions

A graphical summary of the contents of the thesis is given in Fig. 5.1, where the four different parts, their elements, and their relations to the whole are shown.

From Fig. 5.1 it is obvious that all addressed topics have a relation to the processing and analysis of DEMs, satellite images, and remote sensing-based glacier outlines. Many of the applied methodologies and models were initially developed in other studies, and are now integrated here into a comprehensive and harmonized framework.

The spatial focus of the approaches and studies is generally on a larger regional scale, ranging from a group of glaciers within a catchment to entire mountain ranges such as the Alps or subranges of the Himalayas, spanning several Landsat scenes. Geographically, all mountain ranges of the world are potential areas of application. To allow such investigations on a global scale, consistent input data of sufficient quality are required. Thus such studies only became possible with the release of the SRTM DEM at the beginning of the 21st century. Today, with the availability of free and orthorectified Landsat data from USGS and the ASTER GDEM as an alternative and geographic extension to the SRTM DEM, challenging research questions on a global scale can be approached at a level of detail that was virtually impossible one decade ago.

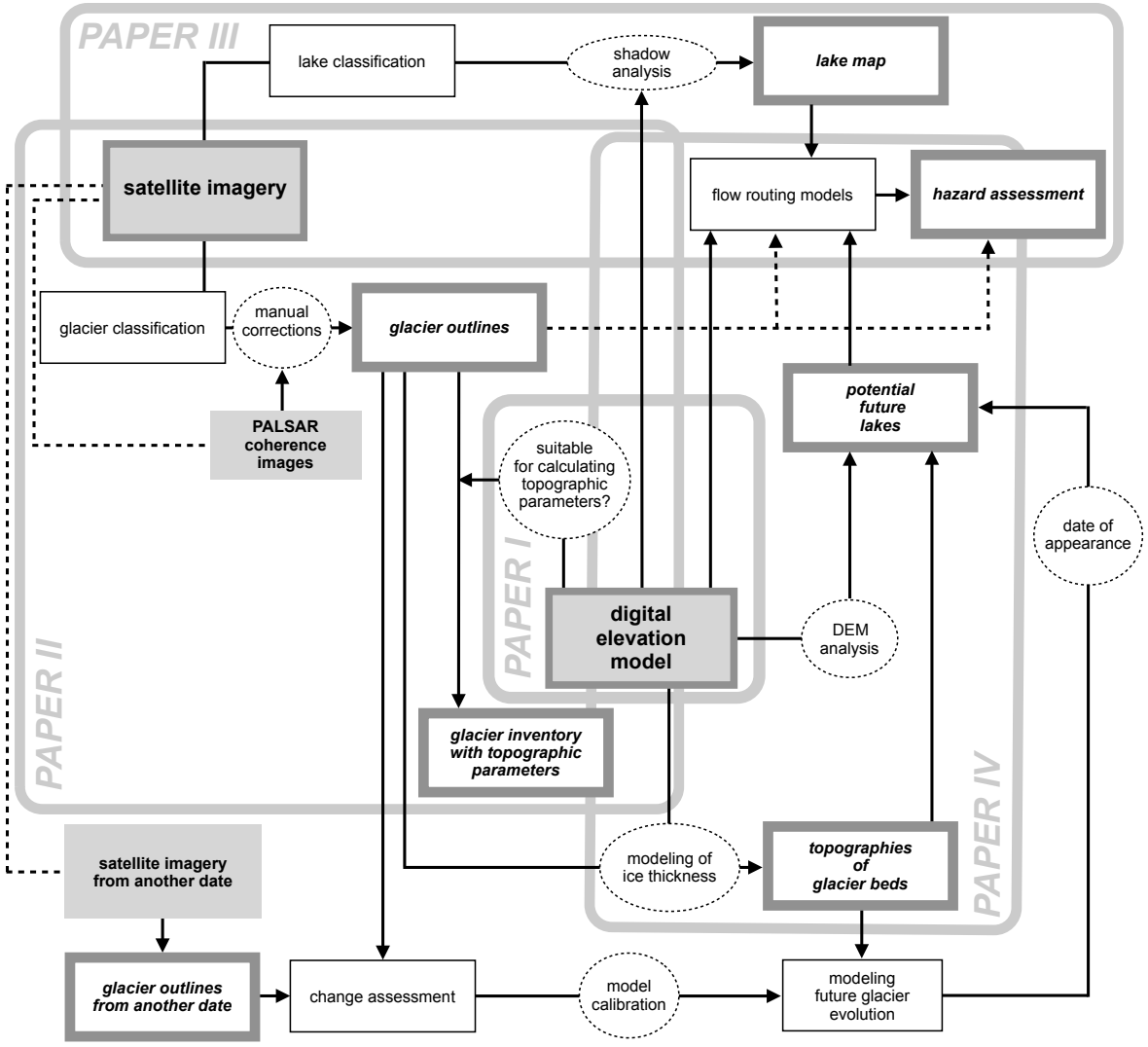

Figure 5.1: *Schematic overview of the elements of this thesis, their connections and structure, as well as the grouping of topics into different research papers.*

Not only DEMs and satellite data, but also glacier outlines in vector format are freely available nowadays. Although a major part of the presented research is dedicated to the compilation of such outlines, they are in turn also used as input data for various other applications, within and beyond the focus of this thesis. To guarantee that related research fields, such as for instance estimations of sea-level rise, runoff, or regional climate modeling, can benefit from this work, it is essential that the glacier data be freely and easily available, for instance through the GLIMS glacier database.

The glacier inventory compiled for the western Himalayas (*Paper II*) closed a prominent gap in the global picture of glaciers and ice caps. Although glacier outlines are still lacking for regions northwest of the study region, this study demonstrated that accurate glacier mapping based on Landsat imagery is possible, even under the challenging conditions of this region. This work, together with the results and success of the entire GlobGlacier project, demonstrated that data and methods available today have the potential to accomplish the difficult task of compiling a consistent and detailed inventory of the Earth's glaciers and ice caps; a goal that has been pursued for more than half a century now (e.g. *Ommanney*, 1986). Although the methodological basics and the data required for the production of such a global glacier dataset have existed for many years (e.g. *Paul and Kääb*, 2005, *Williams and Ferrigno*, 2010), still many urgently needed data are missing in the current glacier databases (e.g. *Cogley*, 2009, *Ohmura*, 2009, *Gardner et al.*, 2011, *Radić and Hock*, 2011). Therefore it is important that (1) funding is provided for application-oriented projects like ESA's Glaciers_cci (the successor of GlobGlacier) or the EU FP7 ice2sea; and (2) that the derived data is freely and easily available to the scientific community for all kinds of further applications. In parallel to the data generation, research aimed at methodological improvements and the development of models to further use and exploit this data is required.

Combinations of the generated data with such modeling approaches can be bidirectional: On the one hand, the generated data can be fed into these models in order to extract new information, for instance a DEM and glacier or lake outlines can be used as input data for flow-routing models for a preliminary hazard assessment. On the other hand, the output of models can also be further used, for instance, the results from a glacier retreat model can be used to determine the date of appearance of expected future lakes. Also combinations of these two cases exist, such as the modeling of the ice thickness distribution: a DEM and glacier outlines are used as input for the model (*Linsbauer et al.*, 2009), and resulting glacier bed topographies in turn can help to identify sites with potential glacier lake formation.

By integrating all aspects included in Fig. 5.1, a comprehensive overview of the current conditions and characteristics as well as potential future evolutions of glaciers and glacier lakes is possible. For instance, the formation of new glacier lakes and their asso-

ciated hazard potentials will pose major challenges to stakeholders in many glacierized mountain regions of the world. The presented approaches provide tools to anticipate potential future situations in advance, to continuously assess and monitor the situations of a larger region and to provide information for a detailed, case-specific hazard assessment.

5.3 Perspectives for future research

Based on the current state of research and the findings of this thesis, research topics that could be addressed in the future are outlined in the following. They are grouped into the fields 'compilation of remotely sensed glacier inventories', 'exploiting the potential of glacier inventory data', 'DEMs', and 'prediction of glacier lake formation'.

Compilation of remotely sensed glacier inventories

A complete and detailed glacier inventory of all glaciers and ice caps in the world would be an invaluable dataset for many further applications. Although this goal has been pursued for about half a century, it still has not been accomplished; it will surely require several more years, even with the contemporary possibilities. Future efforts will focus on further automating the mapping and, hence, being able to process large numbers of satellite scenes on an operational basis. The ultimate goal is a 'push-button methodology', though fully automated glacier mapping is probably not possible. A reason for this is the fact that the thresholds for glacier mapping still need to be defined manually. Even more important, the corrections of debris cover, lakes, and clouds, can probably never be fully automated.

Simpler glacier mapping approaches with less accuracy could be a valuable alternative to high-precision glacier inventories, e.g. for automated change assessments. A rough map of clean-ice glacier parts and snow can in principle be derived be applying a fixed threshold to a TM3 / TM5 ratio or, even simpler, by applying a threshold to TM1. This would be a fully automated approach, and, in combination with freely available and orthorectified satellite imagery, would be a fast method for getting at least a rough estimation of the glacier area in a specific region. Of course, water bodies need to be excluded as well, but this could also be achieved automatically (cf. *Paper III*). Such a dataset would certainly exceed the quality of the DCW (digital chart of the world, cf. Section 2.1.2), which is currently the only dataset that covers more or less all glaciers and ice caps of the world at a scale of about 1:1,000,000.

Upcoming challenges in the near future will be related to the termination of the operational lifetimes of the Landsat and Terra platforms. Today, TM, ETM+, and ASTER, i.e., the most frequently used sensors for glacier mapping, are at the end or (far) beyond their designed lifetime. Although the Landsat data continuity mission from NASA / USGS and the Sentinel 2 mission from ESA will guarantee a continuation of earth observation (EO) data acquisitions, mapping procedures may need some adaptations to this new generation of data.

Exploiting the potential of glacier inventory data

In addition to the outlines, glacier-specific attributes such as topographic parameters are basic components of glacier inventories. In combination with a DEM, most topographic parameters can be derived automatically in a GIS. Glacier length, however, is still missing in many glacier inventories, as it is so far not possible to derive this automatically. A procedure that allows an automated calculation of glacier length could probably also be modified to compile central lines for each glacier branch (branch lines), which are required for current modeling approaches related to the reconstruction of glacier bed topography (e.g. *Linsbauer et al.*, 2009, *Farinotti et al.*, 2009). A promising approach to calculating central flowlines is currently developed by *Le Bris et al.* (in prep.). Besides the determination of glacier lengths, such flowlines would also allow the automated calculation of length changes by an intersection with glacier outlines from two points in time.

Haeberli and Hoelzle (1995) presented a parameterization scheme to characterize glaciers based on tabular glacier inventory information and to simulate climate-change effects. Glacier inventories derived by remote sensing, in combination with DEMs of course have a large potential to feed such parameterization schemes, as shown for instance by *Paul and Svoboda* (2009). The considerations underlying the parameterization scheme assume a dynamic response of the glaciers to a perturbation in the climatic forcing. However, in the past decades glaciers in many regions show a downwasting in place, rather than a dynamic response to climate forcing (e.g. *Paul et al.*, 2004b, *Pelto*, 2006). Potential future research could therefore focus on criteria that make it possible to discriminate whether a glacier is still dynamically coupled to the climate system or downwasting, and possibly revise and adapt the parameterization scheme accordingly (*Pelto*, 2010).

Digital elevation models

As mentioned already in Section 4.1, it would be a great asset for data users if ready-to-use versions of the SRTM and the ASTER GDEM were to be generated and offered at no cost. Although the systematic errors found in these datasets by different studies

probably have negative effects on many applications, data users often are not aware of them. Producers of the ASTER GDEM already indicated the potential of such actions by the statement that "[they] hope the work of the user community can help lead to an improved ASTER GDEM in the future" (*METI/NASA/USGS*, 2009). The widespread use of the void-filled SRTM version offered by CGIAR underlines the need and popularity of such preprocessed and globally consistent datasets. The release of a revised version of the ASTER GDEM, the GDEM2 with improved resolution and fewer artifacts, has recently been announced for the end of August 2011 (*Abrams and Kargel*, pers. comm., cf. `https://nsidc.org/pipermail/glims/2011/000475.html`, accessed July 2011).

DEM differencing, i.e., the subtraction of two DEMs acquired at two different points in time, is an efficient method to assess changes in the Earth's surface. However, comparing two datasets with different spatial resolution or acquired with different techniques always involves noise and uncertainties (e.g. *Nuth and Kääb*, 2011). In particular over glacier areas, the acquisition technique has a large influence on the quality of the dataset due to the low optical contrast of snow or the varying penetration depths of a radar signal. A new edition of an existing DEM dataset, having properties identical to those of its predecessor, would significantly increase the accuracy and quality of the result of such a DEM differencing.

A promising DEM for the future is an InSAR DEM from the TerraSAR-X and the TanDEM-X satellites. The two spacecrafts are run by a public-private partnership between DLR and a German company (Astrium GmbH) and were launched in 2007 (TerraSAR-X) and 2010 (TanDEM-X). Using bistatic InSAR, i.e., one satellite operates as the transmitting and receiving antenna, whereas the other sensor acts as the receive antenna only, a DEM with global coverage will be derived. This dataset will have a spatial resolution of 12 m and a relative height accuracy of 2 m (*Krieger et al.*, 2007). In other words, this means that a global DEM would become available with similar or even better accuracy than the Swiss DHM25 at a doubled spatial resolution. If this quality can be achieved, this dataset will offer unprecedented possibilities for various geoscientific applications.

Most methodologies and approaches presented in this thesis could be used in combination with this new DEM, which would improve the results. Data release is planned for 2014, which would be desirable, since SRTM is already a decade old. In combination with SRTM it will be possible to derive volume changes for virtually all glaciers that have digital outlines (currently about 100,000) over a timespan of more than a decade.

Predictions of glacier lake formation

At the current rate of change, historically unknown situations have to be expected in the future as environmental systems are rapidly changing. Thus, simple but robust

tools and strategies for the anticipation of potential future situations will become increasingly important. The presented multi-level strategy for the detection of sites with future glacier lake formation is a promising advance in this direction, but further developments could also enhance the strategy.

A more in-depth validation of the approach would further improve the performance. Detailed historical maps of Switzerland offer a unique opportunity to perform such validations: As a first step, a systematic survey should be performed, looking for sites where the criteria for lake formation were fulfilled in the past, but lake formation has not acutally taken place. In a second step, glacier lakes, whose formation was not indicated in the past, should be identified. Detailed investigations of such cases would provide insights into the mechanisms and processes of glacier lake formation. Based on such findings the prediction accuracy of the proposed strategy could be improved.

In combination with a glacier retreat model it would be possible to include the temporal dimension, in other words, to predict not only the location, but also the point in time of potential anticipated lake formation. In turn, knowledge about sites where lake formation in the course of glacier retreat is expected could also be included in detailed glacier retreat models. Integrating interactions of lake formation and glacier evolution into such models should include different processes: Increasing ablation due to calving and thermokarst effects, but also changing glacier dynamics caused by the termination into a water body and the expected increase in the surface slope (*Chinn et al.*, 2008).

Such glacier retreat models would also support a more detailed assessment of future hazard situations. Besides focusing on glaciers, estimations about the evolution of other processes should be taken into account, including thermal conditions in rock walls and at the bed of steep hanging glaciers, ice contents of moraines, the presence of loose material, and changes in the stress fields of oversteepened slopes.

Combining knowledge of such processes with information on future glacier extent and lake development would allow a fully integrated assessment of future environmental conditions and their potential impacts to be conducted.

References

Abermann, J., Fischer, A., Lambrecht, A., and Geist, T. (2010). On the potential of very high-resolution repeat DEMs in glacial and periglacial environments. *The Cryosphere*, 4: 53–65.

Alean, J. (1985). Ice avalanches: some empirical information about their formation and reach. *Journal of Glaciology*, 31: 324–333.

Allen, S. K., Schneider, D., and Owens, I. F. (2009). First approaches towards modelling glacial hazards in the Mount Cook region of New Zealand's Southern Alps. *Natural Hazards and Earth System Sciences*, 9: 481–499.

Andreassen, L. M., Paul, F., Kääb, A., and Hausberg, J. E. (2008). Landsat-derived glacier inventory for Jotunheimen, Norway, and deduced glacier changes since the 1930s. *The Cryosphere*, 2 (2): 131–145.

Aniya, M., Sato, H., Naruse, R., Skvarca, P., and Casassa, G. (1996). The use of satellite and airborne imagery to inventory outlet glaciers of the Southern Patagonia Icefield, South America. *Photogrammetric Engineering and Remote Sensing*, 62: 1361–1369.

Atwood, D. K., Meyer, F., and Arendt, A. (2010). Using L-band SAR coherence to delineate glacier extent. *Canadian Journal of Remote Sensing*, 36 (1): 186–195.

Augustinus, P. (1995). Glacial valley cross-profile development: the influence of in situ rock stress and rock mass strength, with examples from the Southern Alps, New Zealand. *Geomorphology*, 14 (2): 87–97.

Bajracharya, S. R. and Mool, P. (2009). Glaciers, glacial lakes and glacial lake outburst floods in the Mount Everest region, Nepal. *Annals of Glaciology*, 50 (53): 81–86.

Baldridge, A. M., Hook, S. J., Grove, C. I., and Rivera, G. (2009). The ASTER spectral library Version 2.0. *Remote Sensing of Environment*, 113: 711–715.

Ballantyne, C. K. (2002). Paraglacial geomorphology. *Quaternary Science Reviews*, 21: 1935–2017.

Baltsavias, E. P., Favey, E., Bauder, A., Bösch, H., and Pateraki, M. (2001). Digital Surface Modelling by Airborne Laser Scanning and Digital Photogrammetry for Glacier

Monitoring. *Photogrammetric Record*, 17 (98): 243–273.

Bartelt, P., Salm, L. B., and Gruberl, U. (1999). Calculating dense-snow avalanche runout using a Voellmyfluid model with active/passive longitudinal straining. *Journal of Glaciology*, 45 (150): 242–254.

Benn, D. I., Wiseman, S., and Warren, C. R. (2000). Rapid growth of a supraglacial lake, Ngozumpa Glacier, Khumbu Himal, Nepal. In: *Debris-Covered Glaciers. Proceedings of a workshop held at Seattle, Washington, U.S.A., September 2000. IAHS publications*, (edited by Nakawo, M., Raymond, C., and Fountain, A.), vol. 264, pp. 177–185.

Berthier, E., Arnaud, Y., Vincent, C., and Remy, F. (2006). Biases of SRTM in high-mountain areas: Implications for the monitoring of glacier volume changes. *Geophysical Research Letters*, 33 (L08502). doi: 10.1029/2006GL025862.

Berthier, E., Arnaud, Y., Kumar, R., and Ahmad, S. (2007). Remote sensing estimates of glacier mass balances in the Himachal Pradesh (Western Himalaya, India). *Remote Sensing of Environment*, 108: 327–338.

Berthier, E., Schiefer, E., Clarke, G. K. C., Menounos, B., and Rémy, F. (2010). Contribution of Alaskan glaciers to sea-level rise derived from satellite imagery. *Nature Geoscience*, 3 (2): 92–95. doi: 10.1038/ngeo737.

Bishop, M., Shroder, J. F., and Hickman, B. L. (1999). SPOT panchromatic imagery and neural networks for information extraction in a complex mountain environment. *Geocarto International*, 14 (2): 19–28.

Bishop, M., Bonk, R., Kamp, U., and Shroder, J. F. (2001). Terrain analysis and data modeling for alpine glacier mapping. *Polar Geography*, 25 (3): 182–201.

Bolch, T. and Kamp, U. (2005). Glacier Mapping in High Mountains using DEMs, Landsat and ASTER Data. In: *Grazer Schriften für Geographie und Raumforschung 41: Proceedings of the 8th International Symposium on High Mountain Remote Sensing Cartography, 20.-27.3.2005 - La Paz, Bolivia*, (edited by Kaufmann, V. and Sulzer, W.).

Bolch, T., Buchroithner, M. F., Kunert, A., and Kamp, U. (2007). Automated delineation of debris-covered glaciers based on ASTER data. In: *GeoInformation in Europe: Proceedings of the 27th EARSeL-Symposium, 4.-7.6.07, Bolzano/Bozen, Italy.*, (edited by Gomarasca, M. A.), pp. 403–410. Millpress, Netherlands.

Bolch, T., Menounos, B., and Wheate, R. (2010). Landsat-based inventory of glaciers in western Canada, 1985-2005. *Remote Sensing of Environment*, 114: 127–137. doi: 10.1016/j.rse.2009.08.015.

Bolch, T., Kulkarni, A., Kääb, A., Huggel, C., Paul, F., Cogley, J. G., Frey, H., Kargel, J. S., Fujita, K., Scheel, M., Stoffel, M., and Bajracharya, S. (subm.). The state and fate of Himalayan glaciers. *Science*.

Burrough, P. A. and McDonnell, R. A. (1998). *Principles of geographical information systems for land resources management*. Oxford University Press, New York, 2nd ed.

Carabajal, C. C. and Harding, D. J. (2006). SRTM C-band and ICESat laser altimetry elevation comparisons as a function of tree cover and relief. *Photogrammetric Engineering and Remote Sensing*, 72 (3): 287–298.

Carabajal, C. C. and Harding, J. D. (2005). ICESat validation of SRTM C-band digital elevation models. *Geophysical Research Letters*, 32 (L22S01). doi: 10.1029/2005GL023957.

Carey, M. (2007). The history of ice: How Glaciers became an endangered species. *Envirnmental History*, 12: 497–527.

Casson, B., Delacourt, C., Baratoux, D., and Allemand, P. (2003). Seventeen years of the "La Clapière" landslide evolution analysed from ortho-rectified aerial photographs. *Engineering Geology*, 68: 123–139.

Chinn, T., Salinger, J., Fitzharris, B., and Willsman, A. (2008). Glaciers and climate. *Bulletin of the Federated Mountain Clubs of NZ*, 171: 1–15.

Christen, M., Bartelt, P., Kowalski, J., and Stoffel, L. (2008). Calculation of dense snow avalanches in three-dimensional terrain with the numerical simulation program RAMMS. *Proceedings of the International Snow Science Workshop, Whistler, BC, Canada*, pp. 709–716.

Clague, J. and Evans, S. (1994). Formation and failure of natural dams in the Canadian Cordillera. *Geological Survey of Canada Bulletin*, 464: 35 pp.

Clague, J. and Evans, S. (2000). A review of catastrophic drainage of moraine-dammed lakes in British Columbia. *Quarternary Science Reviews*, 19: 1763–1783.

Cogley, J. (2009). A more complete version of the World Glacier Inventory. *Annals of Glaciology*, 50 (53): 32–38.

Cogley, J. G. (2003). GGHYDRO - Global Hydrographic Data, Release 2.3.1. *Trent Technical Note 2003-1*.

Copland, L., Sharp, M. J., and Dowdeswell, J. A. (2003). The distribution and flow characteristics of surge-type glaciers in the Canadian High Arctic. *Annals of Glaciology*, 36: 73–81.

Costa, J. and Schuster, R. (1988). The formation and failure of natural dams. *Geological Society of America Bulletin*, 7: 1054–1068.

Crippen, R. E. (1988). The dangers of underestimating the importance of data adjustments in band ratioing. *International Journal of Remote Sensing*, 9 (4): 767–776.

Danko, D. M. (1992). The digital chart of the world project. *Photogrammetric Engineering and Remote Sensing*, 58 (8): 1125–1128.

DLR (2011). Elevation models from SRTM now available for download free of charge. *Press release Deutsches Zentrum für Luft- und Raumfahrt, 25 May 2011*.

Dozier, J. (1989). Spectral signature of alpine snow cover from the landsat thematic mapper. *Remote Sensing of Environment*, 28: 9–22.

Drinkwater, M. R., Long, D. G., and Bingham, A. W. (2001). Greenland snow accumulation estimates from satellite radar scatterometer data. *Journal of Geophysical Research*, 106 (D24): 33935–33950.

Dyurgerov, M. B. and Meier, F. (2000). Twentieth century climate change: Evidence from small glaciers. *Proceedings of the National Academy of Sciences USA (PNAS)*, 97 (4): 1406–1411.

Dyurgerov, M. B. and Meier, M. F. (2005). Glaciers and the changing Earth system: a 2004 snapshot. *Occasional paper 58, Institute of Arctic and Alpine Research, University of Colorado, Boulder, Colorado*.

Egli, M., Wernli, M., Kneisel, C., Biegger, S., and Haeberli, W. (2006). Melting Glaciers and Soil Development in the Proglacial Area Morteratsch (Swiss Alps): II. Modeling the Present and Future Soil State. *Arctic, Antarctic, and Alpine Research*, 38 (4): 510–521.

Eineder, M. and Holzner, J. (2001). Interferometric DEMs in rugged terrain. *Proceedings IGARSS 2001*, 5: 2040–2042.

Evans, S. and Clague, J. (1994). Recent climatic change and catastrophic geomorphic processes in moutnain environments. *Geomorphology*, 10: 107–128.

Faillettaz, J., Pralong, A., Funk, M., and Deichmann, N. (2008). Evidence of log-periodic oscillations and increasing icequake activity during the breaking-off of large ice masses. *Journal of Glaciology*, 54 (187): 725–737.

Farinotti, D., Huss, M., Bauder, A., Funk, M., and Truffer, M. (2009). A method to estimate the ice volume and ice-thickness distribution of alpine glaciers. *Journal of Glaciology*, 55 (191): 422–430.

Farr, T. G., Rosen, P. A., Caro, E., Crippen, R., Duren, R., Hensley, S., Kobrick, M., Paller, M., Rodriguez, E., Roth, L., Seal, D., Shaffer, S., Shimada, J., Umland, J., Werner, M., Oskin, M., Burbank, D., and Alsdorf, D. (2007). The Shuttle Radar Topography Mission. *Reviews in Geophysics*, 45 (2): 1–33. doi: 10.1029/2005RG000183.

Fischer, L., Amann, F., Moore, J. R., and Huggel, C. (2010). Assessment of periglacial slope stability for the 1988 Tschierva rock avalanche (Piz Morteratsch, Switzerland). *Engineering Geology*, 116 (1–2): 32–43. doi: 10.1016/j.enggeo.2010.07.005.

Fischer, L., Eisenbeiss, H., Kääb, A., Huggel, C., and Haeberli, W. (2011). Monitoring topographic changes in a periglacial high-mountain face using high-resolution DTMs, Monte Rosa East Face, Italian Alps. *Permafrost and Periglacial Processes*.

Forel, F. A. (1895). *Les variations périodique des glaciers. Discourse préliminaire*. Extrait des Archives des Sciences physiques et naturelles, XXXIV.

Fowler, A. C., Murray, T., and Ng, F. S. L. (2001). Thermally controlled glacier surging. *Journal of Glaciology*, 47 (159): 527–538.

Fraser, R. N. (1998). Multispectral remote sensing of turbidity among Nebraska Sand Hills lakes. *International Journal of Remote Sensing*, 19 (15): 3011–3016.

Frey, H. (2007). Identifikation und Analyse von Gletscherseen mit Fernerkundung und GIS. Master's thesis, Department of Geography, University of Zurich.

Frey, H. and Paul, F. (in press). On the suitability of the SRTM DEM and ASTER GDEM for the compilation of topographic parameters in glacier inventories. *International Journal of Applied Earth Observation and Geoinformation*. doi: 10.1016/j.jag.2011.09.020.

Frey, H., Haeberli, W., Linsbauer, A., Huggel, C., and Paul, F. (2010a). A multi-level strategy for anticipating future glacier lake formation and associated hazard potentials. *Natural Hazards and Earth System Sciences*, 10: 339–352.

Frey, H., Huggel, C., Paul, F., and Haeberli, W. (2010b). Automated detection of glacier lakes based on remote sensing in view of assessing associated hazard potentials. In: *Grazer Schriften der Geographie und Raumfoschung 45: Proceedings of the 10th Internatinal Symposium on High Mountain Remote Sensing Cartography, 8.-11.9.2008, Kathmandu, Nepal.*, (edited by Kaufmann, V. and Sulzer, W.), pp. 261–272.

Frey, H., Paul, F., and Strozzi, T. (in rev.). Compilation of a glacier inventory for the western Himalayas from satellite data: Methods, challenges and results. *Remote Sensing of Environment*.

Fujisada, H., Bailey, G. B., Kelly, G. G., Hara, S., and Abrams, M. J. (2005). ASTER DEM performance. *IEEE Transactions on Geoscience and Remote Sensing*, 43 (12): 2707–2714.

Fujita, K., Suzuki, R., Nuimura, T., and Sakai, A. (2008). Performance of ASTER and STRM DEMs, and their potential for assessing glacier lakes in the Lunana region, Buthan Himalaya. *Journal of Glaciology*, 54 (185): 220–228.

Gao, J. and Liu, Y. (2001). Applications of remote sensing, GIS and GPS in glaciology: a review. *Progress in Physical Geography*, 25 (4): 520–540.

Gardelle, J., Arnaud, Y., and Berthier, E. (2011). Contrasted evolution of glacial lakes along the Hindu Kush Himalaya mountain range between 1990 and 2009. *Global and Planetary Change*, 75 (1-2): 47–55. doi: 10.1016/j.gloplacha.2010.10.003.

Gardner, A. S., Moholdt, G., Wouters, B., Wolken, G. J., Burgess, D. O., Sharp, M. J., Cogley, J. G., Braun, C., and Labine, C. (2011). Sharply increased mass loss from glaciers and ice caps in the Canadian Arctic Archipelago. *Nature*, 473: 357–360. doi: 10.1038/nature10089.

GCOS (1997). GHOST - Global Hierarchical Observing Strategy. *GCOS-33*, WMO/TD-No. 798: 12pp.

GCOS (2003). The second report on the adequacy of the global observing systems for climate in support of the UNFCCC. *Reports GCOS - 82 (WMO/TD No. 1143)*, p. 85pp.

Geist, T., Lutz, E., and Stötter, J. (2003). Airborne laser scanning technology and its potential for applications in glaciology. In: *Proceedings of the ISPRS working group III/3 workshop '3-D reconstruction from airborne laserscanner and InSAR data' Dresden, Germany, 8-10 October 2003*, (edited by Maas, H.-G., Vosselman, G., and Streilein, A.), vol. XXXIV, Part 3/W13 , pp. 101–106.

Gesch, D., Oimonen, M., Grennlee, S., Nelson, C., Steuck, M., and Tyler, D. (2002). The National Elevation Dataset. *Photogrammetric Engineering and Remote Sensing*, 68 (1): 5–11.

Goward, S. N., Tucker, C. J., and Dye, D. G. (1985). North American vegetation patterns observed with the NOAA-7 advanced very high resolution radiometer. *Vegetatio*, 64 (1): 3–14. doi: 10.1007/BF00033449.

Gruber, S., Huggel, C., and Pike, R. (2008). Modelling mass movements and landslide susceptibility. In: *Geomorphometry - Concepts, Software, Applications*, (edited by Hengl, T. and Reuter, H. I.), vol. 33 of *Developments in Soil Science*, pp. 527–550. Elsevier, B.V.

Haeberli, W. (1998). Historical evolution and operational aspects of worldwide glacier monitoring. In: *Into the second century of worldwide glacier monitoring: prospects and strategies*, (edited by Haeberli, W., Hoelzle, M., and Suter, S.). UNESCO Studies and Reports in Hydrology, Vol. 56.

Haeberli, W. (2005). Changing views on changing glaciers. In: *The Darkening Peaks: Glacial Retreat in Scientific and Social Context*, (edited by B. Orlove, E. W. and Luckman, B.). Berkeley: University of California Press.

Haeberli, W. (2006). Integrated perception of glacier changes: a challenge of historical dimensions. In: *Glacier Science and Environmental Change*, (edited by Knight, P. G.), pp. 423–430. Blackwell Publishing.

Haeberli, W. and Beniston, M. (1998). Climate change and its impacts on glaciers and permafrost in the Alps. *Ambio*, 27 (4): 258–265.

Haeberli, W. and Hoelzle, M. (1995). Application of inventory data for estimating characteristics of and regional climate-change effects on mountain glaciers: a pilot study with the European Alps. *Annals of Glaciology*, 21: 206–212.

Haeberli, W. and Hohmann, R. (2008). Climate, Glaciers and Permafrost in the Swiss Alps 2050: Scenarios, Consequences and Recommendation. In: *Proceedings of the Ninth International Conference on Permafrost 2008, Fairbanks, Alaska, USA*, (edited by Kane,

D. L. and Hinkel, K. M.), vol. 1, pp. 607–612.

Haeberli, W., Rickenmann, D., Zimmermann, M., and Rösli, U. (1991). Murgänge. In: *Ursachenanalyse der Hochwasser 1987, Ergebnisse der Untersuchungen. Mitteilungen des Bundesamtes für Wasserwirtschaft*, vol. 4, pp. 77–88.

Haeberli, W., Frauenfelder, R., Hoelzle, M., and Maisch, M. (1999). On rates and acceleration trends of global glacier mass changes. *Geografiska Annaler*, 81A (4): 585–591.

Haeberli, W., Cihlar, J., and Barry, R. G. (2000). Glacier monitoring within the Global Climate Observing System. *Annals of Glaciology*, 31: 241–246.

Haeberli, W., Kääb, A., Paul, F., Chiarle, M., Mortara, G., Mazza, A., and Richardson, S. (2002). A surge-type movement at Ghiacciaio del Belvedere and a developing slope instability in the east face of Monte Rosa, Macunaga, Italian Alps. *Norsk Geografisk Tidskrift - Norwegian Journal of Geography*, 56 (2): 104–111.

Haeberli, W., Huggel, C., Kääb, A., Zgraggen-Oswald, S., Polkvoi, A., Galushkin, I., Zotikov, I., and Osokin, N. (2004). The Kolka-Karmadon rock/ice slide of 20 September 2002: an extraordinary event of historical dimensions in North Ossetia, Russian Caucasus. *Journal of Glaciology*, 50 (171): 533–546.

Haeberli, W., Hoelzle, M., Paul, F., and Zemp, M. (2007). Integrated monitoring of mountain glaciers as key indicators of global climate change: the European Alps. *Annals of Glaciology*, 46: 150–160.

Hall, D., Ormsby, J., Bindschadler, R., and Siddalingaiah, H. (1987). Characterization of snow and ice zones on glaciers using landsat thematic mapper data. *Annals of Glaciology*, 9: 104–108.

Hall, D. K., Riggs, G. A., and Salomonson, V. V. (1995). Development of methods for mapping global snow cover using moderate resolution imaging spectroradiometer data. *Remote Sensing of Environment*, 54 (2): 127–140.

Hardy, C. C. and Burgan, R. E. (1999). Evaluation of NDVI for monitoring moisture in three vegetation types of the western U.S. *Photogrammetric Engineering and Remote Sensing*, 65: 603–610.

Hayakawa, Y. S., Oguchi, T., and Lin, Z. (2008). Comparison of new and existing global digital elevation models: ASTER G-DEM and SRTM-3. *Geophysical Research Letters*, 35 (L17404). doi: 10.1029/2008GL035036.

Hoelzle, M., Haeberli, W., Dischl, M., and Peschke, W. (2003). Secular glacier mass balances derived from cumulative glacier length changes. *Global and Planetary Change*, 36: 295–306.

Hoelzle, M., Chinn, T., Stumm, D., Paul, F., Zemp, M., and Haeberli, W. (2007). The application of glacier inventory data for estimating past climate change effects on

mountain glaciers: A comparison between the European Alps and the Southern Alps of New Zealand. *Global and Planetary Change*, 56: 69–82.

Hubbard, B., Heald, A., Reynolds, J., Quincey, D., Richardson, S., Luyo, M., Portilla, N., and Hambrey, M. (2005). Impact of a rock avalanche on a moraine-dammed proglacial lake: Laguna Safuna Alta, Cordillera Blanca, Peru. *Earth Surface Processes and Landforms*, 30 (10): 1251–1264.

Huggel, C. (2004). Assessment of Glacial Hazards based on Remote Sensing and GIS Modeling. Ph.D. thesis, University of Zurich.

Huggel, C., Kääb, A., Haeberli, W., Teysseire, P., and Paul, F. (2002). Remote sensing based assessment of hazards from glacier lake outbursts: a case study in the Swiss Alps. *Canadian Geotechnical Journal*, 39: 316 – 330.

Huggel, C., Haeberli, W., Kääb, A., Hoelzle, M., Ayros, E., and Portocarrero, C. (2003a). Assessment of glacier hazards and glacier runoff for different climate scenarios based on remote sensing data: a case study for a hydropower plant in the Peruvian Andes. *EARSeL Workshop, Observing our cryosphere from space, Bern, 11.3.-13.3.2002*, pp. 22–33.

Huggel, C., Kääb, A., Haeberli, W., and Krummenacher, B. (2003b). Regional-scale GIS-models for assessment of hazards from glacier lake outbursts: evaluation and application in the Swiss Alps. *Natural Hazards and Earth System Sciences*, 3: 647–662.

Huggel, C., Haeberli, W., Kääb, A., Bieri, D., and Richardson, F. (2004a). An assessment procedure for glacial hazards in the Swiss Alps. *Canadian Geotech Journal*, 41: 1068–1083.

Huggel, C., Kääb, A., Reynolds, J., and Heald, A. (2004b). Impact-oriented models for potential lake outbursts and ASTER-based application in the Peruvian Andes. *Proceedings Fachtagung Schweizerische Geomorphologische Gesellschaft, March 28-29, 2003, Erstfeld*, pp. 129–143.

Huggel, C., Kääb, A., and Salzmann, N. (2004c). GIS-Based modelling of glacial hazards and their interactions using Landsat-TM and IKONOS imagery. *Norsk Geografisk Tidskrift - Norwegian Journal of Geography*, 58 (2): 61 – 73.

Huggel, C., Zgraggen-Oswald, S., Haeberli, W., Kääb, A., Polkvoj, A., Galushkin, I., and Evans, S. (2005). The 2002 rock/ice avalanche at Kolka/Karmadon, Russian Caucasus: assessment of extraordinary avalanche formation and mobility, and application of QuickBird satellite imagery. *Natural Hazards and Earth System Sciences*, 5: 173–187.

Huggel, C., Schneider, D., Miranda, P. J., Delgado Granados, H., and Kääb, A. (2008). Evaluation of ASTER and SRTM DEM data for lahar modeling: A case study on lahars from Popocatépetl Volcano, Mexico. *Journal of Volcanology and Geothermal Research*, 170: 99–110. doi: 10.1016/j.jvolgeores.2007.09.005.

Huss, M., Farinotti, D., Bauder, A., and Funk, M. (2008). Modelling runoff from highly glacierized alpine drainage basins in a changing climate. *Hydrological Processes*.

Huss, M., Bauder, A., and Funk, M. (2009). Homogenization of long-term mass-balance time series. *Annals of Glaciology*, 50: 198–206.

Huss, M., Usselmann, S., Farinotti, D., and A.Bauder (2010). Glacier mass balance in the south-eastern Swiss Alps since 1900 and perspectives for the future. *Erdkunde*, 64 (2): 119–140. doi: 10.3112/erdkunde.2010.02.02.

IPCC (2007). *Contribution of Working Group I to the Fourth Assessment Report of the Intergovernmental Panel on Climate Change, 2007*. Cambridge University Press, Cambridge, United Kingdom and New York, NY, USA.

Jacobs, J. D., Simms, E. L., and Simms, A. (1997). Recession of the southern part of Barnes Ice Cap, Baffin Island, Canada, between 1961 and 1993, determined from digital mapping of Landsat TM. *Journal of Glaciology*, 43: 98–102.

Jiskoot, H., Curran, C. J., Tessler, D. L., and Shenton, L. R. (2009). Changes in Clemenceau Icefield and Chaba Group glaciers, Canada, related to hypsometry, tributary detachment, length–slope and area–aspect relations. *Annals of Glaciology*, 50 (53): 133–143.

Jouvet, G., Huss, M., Blatter, H., Picasso, M., and Rappaz, J. (2009). Numerical simulation of Rhonegletscher from 1874 to 2100. *Journal of Computational Physics*, 228 (17): 6426–6439. doi: 10.1016/j.jcp.2009.05.033.

Kääb, A. (2002). Monitoring high-mountain terrain deformation from repeated air- and spaceborne optical data: examples using digital aerial imagery and ASTER data. *ISPRS Journal for Photogrammetry and Remote Sensing*, 57 (1-2): 39–52.

Kääb, A. (2005a). Combination of SRTM3 and repeat ASTER data for deriving alpine glacier flow velocities in the Bhutan Himalaya. *Remote Sensing of Environment*, 94 (4): 463–474. doi: 10.1016/j.rse.2004.11.003.

Kääb, A. (2005b). Remote Sensing of Mountain Glaciers and Permafrost Creep, Habilitation thesis, University of Zurich.

Kääb, A., Paul, F., Maisch, M., Hoelzle, M., and Haeberli, W. (2002). The new remote-sensing-derived Swiss glacier inventory: II. First Results. *Annals of Glaciology*, 34: 362–366.

Kääb, A., Huggel, C., Paul, F., Wessels, R., Raup, B., Keiffer, H., and Kargel, J. S. (2003a). Glacier monitoring from ASTER imagery: Accuracy and applications. *EARSeL eProceedings*, 2 (1): 43–53.

Kääb, A., Wessels, R., Haeberli, W., Huggel, C., Kargel, J., and Khalsa, S. (2003b). Rapid aster imaging facilitates timely assessment of glacier hazards and disasters. *EOS,*

Transactions, American Geophysical Union, 84 (13): 117 –124.

Kääb, A., Huggel, C., Barbero, S., Chiarle, M., Cordola, M., Epifani, F., Haeberli, W., Mortara, G., Semino, P., Tamburini, A., and Viazzo, G. (2004). Glacier hazards at Belvedere Glacier and the Monte Rosa east face, Italian Alps: Processes and Mitigation. In: *Proceeding of the International Symposium Interpraevent 2004 – Riva/Trient*, pp. 67–78.

Kääb, A., Huggel, C., Fischer, L., Guex, S., Paul, F., Roer, I., Salzmann, N., Schmutz, K., Schneider, D., Strozzi, T., and Weidman, Y. (2005a). Remote sensing of glacier- and permafrost-related hazards in high mountains: an overview. *Natural Hazards and Earth System Sciences*, 5: 527–554.

Kääb, A., Huggel, C., Guex, S., Paul, F., Salzmann, N., Schmutz, K., Schneider, D., and Weidman, Y. (2005b). Glacier hazard assessment in mountains using satellite optical data. *EARSeL eProceedings*, 4 (1): 79–93.

Kamb, B., Engelhardt, H., Fahnestock, M., Humphrey, N., MEIER, M., and Stone, D. (1994). Mechanical and hydrologic basis for the rapid motion of a large tidewater glacier - 2. Interpretation. *Journal of Geophysical Research*, 99 (B8): 15231–15244.

Kargel, J. S., Abrams, M. J., Bishop, M. P., Bush, A., Hamilton, G., Kääb, A., Kieffer, H. H., Lee, E. M., Paul, F., Rau, F., Raup, B., Shroder, J. F., Soltesz, D., Stearns, L., Wessels, R., and the wGLIMS Consortium (2005). Multispectral imaging contributions to Global Land Ice Measurements from Space. *Remote Sensing of Environment*, 99 (1/2): 187–219.

Kaser, G., Cogley, J. G., Dyurgerov, M. B., Meier, M. F., and Ohmura, A. (2006). Mass balance of glaciers and ice caps: Consensus estimates for 1961–2004. *Geophysical Research Letters*, 33 (L19501). doi: 10.1029/2006GL027511.

Kaser, G., Grosshauser, M., and Marzeion, B. (2010). Contribution potential of glaciers to water availability in different climate regimes. *Proceedings of the National Academy of Sciences USA (PNAS)*, pp. 1–5. doi: 10.1073/pnas.1008162107.

Kershaw, J., Clague, J., and Evans, S. (2005). Geomorphic and sedimentological signature of a two-phase outburst flood from moraine-dammed Queen Bess Lake, British Columbia, Canada. *Earth Surface Processes and Landforms*, 30 (1): 1–25.

Khalsa, S. J. S., Dyurgerov, M. B., Khromova, T., Raup, B. H., and Barry, R. G. (2004). Space-based mapping of glacier changes using ASTER and GIS tools. *IEEE Transactions on Geoscience and Remote Sensing*, 42 (10): 2177–2183.

Koblet, T., Gärtner-Roer, I., Zemp, M., Jansson, P., Thee, P., Haeberli, W., and Holmlund, P. (2010). Reanalysis of multi-temporal aerial images of Storglaciären, Sweden (1959–99) –w Part 1: Determination of length, area, and volume changes. *The Cryosphere*, 4: 333–343. doi: 10.5194/tc-4-333-2010.

Koboltschnig, G. R., Schöner, W., Zappa, M., Kroisleitner, C., and Holzmann, H. (2008). Runoff modelling of the glacierized alpine upper salzach basin (austria): multi-criteria result validation. *Hydrological Processes*, 22: 3950–3964. doi: 10.1002/hyp.7112.

Komori, J. (2008). Recent expansions of glacial lakes in the Bhutan Himalayas. *Quaternary International*, 184: 177–186.

Korona, J., Berthier, E., Bernard, M., and Thouvenot, E. (2009). SPIRIT. SPOT 5 stereoscopic survey of polar ice: Reference images and topographies during the fourth international polar year (2007-2009). *ISPRS Journal for Photogrammetry and Remote Sensing*, 64: 204–212.

Korup, O. and Tweed, F. (2007). Ice, moraine, and landslide dams in mountainous terrain. *Quaternary Science Reviews*, 26 (25-28): 3406–3422.

Kotlarski, S., Jacob, D., Pozum, R., and Paul, F. (2010). Representing glaciers in a regional climate model. *Climate Dynamics*, 34 (1): 27–46. doi: 10.1007/s00382-009-0685-6.

Krieger, G., Moreira, A., Fiedler, H., Hajnsek, I., Werner, M., Younis, M., and Zink, M. (2007). TanDEM-X: A Satellite Formation for High-Resolution SAR Interferometry. *IEEE Transactions on Geoscience and Remote Sensing*, 45 (11): 3317–3341. doi: 10.1109/TGRS.2007.900693.

Larsen, C. F., Motyka, R. J., Arendt, A. A., Echelmeyer, K. A., and Geissler, P. E. (2007). Glacier changes in southeast Alaska and northwest British Columbia and contribution to sea level rise. *Journal of Geophysical Research*, 112. doi: 10.1029/2006JF000586.

Le Bris, R., Paul, F., Frey, H., and Bolch, T. (2011). A new satellite-derived glacier inventory for Western Alaska. *Annals of Glaciology*, 52 (59): 135–143.

Le Bris, R., Paul, F., and Frey, H. (in prep.). A semi-automatic method to create central glacier flow lines: A pilot study with Alaskan glaciers. *Computers & Geosciences*.

Le Meur, E., Gerbaux, M., Schäfer, M., and Vincent, C. (2007). Disappearance of an Alpine glacier over the 21st Century simulated from modeling its future surface mass balance. *Earth and Planetary Science Letters*, 261: 367 –374.

Lillesand, T. M., Kiefer, R. W., and Chipman, J. W. (2008). *Remote sensing and image interpretation*. John Wiley & Sons, New York, 6th ed.

Linsbauer, A., Paul, F., Hoelzle, M., Frey, H., and Haeberli, W. (2009). The Swiss Alps without glaciers – A GIS-based modelling approach for reconstruction of glacier beds. In: *Geomorphometry 2009 Conference Proceedings*, (edited by Purves, R., Gruber, S., Straumann, R., and Hengl, T.), pp. 243–247. University of Zurich, Zurich.

Linsbauer, A., Paul, F., and Haeberli, W. (subm.). Modeling the ice thickness distribution of large glacier samples: Application of a fast and robust approach to all Swiss glaciers. *Journal of Geophysical Research*.

Longley, P. A., Goodchild, M. F., Maguire, D. J., and Rhind, D. W. (2011). *Geographic information systems and science*. Wiley, New York, 3rd ed.

Lusch, D. P. (1999). *Introduction to Environmental Remote Sensing*. Center for Remote Sensing and GIS, Michigan State University.

Matsuoka, N. and Masahiro, A. (2002). Rock slope failures associated with deglaciation: some exam- ples from glaciated valleys in the Swiss Alps. *Annual Report of the Institute of Geoscience, University of Tsukuba*, 28: 11–16.

Matthews, J. and Shakesby, R. (2004). A twentieth-century neoparaglacial rock topple on a glacier foreland, Ötztal Alps, Austria. *The Holocene*.

Meier, M. F., Dyurgerov, M. B., Rick, U. K., O'Neel, S., Pfeffer, W. T., Anderson, R. S., Anderson, S. P., and Glazovsky, A. F. (2007). Glaciers dominate eustatic sea-level rise in the 21st century. *Science*, 317: 1064–1067.

METI (2009). Distribution of ASTER Global Digital Elevation Model (ASTER G-DEM). *Press release by Ministry of Economy, Trade, and Industry (METI), 29 June 2009*.

METI/NASA/USGS (2009). ASTER GDEM Validation Summary Report. Tech. rep., ASTER GDEM Validation Team: METI/ERSDAC, NASA/LPDAAC, USGS/EROS. In cooperation with NGA and other Collaborators.

Möller, M. and Schneider, C. (2010). Volume change at Gran Campo Nevado, Patagonia, 1984–2000: a reassessment based on new findings. *Journal of Glaciology*, 56 (196): 363–364.

Möller, M., Schneider, C., and Kilian, R. (2007). Glacier change and climate forcing in recent decades at Gran Campo Nevado, southernmost Patagonia. *Annals of Glaciology*, 46: 136–144.

Noetzli, J., Huggel, C., Hoelzle, M., and Haeberli, W. (2006). GIS-based modelling of rock-ice avalanches from Alpine permafrost areas. *Computers & Geosciences*, 10: 161–178.

Nuth, C. and Kääb, A. (2011). Co-registration and bias corrections of satellite elevation data sets for quantifying glacier thickness change. *The Cryosphere*, 5: 271–290.

O'Callaghan, J. F. and Mark, D. M. (1984). The extraction of drainage networks from digital elevation data. *Computer Vision Graphics and Image Proceedings*, 28: 323–344.

Oerlemans, J. (1994). Quantifying Global Warming from the Retreat of Glaciers. *Science*, 264: 243–245.

Oerlemans, J. (2005). Extracting a climate signal from 169 glacier records. *Science*, 308 (675).

Oerlemans, J., Dyurgerov, M. B., and Van De Wal, R. S. W. (2007). Reconstructing the glacier contribution to sea-level rise back to 1850. *The Cryosphere*, 1: 59–65.

Oerlemans, J., Geisen, H. J., and Van den Broeke, M. R. (2009). Retreating alpine glaciers: increased melt rates due to accumulation of dust (Vadret da Morteratsch, Switzerland). *Journal of Glaciology*, 55 (192): 729–736.

Ohmura, A. (2009). Completing the World Glacier Inventory. *Annals of Glaciology*, 50 (53): 144–148.

Ommanney, C. S. L. (1986). Mapping Canada's glaciers since 1965. *Annals of Glaciology*, 8: 132–134.

Oppikofer, T., Jaboyedoff, M., and Keusen, H.-R. (2008). Collapse at the eastern Eiger flank in the Swiss Alps. *Nature Geoscience*, 1 (8): 531–535.

Østrem, G. and Brugman, M. (1991). Glacier mass-balance measurements. A manual for field and office work [Rev. ed.]. *NHRI Science Report, No. 4*.

Paul, F. (2007). The New Swiss Glacier Inventory 2000 - Application of Remote Sensing and GIS. Ph.D. thesis, Univerisity of Zurich.

Paul, F. (2008). Calculation of glacier elevation changes with SRTM: is there an elevation-dependent bias? *Journal of Glaciology*, 54: 945–946.

Paul, F. (2011). Sea-level rise: Melting glaciers and ice caps. *Nature Geoscience*.

Paul, F. and Andreassen, L. (2009). A new glacier inventory for the Svartisen region, Norway, from Landsat ETM+ data: challenges and change assessment. *Journal of Glaciology*, 55 (192): 607–618.

Paul, F. and Haeberli, W. (2008). Spatial variability of glacier elevation changes in the Swiss Alps obtained from two digital elevation models. *Geophysical Research Letters*, L21502 (21). doi: 10.1029/2008GL034718.

Paul, F. and Hendriks, J. (2010). Optical remote sensing of glaciers. In: *Remote Sensing of Glaciers - Techniques for Topographic, Spatial and Thematic Mapping of Glaciers*, (edited by Pellikka, P. and Rees, W. G.), pp. 137–152. CRC Press, Taylor and Francis Group, Leiden.

Paul, F. and Kääb, A. (2005). Perspectives on the production of a glacier inventory from multispectral satellite data in Arctic Canada: Cumberland Peninsula, Baffin Island. *Annals of Glaciology*, 42: 59–66.

Paul, F. and Kotlarski, S. (2010). Forcing a distributed glacier mass balance model with the regional climate model REMO. part ii: Downscaling strategy and results for two Swiss glaciers. *J Climate*, 23 (6): 1607–1620. doi: 10.1175/2009JCLI3345.1.

Paul, F. and Svoboda, F. (2009). A new glacier inventory on southern Baffin Island, Canada, from ASTER data: II. Data analysis, glacier change and applications. *Annals of Glaciology*, 50 (53): 22–31.

Paul, F., Kääb, A., Maisch, M., Kellenberger, T., and Haeberli, W. (2002). The new remote-sensing-derived swiss glacier inventory: I. methods. *Annals of Glaciology*, 34: 355 – 361.

Paul, F., Huggel, C., and Kääb, A. (2004a). Combining satellite multispectral image data and a digital elevation model for mapping of debris-covered glaciers. *Remote Sensing of Environment*, 89 (4): 510 – 518.

Paul, F., Kääb, A., Maisch, M., Kellenberger, T. W., and Haeberli, W. (2004b). Rapid disintegration of Alpine glaciers observed with satellite data. *Geophysical Research Letters*, 31 (L21402). doi: 10.1029/2004GL020816.

Paul, F., Kääb, A., and Haeberli, W. (2007). Recent glacier changes in the Alps observed by satellite: Consequences for future monitoring strategies. *Global and Planetray Change*, 55 (4): 111–122.

Paul, F., Barry, R. G., Cogley, J. G., Frey, H., Haeberli, W., Ohmura, A., Ommanney, C. S. L., Raup, B., Rivera, A., and Zemp, M. (2009a). Recommendations for the compilation of glacier inventory data from digital sources. *Annals of Glaciology*, 50 (53): 119–126.

Paul, F., Kääb, A., Rott, H., Shepherd, A., Strozzi, T., and Volden, E. (2009b). Globglacier: A new esa project to map the world's glaciers and ice caps from space. *EARSeL eProceedings*, 8 (1): 11–25.

Paul, F., Frey, H., and Le Bris, R. (2011). A new glacier inventory for the European Alps from Landsat TM scenes of 2003: Challenges and analysis. *Geophysical Research Abstracts*, 13.

Paul, F., Frey, H., and Le Bris, R. (in press). A new glacier inventory for the European Alps from Landsat TM scenes of 2003: Challenges and results. *Annals of Glaciology*.

Pelto, M. S. (2006). The current disequilibrium of North Cascade glaciers. *Hydrological Processes*, 20: 769–779. doi: 10.1002/hyp.6132.

Pelto, M. S. (2010). Forecasting temperate alpine glacier survival from accumulation zone observations. *The Cryosphere*, 4: 67–75.

Pietroniro, A. and Leconte, R. (2000). A review of Canadian remote sensing applications in hydrology, 1995–1999 - Pietroniro - 2000 - Hydrological Processes - Wiley Online Library. *Hydrological Processes*, 14: 1641–1666.

Post, A. and Lachapelle, E. R. (2000). *Glacier ice*. University of Washington Press, revised ed.

Pralong, A. and Funk, M. (2006). On the instability of avalanching glaciers. *Journal of Glaciology*, 52 (176): 31–48.

Quincey, D., Richardson, S., Luckman, A., Lucas, R., Reynolds, J., Hambrey, M., and Glasser, N. (2007). Early recognition of glacial lake hazards in the Himalaya using remote sensing datasets. *Global and Planetary Change*, 56: 137–152.

Rabus, B., Eineder, M., Roth, A., and Bamler, R. (2003). The shuttle radar topography mission - a new class of digital elevation models aquired by spaceborne radar. *ISPRS Journal for Photogrammetry and Remote Sensing*, 57: 241–262.

Racoviteanu, A., Arnaud, Y., Williams, M., and Ordoñez, J. (2008a). Decadal changes in glacier parameters in the Cordillera Blanca, Peru, derived from remote sensing. *Journal of Glaciology*, 54 (186): 499–509.

Racoviteanu, A. E., Williams, M. W., and Barry, R. G. (2008b). Optical remote sensing of glacier characteristics: a review with focus on the Himalaya. *Sensors*, 8 (5): 3355–3383. doi: 10.3390/s8053355.

Radić, V. and Hock, R. (2011). Regionally differentiated contribution of mountain glaciers and ice caps to future sea-level rise. *Nature Geoscience*, 4 (2): 91–94. doi: 10.1038/ngeo1052.

Ranzi, R., Grossi, G., Iacovelli, L., and Taschner, S. (2004). Use of multispectral ASTER images for mapping debris-covered glaciers within the GLIMS project. *Geoscience and Remote Sensing Symposium, 2004. IGARSS '04. Proceedings. 2004 IEEE International*, 2: 1144–1147.

Raper, S. C. B. and Braithwaite, R. J. (2006). Low sea level rise projections from mountain glaciers and icecaps under global warming. *Nature*, 439: 311–313. doi: 10.1038/nature04448.

Raup, B. and Singh Khalsa, S. J. (2010). *GLIMS Analysis Tutorial*.

Raup, B., Kieffer, H., Hare, T., and Kargel, J. (2000). Generation of data acquisition requests for the ASTER satellite instrument for monitoring a globally distributed target: glaciers. *IEEE Transactions on Geoscience and Remote Sensing*, 38 (2): 1105–1112.

Raup, B., Kääb, A., Kargel, J. S., Bishop, M. P., Hamilton, G., Lee, E., Paul, F., Rau, F., Soltesz, D., Khalsa, S. J. S., Beedle, M., and Helm, C. (2007a). Remote sensing and GIS technology in the Global Land Ice Measurements from Space (GLIMS) Project. *Computers & Geosciences*, 33: 104–125.

Raup, B., Racoviteanu, A., Khalsa, S. J. S., Helm, C., Armstrong, R., and Arnaud, Y. (2007b). The GLIMS geospatial glacier database: A new tool for studying glacier change. *Global and Planetary Change*, 56 (1-2): 101–110.

Reuter, H. I., Nelson, A., and Jarvis, A. (2007). An evaluation of void filling interpolation methods for SRTM data. *International Journal of Geographic Information Science*, 21 (9): 983–1008.

Reynolds, J. M. (2000). On the formation of supraglacial lakes on debris-covered glaciers. In: *Debris-Covered Glaciers. Proceedings of a workshop held at Seattle, Washington, U.S.A., September 2000. IAHS publications*, (edited by Nakawo, M., Raymond, C., and Fountain, A.), vol. 264, pp. 153–161. IAHS Publication.

Reynolds Geo-Science (2003). *Guidelines for the management of glacial hazards and risks*. Reynolds Geo-Science Ltd, Mold, UK.

Richards, J. A. (1999). *Remote sensing digital image analysis: an introduction*. Springer, Berlin/Heidelberg, 2nd ed.

Richardson, S. and Reynolds, J. (2000). An overview of glacial hazards in the himalayas. *Quaternary International*, 65-66: 31–47.

Richardson, S. D. (2010). Remote sensing approaches for early warning of GLOF hazards in the Hindu Kush-Himalayan region. Final report, Prepared for the United Nations International Strategy for Disaster Reduction (UN/ISDR).

Ridley, J., Huybrechts, P., Gregory, J. M., and Lowe, J. A. (2005). Elimination of the Greenland ice sheet in a high CO2 climate. *Journal of Climate*, 18: 3409–3427.

Rignot, E., Echelmeyer, K., and Krabill, W. (2001). Penetration depth of interferometric synthetic-aperture radar signals in snow and ice. *Geophysical Research Letters*, 28 (18): 3501–3504.

Rignot, E., Rivera, A., and Casassa, G. (2003). Contribution of the Patagonia Icefields of South America to Sea Level Rise. *Science*, 302: 434–437.

Rivera, A., Casassa, G., Bamber, J., and Kääb, A. (2005). Ice-elevation changes of Glaciar Chico, southern Patagonia, using ASTER DEMs, aerial photographs and GPS data. *Journal of Glaciology*, 51 (172): 105–112.

Rott, H. (1994). Thematic studies in alpine areas by means of polarimetric SAR and optical imagery. *Advances in Space Research*, 14 (217-226).

Ruiz, A., Kornus, W., Talaya, J., and Colomer, J. L. (2004). Terrain modeling in an extremely steep mountain: A combination of airborne and terrestrial lidar. *International Archives of Photogrammetry, Remote Sensing and Spatial Information Sciences*, 35 (B3): 281– 284.

Sabins, F. F. (1997). *Remote Sensing - Principles and Interpretations*. W. H. Freeman, New York, third edition ed.

Salzmann, N., Kääb, A., Huggel, C., Allgöwer, B., and Haeberli, W. (2004). Assessment of the hazard potential of ice avalanches using remote sensing and gis-modelling. *Norsk Geografisk Tidskrift - Norwegian Journal of Geography*, 58 (2): 74–84.

Scherler, D., Bookhagen, B., and Strecker, M. R. (2011). Spatially variable response of Himalayan glaciers to climate change affected by debris cover. *Nature Geoscience*,

4 (1): 1–4. doi: 10.1038/ngeo1068.

Scheuner, T., Keusen, H.-R., McArdell, B., and Huggel, C. (2009). Murgangmodellierung mit dynamisch-physikalischem und GIS-basiertem Fliessmodell - Fallbeispiel Rotlauigraben, Guttannen, August 2005. *Wasser Energie Luft*, 101 (1): 15–21.

Schiefer, E., Menounos, B., and Wheate, R. (2007). Recent volume loss of British Columbian glaciers, Canada. *Geophysical Research Letters*, 34 (L16503). doi: 10.1029/2007GL030780.

Schneider, D., Delgado Grandes, H., Huggel, C., and Kääb, A. (2008). Assessing lahars from ice-capped volcanoes using ASTER satellite data, the SRTM DTM and two different flow models: case study on Iztaccíhuatl (Central Mexico). *Natural Hazards and Earth System Sciences*, 8: 559–571.

Schneider, D., Bartelt, P., Caplan-Auerbach, J., Christen, M., Huggel, C., and McArdell, B. W. (2010). Insights into rock-ice avalanche dynamics by combined analysis of seismic recordings and a numerical avalanche model. *Journal of Geophysical Research*, 115 (F04026): 1–20. doi: 10.1029/2010JF001734.

Schneider, D., Huggel, C., Haeberli, W., and Kaitna, R. (in press). Unraveling driving factors for large rock-ice avalanche mobility. *Earth Surface Processes and Landforms*.

Schowengerdt, R. A. (2007). *Remote sensing – Models and methods for image processing*. Academic Press, Amsterdam, 3rd ed.

Sidjak, R. W. and Wheate, R. D. (1999). Glacier mapping of the Illecillewaet icefield, British Columbia, Canada, using, Landsat TM and digital elevation data. *International Journal of Remote Sensing*, 20 (2): 273–284.

Sing Khalsa, S. J., Dyurgerov, M. B., Khromova, T., Raup, B. H., and Barry, R. G. (2004). Space-based mapping of glacier changes using ASTER and GIS tools. *IEEE Transactions on Geoscience and Remote Sensing*, 42 (10): 2177–2183.

Slater, J. A., Heady, B., Kroenung, G., Curtis, W., Haase, J., Hoegemann, D., Shockley, C., and Tracy, K. (2011). Global Assessment of the New ASTER Global Digital Terrain Model. *Photogrammetric Engineering and Remote Sensing*, 77 (4): 335–349.

Snyder, J. P. (1987). Map projections - a working manual. *U.S. Geological Survey professional paper 1395*.

Stevens, N. F., Manville, V., and Heron, D. W. (2002). The sensitivity of a volcanic flow model to digital elevation model accuracy: experiments with digitised map contours and interferometric SAR at Ruapehu and Taranaki volcanoes, New Zealand. *Journal of Volcanology and Geothermal Research*, 119: 89–105.

Stolz, A. and Huggel, C. (2008). Debris flows in the Swiss National Park: the influence of different flow models and varying DEM grid size on modeling results. *Landslides*,

5 (3): 311–319. doi: 10.1007/s10346-008-0125-4.

Svoboda, F. and Paul, F. (2009). A new glacier inventory on southern Baffin Island, Canada, from ASTER data: I. Applied methods, challenges and solutions. *Annals of Glaciology*, 50 (53): 11–21.

Swisstopo (2004). DHM25 - The digital height model of Switzerland. *Product Information*.

Tamburini, A. and Mortara, G. (2005). Tamburini: The case of the "Effimero" Lake at Monte Rosa (Italian Western Alps): studies, field surveys, monitoring. In: *Proceedings of the 10th ERB Conferece, Turin, 13–17 October 2004*. Progress in Surface and Subsurface Water Studies at Plot and Small Basin Scale, Unesco, IHP-VI Technical Documents in Hydroloy, 77.

Taschner, S. and Ranzi, R. (2002). Comparing the opportunities of Landsat-TM and Aster data for monitoring a debris covered glacier in the Italian Alps within the GLIMS project. *Geoscience and Remote Sensing Symposium, 2002. IGARSS '02. 2002 IEEE International*, 2: 1044–1046.

Toutin, T. (2008). ASTER DEMs for geomatic and geoscientific applications: a review. *International Journal of Remote Sensing*, 29 (7): 1855–1875. doi: 10.1080/01431160701408477.

Tucker, C. J., Grant, D. M., and Dykstra, J. D. (2004). NASA's global orthorectified Landsat data set. *Photogrammetric Engineering and Remote Sensing*, 70 (3): 313–322.

USGS (2005). Orthorectified Landsat digital data now available from USGS. USGS Press release.

Van Zyl, J. J. (2001). The Shuttle Radar Topography Mission (SRTM): a breakthrough in remote sensing of topography. *Acta Astronautica*, 48 (5-12): 559–565.

Vilimek, V., Zapata, M., Klimes, J., Patzelt, Z., and Santillan, N. (2005). Influence of glacial retreat on natural hazard of the Palcacocha Lake area, Peru. *Landslides*, 2: 107–115.

Walder, J. and Costa, J. (1996). Outburst floods from glacier-dammed lakes: the effect of mode of lake drainage on flood magnitude. *Earth Surface Processes and Landforms*, 21: 701–723.

Watanabe, T., Ives, J., and Hammond, J. (1994). Rapid growth of a glacial lake in Khumbu Himal, Himalaya: Prospects for a catastrophic flood. *Mountain Research and Development*, 14: 329–340.

Werder, M. A., Bauder, A., Funk, M., and Keusen, H.-R. (2010). Hazard assessment investigations in connection with the formation of a lake on the tongue of Unterer Grindelwaldgletscher, Bernese Alps, Switzerland. *Natural Hazards and Earth System*

Sciences, 10: 227–237.

Wessels, R., Kargel, J., and Kieffer, H. (2002). ASTER measurement of supraglacial lakes in the Mount Everest region of the Himalaya. *Annals of Glaciology*, 34: 399–408.

WGMS (2008a). Fluctuations of glaciers 2000–2005. *ICSU(FAGS)/IUGG(IACS)/UNEP/ UNESCO/WMO, World Glacier Monitoring Service, Zurich, Switzerland*, Volume IX.

WGMS (2008b). *Global Glacier Changes: facts and figures*. UNEP, World Glacier Monitoring Service, Zurich, Switzerland.

Williams, R. S. and Ferrigno, J. G. (2010). Satellite image atlas of glaciers of the world. *USGS Fact Sheet 133-99, revised version*.

Williams Jr, R. (1987). Satellite remote sensing of Vatnajökull, Iceland. *Annals of Glaciology*, 9: 127–135.

Zemp, M., Haeberli, W., Hoelzle, M., and Paul, F. (2006). Alpine glaciers to disappear within decades? *Geophysical Research Letters*, 33 (L13504). doi: 10.1029/2006GL026319.

Zemp, M., Jansson, P., Holmlund, P., Gärtner-Roer, I., Koblet, T., Thee, P., and Haeberli, W. (2010). Reanalysis of multi-temporal aerial images of Storglaciären, Sweden (1959–99) – Part 2: Comparison of glaciological and volumetric mass balances. *The Cryosphere*, 4: 345–357. doi: 10.5194/tc-4-345-2010.

Zeng, Q., Cao, M., Feng, X., Liang, F., X., C., and Sheng, W. (1984). A study of spectral reflection characteristics for snow, ice and water in the north of China. *Scientia Sinica (Series B)*, 46: 647–56.

Zwally, H. J., Schutz, B., Abdalati, W., Abshire, J., Bentley, C., Brenner, A., Bufton, J., Dezio, J., Hancock, D., Harding, D., Herring, T., Minster, B., Quinn, K., Palm, S., Spinhirne, J., and Thomas, R. (2002). ICESat's laser measurements of polar ice, atmosphere, ocean, and land. *Journal of Geodynamics*, 34: 405–445.

Part II

Research papers

Paper I

Frey, H. and Paul, F. (in press). On the suitability of the SRTM DEM and ASTER GDEM for the compilation of topographic parameters in glacier inventories. *International Journal of Applied Earth Observation and Geoinformation*. doi: 10.1016/j.jag.2011.09.020

On the suitability of the SRTM DEM and ASTER GDEM for the compilation of topographic parameters in glacier inventories

Holger Frey, Frank Paul*
Department of Geography, University of Zurich, Winterthurerstrasse 190, CH-8057 Zurich, Switzerland

Contact: Holger Frey: holger.frey@geo.uzh.ch, +4144 635 52 08*
Frank Paul: frank.paul@geo.uzh.ch, +4144 635 51 75

**corresponding author.*

submitted to the

International Journal of Applied Earth Observation and Geoinformation

Abstract

Topographic parameters in glacier inventories are of vital importance for many subsequent applications. In this study we investigate the suitability of the SRTM DEM and the ASTER GDEM for the compilation of topographic attributes, as both datasets have a nearly global coverage and are freely available. For 1786 Swiss glaciers we calculated seven topographic parameters from both DEMs. Each DEM was used in two different resolutions, and the obtained values were compared to parameter values derived from the Swiss national DEM (DHM25), which served as the reference. While large differences can occur on individual glaciers, they average out for larger glacier samples. Parameters that depend on a single DEM value (e.g. minimum- or maximum elevation) have larger variations than parameters that are averaged over the glacier area (e.g. mean elevation or mean slope). Besides artifacts and errors, changes between different acquisition dates, and dataset acquisition techniques (radar, optical and photogrammetric), have a direct influence on the inventory parameters. Although SRTM yielded slightly better results than the ASTER GDEM, both DEMs can be recommended for the compilation of topographic parameters in glacier inventories.

Keywords: SRTM; ASTER GDEM; glacier inventory; topographic parameter; GLIMS

1. Introduction

1.1 Background

One of the most required datasets for an improved calculation of current and future global sea- level rise (e.g. Hock et al., 2009; Radic and Hock, 2010; Raper and Braithwaite, 2006) or regional water resources assessment (e.g. Haeberli and Hoelzle, 1995) is a globally complete glacier inventory (e.g. GCOS, 2006) with topographic attributes (e.g. minimum and maximum elevation, slope, and aspect) for each glacier. While glacier outlines are currently compiled by a global network of regional centers in a 2D vector format for the GLIMS (Global Land Ice Measurements from Space) glacier database (Raup et al., 2007) using satellite imagery (e.g. Paul et al., 2002; Kargel et al., 2005; Bolch et al., 2010), few of the glacier outlines are accompanied by the required topographic information. With the free availability of the digital elevation models (DEMs) from SRTM (available between 60°N and 56°S) and the ASTER GDEM, the topographic inventory parameters can now be calculated for most glacier outlines using automated procedures (Paul et al., 2009). However, both DEMs suffer locally from artifacts (e.g. due to radar shadow, clouds or low contrast) that result in erroneous elevation values, which in turn can influence the topographic inventory parameters. For the analyst it is often unclear, which of the available DEMs is the most appropriate for the calculation of topographic information. We thus decided to perform a quantitative evaluation of both DEMs based on a large sample of glaciers in Switzerland.

1.2 Study design

To quantify the impact of artifacts and errors on the glacier inventory parameters, we have calculated a set of seven parameters (minimum, mean, median, and maximum elevation, mean slope, mean aspect, and mean aspect sector) for 1786 glaciers in the Swiss Alps and three different DEMs (SRTM, ASTER GDEM and DHM25 from swisstopo). As all three DEMs have different spatial resolutions (90 m, 30 m, and 25 m, respectively), we also tested the influence of resolution alone on the derived parameters for the DHM25 with 25 m, 50 m and 100 m cell size. Such resolution related effects can have some impact on the derived glacier parameters as Möller and Schneider (2010) and Paul (2008) showed for the case of glacier elevation changes. The comparison of values performed here should identify the error bounds that have to be expected for each parameter when the SRTM or the ASTER GDEM is used for the related calculations, e.g. in regions where national DEMs of sufficient quality are not available or outdated.

As mentioned above, the purpose of this study is to evaluate different DEMs for their suitability to derive topographic parameters for a glacier inventory. We do not perform a glaciological characterization of the parameters or an assessment of their changes over time (such analyses for Swiss glaciers can be found in Kääb et al. (2002) and Paul (2007)). As the DEMs used in this study were compiled at different points in time (with a few years in-between, cf. section 2), changes of topographic parameters can be caused by (1) different characteristics of the DEM and (2) changes of the glaciers. In this study we are interested only in (1) and thus seek to reduce the influence of (2). Glacier changes over time occur in the form of (a) changes in glacier extent (i.e. area and length) and (b) changes of surface elevation as represented in the respective DEM. To reduce the influence of (a), we here use the same glacier extents for all calculations. This guarantees that all calculated topographic parameters refer to the same entities. The influence of (b) is difficult to quantify and hence to reduce, as all three DEMs originate from different sources and include extent changes to some degree.

During glacier retreat, minimum, mean and median elevation should increase as the lower glacier parts disappear first (Paul et al. 2007). On the other hand, if glacier extents remain constant, the glacier surface lowering leads to decreasing values of these parameters. In our

calculations we keep the outlines constant, but allow the real surface lowering and extent change as given by the different DEMs. This compensates these two effects to some extent and results in a likely very small net effect. We thus assume for this study that differences in the values of the topographic parameters are mainly caused by differences in the characteristics of the compared DEMs.

2. Test site and datasets

The Swiss Alps were chosen as a test site for this study since we have a high-quality DEM for comparison and glacier outlines for the entire region from about the same point in time as the DEMs were acquired. Moreover, the steep high-mountain topography that is found here is likely representative for many mid-latitude glaciers as it has the typical challenges and uncertainties related to DEM production and analysis in such regions.

We used glacier outlines from the Swiss glacier inventory (SGI2000), which was compiled by remote-sensing-based glacier mapping with Landsat 5 Thematic Mapper (TM) scenes acquired in 1998 and 1999 (Paul et al., 2002; Paul, 2007). Figure 1 gives an overview of the entire study region with the specific test sites (Rhonegletscher and Wächselgletscher) marked. In total, this inventory contains 2607 glacier entities, of which 1786 were used in this study. The remaining 822 glaciers were too small to calculate glacier-specific statistics based on the 100 m resolution DEMs (less than 0.01 km^2, i.e. less than a 100 m x 100 m cell, see section 3). Small glaciers (< 1 km^2) dominate in the dataset by number, but the 173 glaciers larger than 1 km^2 cover 81% of the total area (Fig. 2).

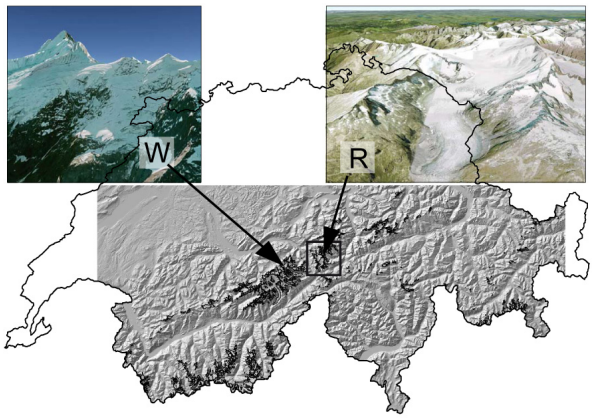

Fig. 1: Overview of the study region. Outlines of Switzerland are shown, the hillshade-view (from SRTM) indicates the extent of the DEMs. Small inset pictures are bird's eye-views of Wächselgletscher (W) and Rhonegletscher (R) from GoogleEarth™, which were used for comparisons of hypsographies (cf. Fig. 7 and 8). The rectangle around Rhonegletscher indicates the extent of Fig. 3.

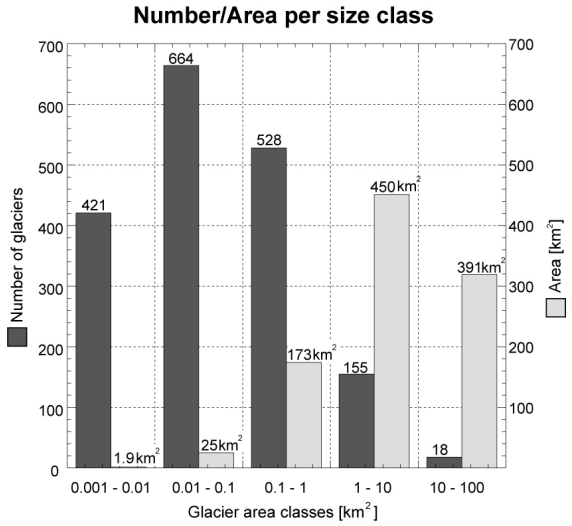

Fig. 2: Distribution of the 1786 glaciers used in this study by area. Dark grey bars show the number of glaciers in each size class; light grey bars show the area covered by all glaciers of each size class.

The inventory parameters that served as a reference were calculated with the Level 2 version of the DHM25 from the Federal Office of Topography (swisstopo). This DEM is derived by interpolation of contour lines from the Swiss Topographic Map series at 1:25,000 scale, including lake outlines, break lines, and spot heights. Two versions of the DHM25 exist, Level 1 (acquired around 1985) and Level 2 (acquired around 1995). Apart from the different dates, the Level 2 version has partly updated glacier elevations (in general in the ablation region only), more break lines were included and an improved interpolation algorithm was applied to create the raster data. The spatial resolution is 25 m, the reported vertical accuracy in the Alps is between 4 and 10 m (Swisstopo, 2004). Values calculated based on this DEM are considered as the reference values for the respective inventory parameters in this study.

The SRTM DEM was acquired by radar interferometry (InSAR) during 10 days in February 2000, when a Space Shuttle mapped the Earth surface between 60°N und 56°S with C band radar. From these data, among other products, a near global DEM with 3 arc-seconds resolution (~90 m, SRTM3) was derived and distributed for free. Validation through comparison with ground control points revealed vertical and horizontal errors of approximately 10 m (Farr et al., 2007). In mountainous terrain with its steep slopes, geometrical constraints of the acquisition method (e.g. radar shadow and layover) result in numerous data voids, which affect 942 (53%) of the 1786 glaciers used in this study, but only five voids are larger than 2 km^2. The Consultative Group on International Agricultural Research (CGIAR) offers a void-filled version of the SRTM3 dataset (SRTM3v4), where the data gaps were filled with different interpolation algorithms and auxiliary DEMs if available, hence some regions are influenced by the lower accuracy of these void-filled regions. Reuter et al. (2007) give a thorough description of the applied methodology for the void filling. In this study we used the tiles srtm_38_03 and srtm_39_03 of this complete version of the SRTM3 DEM (hereafter SRTM).

The ASTER sensor on board of the Terra spacecraft (launched in 1999) has an along-track stereoscopic capability due to a nadir- and 27.6° backward-looking telescope in the Near Infrared (NIR) spectral band. This instrumental setup allows for photogrammetric DEM generation with vertical accuracies of ±15-30 m (Toutin, 2008), but in rough mountainous conditions with steep slopes and snowfields with little contrast, RMS values of ±60 m are

reported (Kääb, 2002). The Ministry of Economy, Trade, and Industry (METI) of Japan and NASA released in June 2009 the ASTER global DEM (GDEM) that was produced by automated processing of the complete ASTER archive from 2000 to 2007, containing more than 1.5 million scenes (METI, 2009). The ASTER GDEM has a horizontal resolution of 1 arc-second (~30 m) and covers the earth's surface between 83°N und 83°S. For this study the ASTER GDEM tiles N45E006, N45E007, N45E008, N46E006, N46E007, N46E008, N46E009 and N46E010 were used.

3. Methods

3.1 Data preparation

First, the DHM25 and the SGI2000 datasets were reprojected from the Swiss map projection to the Universal Transverse Mercator (UTM) coordinate system, zone 32. Originally, both datasets had the Swiss map projection; an oblique conformal cylindrical projection with the Bessel 1841 ellipsoid and a user defined Datum (CH1903). After downloading and merging the tiles of the SRTM DEM (3 arc seconds spatial resolution) and the ASTER GDEM (1 arc second resolution), both datasets were reprojected to UTM zone 32, and then clipped to the extent of the SGI2000. Finally, the three DEMs were resampled with bilinear interpolation from their original resolution to 25 m and 100 m for the SRTM DEM and the ASTER GDEM, and 50 m and 100 m for the DHM25. These three cell sizes have been selected for the following reasons: (1) for the calculation of the topographic parameters an internal vector-to-raster conversion is applied by the software to all glacier outlines in order to align them with the DEM cells. It is therefore essential that all DEMs have the same spatial resolution or cell sizes that are integer factors of the highest resolution (i.e. 25 m, 50 m, 100 m). (2) The 25 m resolution corresponds to the original resolution of DHM25 to which the values were compared; and (3) 25 m is relatively close to the original resolution of the ASTER GDEM (~30 m), whereas 100 m is similar to the original resolution of SRTM (~90 m). In this way, seven different DEMs were compiled for the calculation of topographic parameters. They have the following shortcuts: DHM25_25 (which is the reference), DHM25_50, DHM25_100; SRTM_25, SRTM_100; GDEM_25 and GDEM_100.

To get an impression of the quality and typical characteristics of the three DEMs, they were compared to each other at 25 m resolution using hillshade views and direct subtraction. This facilitates the quality assessment, because the spatial distribution of differences gives information about potential horizontal shifts of the DEMs relative to each other and artifacts and errors are more easily detectable. An overview of potential DEM errors can be found in Hebeler and Purves (2009) and a report about typical artifacts and errors in the GDEM is given in METI/NASA/USGS (2009) and Abrams et al. (2010).

3.2 Compilation of inventory parameters

For the calculation we followed the 'recommendations for the compilation of glacier inventory data from digital sources' by Paul et al. (2009). For each of the 1786 selected glaciers, seven basic inventory parameters were calculated with each DEM in a Geographic Information System (GIS): Minimum-, maximum-, mean- and median elevation; mean slope; mean aspect in degree and mean aspect sector (according to the eight cardinal directions). To obtain mean slope and mean aspect values, a slope and aspect grid was calculated from each DEM. As aspect is a circular parameter (north is represented by two values 0° and 360°) it must be decomposed in a sine and a cosine grid (cf. Evans, 2006). Mean aspect values are then calculated with the arctangent function using the mean sine and cosine values of the aspect grid following Paul (2007).

3.3 Comparisons

Inventory parameters compiled with the different DEMs were compared in two ways: first, the values as calculated with the original DHM25 (25 m resolution) were compared to values obtained from the DHM25 in 50 m and 100 m resolution, respectively, to investigate the influence of different resolutions alone. In a second step, the parameters from the DHM25 – which were taken as the reference – were compared to the parameters compiled from the 25 m and a 100 m version of SRTM and the ASTER GDEM.

In consequence, each glacier has seven values for each of the seven parameters, according to the seven DEM versions. The differences of the respective value to the reference value obtained from the DHM25 were calculated and are shown in the related scatter plots (Fig. 5). To better assess the size dependent variability of the differences, the 1786 glaciers were further subdivided into five size categories, one class for each exponent to the base of 10, ranging from 10^3 to 10^7 m^2.

4. Results

4.1 Differencing of DEMs

Differences from the direct DEM subtractions are depicted in Fig. 3 for the region around Rhonegletscher. As the datasets have been acquired in different years and seasons, the specific changes mentioned above can be recognized over glaciers and outside of glaciers. Table 1 gives mean differences and standard deviations of the three comparisons calculated for the total extent of the datasets (cf. Fig. 1).

In the SRTM DEM, glacier surface elevations are clearly lower compared to the DHM25 (-10.83 m), due to lowering of the ice surfaces over the 15 years between the respective DEM acquisition dates (cf. Paul and Haeberli, 2008). Lower lake levels of storage lakes in winter during the acquisition of the SRTM (February) are the reason for the negative values in the area of the Göscheneralp storage lake ((L) in Fig. 3a). Furthermore, the SRTM DEM has a slight shift of about 55 m in south-western direction, which results in positive difference values on south-west exposed slopes and negative differences on north-east exposed slopes. However, this shift was not corrected for the further analyses because location accuracy is an important factor of the quality and in regions where no reference DEM is available such a shift is difficult to determine. A comparison of the void-filled SRTM version and the SRTM3 version from NASA with voids (not shown here) also reveals a systematic shift of 35 m. This indicates that the geolocation of SRTM data depends on the download source.

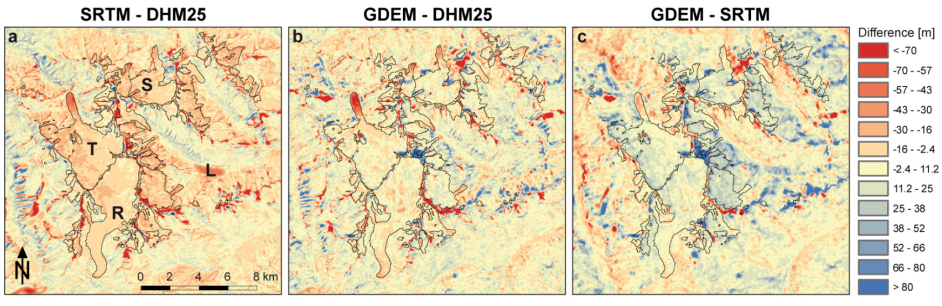

Fig. 3: Differences of the three DEMs in the region of Rhonegletscher (R), Triftgletscher (T), and Steingletscher (S). (L) indicates the location of the Göscheneralp storage Lake. The Color table corresponds to half standard deviations of SRTM – DHM25.

Differences between the ASTER GDEM and the DHM25 (Fig. 3b) are distributed more randomly and are larger than between SRTM and DHM25. Differences of more than ±500 m occur more than ten times more often in the ASTER GDEM (they cover 3.59 km^2) than in the SRTM DEM (0.24 km^2). Over glacier areas on the other hand, the differences are generally smaller and slightly positive (+ 2.33 m) when comparing the GDEM with the DHM25 (Table 1). This indicates a considerable influence of artifacts, as nearly all glacier tongues are lower in the GDEM. This is supported by the larger standard deviations over glaciers and outside of glaciers that are found for the differences between the GDEM and the DHM25 in comparison to the differences of SRTM and the DHM25. A prominent feature in all difference images is the massive lowering of the tongue of Triftgletscher ((T) in Fig. 3a). At this location, the formation of a glacier lake took place from around 2000 to 2006. In general, the surface elevation of glaciers has undergone rapid changes during recent years, as pointed out by numerous studies around the world (e.g. Larsen et al., 2007; Möller and Schneider, 2010; Paul and Haeberli, 2008) and the terrain outside of glaciers is considered to be more stable. We therefore derived mean differences and standard deviations for glacier regions and terrain outside glaciers separately (Table 1). However, the non-glacier areas do not affect our analysis since they are not included in the statistics of the topographic inventory parameters.

Table 1: Mean differences and standard deviations of DEM subtractions, calculated for the total extent of the datasets.

		SRTM – DHM25	GDEM – DHM25	GDEM – SRTM
over glaciers	mean	-10.83	2.33	13.16
[m]	std. dev	15.57	26.75	25.42
outside glaciers	mean	2.23	4.62	0.78
[m]	std. dev	21.64	27.50	25.93

The ASTER GDEM compared to SRTM (Fig. 3c) also shows large standard deviations. Higher elevation values in the ASTER GDEM over accumulation regions are a dominant feature, likely due to the different acquisition technique: whereas the optical ASTER sensor measures the surface of the snow pack, which typically has low contrast, the C-band radar of SRTM penetrates the snow pack to a certain extent, depending on the physical and electrical properties of the snow (Rignot et al., 2001). Considering the different acquisition dates and techniques, the observed differences can, to a certain extent, be explained.

4.2 Glacier parameters derived from the DHM25 in different resolutions

To detect trends that only depend on the resolution, the DHM25 was resampled to 50 and 100 m cell-size and the calculated topographic parameters compared to its original resolution (25 m). The following trends were observed: with decreasing resolution, minimum elevation values tend to increase, whereas values for maximum elevation decrease. This trend is stronger for minimum elevation than for maximum elevation. In Fig. 4a scatter plots of the differences between the values from the 25 m resolution DHM25 and the respective resampled version are shown. There is no dependency of the differences on glacier size recognizable, but it can be noted that for minimum elevation there are fewer glaciers which do not follow the trend described above than in the sample for maximum elevation. Histograms of the differences are shown in Fig. 4b, indicating that for minimum elevation the maxima of both resampled DEMs are in the first positive bin (+5 to +15 m), whereas for maximum elevation the maximum of the histograms only becomes negative in the 100 m version, but is in the bin containing zero (-5 to +5 m) for the 50 m version. For minimum elevation, the mean differences to the original 25 m resolution version are 7.7 and 24.8 m for the 50 and 100 m version, respectively (cf. Table 2); only 207 glaciers (11.6 % of the total

sample) have lower minimum elevation values in the 100 m version than in the original DHM25. For maximum elevation the mean differences are -4.7 and -20.0 m, and 355 glaciers (20% of the total sample) have higher maximum elevations in the 100 m version than in the original DEM. Standard deviations of both parameters are higher for the 100 m resolution version (cf. Table 2).

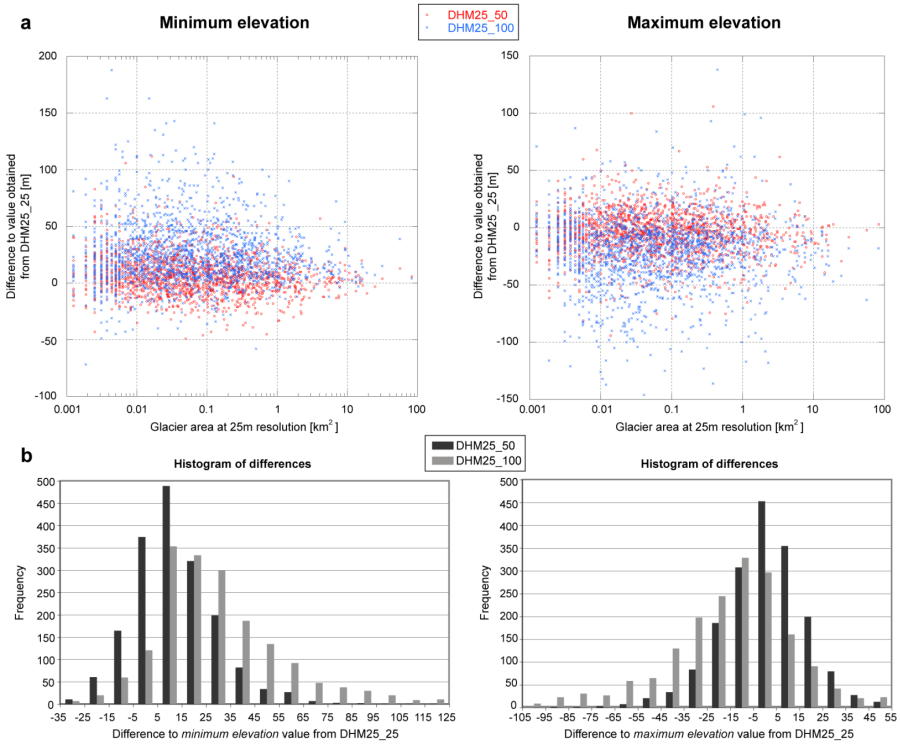

Fig. 4: a: Differences of minimum- and maximum elevation values between DHM25 at 25 m resolution and DHM25 at 50 m and 100 m resolution, respectively. b: Histograms of these differences.

Mean- and median elevations are not affected by the smoothing effect because the different values for the individual grid cells compensate each other. The differences of mean slope do not show a tendency either, the mean differences are only -0.01° and 0.23°; for glaciers larger than 0.1 km^2 most differences are smaller than 5°, and for glaciers larger than 1 km^2 all values are within ±2.5°.

4.3 Comparisons of glacier parameters derived from SRTM, ASTER GDEM and DHM25

All differences of the topographic glacier parameters calculated with the different DEM versions to the reference values are shown in the scatter plots of Fig. 5; mean differences and standard deviations for the entire sample of glaciers are listed in Table 2.

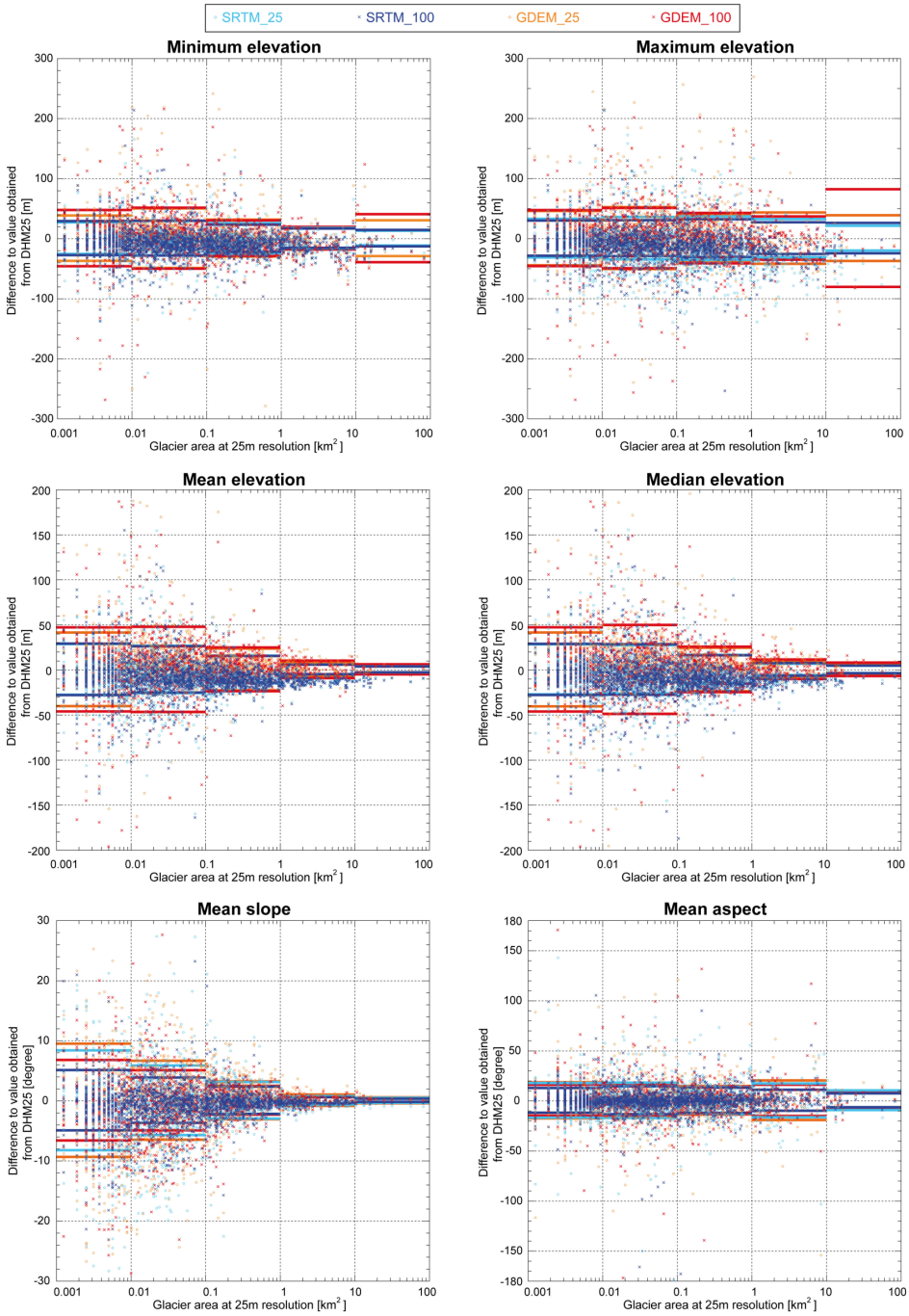

Fig. 5: Scatter plots for all topographic parameters (except mean aspect sector). Some extreme outliers are not plotted (cf. Table 2 for maximal differences). The horizontal bars indicate the standard deviations for the respective size class.

Table 2: Mean differences, standard deviations and maximal positive and negative differences of topographic inventory parameters derived from the four different DEM versions compared to values from DHM25 at 25 m resolution (scatter plots in Fig. 5).

		DHM25 50	DHM25 100	SRTM 25	SRTM 100	GDEM 25	GDEM 100
Minimum elevation [m]	mean	7.68	24.79	-6.52	-9.09	4.41	-1.16
	std. dev	17.63	27.20	26.03	26.07	39.86	42.29
	max. diff (+)	112	188	166	114	679	777
	max. diff (-)	-49	-72	-318	-309	-718	-575
Maximum elevation [m]	mean	-4.66	-19.95	-13.76	-11.40	3.74	-0.94
	std. dev	19.20	30.80	35.14	30.07	45.80	46.44
	max. diff (+)	106	138	213	214	750	748
	max. diff (-)	-94	-308	-143	-253	-385	-550
Mean elevation [m]	mean	2.16	2.75	-8.00	-9.23	6.39	0.97
	std. dev	12.34	18.97	22.69	22.42	37.40	38.99
	max. diff (+)	71	141	211	214	764	764
	max. diff (-)	-47	-149	-214	-205	-484	-408
Median elevation [m]	mean	0.94	-1.18	-7.74	-9.00	6.65	1.32
	std. dev	13.41	23.50	23.03	23.69	38.50	40.25
	max. diff (+)	83	148	219	214	772	801
	max. diff (-)	-57	-153	-230	-187	-498	-393
Mean slope [°]	mean	-0.23	-0.31	-0.94	-0.87	-0.49	-0.87
	std. dev	3.08	4.80	5.62	3.57	6.38	4.68
	max. diff (+)	30.3	21.9	43.9	23.2	30.9	27.7
	max. diff (-)	-22.5	-40.7	-30.4	-21.4	-36.0	-35.7
Mean aspect [°]	mean	0.19	4.36	0.04	0.19	0.23	0.56
	std. dev	29.15	57.51	16.18	12.89	16.70	15.32
	max. diff (+)	122	164	143	105	121	171
	max. diff (-)	-66	-168	-179	-173	-154	-177
Mean aspect sector [sector] (1 sector = 1.0)	mean	-0.009	0.018	0.006	0.003	0.019	0.004
	std. dev	0.356	0.537	0.510	0.425	0.500	0.478
	max. diff (+)	3	4	3	2	4	3
	max. diff (-)	-2	-3	-4	-4	-3	-4

For minimum-, maximum-, mean-, and median elevation, the standard deviations of each size class differ more strongly between the different DEMs than between the different resolutions of the same DEMs. On the other hand, standard deviations of mean slope are more strongly influenced by the resolution than by the DEM source. For none of the parameters could a dependence on glacier size be detected, linear regressions (not shown here) revealed R^2 values smaller than 0.02 for all parameters and datasets, and in most cases R^2 values were even smaller than 0.003. Nevertheless, parameters that include all DEM cells of a specific glacier area (mean- and median elevation, mean slope) show a funnel-shaped distribution of the differences with a stronger scatter for small glaciers than for large glaciers. For the other parameters, which depend more on individual values (minimum- and maximum elevation), the glacier area does not affect the range of differences. Mean aspect is an exception; although this parameter is averaged over the glacier area, standard deviations of differences are similar for all size classes.

The influence of aspect was investigated by comparing parameter values from SRTM_25 and GDEM_25 with the reference values from DHM25. For this purpose, the glaciers were split into eight classes, according to their mean aspect sector (calculated with the DHM25). For each aspect bin, mean, quartiles (25% and 75%), as well as the 5% and the 95% percentile of

the differences were calculated (Fig. 6). In general, the values calculated from the three DEMs vary almost twice as much for the northern sectors (NW, N, NE) than for the southern sectors (SE, S, SW).

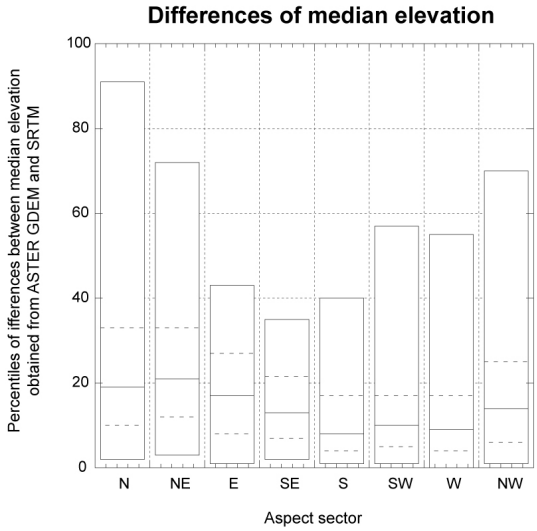

Fig. 6: Absolute differences between mean elevation value from ASTER GDEM and SRTM, plotted for the eight aspect sectors. The bottom and top of each box represent 5% and 95% of the data, the middle line represents the median value (50%), while the lower and upper dashed lines represent 25% and 75% of the data, respectively.

It also appears that the standard deviations of differences are smaller in the versions with a resolution closer to the original version of the respective dataset (100 m for SRTM and 25 m for the ASTER GDEM, Table 2). Although these differences are rather small, the fact that the SRTM_100 performs better than the SRTM_25, but the GDEM_25 leads to smaller differences than the GDEM_100 can be observed for almost all parameters. This is also the case when analyzing the standard deviations in Fig. 5 and Table 2.

Glacier hypsography, or the distribution of area with elevation, is similar in the different DEMs for most glaciers (Figs. 7 and 8). Local differences in the DEMs have only a small influence on the hypsography of larger glaciers, whereas the largest differences occur in the hypsography of small and north-oriented glaciers that can be situated in a radar shadow region of SRTM and/or in cast shadow of the ASTER scenes. Here, the hypsography for Rhonegletscher (16 km^2) as a larger glacier, and Wächselgletscher (0.58 km^2) as a small and north-exposed glacier, are illustrated as an example. Figure 7 shows these glaciers with hillshaded versions of DHM25, ASTER GDEM and the SRTM DEM in the background, all at 25 m resolution for better comparability.

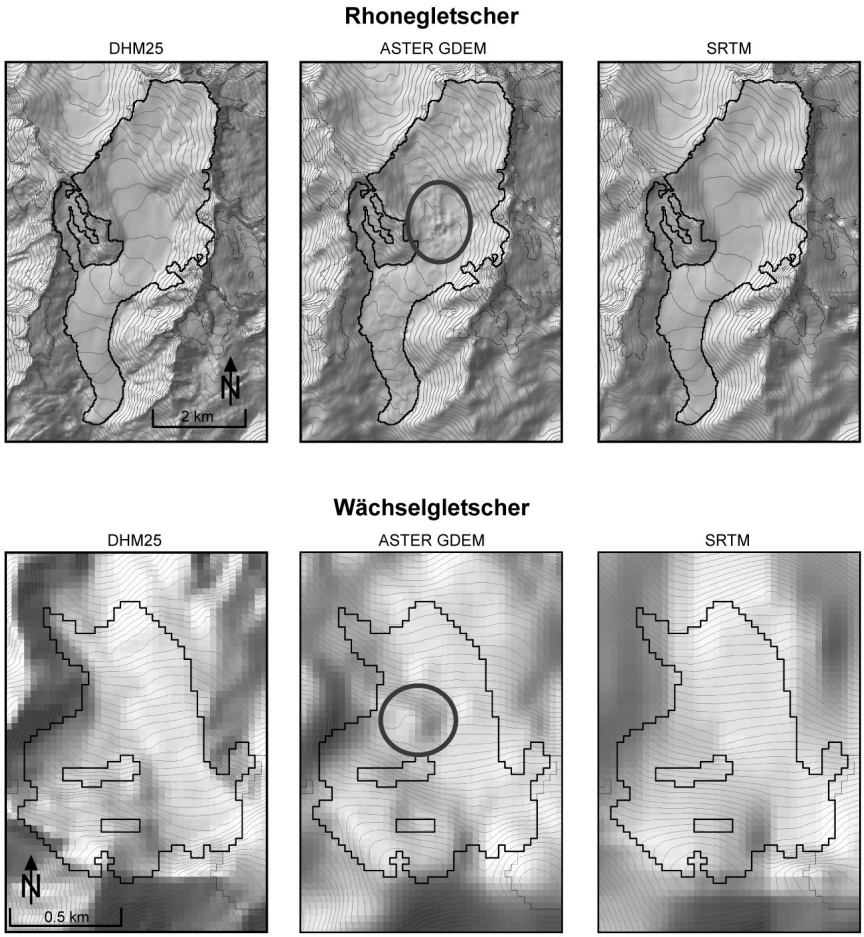

Fig. 7: Hillshade-views with contour lines for Rhonegletscher (top) and Wächselgletscher (bottom) from the three different DEMs. Equidistances are 50 m for Rhonegletscher and 20 m for Wächselgleschtscher. Grey circles indicate artifacts in the ASTER GDEM.

For Rhonegletscher, all three DEMs give similar hypsographies, even the artifacts in the ASTER GDEM in the central part of the glacier have little influence on the values (Fig. 8). The hypsography for Wächselgletscher from the SRTM DEM looks similar to the one from the DHM25, whereas the ASTER GDEM hypsography shows larger differences in the middle elevation ranges of this glacier. This may be caused by the artificial bump in the ASTER GDEM (Fig. 7). For this small glacier, the absolute differences in each 100 m elevation bin are in the same range as for Rhonegletscher, but the relative errors are much larger, in particular in the ASTER GDEM. However, other parameter values that are averaged over the total area do not show large differences, even for the small Wächselgletscher. Mean elevation difference values, for instance, are small: Compared to the value from DHM25 (2763 m.a.s.l.) the values differ by -26 m and -7 m in the two SRTM DEM versions (25 m and 100 m resolution) and 19 m and 24 m in the ASTER GDEM. Again, SRTM_100 and GDEM_25 show smaller differences than SRTM_25 and GDEM_100.

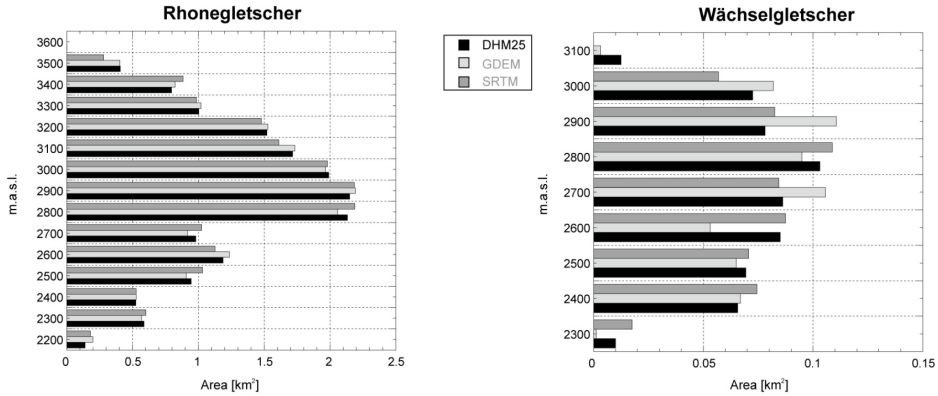

Fig. 8: Hypsographies of Rhonegletscher and Wächselgletscher derived from the three different DEMs.

5. Discussion

5.1 Results of this study

Two important findings emerge from the comparison of inventory parameters derived from the different DEM versions. First, both global elevation datasets (void-filled SRTM DEM and ASTER GDEM) are suitable for the compilation of topographic parameters in a glacier inventory. Although for individual glaciers and specific parameters large differences might occur, the performance over an entire inventory is adequate: the mean differences from the parameter values from the DHM25 are not larger than ±7 m for the elevation parameters, which is in the same order of magnitude than the vertical accuracy of these DEMs. Indeed, to some extent these differences can also be caused by real changes in glacier elevation due to glacier melt. Secondly, results from SRTM show slightly smaller differences from the reference values than the parameters derived with the ASTER GDEM. On the scale of individual glaciers the SRTM DEM has fewer artifacts as the GDEM (cf. Figs. 3 and 7). This is because with optical sensors the contrast over snow is low and correlation algorithms fail more often (Kääb, 2002; Svoboda and Paul, 2009). On the other hand, glacier surfaces are smooth compared to other high-mountain landforms and the SRTM DEM captures glaciers very well (Paul and Haeberli, 2008).

Local undulations and artifact-related roughness variations of the ASTER GDEM have only marginal effects on parameters that are averaged over the entire glacier (mean-, median elevation, mean slope and –aspect) as the averaging compensates for most of the deviations. In contrast, for maximum and minimum elevation only one cell counts. For these parameters, the errors in the ASTER GDEM have a larger influence as no averaging is applied for the calculation of the value. In particular maximum elevation is error prone, as these regions are often located in low-contrast or shadowed terrain (Kääb et al., 2003). This is confirmed by the higher standard deviations for this parameter compared to the others (cf. Table 2). Minimum and maximum elevation are also influenced by the spatial resolution of the DEM. Due to the smoothing of the terrain at a lower spatial resolution, both tend to increase or decrease, respectively (cf. Fig. 4).

Our analysis reveals that the use of SRTM for the calculation of glacier inventory parameters it slightly preferable over the ASTER GDEM from a theoretical point of view and the comparison in this region. If both DEMs are available, it is recommended to carefully analyze them over glaciers, using hillshade views and a visualization of their differences. This might lead to favor the GDEM over SRTM in other regions. Nuth and Kääb (2011) suggest a

methodological framework that should be applied to DEMs before they are used for glaciological applications. North of 60° N and south of 56° S, where many unmapped and huge glaciers and icecaps are located (Cogley, 2009), the GDEM is often the only available dataset. In any case, the availability of local or national DEMs (e.g. from national mapping agencies) should be investigated as they might be even better suited. The better performance of SRTM in this study is in contrast to the study by Hayakawa et al. (2008), who find the ASTER GDEM performing better for geoscientific studies. We assume that glaciers are a special case in this regard due to their particular reflectance and geomorphometric properties.

The main difficulties of assessing the quality differences between the three DEMs emerge from the interpretation of the DEM differences (see section 4.1 and Fig. 3). Those differences can be explained by three factors: (a) the type of dataset, (b) the acquisition technique, and (c) real changes like surface lowering between the acquisition dates. In regard to (a), it is important to consider that the DHM25 is a terrain model, which represents the topography of the Earth's surface without vegetation and buildings, whereas SRTM and the GDEM represent the surface including vegetation and snow (in principle also buildings, but they are too small to be resolved at these resolutions). Additionally, the lower resolution of the SRTM DEM influences the differences by underestimating the elevation of ridges and overestimating the elevation of narrow valleys (Paul, 2008).

Moreover, the acquisition technique (b) influences the elevation values, as the C-band radar from SRTM penetrates a dry snow pack and the vegetation to a certain extent (e.g. Rignot et al., 2001; Carabajal and Harding, 2006), and the low optical contrast of snow-covered regions reduces the quality of the ASTER GDEM over glaciers. Finally (c), real changes such as surface lowering over glaciers took place between the acquisitions of the different DEMs. While the former effect can be used to assess glacier volume changes over time (e.g. Larsen et al., 2007; Paul and Haeberli, 2008), it also influences the values obtained in this study.

Whereas real elevation changes over time are likely small at the highest glacier point (i.e. maximum elevation should only change due to the characteristics of the respective DEM), elevation changes at the lowest glacier parts could be large. The related effects for the here used constant glacier extents are described in section 1.2. For the averaged parameters mean and median elevation, the change in surface elevation might also play a role. In principle, both should lower through time for the same glacier when the surface itself is lowered. Actually, such a trend can be observed for the comparison of the DHM25 with SRTM, but it is vice versa for the GDEM (i.e. the GDEM surface is often higher than SRTM). This can also be seen in the direct comparison of Fig. 3. The differences of mean and median elevation between the DHM25 and the GDEM thus largely result from the GDEM characteristics, whereas the respective SRTM-derived parameter values are slightly lower for the lager glaciers.

From a theoretical point of view, mean slope should increase for a glacier surface with a stronger surface lowering towards its lower parts, but a recognizable effect is only expected for large glaciers with tongues at low elevations that experienced a sufficiently strong lowering. For the ASTER GDEM the influence of this effect should be smaller as the elevation differences to the earlier DHM25 are more irregular (see Fig. 3). Mean aspect should not be influenced from the elevation change over time, as the required strong local changes in elevation are difficult to achieve from natural processes. In fact, both parameters show neither a trend with glacier size nor with the acquisition date of the respective DEM, confirming the above theoretical considerations.

5.2 General findings

For the compilation of topographic glacier inventory parameters, the acquisition year of the DEM and the glacier outlines should be close, because changes in glacier extent directly affect topographic parameters. Elevation changes caused by glacier retreat or advance are particularly strong close to the glacier terminus. Hence, for minimum elevation it is recommended to consider the DEM that has been acquired most closely to the acquisition date of the glacier outlines. In particular in phases of glacier retreat, minimum elevation should be calculated with a DEM acquired after the glacier outlines, otherwise this parameter might be measured on the old glacier surface and will therefore be too high. But this has actually only a small influence on the value of minimum elevation when glacier outlines of a larger, previous extent are used, as the point of the measurement will be located in the stable glacier forefield. In reality the glacier terminus might have retreated to a slightly higher elevation.

One of the major drawbacks of the ASTER GDEM is the undefined acquisition date as it is based on ASTER scenes acquired between 2000 and 2007. This terrain thus represents a somehow averaged mean value over a 7-year period. The elevation changes visible in Fig. 3 are thus difficult to interpret. For SRTM, the acquisition date is well defined (11-22 February 2000), but many uncertainties emerge from the unknown radar penetration and the interpolated topography in the voids of the original data. In these regions only artificial terrain without a date is represented. The elevation values from the interpolated regions can have a considerable influence on the topographic parameters of the investigated glaciers, in particular when they are large compared to the glacier size. In total, data voids in SRTM affect more than 50% of the glaciers and 5% (54 km^2) of their total area. Some of the outliers visible in the scatter plots of Fig. 5 are likely due to such voids. The locations of data voids in the original SRTM3 version are more slope-dependent rather than aspect-dependent: the increasing roughness of the terrain leads to more frequent data voids (Hall et al., 2005).

As a consequence of the sun-synchronous orbit of the Terra spacecraft, ASTER scenes are acquired always around 10:30 a.m. local time. This implies similar illumination azimuths in all scenes, i.e., in the mid-latitudes of the northern hemisphere the sun is in the south-east at this time and, hence, in the shadowed north and north-west exposed steep slopes the quality of the ASTER GDEM is inferior compared to slopes in other expositions. Additionally, they are often totally hidden for the back-looking telescope (Kääb et al., 2003). This is confirmed in this study with median elevation values showing larger differences for northerly exposed glaciers (Fig. 6). Though, the ASTER GDEM shows partly more details than the SRTM DEM, it has also more artifacts, even in glacier regions at low elevations. This might be caused by the use of partly snow-covered scenes for the compilation of this dataset. It has also to be mentioned, that the resolved topographic detail in the ASTER GDEM appears to be similar to SRTM, i.e. lower than the 30 m cell size of the dataset promises.

On a global scale, the quality of the ASTER GDEM varies from region to region, as the conditions of the source images can be constantly poor, for example due to frequent cloud cover or long-lasting snow cover. The‘num’-file provided with each ASTER GDEM tile contains for each cell the number of scenes used to derive the DEM. This information allows the identification of regions where only few scenes were used for DEM production. This might be used as an indicator of lower DEM quality and a higher probability of artifacts. For the ASTER GDEM mosaic used in this study, on average 12.8 ASTER scenes were used to compile the DEM (with a range from 1 to 46).

Both global DEMs analyzed here can be used to derive glacier specific hypsographies at 100 m elevation bins. Small glaciers in steep and shadowed slopes are more susceptible to artifacts, whereas errors tend to be more smoothed for larger glaciers. A comparison of the hypsographies of all glaciers (not shown here) revealed that the differences between the two

DEMs are small in the mean (mostly less than 1%) except for the lowest and highest elevation bands where the total glacier area is less than 0.1 km^2 in the DHM25. From the analysis of the elevation depended differences we conclude that the surface lowering at low elevations between the different DEM dates can be recognized for the tongues of the largest glaciers, but not for the smaller glaciers. Here the artifacts cause more irregular differences.

6. Conclusions

Based on the analysis and results of this study, we make the following conclusions:

- Both global DEMs (SRTM and ASTER GDEM) are suitable for the compilation of topographic glacier inventory parameters.
- For regions where SRTM data are available but no local DEM of higher quality is at hand, the use of the SRTM DEM is preferable over ASTER GDEM. Radar systems have advantages over optical systems for DEM acquisition due their ability to penetrate clouds and their independence from optical contrast. The relatively smooth geometry of glaciers and the low optical contrast of snow covered areas also favor radar systems.
- On the scale of individual glaciers, larger differences to reference values might occur, but careful analyses and elimination of artifacts can reduce them.
- For larger glacier samples mean differences to the reference values are small for all investigated parameters.
- A resampling to a resolution close to the original resolution of the dataset (i.e., 90 m for SRTM, 30 m for the ASTER GDEM) leads to slightly smaller differences of the derived parameters to the reference value.
- A coarser DEM resolution decreases maximum and increases minimum elevation, but the other parameters are nearly unchanged.
- Differences from reference values are larger for parameters that depend on single cell values (minimum and maximum elevation), than for the other parameters, which are averaged over the entire glacier area. These single-cell values also depend more strongly on the resolution of the DEM. Furthermore, the differences from reference values are generally larger for north-exposed glaciers.
- For the calculation of minimum elevation, the acquisition date of the DEM should be as close as possible to the acquisition date of the glacier outlines, especially in regions with strong changes in glacier extent. For glaciers in retreat, the DEM should not be older than the glacier outlines (and vice versa).

Many inventoried glaciers in the GLIMS database are lacking topographic parameters, although it is important that existing and newly compiled glacier inventories include such topographic information for various applications. We therefore recommend supplementing current glacier outlines in the GLIMS database with topographic information based on either the SRTM DEM, the ASTER GDEM or any DEM of higher quality and appropriate temporal coincidence with the acquisition date of glacier outlines. These parameters can be automatically calculated from existing and freely available DEMs and would make a significant contribution to our understanding of the world's glaciers and ice caps.

Acknowledgements

We are indebted to two anonymous reviewers for their helpful comments on the manuscript. Furthermore, we would like to thank J. Fiddes for improving the language. The DHM25 is a product of swisstopo and it is reproduced with the permission of swisstopo (BA100734). The ASTER GDEM is a product of METI and NASA; SRTM is a product of NASA, the void-filled version used in this study is produced by CGIAR-CSI. This study was funded by the ESA Project GlobGlacier (21088/07/I-EC).

References

Abrams, M., Bailey, B., Tsu, H., Hato, M., 2010. The ASTER Global DEM. Photogrammetric Engineering and Remote Sensing 76 (4), 344–348.

Bolch, T., Menounos, B., Wheate, R., 2010. Landsat-based inventory of glaciers in western Canada, 1985-2005. Remote Sensing of Environment 114, 127-137.

Carabajal, C.C., Harding, D.J., 2006. SRTM C-band and ICESat laser altimetry elevation comparisons as a function of tree cover and relief. Photogrammetric Engineering and Remote Sensing 72 (3), 287-298.

Cogley, J.G., 2009. A more complete version of the World Glacier Inventory. Annals of Glaciology 50 (53), 32-38.

Evans, I.S., 2006. Local aspect asymmetry of mountain glaciation: A global survey of consistency of favoured directions for glacier numbers and altitudes. Geomorphology 73, 66-184.

Farr, T.G., Rosen, P.A., Caro, E., Crippen, R., Duren, R., Hensley, S., Kobrick, M., Paller, M., Rodriguez, E., Roth, L., Seal, D., Shaffer, S., Shimada, J., Umland, J., Werner, M., Oskin, M., Burbank, D., Alsdorf, D., 2007. The Shuttle Radar Topography Mission. Reviews in Geophysics 45 (2), 1-33.

GCOS, 2006. Systematic observation requirements for satellite-based products for climate. Supplemental details to the satellite-based component of the "Implementation Plan for the Global Observing System for Climate in Support of the UNFCCC". GCOS Reports - 107 (WMO/TD No. 1338).

Haeberli, W., Hoelzle, M., 1995. Application of inventory data for estimating characteristics of and regional climate-change effects on mountain glaciers: a pilot study with the European Alps. Annals of Glaciology 21, 206-212.

Hall, O., Falorni, G. and Bras, R.L., 2005. Characterization and Quantification of Data Voids in the Shuttle Radar Topography Mission Data. IEEE Geoscience and Remote Sensing Letters 2 (2), 177-181.

Hayakawa, Y.S., Oguchi, T., Lin, Z., 2008. Comparison of new and existing global digital elevation models: ASTER G-DEM and SRTM-3. Geophysical Research Letters 35, L17404.

Hebeler, F., Purves, R.S., 2009. The influence of elevation uncertainty on derivation of topographic indices. Geomorphology 111, 4-16.

Hock, R., De Woul, M., Radić, V., Dyurgerov, M., 2009. Mountain glaciers and ice caps around Antarctica make a large sea-level rise contribution. Geophysical Research Letters 36, L07501.

Kääb, A., 2002. Monitoring high-mountain terrain deformation from repeated air- and spaceborne optical data: examples using digital aerial imagery and ASTER data. ISPRS Journal for Photogrammetry and Remote Sensing 57, 39-52.

Kääb, A., Paul, F., Maisch, M., Hoelzle, M., Haeberli, W., 2002. The new remote-sensing-derived Swiss glacier inventory: II. First Results. Annals of Glaciology, 34, 258-264.

Kääb, A., Huggel, C., Paul, F., Wessels, R., Raup, B., Keiffer, H., Kargel, J.S., 2003. Glacier monitoring from ASTER imagery: Accuracy and applications. EARSeL eProceedings 2, 43-53.

Kargel, J.S., Abrams, M.J., Bishop, M.P., Bush, A., Hamilton, G., Kääb, A., Kieffer, H.H., Lee, E.M., Paul, F., Rau, F., Raup, B., Shroder, J.F., Soltesz, D., Stearns, L., Wessels, R., 2005. Multispectral imaging contributions to Global Land Ice Measurements from Space. Remote Sensing of Environment 99, 187-219.

Larsen, C.F., Motyka, R.J., Arendt, A.A., Echelmeyer, K.A., Geissler, P.E., 2007. Glacier changes in southeast Alaska and northwest British Columbia and contribution to sea level rise. Journal of Geophysical Research 112, F01007.

METI, 2009. Distribution of ASTER Global Digital Elevation Model (ASTER G-DEM). Press release by Ministry of Economy, Trade, and Industry (METI), 29 June 2009. (http://www.meti.go.jp/english/press/data/20090626_03.html; accessed February 2011).

METI, NASA, & USGS, 2009. ASTER GDEM Validation. Summary Report, 28 pp.

Möller, M., Schneider, C., 2010. Volume change at Gran Campo Nevado, Patagonia, 1984-2000: a reassessment based on new findings. Journal of Glaciology 56 (196). 363-364.

Nuth, C., Kääb, A., 2011. Co-registration and bias corrections of satellite elevation data sets for quantifying glacier thickness change. The Cryosphere, 5, 271–290. doi:10.5194/tc-5-271-2011

Paul, F., 2007. The New Swiss Glacier Inventory 2000 - Application of Remote Sensing and GIS. Schriftenreihe Physische Geographie 52. PhD thesis, University of Zurich.

Paul, F., 2008. Calculation of glacier elevation changes with SRTM: is there an elevation-dependent bias?. Journal of Glaciology 54 (188), 945-946.

Paul, F., Haeberli, W., 2008. Spatial variability of glacier elevation changes in the Swiss Alps obtained from two digital elevation models. Geophysical Research Letters 35, L21502. F

Paul, F., Kääb, A., Maisch, M., Kellenberger, T.W., Haeberli, W., 2002. The new remote-sensing-derived Swiss glacier inventory: I. Methods. Annals of Glaciology 34, 355-361.

Paul, F. Maisch, M., Rothenbühler, C., Hoelzle, M., Haeberli, W., 2007. Calculation and visualisation of future glacier extent in the Swiss Alps by means of hypsographic modelling. Global and Planetary Change 55 (4), 343-357.

Paul, F., Barry, R.G., Cogley, J.G., Frey, H., Haeberli, W., Ohmura, A., Ommanney, C.S.L. Raup, B., Rivera, A., Zemp, M., 2009. Recommendations for the compilation of glacier inventory data from digital sources. Annals of Glaciology 50 (53), 119-126.

Radić, V., Hock, R., 2010. Regional and global volumes of glaciers derived from statistical upscaling of glacier inventory data. Journal of Geophysical Research 115, F01010.

Raper, S.C.B., Braithwaite, R.J., 2006. Low sea level rise projections from mountain glaciers and icecaps under global warming. Nature 439, 311-313.

Raup, B., Racoviteanu, A., Khalsa, S.J.S., Helm, C., Armstrong, R., Arnaud, Y., 2007. The GLIMS geospatial glacier database: A new tool for studying glacier change. Global and Planetary Change 56, 101-110.

Reuter, H.I., Nelson, A., Jarvis, A., 2007. An evaluation of void filling interpolation methods for SRTM data. International Journal of Geographic Information Science 21, 983-1008.

Rignot, E., Echelmeyer, K., Krabill, W., 2001. Penetration depth of interferometric synthetic-aperture radar signals in snow and ice. Geophysical Research Letters 28 (18), 3501-3504.

Svoboda, F., Paul, F., 2009. A new glacier inventory on southern Baffin Island, Canada, from ASTER data: I. Applied methods, challenges and solutions. Annals of Glaciology, 50 (53), 11-21.

Swisstopo, 2004. DHM25 - The digital height model of Switzerland. Product Information. (http://www.swisstopo.admin.ch/internet/swisstopo/en/home/products/height/dhm25.html; accessed February 2011).

Toutin, T., 2008. ASTER DEMs for geomatic and geoscientific applications: a review. International Journal of Remote Sensing 29 (7), 1855-1875.

Paper II

Frey, H., Paul, F., and Strozzi, T. (in rev.). Compilation of a glacier inventory for the western Himalayas from satellite data: Methods, challenges and results. *Remote Sensing of Environment*

Compilation of a glacier inventory for the western Himalayas from satellite data: Methods, challenges and results

Holger Frey[1] +, Frank Paul[1], Tazio Strozzi[2]

[1]Department of Geography, University of Zurich, Switzerland
[2]Gamma Remote Sensing, Gümligen, Switzerland

[+]Corresponding author (holger.frey@geo.uzh.ch)

submitted to Remote Sensing of Environment

Abstract

Due to their sensitive reaction to changes in climatic conditions, glaciers have been selected as an essential climate variable (ECV). Although a large amount of ice is located in the Himalayas, this region is yet only sparsely represented in global glacier databases. Accordingly, a sound and comprehensive change assessment or determination of water resources was yet not possible. In this study, we present a new glacier inventory for the western Himalayas that was compiled from Landsat ETM+ scenes acquired between 2000 and 2002, coherence images from the ALOS PALSAR image pairs, the SRTM digital elevation model (DEM) and the ASTER Global DEM (GDEM). Several specific challenges for glacier mapping were found in this region and addressed. They are related to debris cover, orographic clouds, locally variable snow conditions, and creeping permafrost features in cold-dry regions. Additional to seven topographic parameters that are obtained from the ASTER GDEM for each glacier, we also determined the relative amount of debris cover on the glacier surface. The inventory contains 11'550 glaciers larger than 0.02 km^2, which cover a total area of 9370 km^2. A more detailed analysis of the inventory data revealed a dependency of the mean glacier elevation and the relative amount of debris cover on the highly variable climatic conditions (e.g. in precipitation amounts) within the mountain range. The full dataset will be made freely available in the GLIMS glacier database to foster further analyses and modeling of the glaciers in this region.

Keywords: Himalaya, glacier inventory, glacier mapping, debris-covered glaciers, coherence images, SRTM, ASTER GDEM, glacier characteristics

1. Introduction

The creation of glacier inventories from automated multi-spectral classification of optical satellite data in combination with a digital elevation model (DEM) is meanwhile a well-established procedure (e.g. Andreassen et al., 2008; Bolch et al., 2010; Paul & Kääb, 2005; Paul et al. 2009). There is also no question that a globally complete and detailed glacier inventory is urgently required (e.g. Cogley, 2009; GCOS, 2006; Ohmura, 2009) for a wide range of purposes, among others the modeling of the past and future contribution of glaciers to global sea-level rise (Hock et al., 2009; Kaser et al., 2006; Raper & Braithwaite, 2006;), determination of water resources and hydrological modeling on a regional scale (Koboltsching et al., 2008, Kaser et al. 2010), as well as for accurate assessment of glacier changes (e.g. Paul et al., 2004). In particular the latter requires the availability of digital vector lines to refer glacier-specific changes to exactly the same entities.

For the heavily glacierized region of the Himalaya (also called the 'Third pole') all of the above purposes apply, but very little information is available in digital form for sound assessments. This results in high uncertainties when local observations need to be generalized (Raina, 2009). Though strong efforts have been made recently to make glacier extents for the Himalaya region available, large parts are still missing in the glacier database of the global land ice measurements from space (GLIMS) initiative (cf. Raup et al., 2007). The uncertainties and limited knowledge recently launched debates in the media about state and future developments of glaciers in this region (Cogley et al., 2010; Schiermeier, 2010) One of the regions with missing glacier outlines is the western Himalayan part of India, which was hence selected as a key region for this study. Glacier as essential climate variables (ECVs) are easily understandable and reliable climate indicators, which makes their investigation especially important in regions with sparse climatic records and where is still under debate whether climate change is occurring or not (Roy & Balling, 2004; Yadav et al., 2004).

There are a number of glaciological studies in this region focusing on individual glaciers or on glacier inventories of smaller sub basins (e.g. Bhambri et al., in press; Kulkarni et al., 2007). Namely on Chhota Shigri glacier, which is part of the mass balance network of the World Glacier Monitoring Service (WGMS) since 2003 (WGMS, 2007), a lot of research related to mass balance observation has been done (e.g. Hasnain et al., 2010; Kumar & Dobhal, 1997). Bhambri and Bolch (2009) provide an overview of studies and data obtained for Indian glaciers and give an overview of glacier mapping methods. Racoviteanu et al. (2008) describes techniques to map Himalayan glaciers based on optical satellite imagery using semi-automated techniques. Due to the remoteness and difficult access to many of these glaciers, field observations are very laborious and time consuming. However, satellite data provide an ideal tool to investigate glaciers in this part of the world. Besides mapping of glacier outlines, remote sensing techniques were also used for assessing mass balance, volumetric changes and mass loss of Indian glaciers (e.g. Berthier et al., 2007; Kulkarni et al., 2004; Matsuo & Heki, 2010).

Dyurgerov and Meier (2005) estimated that glaciers in the entire Himalayas might cover about 33000 km^2. However, a freely available and comprehensive inventory of these glaciers in digital format does not exist. There are efforts made by Indian governmental institutions to complete a national glacier inventory (Raina & Shrivastava, 2008; Sangewar & Shukla, 2009), which partly includes inventory work already compiled for several basins (e.g. Kaul, 1999, Vohra, 2010). These inventories are in tabular form, including topographic information such as minimum and maximum elevation, mean elevation of accumulation and ablation region, maximum glacier length, mean width, area, accumulation area ratio (AAR), and estimation of mean depth and resulting glacier volume. Glacier outlines were obtained from topographic maps with additional information from aerial photography and satellite imagery if available. But as these outlines are not available in a digital form, it is difficult to assess the quality and accuracy of these datasets. In most cases, it looks like the efforts focused on the tongues of larger glaciers as glacier boundaries in the accumulation regions seem to be strongly generalized and for some studies smaller glaciers are missing completely.

In general, a whole range of glacier inventories can be distinguished with the main differences being related to issues like: (1) digital or analog (printed) form, (2) point information (all data related to coordinates) or vector outlines, (3) data compiled based on maps or satellite imagery, using (4) mostly automated or manual digitization with the work done by (5) glaciologists or cartographers. Of course, when any of these issues are different for two inventories that should be compared, a change in glacier area might be observed independent of a real change. This greatly reduces the possibility for a sound change assessment when inventories from two different sources are compared.

To overcome the major shortcomings of this situation, we here present a digital glacier inventory in vector format that has been compiled using semi-automated mapping techniques applied to different kinds of satellite imagery. For the special challenges in this region such as heavily debris-covered glacier tongues, frequent orographic clouds, seasonal snow, and glaciers ending in permafrost, we present best effort approaches to solve them. In particular we apply a recently introduced new technique for improved delineation of debris-covered glaciers with coherence images from the ALOS PALSAR sensor (Atwood et al. 2010, Strozzi et al. 2010). Without this information it turned out to be very difficult to identify the boundary of debris-covered glacier parts with sufficient quality.

2. Study region and data

2.1. Study region

The study region covers an area of more than 100'000 km^2 and reaches from the town Kargil and the Amarnath caves near Srinagar in the Northwest to the Tehri dam and the Alaknanda basin in southeast (Fig. 1). Most of the glaciers are located in India, including the states of Jammu and Kashmir, Himachal Pradesh, and Uttaranchal, but some glaciers northwest of the Himalayan main range are located in the territory of the autonomous region Tibet (China). It includes the parts of the Ladakh Range south of Indus, the Zanskar Range and parts of the Garhwal Himalaya.

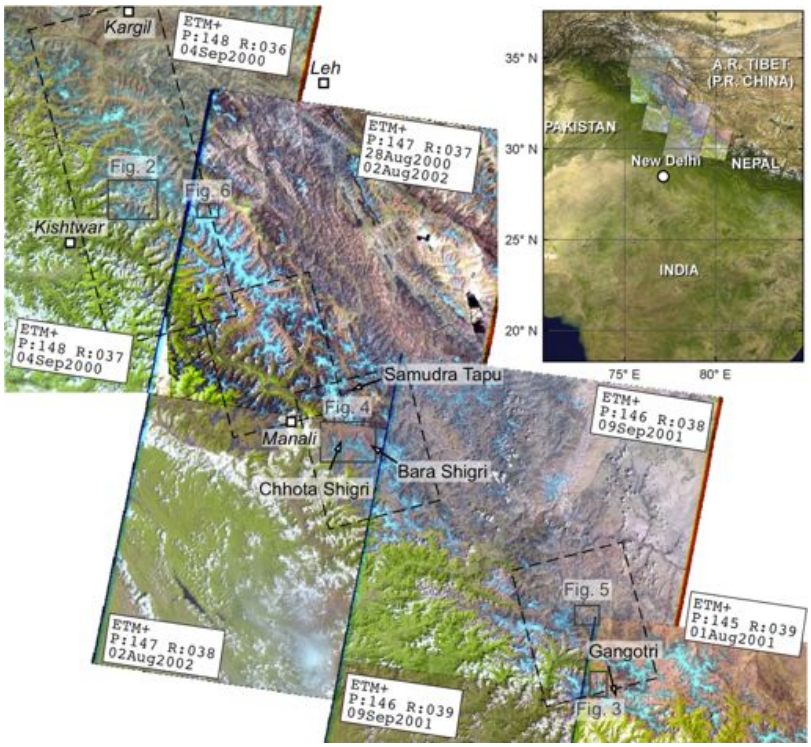

Fig. 1: Overview of the study region, satellite data and location of figures, map in the top right corner shows the surrounding territories. Dashed rectangles indicate the outlines of the coherence images.

Precipitation patterns are governed by the Indian summer monsoon and the mid-latitude westerlies (Böhner, 2006). This results in decreasing amounts of precipitation from south to north due to the barrier effect of the mountain range and an east-west gradient caused by the weakening influence of the summer monsoon (Bookhagen & Burbanks, 2006). The latter is compensated to a certain degree by the growing influence of the moisture-bearing westerly winds in the western Himalayas (Hatwar et al., 2005).

2.2. Satellite scenes

The USGS archive (http://glovis.usgs.org) was searched for Landsat scenes of the study region with as low snow and cloud cover as possible and therefore suitable for automated glacier mapping. Our time horizon was the year 2000 ±2 years to have a good temporal agreement with the digital elevation model (DEM) from SRTM. We finally selected three scenes from 2000, three from 2001 and two from 2002 (due to complementary cloud cover, two scenes were chosen for P147R037, one from 2000 and one from 2002). Table 1 gives an overview on the used satellite data. To facilitate the mapping of debris-covered glaciers parts, coherence images were created from four ALOS PALSAR image pairs. The sequential ALOS PALSAR scenes have been acquired from the ascending orbit in Fine-Beam Dual mode (FBD - HH/HV) with a 275 m baseline and a 46 days time interval during the snow-free period in 2007 (cf. 3.1.2 and Tab.1).

Table 1: List of used satellite data.

Purpose	Platform and Sensor	ID (P=path, R=row, T=Track, F=Frame, B=Baseline)		Date (dd/mm/yyyy)
Glacier mapping	Landsat ETM+	P:145 R:039		01/08/2001
	Landsat ETM+	P:146 R:038		09/09/2001
	Landsat ETM+	P:146 R:039		09/09/2001
	Landsat ETM+	P:147 R:037		28/08/2000, 02/08/2002
	Landsat ETM+	P:147 R:038		02/08/2002
	Landsat ETM+	P:148 R:036		04/09/2000
	Landsat ETM+	P:148 R:037		04/09/2000
Coherence images	ALOS PALSAR	T:525 F:650-670	B:275m	12/07/2007, 27/08/2007
	ALOS PALSAR	T:524 F:640	B:46m	10/08/2007, 25/09/2007
	ALOS PALSAR	T:523 F:630	B:270m	27/07/2007, 08/09/2007
	ALOS PALSAR	T:521 F:610	B:-216m	05/08/2007, 20/09/2007

On the pre-processing stage, the selected Landsat ETM+ scenes were downloaded and different color composites were generated (RGB 321 for near true-color images and RGB 543 for discriminating clouds, ice, snow and debris). In the USGS archive, all scenes are in Universal Transverse Mercator (UTM) projection, with the scene center coordinates defining the zone. The scenes in our study region belong to UTM zones 43N and 44N and for practical purposes we decided to have the mosaiced inventory in a single UTM zone (43N).

2.3. Digital Elevation Models

To derive specific topographic inventory parameters such as minimum-, maximum-, mean-, and median elevation, mean slope, and mean aspect, a DEM of appropriate quality and resolution is required (Paul et al., 2009). For the study region, no local or national DEM with such conditions is publicly available. However, with the DEM from the Shuttle Radar Topography Mission (SRTM) and ASTER GDEM, there are two DEMs available, which cover almost the entire world, at least outside the polar regions, and that fulfill the requirements to be used for compiling topographic glacier inventory data (Frey & Paul, subm.). The SRTM DEM has been used in numerous glaciological studies, mainly related to the assessment of ice volume variations with time (e.g. Berthier et al., 2007; Paul & Haeberli, 2008; Schiefer et al., 2007; Surazakov and Aizen, 2006); on the other hand only a few studies used the ASTER GDEM so far (e.g. Shugar et al., 2010). The SRTM DEM was acquired using radar interferometry (InSAR) (Farr et al., 2007), which causes data voids, especially in rough high-

mountain terrain due to radar shadow and layover effects. The Consultative Group for International Agriculture Research (CGIAR) compiled a void-free version (SRTM3v4) by interpolating the terrain in data voids. This void-free version of SRTM is available in 5 by 5 degree tiles. Tile 'srtm_52_06' covers the entire study region and was downloaded from CGIAR (http://srtm.csi.cgiar.org/, accessed March 2011, Tab. 2). It has to be noted that also the operational orthorectification provided for the level 1T product of Landsat imagery from USGS is based on the GLSDEM, which consists of this void-filled SRTM version in this region. Hence, elevation errors in this DEM cause geolocation shifts in the provided satellite imagery.

The ASTER GDEM with a spatial resolution of 30 m was compiled by applying automated photogrammetric techniques to all suitable scenes available from the ASTER data archive (Hayakawa et al., 2008). Especially in rough terrain and in accumulation regions with reduced optical contrast, artifacts like local bumps and holes are frequent and reduce the quality of this data. Frey and Paul (subm.) found in a study for the Swiss Alps that the topographic parameters derived from SRTM are slightly more accurate than the ones derived from the ASTER GDEM, but both datasets can be used for this purpose. To cover the entire study region, 16 ASTER GDEM tiles with a 1 by 1 degree coverage were downloaded.

Table 2: *List of used DEM tiles*.

Dataset	ID
ASTER GDEM	N30E078, N30E079, N30E080
ASTER GDEM	N31E077, N31E078, N31E079
ASTER GDEM	N32E076, N32E077, N32E078, N32E079
ASTER GDEM	N33E075, N33E076, N33E077, N33E078
ASTER GDEM	N34E075, N34E076
SRTM3v4	srtm_52_06

Initially, our intention was to use the void-filled version of the SRTM DEM for this study, because it is more consolidated than the ASTER GDEM. However, after downloading the tile and reprojecting it from WGS84 to UTM Zone 43N, we realized that large parts of the tile are affected by gross artifacts. Subtracting the ASTER GDEM from SRTM revealed in many regions differences of several hundred meters up to 1.5 km (Fig. 2a). By extracting the extents of the data voids from the original SRTM3 version (without void filling, downloaded from USGS), we then found that the large differences are congruent with the data voids. This suggests that these differences are caused by erroneous interpolations in the SRTM data voids. In the hillshade-views of the DEMs (Figs. 2b and 2c), this becomes clearly visible: although the interpolated terrain in the SRTM voids looks reasonable, all the interpolated regions seem to be systematically too low, resulting in distinct shadows in the hillshade-view at the margins of these crater-like features. Here, the SRTM measured terrain drops down to the interpolated surface. The ASTER GDEM on the other hand shows some of the typical artifacts, but is much more consistent throughout the whole study region. We thus decided to use here the ASTER GDEM instead of SRTM, as the gross errors in the interpolated voids of SRTM would have a strong negative influence on the topographic parameters and the calculation of drainage divides. However, for the processing of the ALOS PALSAR coherence images (cf. 3.1.2.) we stuck to the SRTM DEM to remove the topographic related phase and for terrain geocoding. This is because the artificial bumps and holes of the ASTER GDEM are introducing artifacts nearly impossible to be detected and removed. On the other hand, the SRTM DEM has a validity mask that was applied to the coherence images before analyzing them for terrain properties.

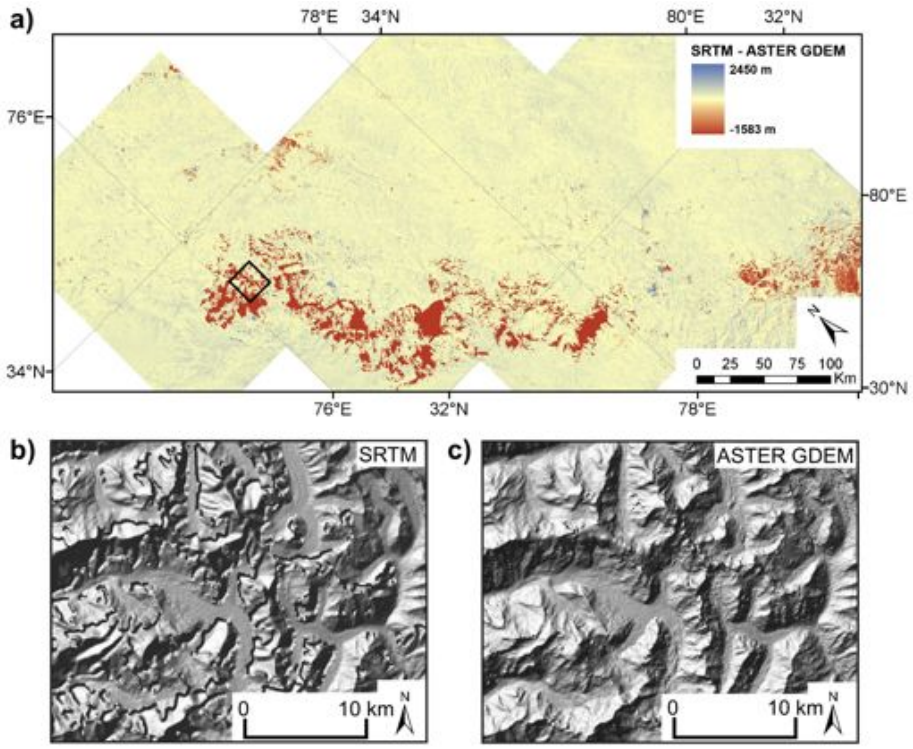

Fig. 2: a) Difference of SRTM – ASTER GDEM for the whole extent of the ASTER GDEM mosaic. Red areas (void-filled SRTM up to 1.5 km lower than ASTER GDEM) are congruent with data voids in the SRTM raw version. The black rectangle indicates the location of the hillshade views shown in b) and c) (with illumination coming from northwest). b) Zoom to the hillshade view of SRTM, c) zoom to the hillshade view of ASTER GDEM. Note the artifacts in the SRTM DEM, causing the large differences shown in a). The dark parts at margins of the interpolated data voids are shadow areas caused by the fall of the terrain of several hundred meters.

3. Methods

3.1. Glacier mapping

On the main-processing stage, we computed band ratios of band 3 (green, TM3) and band 5 (short wave infrared (SWIR), TM5), with a specific threshold applied to each scene (Bolch et al., 2010; Paul et al., 2002; Paul et al., 2009). Due to the rather strong contrast between ice/snow and rock/debris, the mapping result was not very sensitive to changes of the thresholds and mapping results for thresholds between 1.8 and 2.2 varied only slightly. One reason for this is the relatively high sun elevation in these low latitudes (in all scenes the sun elevation at acquisition was between 55° and 63°), which results in only small glacier regions in cast shadow. We therefore resigned to apply an additional threshold to band 1 as suggested by Paul & Kääb (2005). As a last step of the main processing, a 3x3 kernel size median filter was applied to reduce noise, i.e. to eliminate isolated pixels and fill small gaps in glacier areas.

The more time-consuming part of the glacier mapping is related to the post-processing stage, where all misclassifications need to be manually corrected. This includes elimination of erroneously classified features like turbid water surfaces (lakes and wide rivers), clouds and remaining snow avalanche deposits as well as mapping of debris-covered glacier parts. The latter are widespread in the Himalayas, in particular in the ablation zones of large valley glaciers. The editing work was performed within a Geographic Information System (GIS), where the false color composites were imported in Geo-TIFF format and the raw glacier map (binary image) was converted to vector format before the manual editing (cf. Paul et al. 2002).

The separate acquisition of clean ice areas (automated) and debris-covered glacier parts (manual delineation), allows a straightforward distinction of debris-covered and debris-free regions. To keep record of this information, the amount of debris-cover on the total glacier area is stored for each glacier. This allows specific analyses of these glacier regions and is valuable information for various modeling applications concerning for instance future glacier developments (Quincey et al., 2007) and melt water production (e.g., Huss et al., 2008; Kaser et al., 2010).

3.1.1. Multitemporal mapping of cloud-covered glaciers

In particular on the southern margin of the Himalayan range orographic clouds are prevalent due to lift up of moisture transported by monsoon winds. These clouds cover glaciers partly or entirely and make their complete mapping often impossible. In some cases overlapping neighboring scenes or a scene from another date was used to map the hidden glaciers or missing parts (Fig. 3). To keep track of the source scene for each glacier, a 'scene' field with the ID (path and row) and the date of the source satellite image was added to the database. However, since glaciers are affected by clouds in all scenes, we further added a field 'cloud_cov', which indicates whether a glacier polygon is affected by cloud cover ('cloud_cov' = 1) or not ('cloud_cov' = 0). This allows us to exclude only partly mapped glaciers from further analyses, but still keep the mapped parts of their outlines in the database.

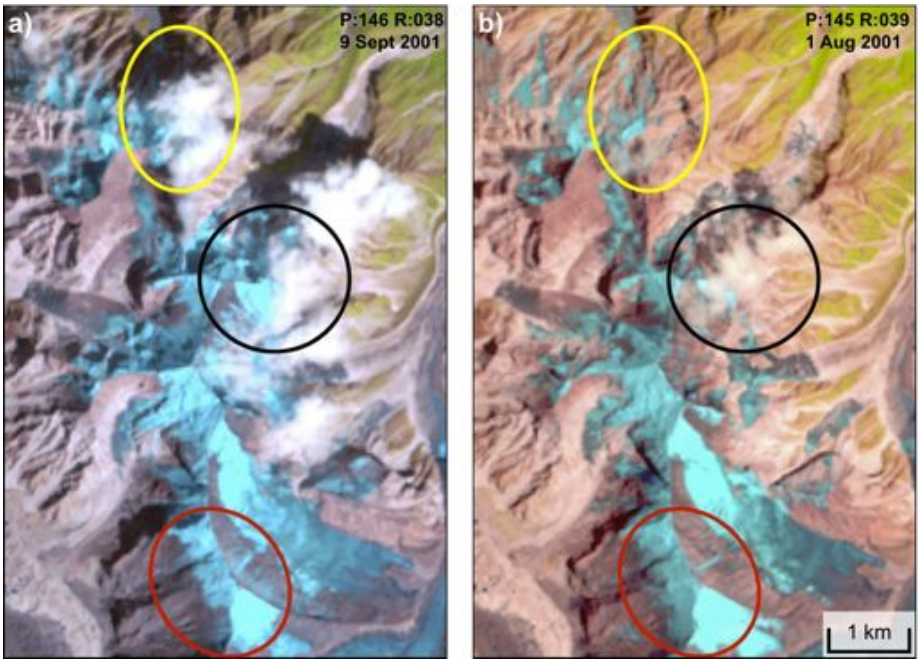

Fig. 3: Differing snow and cloud conditions in two adjacent satellite scenes. Yellow circle: cloud in scene a but not in scene b (glacier is mapped based on scene b). Black circle: cloud exists in both scenes (glaciers cannot be mapped completely and are flagged to be cloud-covered). Red circle: differing snow conditions on the two sides of the ridge. On the western side of the ridge glaciers are mapped with scene a, which has less snow at this location, whereas on the eastern side of the ridge, snow conditions are better in scene b.

3.1.2. Mapping of debris-covered glaciers with coherence images

Editing of debris-covered glacier parts is one of the most time consuming tasks in the compilation of a glacier inventory for a mountainous region, in particular in the Himalayas (e.g. Racoviteanu et al., 2008; Bhambri et al., in press). The high sun elevation considerably reduces the optical contrast and the convex shape of the tongues or the break in slope at the contact to lateral moraines that can normally be used to track the glacier boundary from small differences in illumination are hardly visible (cf. Paul et al., 2004).

Using the coherence of interferograms from radar images allows an accurate mapping of glacier margins under debris cover (Atwood et al., 2010; Strozzi et al., 2010). The degree of coherence is a measure of the phase noise of the interferogram. It depends on sensor parameters (wavelength, polarization, system noise, slant range resolution), parameters related to the imaging geometry (interferometric baseline, local incidence angle), and target parameters. Volume scattering and temporal change (i.e. random motion of the scatterers, change of the scatterers) decrease the degree of coherence. The system and geometry dependent effects are pretty well understood and can be mostly taken into account by appropriate interferometric processing. The decorrelation caused by volume scattering and temporal change, on the other hand, is important in order to characterize the target properties. During summer time most of the seasonal snow has disappeared and changes of the surface are mainly related to ice flow and ice and snow melting.

The SAR processing of the ALOS PALSAR data included radiometric calibration for the antenna gain and slant range distance, radio frequency interference filtering, and common band filtering of the azimuth and range spectra. The resulting single look complex (SLC) images were well focused and allowed to produce interferograms of high quality after accurate co-registration of master and slave images. The interferometric processing combined pairs of SLC images at HH-polarization into an interferogram. Because of rugged areas, a simulated phase image, which corresponds to the topographic phase, was first computed from the void-filled SRTM DEM and then subtracted from the interferometric phase. For coherence estimation an adaptive window size was used. In the first step, the coherence was estimated with a fixed, relatively small window size. In the second step, the window size was determined based on the first estimate, applying larger windows in order to estimate lower coherence. The estimator window size was varied between 3 x 3 and 9 x 9 pixels for a 4 azimuth-looks interferogram. In addition, a weighting function, decreasing linearly with increasing distance, was applied (Wegmüller and Werner, 1996). With this procedure reliable values at the pixel level were found without compromising the spatial resolution. In conclusion, terrain-corrected geocoding of the coherence images was performed and a mask including layover and shadow of the scene under investigation and the SRTM voids was applied.

As shown in Fig. 4, glaciers (clean and debris-covered parts) and water bodies show very low coherence values (dark) due to the change in the geometrical configuration of the scatterers. Since the identification and exclusion of water bodies is straightforward with the optical satellite scenes, the identification of the moving glaciers is strongly facilitated by these coherence images. However, due to data gaps and other disturbances like water bodies and mass movements outside glaciers, an automated mapping is not possible here and manual corrections by a trained glaciologist using optical imagery is required as a guideline and reference.

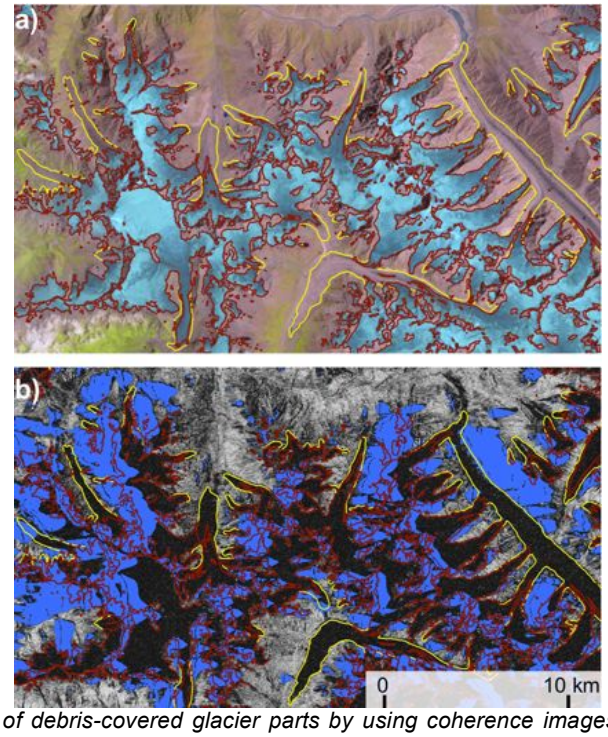

Fig. 4: Mapping of debris-covered glacier parts by using coherence images in the region of Chhota Shigri (the north-facing glacier east of the image center). The long debris-covered tongue on the eastern part of the image is Bara Shigri glacier. Red lines show the raw glacier outlines resulting from the ETM3/ETM5 ratio, corrected glacier outlines are shown in yellow. a) Shows a false-color composite of the ETM+ scene (RGB 543), b) is a coherence image from two ALOS PALSAR scenes. Note the low coherence (dark pixels) over glacier areas, independent of the amount of debris cover. Data voids (blue areas) are large, but normally they are restricted to steep terrain an do not affect the glacier tongues. Also the water area in front of the terminus of Bara Shigri results in decorrelation, however, water can easily be discriminated in the optical satellite image (a).

3.1.3. Limits of geomorphologic definitions

Due to the cold-arid climate, glacier tongues lie in continuous permafrost in the northwestern part of the study region. It is often hard to discriminate between forms of creeping scree and debris-covered glacier tongues as they exhibit a similar surface structure and identical spectral properties. Moreover, these features are a mix of glacial and periglacial forms and simple differentiations between glaciers and rock glaciers are even on-site not possible (e.g. Whalley et al., 1986). Some hints in interpreting these features are provided by the InSAR coherence images; however, a loss of coherence is visible in large parts of these regions as well, due to the movement of rockglaciers and other creeping features (Fig. 5b).

As a consequence, we proceeded in regions north of the main range as follows: rockglaciers were not considered for this inventory, although they can contain a considerable amount of ice and are therefore interesting freshwater resources. This is justified as the aim of the study is to map the Essential Climate Variable (ECV) ‘glaciers and ice caps’ as defined by the Global Climate Observing System (GCOS). In this regard, rockglaciers are part of ‘permafrost and seasonally-frozen ground’ (GCOS, 2003). Apart from the different genesis and characteristics, the latter also show a different reaction to climate change than glaciers. The main criterion to discriminate between debris-covered glaciers and rockglaciers is the visibility of clean ice. The delineation of the terminus of the debris-covered tongue is then the most challenging part, as often a smooth transition to creeping permafrost features next to the glaciers occurs, which makes the interpretation of the coherence images difficult. Basically, only a minimal possible extent (clean ice part) and a maximum possible extent (margin of the

entire convex-shaped creeping feature) are known. The real glacier margins lay somewhere between these extremes. In some cases typical structures of the surface like elongated features of debris-covered glacier tongues or lobes on rockglaciers, respectively, can be used to guide the delineation, in other cases the extent of the glacier tongue can be directly extracted from the coherence image (Fig. 5).

However, the uncertainty of the outlines from debris-covered glaciers in cold-arid regions is higher than in other regions and for the mapping both the optical satellite image as well as the coherence images must be considered and the analyst requires good glaciological knowledge.

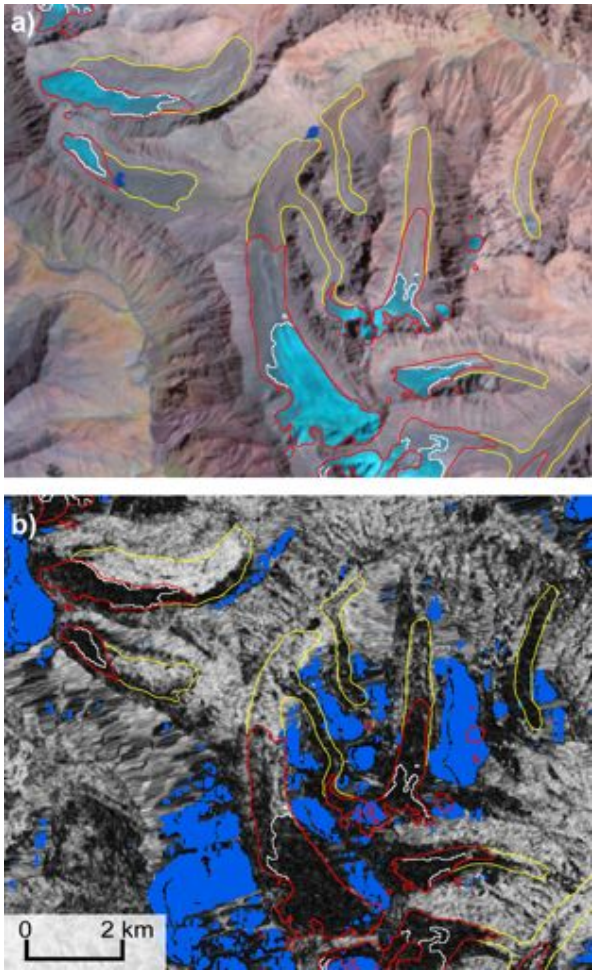

Fig. 5: Challenging mapping situation in the dry-cold north of the study region where glacier tongues lay in the zone of continuous permafrost. White lines represent the raw glacier outlines after thresholding the ETM3/ETM5 ratio image (i.e. the clean-ice areas); yellow lines delineate the maximum extent of the features with a glacier-tongue shape, including rock glaciers and potential non-moving dead-ice parts. The corrected glacier outlines of the inventory are shown in red. The background is a false-color composite (RGB 543) of the ETM+ scene (a); and the coherence image of an ALOS PALSAR image pair (with no-data areas shown in blue) (b).

Avalanche-fed glacier tongues are another special type of glacier in this region. Some glacier tongues under steep slopes are only fed by ice and snow avalanches but are otherwise completely separated from the accumulation region. Each of these multi-part glaciers is represented by two or more polygons in the inventory. An automatic assignment of such

separated glacier tongues to their respective higher reaches is not straightforward, even by manual inspection it is challenging to identify such multipart glaciers and to distinguish them from independent small glaciers. Furthermore, many topographic parameters like for instance mean and median elevation loose their validity in such cases. Benn and Lehmkuhl (2000) propose the term 'reconstituted glaciers' for them; they also presented a photo of such a glacier from the Chandra valley, which is part of our study region. As it is difficult to identify these glaciers, an exact number of these features cannot be given, but there are several dozens of them spread over the study region.

3.2. Separation of individual glaciers and calculation of topographic parameters

To get the extent of individual glaciers, the manually edited glacier map has to be separated along the hydrologic divides. For compiling the drainage divides we first followed the automated approach described by Bolch et al. (2010) and derived the hydrological basins with the DEM that had been clipped to a buffer of 700 m around the glacier outlines. However, a comparison of these drainage divides with the satellite imagery revealed some larger discrepancies caused by the lower quality of the DEM in the accumulation region, e.g. many sliver polygons along the glacier margins (Fig. 6). Furthermore, many glaciers are already separated by steep rock ridges that are free of ice and snow and, thus, do not need to have a further divide. We hence decided to digitize the drainage divides manually using the automatically derived hydrological basins only as a guide. Additionally we used a hillshade view, a flowdirection raster of the DEM and the satellite scenes for interpretation. In situations where ridges were recognizable in the satellite image due to illumination differences, the divides were drawn along them as the information from the satellite image was considered to be superior to the DEM.

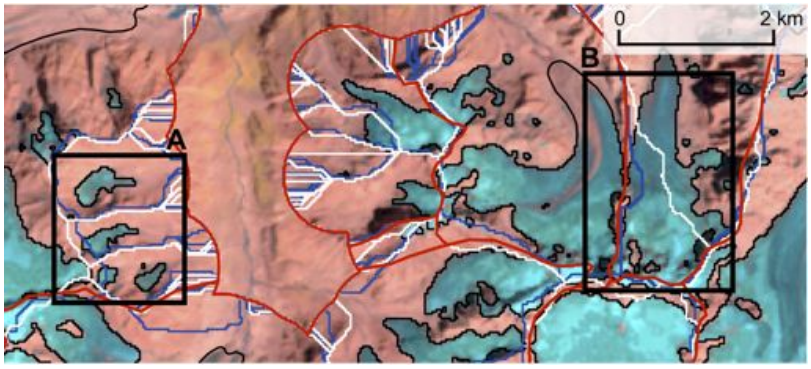

Fig. 6: Basins derived from SRTM (blue lines), ASTER GDEM (white lines), and the manually corrected final basins (red lines). Many glaciers are already completely isolated by ridges and do not need to be separated by drainage divides (box A). Besides many sliver-polygons along the margins in the upper parts of glaciers at some places large differences occur between basins derived from SRTM and ASTER GDEM (box B).

After intersecting the glacier map with the drainage divides, glacier specific parameters could be calculated. Besides an internal ID and the aforementioned percentage of debris-cover, the ID of the source scene, the cloud-cover flag, the area and topographic parameters were assigned to each glacier. Following the recommendations of Paul et al. (2009), minimum-, maximum-, mean- and median elevation, mean slope, and mean aspect in degree and mean aspect sector (from 1 to 8, according to the cardinal and intermediate directions, with 1 being North, i.e. 337.5° to 22.5°) were calculated.

4. Results

After separating the individual glaciers by clipping the glacier mask with the drainage divides, a total of 26001 polygons resulted. However, polygons with an area smaller than 0.02 km^2 are more likely seasonal or perennial snow patches rather than glaciers; therefore 14218 polygons smaller than this were not considered for the inventory. This resulted in 11783 mapped glaciers larger than 0.02 km^2, covering a total area of 9372 km^2 Additionally, 938 of

these glacier polygons were excluded due to partial cloud cover, thus 10845 glaciers (8872 km^2) were analyzed.

The distribution of glaciers by number and by area per size class (Fig. 7a) and per mean aspect sector (Fig. 7b) shows the typical patterns of mountain glaciers in mid-latitudes: 86% of all analyzed glaciers are smaller than 1 km^2, but they share only 20.2% of the total area. On the other hand there are only 13 glaciers (0.12% of the total number) larger than 50 km^2, but they cover more than 11% of the glacierized area (1012 km^2). The mean aspect of 60.4% (64.5%) of the number (area) of glaciers is in a northern sector (NE, N, or NW), whereas southern sectors (SE, S, and SW) contain only 15% (21.7%) of the glaciers by number (area).

Additionally, we calculated the mean elevation of each aspect sector (Fig. 7c). Mean elevation versus aspect sector reveals a 100 m higher mean glacier elevation in eastern sectors (NE, E, SE) than in western sectors (SW, W, NW). This reflects the general atmospheric circulation patterns in the western Indian Himalayas, with moisture transported by the monsoon and the westerlies generally from west to east that results in a lower mean elevation for glaciers exposed to the west.

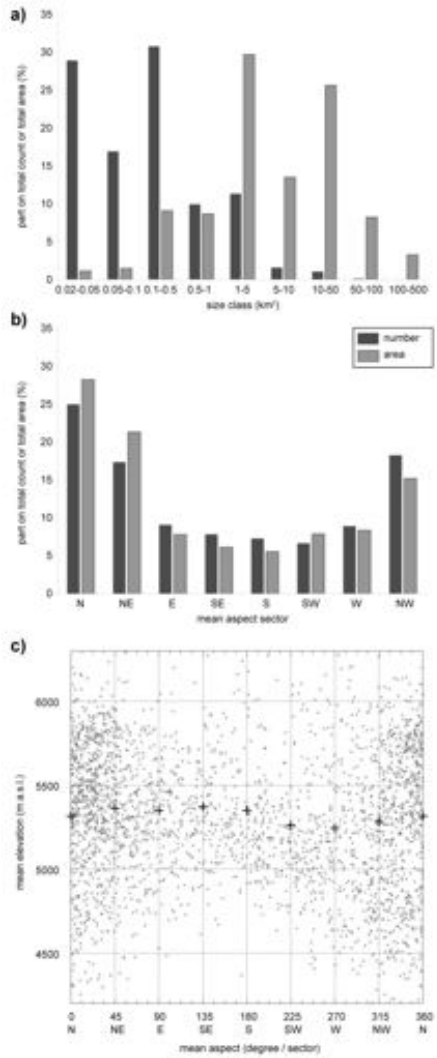

Fig. 7: Distribution of the number of glaciers and glacier area per size class (a) and per aspect sector (b). The bars show the relative amount on total glacier number (dark grey) and area

(light grey). (c) Mean elevation per aspect sector of glaciers larger than 0.5 km2. Each glacier is represented by a grey cross; black pluses indicate the average mean glacier elevation of all glaciers per aspect sector.

A characteristic of Himalayan glaciers is the extensive debris cover as described above; in total 14.9% (1325.5 km^2) of the analyzed glacier area is debris-covered. In order to investigate the distribution of debris-covered glacier parts, we split the total glacier area into debris-covered and debris-free ice and calculated overall measures for these two classes separately: debris-free (debris-covered) areas have an overall mean elevation of 5323 m a.s.l. (4755 m a.s.l.) and mean slope is 22.5° (15.4°). This confirms the previously made observation that debris-cover occurs mainly on the low lying and less inclined tongues of large valley glaciers. The largest completely debris-free glacier has an area of 7.4 km^2, but all other debris-free glaciers are smaller than 3.8 km^2.

The distribution of glacier area by elevation (i.e. the hypsography) of all analyzed glaciers is depicted in Fig. 8. Besides the total glacier surface, also the hypsographies for clean and debris-covered ice is given. Although more than 85% of the total glacier area is debris-free, the amount of debris-covered ice in the elevation band between 3200 m a.s.l. and 4400 m a.s.l. is larger than the clean-ice area; between 3500 m a.s.l. and 4100 m.a.s.l even more than 75% of the total glacier area is debris covered.

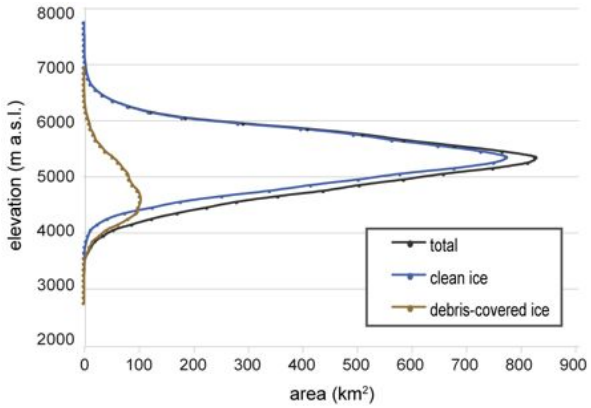

Fig. 8: Hypsometry of all glaciers of the study region. Clean ice in blue, debris-covered glacier parts in brown, and total glacier are in black.

A fundamental glaciological parameter of each glacier is the equilibrium line altitude (ELA), which divides a glacier into accumulation and ablation areas (e.g. Braithwaite & Raper, 2009). Assuming that a glacier (1) is in balance with the current climatic conditions, (2) has a constant mass balance gradient with altitude and (3) has a symmetrical area-elevation distribution, the ELA is equal to mean elevation (Braithwaite & Raper, 2009). Although probably none of the glaciers in the inventory completely fulfils all three criteria, mid-range elevation is still a very good approximation for the balance-budget ELA and thus a suitable parameter to analyze the governing climatic conditions. This becomes visible when looking at the spatial distribution of glacier specific mean elevation values (Fig. 9): at the southwestern margin of the Himalayan main range, the monsoon-dominated, relatively maritime climate results in mean elevations of glaciers below 4800 m a.s.l., whereas in the Tibetan Plateau northeast of the main range mean elevations are mostly above 5700 m a.s.l., reflecting the cold-dry climatic conditions. In a study about flow velocities in the Bhutan Himalaya, Kääb (2005) observed that glaciers south of the main range exhibit a considerably higher amount of debris-covered area than northbound glaciers; presumably due to debris supply from the steep rock faces surrounding the glaciers in the south. We therefore averaged the individual relative amounts of debris cover for the mean elevation classes as shown in Fig. 9 (numbers given in the legend). The observed decrease of debris cover with increasing (mean) glacier elevation from 22% in the southwest to only 6% in the northeast is in agreement with the findings of Kääb (2005).

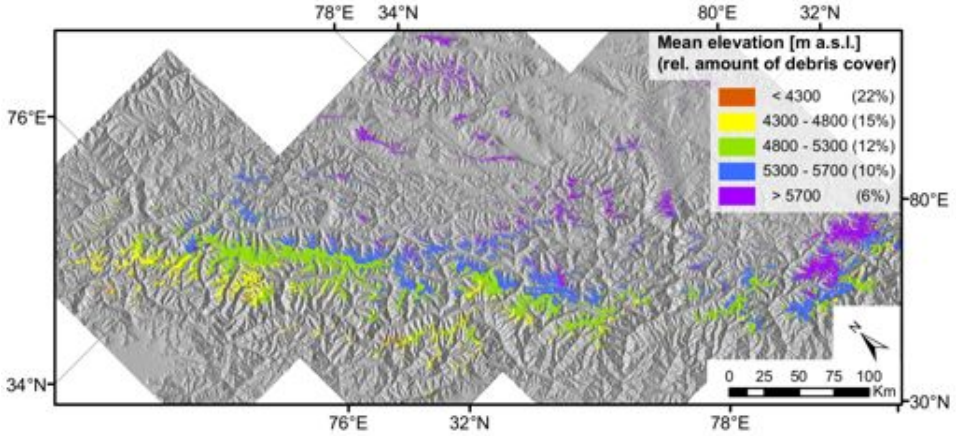

Fig. 9: Mean glacier elevation and relative amount of debris cover is spatially correlated: Mean elevation is increasing from southwest to northeast, whereas the debris cover (indicated by the number in brackets in the legend) is decreasing along this gradient.

An additional analysis of accumulation and ablation areas is possible by cutting glaciers at their mean elevation. As expected, debris cover predominantly occurs in ablation regions (23.1%), accumulation regions only have 3.1% of debris cover. Moreover, considerably lower mean slope values were found for ablation regions (16.8°) than for accumulation regions (25.8°).

5. Discussion

5.1. Inventory parameters

The difference in mean slope of accumulation and ablation regions separated by mean elevation implies that a larger amount of glacier volume is located at lower elevations, since flat glacier parts tend to be thicker than steeper regions (i.e. if basal shear stress is assumed to be constant and basal and lateral drag are neglected, ice thickness directly depends on the surface slope, cf. Paterson (1994)). Although melting is expected to be reduced under the debris cover on these low-laying glacier parts (e.g. Benn & Lehmkuhl, 2000), the surface properties possibly have only limited influence on this: in their study in the Himachal Pradesh, Berthier et al. (2005) observed the strongest lowering of glacier surfaces at low elevations, independent of the amount of debris cover; Paul & Haeberli (2008) found the same for the European Alps. As a consequence, with a continuation of the observed atmospheric warming, large amounts of the freshwater reserves of these Himalayan glaciers will be show accelerated melting in the future. This might have considerable impacts on local and regional runoff regimes (Kaser et al, 2010) but might also result in a significant contribution of these glaciers to global sea-level rise.

5.2. Debris-cover mapping and accuracy

The most laborious processing step during the compilation of this glacier inventory was to manually add debris-covered parts to the automatically mapped clean-ice outlines. For this task the use of ALOS PALSAR coherence images acquired during summer proved to be very helpful as they strongly facilitated the identification of the (moving) debris-covered tongues. Especially the large valley glaciers in the main range and on the southwestern part of the study region with extensive debris cover could be mapped much more efficient and precisely by using this information. However, the compilation of coherence images requires specific software and know-how, and also possible acquisition costs of the underlying raw scenes need to be considered. As the coherence images always contain data voids in steep and mountainous topography, automated glacier mapping based solely on such data is difficult for this region. This finding is in contrast to the study of Atwood et al. (2010), who have been successful in mapping all glaciers in sub-regions of the Wrangell Mountains and the Juneau Ice Field in Alaska from coherence imagery alone. Nevertheless, this combination of optical

an microwave remote sensing data is very promising and might be expanded in the future to other regions and other purposes, like for instance identification of glaciers under persistent orographic cloud cover that also works quite well. Summer coherence images computed from SAR images of other sensors characterized by shorter wavelengths and acquisition time intervals like TerraSAR-X or Cosmo-SkyMed are an alternative to ALOS PALSAR. The relatively long acquisition time interval of ERS and ENVISAT data, on the other hand, results in a strongly reduced distinction between debris-covered glaciers and the surrounding non-moving areas.

For clean glaciers without debris cover, an accuracy of +/-1 pixel (30 m) is assumed since the applied automated mapping method is very robust. Larger differences and uncertainties can occur in shadowed regions and for glacier divides (ice – ice margins) in accumulation regions, but the latter have no influence on the total area of multi-part glacier ensembles. To assess the accuracy of the outlines of debris-covered glaciers, a digitizing experiment with three experienced analysts was performed. Each analyst digitized five predefined debris-covered glacier tongues five times with a break of least one day between two digitizing sessions. The different outlines were then compared only relative to each other, since there is no known ground truth for comparison. Although the standard deviations of relative area differences between the five digitizing sessions were normally below 3%, the position of the outlines shows partly large variations, in particular between the different analysts. We therefore assigned a local uncertainty of +/-2 pixels (60 m) for glaciers that are partly debris-covered. In most cases, the differences at the margins along the glacier tongue where smaller than this value but larger for the glacier terminus. A third local uncertainty value of +/- 5 pixels (150 m) finally was assigned to debris-covered glaciers in the north, which are often merged with periglacial forms (see 3.1.3 and Fig. 5).

5.3. DEM accuracy

Apart from the glacier outlines, the accuracy of the glacier inventory strongly depends on the quality of the used DEM, because the compilation of drainage divides and the calculation of topographic parameters is directly based on these data. The void filled SRTM DEM exhibited gross errors in the investigated region. As shown by Frey and Paul, (subm.), the ASTER GDEM provides a valuable alternative to SRTM for the compilation of topographic parameters. Unfortunately, a quantitative accuracy assessment of the ASTER GDEM was not possible as no other independent DEM of sufficient quality was available for this purpose. A visual inspection of hillshade views revealed artifacts like holes and bumps that are characteristic for this dataset. Such errors can have a strong influence on the topographic parameters minimum and maximum elevation as these values are obtained from a single DEM cell. For the other parameters the DEM values are averaged over the entire glacier area, and they are thus less influenced by such artifacts. An advantage of the applied workflow for inventory compilation is the separation of the mapping process from the processing steps that require a DEM. It allows a fast reprocessing of drainage divides or topographic parameters or both if a suitable DEM of higher quality becomes available.

Due to the errors found in the void-filled SRTM version we used the ASTER GDEM for digitizing the drainage divides and calculating the topographic parameters. However, the quality of the void-filled SRTM affected also our results. First, it was used for removing the topographic phase of the SAR scenes during the processing of the coherence images. Although many glaciers tongues were not affected, our coherence images have large data voids (Fig. 4), much more than the coherence images produced in the study of Atwood et al. (2010) in Alaska. The second influence of these local errors is related to the geolocation accuracy of the satellite scenes and therefore the positional accuracy of the glacier outlines. As described in the metadata files of the used Landsat scenes, the orthorectification of these satellite images was performed with the Global Land Survey DEM (GLS DEM), which consists of void-filled SRTM data from CGIAR in our study region (http://www.glcf.umd.edu/data/glsdem/description.shtml, accessed March 2011). In part, we found some pixels that were more than 5 pixels (150 m) shifted away from their location indicated by the drainage divides in the ASTER GDEM. It is difficult to evaluate this effect more quantitatively as the shift depends on elevation, the elevation error, and, due to the cross track scanning of Landsat, on the distance of the pixel from the center (nadir) line of the scene (e.g. Schowengerdt, 2007).

5.4. Outlook

Due to its high degree of detail and completeness as well as the large area covered, the here created datasets can provide a baseline for future change assessment and more detailed investigations of climate change impacts on glaciers in the Himalayas. Considering the availability of earlier Landsat data including Multi-Spectral Scanner (MSS) scenes from the 1970s, a remote sensing-based assessment of glacier changes over a time span of almost 40 years would be possible. Also Vohra (2010) mentioned that several MSS scenes with suitable conditions for glacier terminus mapping are available. As the presented dataset is a snapshot of the situation between 2000 and 2002, glacier changes of the last decade can be determined as well once a more recent inventory becomes available.

For such change assessments, there are several challenges to be considered: (1) the two datasets that are compared must have the same level of detail, i.e. they should be compiled using the same methodology and source information of identical quality. (2) A straightforward comparison of total glacier areas is not possible. Changing conditions in steep headwalls covered with snow, ice and avalanche deposits have a strong influence on the mapped glacier area (cf. Fig. 3) and would lead to larger area variations than 'real' changes of glacier extent (Bhambri & Bolch, 2009). To address this problem, the areas that are compared must be restricted somehow, for example by excluding the steep headwall areas or by restricting the analysis to regions below mean elevation. (3) The same drainage divides must be used to separate glaciers in different catchments in order to perform a change assessment based on individual glaciers (e.g. Paul & Andreassen, 2009). (4) To deal with glaciers that disintegrate and split into multipart glaciers during retreat, it must be assured that a consistent labeling for both inventories exists, e.g. by using the 'parent-child relations' of the GLIMS glacier database (e.g. Andreassen et al., 2008).

Additional data compilation as well as modeling and field studies are required in the future to get a better understanding of the interactions of Himalayan glaciers with climate and also to model the potential future behavior of these glaciers. In this regard, it also needs to be assessed to which degree models that were developed and calibrated for other glacier regions can be transferred to and applied in this region, as the topographic and glacier characteristics are partly very different from other mid-latitude mountain ranges.

6. Conclusions

Several conclusions can be drawn from this study. On the one hand, from the application of established glacier mapping techniques to a large region with challenging conditions new methodological and technical solutions were found, addressing the specific points. On the other hand, the large extent and high degree of completeness of this glacier inventory, along with the analysis of the topographic glacier parameters allowed new findings about the characteristics of glaciers in a so far only sparsely analyzed mountain region:

- In a high-mountain region of about 100'000 km^2, more than 10'000 glaciers larger than 0.02 km^2 and covering an area of almost 10'000 km^2 where mapped by a semi-automated mapping technique based on 8 Landsat ETM+ scenes acquired between 2000 and 2002.
- About 15% of the total glacier area is debris-covered; however, debris cover is restricted to less inclined and lower elevations. Between 3200 m a.s.l. and 4400 m a.s.l. the amount of debris-covered glacier parts exceeds the clean ice areas.
- Across the Himalayan range, from the monsoon dominated southwest to the cold-arid northeast, an increase of mean glacier elevation by about 1500 m and a decrease in the amount of relative debris-cover from 22% to 6% was observed, reflecting the different governing climatic and topographic conditions.
- Ablation regions have much gentler slopes than accumulation regions and do likely include most of the ice in the region.
- The most laborious task for glacier mapping was the manual delineation of debris-covered glacier parts, which was strongly facilitated by the coherence images from microwave sensors. Differentiation between debris-covered glacier parts and creeping

permafrost features was particularly challenging for the northbound glaciers under cold-arid climate conditions.
- Cloud- and snow cover in the satellite scenes where partially challenging and were addressed by applying multi-temporal mapping approaches and additional meta information.
- The void-filled SRTM DEM revealed gross artifacts in interpolated data voids and was thus considered to be unsuitable in this region. Therefore, the ASTER GDEM was used to compile drainage divides along which individual glaciers were separated. The latter was then also used to calculate glacier specific topographic parameters.

This inventory is a baseline dataset for various future studies, including change assessments, modeling of future glacier developments and related changes in river runoff of Ganges and Indus and estimates of ice volumes potential sea-level rise contribution. The entire dataset will be submitted to the GLIMS glacier database to make it freely available.

Acknowledgements

The ASTER GDEM is a product of METI and NASA; SRTM is a product of NASA, the void-filled version used in this study is produced by CGIAR-CSI. Landsat scenes were provided by the USGS. This study was funded by the ESA project GlobGlacier (21088/07/I-EC).

References

Atwood, D. K., Meyer, F., & Arendt, A. (2010). Using L-band SAR coherence to delineate glacier extent. *Canadian Journal of Remote Sensing, 36*(1), 186-195.

Benn, D. I. & Lehmkuhl, F. (2000). Mass balance and equilibrium-line altitudes of glaciers in high-mountain environments. *Quaternary International, 65/66,* 15-26.

Berthier, E., Arnaud, Y., Kumar, R., & Ahmad, S. (2007). Remote sensing estimates of glacier mass balances in the Himachal Pradesh (Western Himalaya, India). *Remote Sensing of Environment, 108*, 327-338.

Bhambri, R., & Bolch, T. (2009). Glacier mapping: a review with special reference to the Indian Himalayas. *Progress in Physical Geography, 33*(5), 672-704. doi: 10.1177/0309133309348112

Bhambri, R., Bolch, T., Chaujar, R. K., & Kulshreshtha, S. C. (in press). Glacier changes in the Garhwal Himalayas, India 1968 - 2006 based on remote sensing. *Journal of Glaciology*.

Böhner, J. (2006). General climatic controls and topoclimatic variations in Central and High Asia. *Boreas, 35*, 279–295.

Bolch, T., Menounos, B., & Wheate, R. (2010). Landsat-based inventory of glaciers in western Canada, 1985–2005. *Remote Sensing of Environment, 114*, 127-137.

Bookhagen, B., & Burbank, D. W. (2006): Topography, relief, and TRMM-derived rainfall variations along the Himalaya. *Geophysical Research Letters, 33*, L08405.

Braithwaite, R. J., & Raper, S. C. B. (2009): Estimating equilibrium-line altitude (ELA) from glacier inventory data. *Annals of Glaciology, 50*(53), 127-132.

Cogley, J. G., Kargel, J. S., Kaser, G., & van der Ween, C. J. (2010). Tracking the source of glacier misinformation. *Science, 327*(5965), 522-522.

Dyurgerov, M. B., & Meier, M. F. (2000). Twentieth century climate change: Evidence from small glaciers. *Proceedings of the National Academy of Sciences of the United States of America, 97*(4), 1406−1411.

Farr, T. G., Rosen, P. A., Caro, E., Crippen, R., Duren, R., Hensley, S., Kobrick, M., Paller, M., Rodriguez, E., Roth, L., Seal, D., Shaffer, S., Shimada, J., Umland, J., Werner, M., Oskin, M., Burbank, D., & Alsdorf, D. (2007). The shuttle radar topography mission. *Reviews in Geophysics, 45*(2), 1-33.

Frey, H., & Paul, F. (sumb.). On the suitability of the SRTM DEM and the ASTER GDEM for the compilation of topographic parameters in glacier inventories. *International Journal of Applied Earth Observation and Geoinformation.*

GCOS (2003). *The second report on the adequacy of the global observing systems for climate in support of the UNFCCC*. GCOS Reports - 82 (WMO/TD No. 1143), 85 pp.

Hasnain, S. I., Kumar, R., Ahmad, S, & Tayal, S. (2010). A study of selected glaciers under the changing climate regime. In R.S. Williams & J.G. Ferrigno (Eds.), *Satellite image atlas of glaciers of the world*. Denver, CO, United States Geological Survey, F259-F274. (USGS Professional Paper 1386-F)

Hatwar, H. R., Yadav, B. P., & Rama Rao Y. V. (2005). Prediction of western disturbances and associated weather over western Himalayas. *Current Science, 88*(6), 913-920.

Hayakawa, Y. S., Oguchi, T., & Lin, Z. (2008). Comparison of new and existing global digital elevation models: ASTER G-DEM and SRTM-3. *Geophysical Research Letters, 35*(17), L17404. doi:10.1029/2008GL035036

Huss, M., Farinotti, D., Bauder, A., & Funk, M. (2008). Modelling runoff from highly glacierized alpine drainage basins in a changing climate. *Hydrological Processes, 22*(19), 3888–3902. doi:10.1002/hyp.7055

Kääb, A. (2005). Combination of SRTM3 and repeat ASTER data for deriving alpine glacier flow velocities in the Bhutan Himalaya. *Remote Sensing of Environment, 94*(4), 463-474.

Kaser, G., Grosshauser, M., & Marzeion, B. (2010). Contribution potential of glaciers to water availability in different climate regimes. *Proceedings of the National Academy of Sciences, 107*, 20223-20227.

Kaul, M. K. (1999). *Inventory of the Himalayan glaciers: a contribution to the International Hydrological Programme*. Kolkata: Geological Survey of India, 165 pp. (Geological Survey of India, Special Publication, No. 34)

Koboltschnig, G. R., Schöner, W., Zappa, M., Kroisleitner, C., & Holzmann, H. (2008). Runoff modelling of the glacierized Alpine Upper Salzach basin (Austria): multi-criteria result validation. *Hydrological Processes, 22*, 3950-3964.

Kulkarni, A. V., Rathore, B. P., & Alex, S. (2004). Monitoring of glacial mass balance in the Baspa basin using accumulation area ratio method. *Current Science, 86*(1), 101-106.

Kulkarni, A. V., Bahuguna, I. M., Rathore, B. P., Singh, S. K., Randhawa, S. S., Sood, R. K., & Dhar, S. (2007). Glacial retreat in Himalaya using Indian Remote Sensing satellite data. *Current Science, 92*(1), 69-74.

Kumar, S., & Dobhal, D. P. (1997). Climatic effects and bed rock control on rapid fluctuations of Chhota Shigri glacier, northwest Himalaya, India. *Journal of Glaciology, 43*(145), 467-472.

Matsuo, K., & Heki, K. (2010). Time-variable ice loss in Asian high mountains from satellite gravimetry. *Earth and Planetary Science Letters, 290(1-2)*, 30-36.

Paterson, W. (1994). The physics of glaciers. New York: Pergamon Press.

Paul, F., & Kääb, A. (2005). Perspectives on the production of a glacier inventory from multispectral satellite data in Arctic Canada: Cumberland Peninsula, Baffin Island. *Annals of Glaciology, 42*, 59-66.

Paul, F., & Haeberli, W. (2008). Spatial variability of glacier elevation changes in the Swiss Alps obtained from two digital elevation models. *Geophysical Research Letters, 35*(21), L21502. doi: 10.1029/2008GL034718

Paul, F., & Andreassen, L. M. (2009). A new glacier inventory for the Svartisen region, Norway, from Landsat ETM+ data: challenges and change assessment. *Journal of Glaciology, 55*(192), 607-618.

Paul, F., Kääb, A., Maisch, M., Kellenberger, T., & Haeberli, W. (2002). The new remote-sensing-derived Swiss glacier inventory: I. Methods. *Annals of Glaciology, 34*, 355-361.

Paul, F., Huggel, C., & Kääb, A. (2004). Combining satellite multispectral image data and a digital elevation model for mapping of debris-covered glaciers. *Remote Sensing of Environment, 89*(4), 510-518.

Paul, F., Barry, R. G., Cogley, J. G., Frey, H., Haeberli, W., Ohmura, A., Ommanney, C. S. L., Raup, B., Rivera, A., & Zemp, M. (2009). Recommendations for the compilation of glacier inventory data from digital sources. *Annals of Glaciology, 50*(53), 119-126.

Quincey, D. J., Richardson, S. D., Luckman, A., Lucas, R. M., Reynolds, J. M., Hambrey, M. J., & Glasser, N.F. (2007). Early recognition of glacial lake hazards in the Himalaya using remote sensing datasets. *Global and Planetary Change, 56*(1-2), 137-152.

Racoviteanu, A. E., Williams, M. W., & Barry, R. G. (2008). Optical remote sensing of glacier characteristics: a review with focus on the Himalaya. *Sensors, 8*, 3355-3383. doi: 10.3390/s8053355

Raina, V. K., & Srivastava, D. (2008). *Glacier atlas of India*. Bangalore: Geological Society of India, 316 pp.

Raup, B., Kääb, A., Kargel, J. S., Bishop, M. P., Hamilton, G., Lee, E., Paul, F., Rau, F., Soltesz, D., Khalsa, S. J. S., Beedle, M., & Helm, C. (2007). Remote sensing and GIS technology in the Global Land Ice Measurements from Space (GLIMS) Project. *Computers & Geosciences, 33*, 104-125.

Roy, S. S., & Balling R. C. (2005). Analysis of trends in maximum and minimum temperature, diurnal temperature range, and cloud cover over India. *Geophysical Research Letters, 32*(12), L12702. doi:10.1029/ 2004GL022201

Sangewar, C. V., & Shukla, S. P. (2009). Inventory of the Himalayan Glaciers: A Contribution to the International Hydrological Programme. *Special Publication, Geological Survey of India, 34*: An Updated Edition, 594 pp.

Schiefer, E., Menounos, B., & Wheate, R. (2007). Recent volume loss of British Columbian glaciers, Canada. *Geophysical Research Letters, 34*(16), L16503. doi: 10.1029/2007GL030780.

Schiermeier, Q. (2010). Glacier estimate is on thin ice. *Nature, 463(7279)*, 276-277.

Schowengerdt, R. A. (2007). *Remote sensing – Models and methods for image processing* (Third edition). Amsterdam : Academic Press, 515 pp.

Shugar, D. H., Rabus, B. T., & Clague, J. J. (2010). Elevation changes (1949–1995) of Black Rapids Glacier, Alaska, derived from a multi-baseline InSAR DEM and historical maps. *Journal of Glaciology, 56(198),* 625-635.

Strozzi, T., Paul, F., & Kääb, A. (2010). Glacier mapping with ALOS PALSAR within the GlobGlacier project. *Proceedings of the ESA Living Planet Symposium 2010, 28. June – 02 July 2010, Bergen, Norway*.

Surazakov, A. B., & Aizen, V. B. (2006). Estimating volume change of mountain glaciers using SRTM and map-based topographic data. *IEEE Transactions on Geoscience and Remote Sensing, 44*(10), 2991-2995.

Vohra, C. P. (2010): Glaciers of India – A brief overview of the state of glaciers in the Indian Himalaya in the 1970s and the end of the 20th century. In R.S. Williams & J.G. Ferrigno (Eds.), *Satellite image atlas of glaciers of the world.* Denver, CO, United States Geological Survey, F259-F274. (USGS Professional Paper 1386-F)

Wegmüller, U., & . Werner, C. (1996). Land applications using ERS-1/2 tandem data. *Proceedings of the Fringe 96 Workshop: ERS SAR Interferometry, Zurich, 30 September - 2 October 1996, ESA SP-406,* 97-112.

WGMS (2007). *Glacier Mass Balance Bulletin No. 9 (2004-2005)*. W. Haeberli, M. Hoelzle, & M. Zemp (Eds.), ICSU(FAGS)/IUGG(IACS)/UNEP/UNESCO/WMO, World Glacier Monitoring Service, Zurich, 100 pp.

Whalley, W. B., Marin, H. E., & Gellatly, A. F. (1986). The problem of "hidden" ice in glacier mapping. *Annals of Glaciology, 8*, 181-183.

Yadav, R. R., Park, W.-K., Singh, J., & Bhasha, D. (2004). Do the western Himalayas defy global warming? *Geophysical Research Letters, 31*(17). doi:10.1029/2004GL020201

Paper III

Frey, H., Huggel, C., Paul, F., and Haeberli, W. (2010b). Automated detection of glacier lakes based on remote sensing in view of assessing associated hazard potentials. In: *Grazer Schriften der Geographie und Raumfoschung 45: Proceedings of the 10th Internatinal Symposium on High Mountain Remote Sensing Cartography, 8.-11.9.2008, Kathmandu, Nepal.*, (edited by Kaufmann, V. and Sulzer, W.), pp. 261–272

138 Grazer Schriften der Geographie und Raumforschung Band 45/2010 pp. 261 - 272

Automated detection of glacier lakes based on remote sensing in view of assessing associated hazard potentials

H. Frey, C. Huggel, F. Paul and W. Haeberli
Glaciology, Geomorphodynamics & Geochronology; Department of Geography; University of Zurich; Switzerland

Abstract

An approach for semi-automatic lake detection based on multispectral optical remote sensing data and digital elevation models (DEM) is presented in this contribution. After preprocessing of the satellite images, all data are processed in a Geographic Information System (GIS). Preliminary hazard assessment of the detected lakes in a test region was performed: Potential ice avalanches and debris flows originating in glacier lake outbursts are modeled by means of hydrological flow-routing models. The strength of the presented methods is the ability to quickly create an overview of the glacier lake situation and related hazard potentials over large regions. With few adjustment works, the presented approach can be applied to mountain regions all over the world.

KEY WORDS: glacier lake, remote sensing, gis, semi-automatic

1. Introduction

All over the world, glaciers react with retreat or even downwasting to ongoing atmospheric warming. Besides its impact on the natural scenery, these changes in high-mountain environment can also cause the formation or enlargement of glacier lakes (Clague and Evans, 2000; Richardson and Reynolds 2000) and result in new potential hazards such as rock fall from warming permafrost zones (Gruber and Haeberli 2007) and destabilized, oversteepened rock walls (Korup and Tweed 2007; Haeberli and Hohmann 2008); new potential ice avalanche detachment zones caused by glacier shrinkage (Clague and Evans 2000) and increasing basal ice temperatures of hanging glaciers (Alean 1985). With the extension of human activities into high mountain regions, conflicting situations with changing glacier hazards are becoming more critical (Richardson and Reynolds 2000). The typically remote location of the source zones of glacier hazards with their difficult access and the accelerated changes of the glacial and periglacial environment due to climatic change requires a continuously updated information base. Remote sensing techniques in combination with Geographic Information Systems (GIS) can satisfy the needs for large area detection and monitoring of such phenomena (Huggel et al. 2002; Kääb et al. 2005).

Outbursts of glacier lakes are considered to be the most far-reaching glacier hazards. Glacier lakes can develop within very short times, especially lakes dammed by landslide / avalanche deposits or surging glaciers form a tributary valley (Costa and Schuster 1988; Huggel et al. 2002; Kääb et al. 2005; Korup and Tweed 2007). Due to the rapid dynamics of formation and evolution of these lakes, there is a need for simple but robust approaches to quickly obtain an overview over large areas with only minimal input data and effort. In this contribution, we present such an approach, consisting first of a GIS-tool for semi-automatic lake detection based on multispectral optical satellite imagery and digital terrain modelling and second of two flow-routing models to assess the hazard potential of ice avalanches and debris flows originating from glacier lake outbursts.

The methods were developed and tested in two regions in the Eastern Swiss Alps (Engadin) and then applied to three Landsat TM scenes from the Alps in order to compile a corresponding lake inventory. For the test region in the Engadin also the first-order hazard assessment has been applied.

2. Data and study area

Lake detection and related hazard assessment with the presented approach requires multispectral satellite imagery and digital elevation data. The Alps were chosen as study area due to their comparably good accessibility for fieldwork and the high-quality data (DEM25 for Switzerland form swisstopo with 25 m resolution and high accuracy (4–6 m vertical, Rickenbacher 1998; Swisstopo 2004), up to date high-precision topographic maps of 1:25,000 scale for validation and the remote sensing-based Swiss Glacier Inventory (SGI 2000) (Paul 2007).

Parts of three Landsat Thematic Mapper (TM) scenes from 2003 have been selected for processing (Fig. 1). Snow and cloud conditions are the most crucial selection criteria for

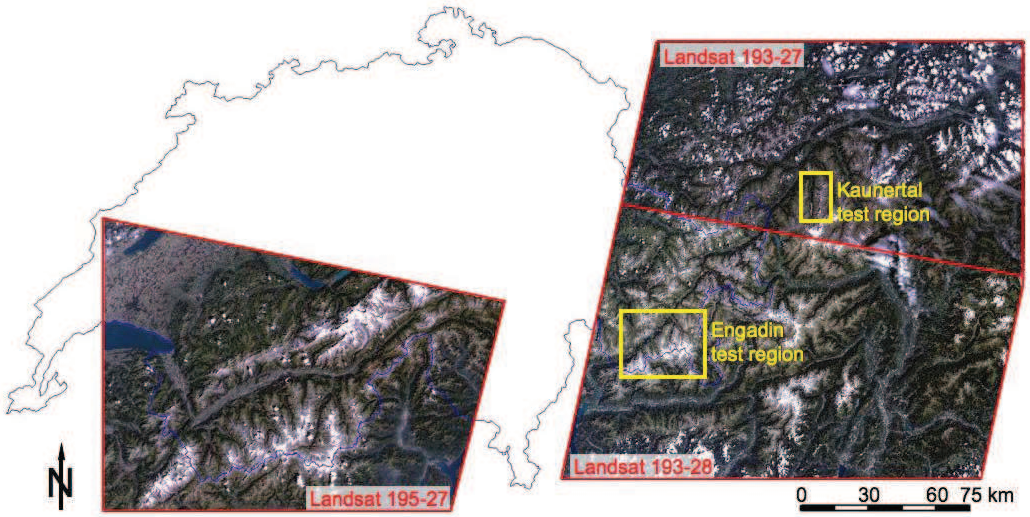

Figure 1: Overview of the three processed Landsat TM scenes and the two test regions. Image parts are restricted to mountainous regions. Outline of Switzerland is shown in the background.

the satellite scenes because snow cover hampers glacier mapping, clouds shroud the surface and inhibit classification of the ground and cloud shadows can be misclassified as lakes. Thus, for lake mapping as well as for glacier mapping cloud free scenes from the end of the ablation period are most favorable (Paul et al. 2002).

Development, testing and validation of the mapping tool were carried out in a test region in the Upper Engadin Valley in Switzerland. Based on 1:25,000 topographic maps from the same year as the satellite scenes (2003), a ground-truth map was generated for validation purposes. In the Kaunertal test region in Austria, the model was tested with elevation data from the Shuttle Radar Topography Mission (SRTM) (Rabus et al. 2003; Van Zyl 2001). In comparison to the DEM25 from Switzerland, the SRTM-DEM has a lower spatial resolution (3 arc seconds ~ 90 m) and contains voids due to shadowing effects and poor signal returns in rough topography. However, it covers land surface between 60° North and 56° South and can thus be used for many glacierized mountain belts of the world. For this work, data voids in the SRTM3 data set were filled with SRTM30 data (resolution of 30 arc seconds, which is ~1 km).

3. Methods

3.1. Tool for semi-automatic lake detection

In order to develop a tool for automatic or semi-automatic lake classification, a model was generated within the model builder of the ArcGIS Software (general workflow in Fig. 2). After the preprocessing of the satellite image (georeferencing, orthorectification and cubic convolution resampling to 25 m to match the DHM25 grid), TM bands 1 (blue), 4 (near infrared (NIR)) and 5 (short wave infrared (SWIR)) was imported into the ArcGIS environment as single 8bit raster layers. All the following image processing (described below) was then performed with raster calculation tools within the ArcGIS environment.

Lakes in glacierized areas show a wide range of turbidity, ranging from light blue or green to almost black. The major influences are sediment influx, water depth, the properties of the lake bottom, and the origin of the lake water (Wessels et al. 2002). Due to these different spectral information of lakes, unsupervised classification methods cannot be used for automated lake mapping. Based on the normalized difference vegetation index (NDVI) (Hardy and Burgan 1999), Huggel et al. (2002) developed the normalized difference water index (NDWI). Both these indices use two spectral bands with maximum reflectance differences for an object (water for NDWI): For lake classification, a blue channel with maximum reflection (Bblue)

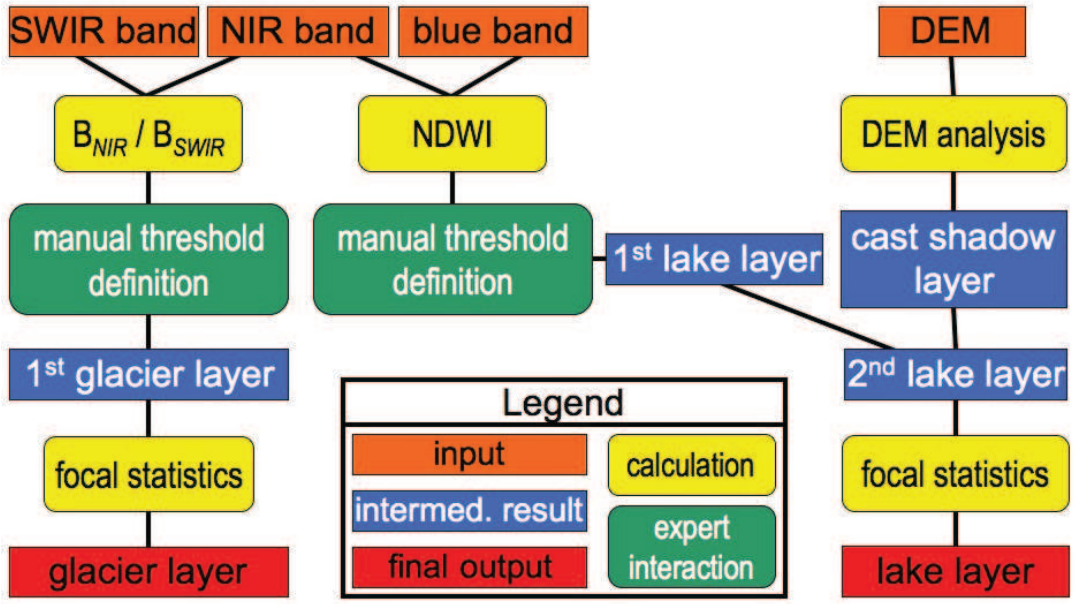

Figure 2: General workflow of the GIS-tool for semi-automatic lake detection.

and a NIR channel with minimum reflection (BNIR) are required. The NDWI is calculated as follows:

$$NDWI = \frac{B_{NIR} - B_{blue}}{B_{NIR} + B_{blue}}$$

In comparison to a simple channel ratio (e.g. BNIR / Bblue), the NDWI shows better contrast between water and the surrounding environment, and has a normalized numeric range between -1 and 1 (Huggel et al. 2002). Lake areas typically have low (dark) NDWI values (between -0.60 and -0.85), thus a scene dependent threshold can be defined and used as the classification criterion to distinguish between lake and non-lake pixels (Fig. 3). For threshold definition, lakes appearing dark (in a true-color view) should be examined due to their higher NDWI values caused by lower reflection in the blue channel. In the given context of hazard assessment, it is important to detect all lakes, even if a lower overall accuracy has to be accepted. This can be justified by the higher feasibility to manually correct misclassifications than finding undetected lakes.

Besides the erroneous classification of several isolated pixels, the prevalent misclassification of cast shadow regions is the main problem of the NDWI (red circles in Fig. 3), especially in terms of an automatic application of the method. The reason is, that shortwave radiation (here blue) is susceptible to atmospheric scattering, thus even in cast shadow regions there is always a signal in the blue channel. To reduce the shortwave scattering component, a dark object subtraction (DOS) was applied to the blue channel (Crippen 1988). However, only small improvements have been achieved by this subtraction. To avoid misclassifications of cast shadow areas more efficiently, a cast shadow mask was derived based on a DEM and the sun position at the time of image acquisition, which is given in the metadata of the satellite scene.

In ArcGIS, the hillshade procedure calculates the luminosity of a pixel based on the cosine of the surface normal and the direction of the illumination source (ESRI 2006), resulting in a raster with values between 0 (black, no light) and 255 (white, vertical irradiation). To define a threshold for cast shadow classification, the results from the hillshade procedure were compared to the cast shadow algorithm based on a viewshed analysis of the light source (Dozier

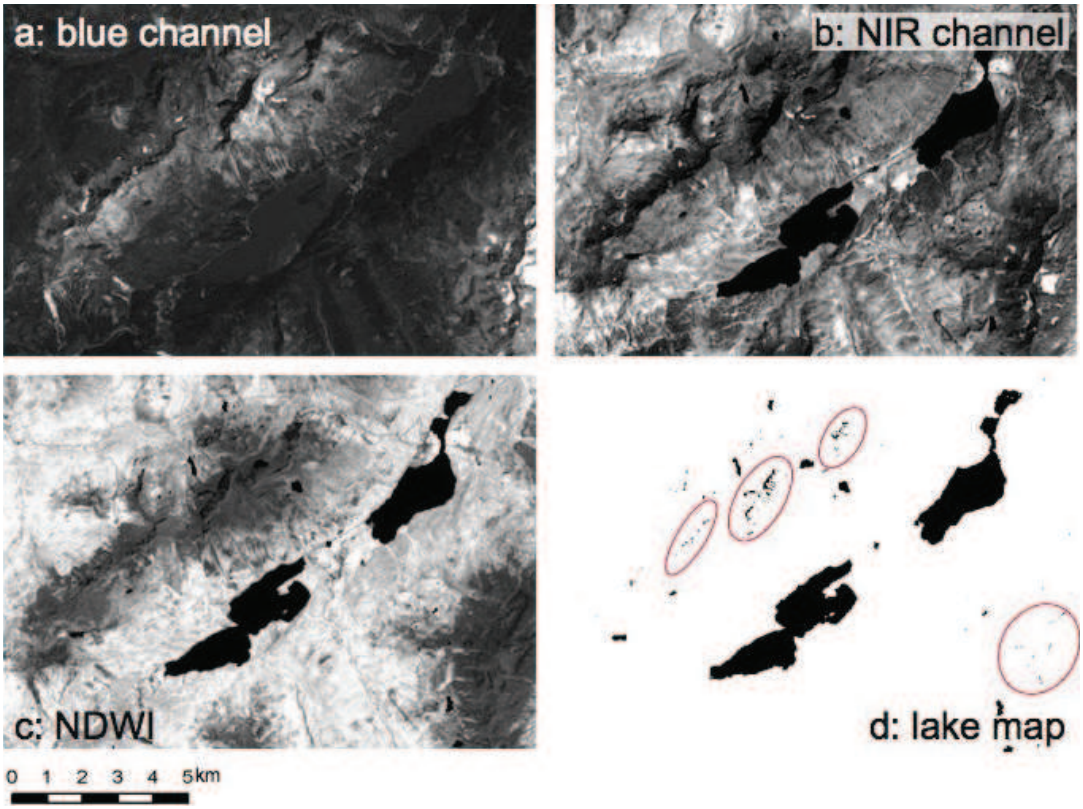

Figure 3: Illustration of lake mapping with the NDWI. a, b: the two channels (grayscale view); c: the NDWI values from -1 (black) to +1 (white); d: the lake map after thresholding. Erroneously classified cast shadow areas are indicated with red circles.

and Frew 1990) and it was found that regions with hillshade values from 0 to 4 is almost congruent with the calculated cast shadow areas from the viewshed analysis. Due to much lower computational cost, the classified hillshade procedure was used for cast shadow modeling.

Misclassifications of cast shadow can be avoided with this correction but the deficit of this procedure is, that lakes located completely in cast shadow are not detected at all, a problem that is emphasized for scenes with low sun elevations and, hence, large cast shadow areas. Furthermore, lake areas may be incorrectly classified, if a part of a lake is covered by cast shadow and thus not detected. For the correction of other small-area errors a 3 by 3 median filter was applied after the application of the threshold. With such a filter, gaps within closed lake areas are filled and isolated lake pixels are deleted (Paul et al. 2002). Lakes with areas smaller than 1875 m2 (three 25 m pixels) are deleted; this helps to eliminate a majority of the small-area errors.

Due to their importance for hazard assessment of glacier lakes, glaciers are included in the mapping. Paul et al. (2002) showed, that for mapping clean ice the channel ratio of a NIR band and a SWIR band provides best results, also in shadowed areas. A simple threshold applied to this ratio image then allows discriminating ice and snow from all other surface types. Debris-covered glacier parts cannot be mapped automatically, because they have the same spectral reflectance properties as the surrounding rock and debris areas (Paul et al. 2004), thus the results of the automatic glacier mapping are only a first approximation and should be replaced with (recent) two-dimensional glacier inventory data of the investigated region if available (Fig. 9). Manual corrections based on the satellite image is possible as well, but laborious.

3.2. Hazard assessment

Flood waves and debris flows originating from outburst of glacier lakes can be far-reaching (>100 km) and highly destructive to human lives and infrastructure (Huggel et al. 2002; Kääb et al. 2005). Due to the dynamic nature of the related processes in high-mountain environments, not only glacier lakes but also the factors influencing the hazard situation of these lakes must be (re-) assessed frequently.

Depending on the lake stability, ice / rock avalanches can trigger outbursts of glacier lakes (Richardson and Reynolds 2000). Heavy rainstorms, calving at the glacier front, snow avalanches and debris-flows or water influx from upstream lakes can also cause glacier lake floods, but exact forecasting of such an event is generally difficult. Space-borne remote sensing techniques, combined with modeling, can help to assess the related hazard potential rather than predict the timing of an event (Kääb et al.,2005).

Occurrence, frequency and magnitude of all mentioned processes have a relation to climatic conditions. The hazard situations of rapid mass movements such as ice- and rock avalanches are most directly influenced by changes of glacier extent: Retreating glaciers cause loss of support and changes in the stress field of over-steepened rock walls and thus lead to long-term destabilizations (Matthews and Shakesby 2004; Korup and Tweed 2007; Haeberli and Hohmann 2008). Modified glacier extents can result in new cliff-type ice avalanche starting zones whereas changing basal ice temperatures and melt water availability at the ice/bedrock interface of hanging glaciers reduces the strength and can cause ramp-type ice avalanche starting zones (Fig. 4; Alean 1985; Huggel et al. 2004a).

In this study, ice avalanches are the only mass movements considered for triggering glacier lake outbursts (besides triggering by a debris flow from an upstream lake outburst). From an investigation of 26 glacier lake-outbursts in the Himalayas, Richardson and Reynolds (2000) found that 53% were initiated by displacement waves from ice avalanches that collapsed into the lakes from hanging or calving glaciers. The applied flow-routing algorithm for modeling lake outburst floods is based on the D8 (eight possible directions) approach from O'Callaghan and Mark (1984), which assigns the flow direction from one cell of a DEM to the one of its eight neighbors with the steepest descent. In combination with an empirically acquired maximum runout distance (see below), this method is useful to model flow trajectories of ice avalanches (Huggel et al., 2003; Huggel et al. 2004b; Salzmann et al. 2004). Huggel et al. (2003) developed the modified single flow model (MSF) that is based on the D8 algorithm, but the flow trajectory of the MSF model is allowed to spread in less steep terrain and on the fan. In both models erosion, deposition, mass and changing channel geometries are not considered.

For lake outburst modeling, starting zones are defined by the detected lakes. To define starting zones for ice avalanche assessment, the mapped glacier areas are combined with a slope map derived from the DEM, to detect glacier parts steeper than 25°. According to Alean (1985), this is approximately the critical slope for the detachment of ice avalanches from temperate glaciers with ramp type starting situations (see Fig. 4). The fact that debris-covered glacier parts are not detected with the applied mapping algorithm (band ratio) does not significantly affect the results, since debris coverage is generally restricted to flat glacier parts (Maisch et al. 1999; Paul et al. 2004). For the determination of glacier lake outburst floods runout distance (maximum trajectory length), worst-case scenarios based on empirical studies in the Alps are used. It has been

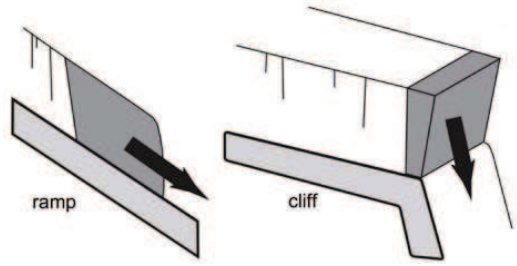

Figure 4: Types of ice avalanche starting zones (modified from Huggel et al., 2004a; based on Alean, 1985)

found, that the average slope angle (α) related to maximum runout distance does not fall below 11° (tan α = 0.19) for granular debris flows from glacier / ice dammed lakes (Haeberli 1983; Huggel et al. 2002) and 17° (tan α = 0.31) for ice avalanches, respectively (Alean, 1985). These values are implemented into the models, but depending on expected flow processes (e.g. sediment concentration) they need to be reassessed for applications in other regions.

One of the main strength of these models is, that they can be applied to large regions and thus provide a first-level hazard assessment. This is important to gain a first overview, to detect further potential chain reactions (e.g. damming of a downstream river) (Huggel et al. 2004b) and, hence, such investigations should be included into any hazard assessment, regardless of the level of detail. If such a first-level hazard assessment reveals that a lake is potentially susceptible to failure, the lake should be investigated on a further level of detail including high resolution satellite imagery, aerial photography, more detailed lake outburst modeling and, if required, field surveys and

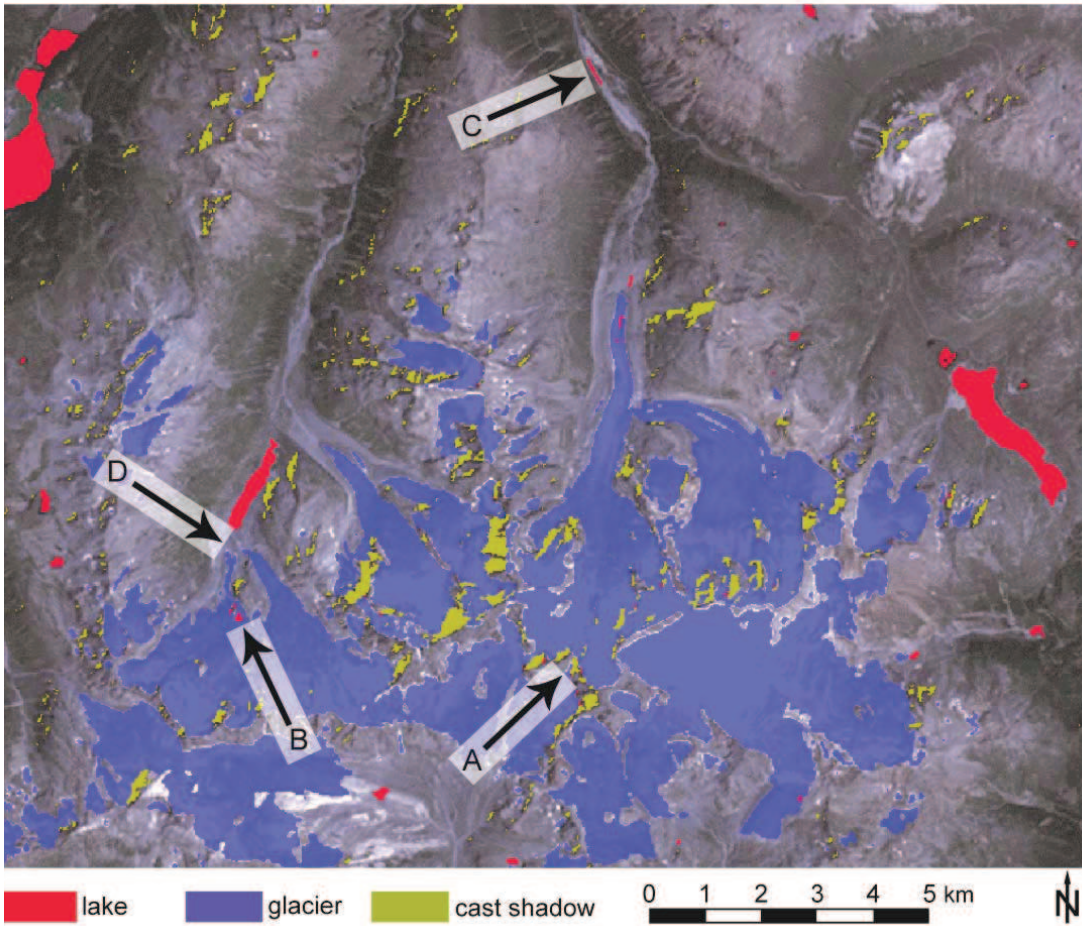

Figure 5: Result from the lake detection tool. Main error sources are: A: inaccurate cast shadow modeling (see also Fig. 6); B: channel saturation of near-surface water on glacier; C: broad river part (literally no misclassification). D shows debris-covered glacier parts that are not mapped (see Fig. 9 for detail).

geophysical investigations (Reynolds 1998; Haeberli et al. 2001). On the final level of hazard assessment, more process-oriented models should be applied, which require more detailed input data that might be difficult to obtain.

4. Results

4.1. Lake detection

Regarding the image classification with the NDWI, there is no discrimination made between glacier lakes and "other" lakes. Thus, the applied algorithm produces rather a general lake inventory than a specific glacier lake inventory. Most misclassifications of the GIS-based classification tool can be related to three main types of errors (Fig. 5):

A. Inaccurate cast shadow modeling: If no cast shadow is modeled for a pixel that is actually in cast shadow, it is highly probable that the pixel is misclassified as lake. Frequency and magnitude of these errors are closely linked to DEM quality, therefore the lake map contains significantly more errors in regions where the SRTM DEM was used for cast shadow calculation (e.g. Kaunertal test region, Fig. 6).

B. Channel saturation: Snow and ice have high reflectivity in the visible range of the electromagnetic spectrum. Pixels with a certain slope and aspect can reflect the incoming sunlight directly into the sensor and cause a saturation of the blue channel. This can lead to misclassifications due to high blue channel values.

C. In hot summer months the occurrence of water on or near the glacier surface is possible. Both melt water on ice and expanded parts of rivers are not a misclassification in technical terms, but need to be adjusted for lake inventory compilation.

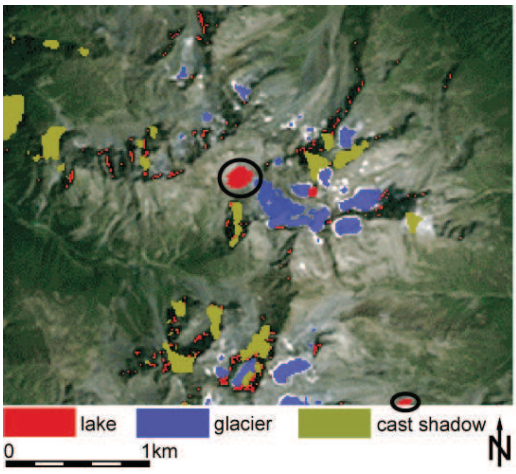

Figure 6: Inaccurate cast shadow modelling (due to lower resolution of DEM) leads to many small-area misclassifications. The only real lakes are marked with black circles; all other red areas are misclassifications. Image detail from the Kaunertal test regi-

For a lake inventory the detected lake areas need to be checked for lake parts covered by cast shadow. Otherwise some lake areas can be underestimated.

For the regions covered by the Landsat scenes shown in Fig. 1, a preliminary lake inventory was compiled. This inventory contains all kind of water surfaces with an area of at least 1875 m2 (three 25 m pixels) without any manual corrections. It is, thus, not confined to glacier lakes only. Nevertheless, such an inventory is a snapshot of the lake situation in 2003 (all used satellite scenes date between 30th July 2003 and 13th August 2003) and provides a baseline for change assessments in the future. Each lake has an inventory number and values for area, as well as x- and y-coordinates in the Swiss projection system.

4.2. Hazard assessment

The applied flow routing models are appropriate for application to large areas (e.g. complete Landsat scenes, Figs. 7 & 8). This is very useful to gain a first overview and detect potential chain reactions, especially in regions with a poor database and/or difficult accessibility. However, there is a need for manual editing and/or expert judgment. The independence of the flow routing models from outburst/avalanche volumes is reasonable although small events and especially misclassifications are emphasized disproportionally (C in Fig. 8). However, for a first-order approach determination of lake volume on this fist level of hazard assessment is related with uncertainties and in many cases an outburst/ice avalanche does not implicitly involve the whole lake volume/steep glacier part.

5. Discussion

Lakes in cast shadow cannot be detected; this is the most critical element in the suggested procedure. To avoid an unacceptable number of misclassifications, a cast shadow mask was modeled by DEM-analysis and the sun position at the time and date of image acquisition and all mapped lake pixels in the modeled shadow regions areas deleted. Cast shadow modeling is the main cause of errors and implicates that a compiled lake inventory cannot be complete, that lake areas crossing shadow zone are underestimated and that small lakes within cast shadow are not detected at all.

A DEM from around the date of satellite image acquisition would open new options for corrections and enhance the quality of the model, e.g. a sensor with along-track stereo capability such as ASTER could be used. For this reason, ASTER DEMs, which have a vertical accuracy of about 15 m in mountainous terrain, are considered to be very useful

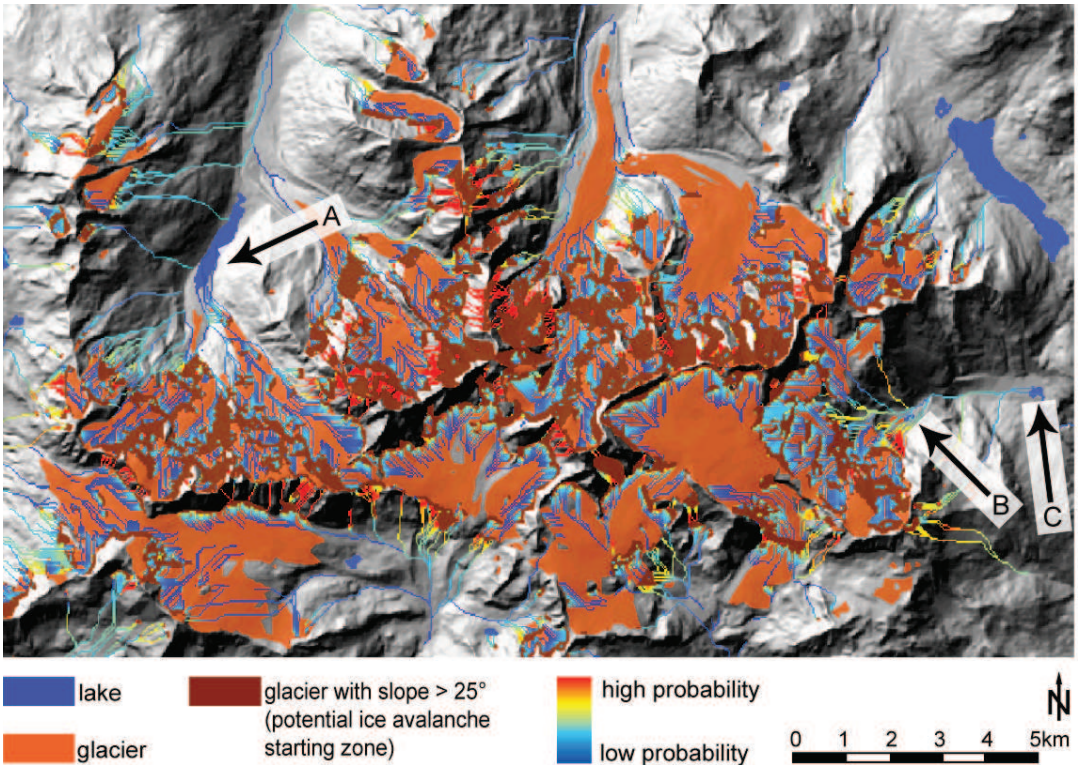

Figure 7: Modelling of potential ice avalanches with flow routing modeling. Glacier parts with a slope > 25° (brown areas) are considered as potential starting zones of ice acalanches. Many lakes could be hit by ice avalanches. For instance A: Lake Rosegg, with an area of approx. 343'000 m2; B: a newly formed lake at the terminus of Palü Glacier and C: a small storage lake at Alp Grüm, downstream of B. DEM25 reproduced by permission of swisstopo (BA081538).

in a glaciological context (Kääb et al. 2003; Racoviteanu et al. 2007; Toutin 2008). By means of zonal statistics of detected lake polygons and the up-to-date DEM, a threshold for maximum elevation differences within one lake polygon could help to eliminate most erroneous lakes, regardless of the reason for misclassification. Time differences between the date of the satellite scene and DEM acquisition make such corrections nearly impossible, because pre-lake formation surfaces in high-mountain areas can be subject to large altitude differences (e.g. due to a retreating glacier terminus, melting of debris covered glacier / dead ice, etc.).

The Quality of the applied hazard assessment over large area relies on the quality of the DEM as well as the lake detection and steep glacier classification. Lake-misclassifications and mistakes in evaluation of avalanche-prone steep glacier parts (due to debris cover, unknown basal ice conditions and internal structure, and DEM errors) degrade the model output. If glacier outlines from a (regional) glacier inventory are available, they should be used instead of the unrevised (first level) glacier map from the semi-automatic classifications (Fig. 9). A shortcoming of the hazard assessment presented here is the fact that only ice avalanches and water influx from upstream lakes are considered as triggers for lake outbursts but other processes like rock fall or landslides / debris flows originating in steep debris reservoirs (Huggel et al. 2004b) are ignored. Further efforts will be directed to better include such potential outburst trigger processes.

6. Conclusions

The presented GIS-tool for semi-automatic lake and glacier mapping and the flow-routing approach for ice avalanches and debris flows modelling is a powerful tool to quickly obtain an overview over large regions (e.g. an entire Landsat scene) and can provide a baseline for following assessments. Based only on multispectral satellite imagery and digital elevation information, the method is directly applicable to mountain ranges all over the world given that the quality of the used DEM is sufficient. A model limitation is currently that with the applied NDWI does

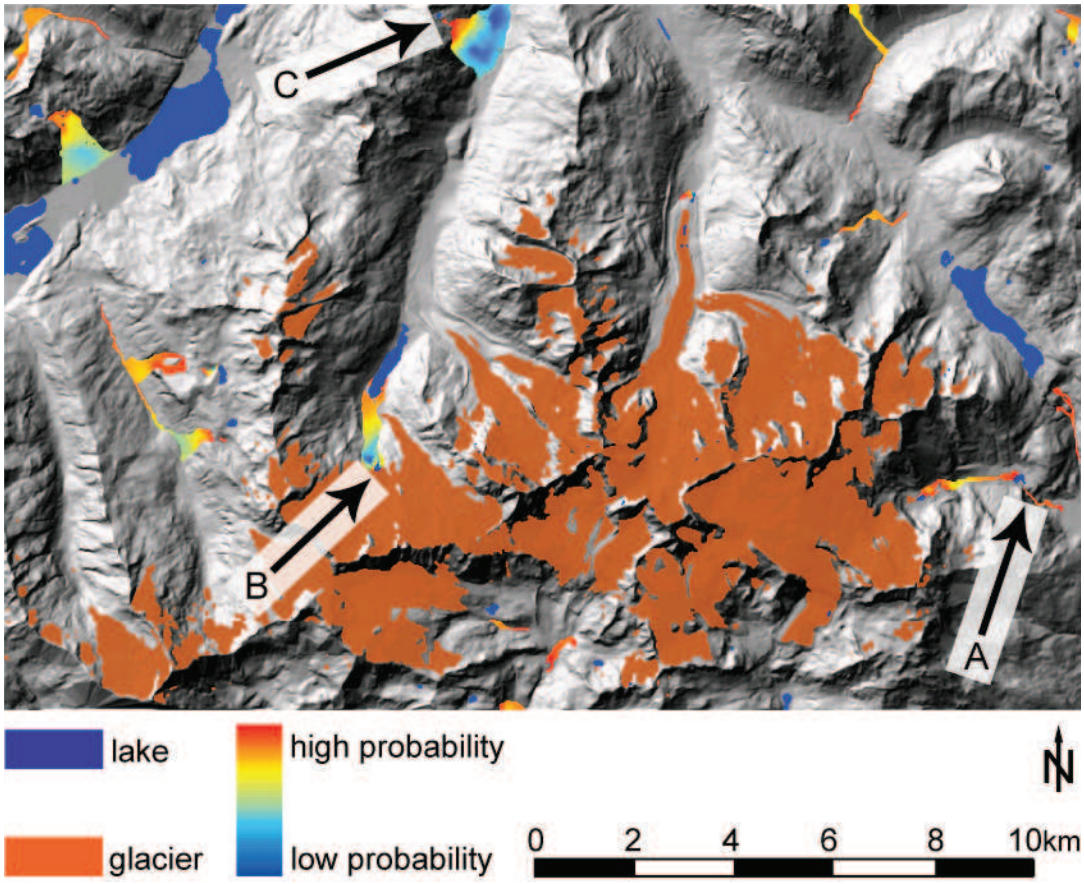

Figure 8: Modeling of potential debris flows originating in glacier lake outbursts. Besides the assessment of isolated lake outbursts, potential chain reaction can be detected, such as a downstream lake in the runout path (A). Due to the independence of the model from the outburst volume especially misclassifications (B) distort the image and outbursts from small area lakes (C) look emphasized. DEM25 reproduced by permission of swisstopo (BA081538).

not detect lakes in cast shadow automatically and some small-area misclassifications remain. DEMs from the same date as the used satellite image would be helpful to eliminate many errors.

For the hazard assessment, ice avalanches and debris flows originating from glacier lake outbursts are modeled, but other potential outburst mechanisms and triggers are not considered. The model was calibrated with empirically derived values of avalanche and outburst floods of the Swiss Alps and therefore needs to be adjusted for application in other mountain regions. A significant asset of the model is the identification of potential chain reactions related to glacier lake outburst floods that often cause the most severe disasters.

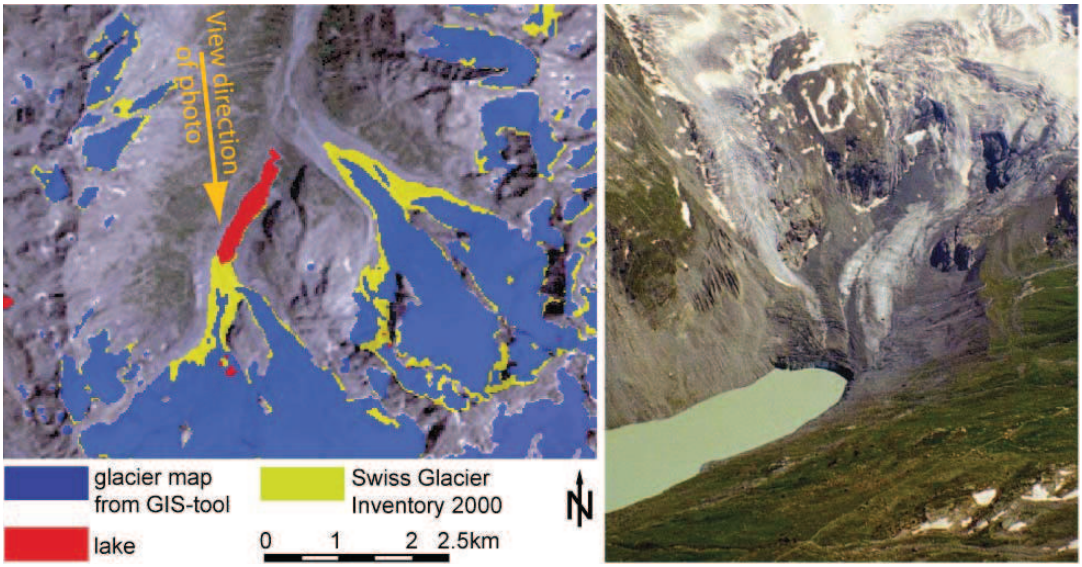

Figure 9: Comparison of the glacier map from the GIS-tool (blue) where debris cover is not mapped and the Swiss Glacier Inventory 2000 (SGI 2000) including debris covered glacier parts. The air photo shows the situation in the same year than the satellite image (Photo: C. Rothenbühler).

References

ALEAN, J., 1985: Ice avalanches: Some empirical information about their formation and reach. Journal of Glaciology, 31:324-333.

CLAGUE, J.J. and EVANS, S.G., 2000: A review of catastrophic drainage of moraine-dammed lakes in British Columbia. Quaternary Science Reviews, 19:1763-1783.

COSTA, J.E. and SCHUSTER, R.L., 1988: The formation and failure of natural dams. Geological Society of America Bulletin, 7:1054-1068.

CRIPPEN, R.E., 1988: The dangers of underestimating the importance of data adjustments in band rationing. International Journal of Remote Sensing, 9(4):767-776.

DOZIER, J. and FREW, J., 1990: Rapid calculation of terrain parameters for radiation modeling from digital elevation data. IEEE Transactions on Geoscience and Remote Sensing, 28(5):963-969.

ESRI, 2006: ArcGIS 9.2 desktop help. Environmental Systems Research Institute Inc.

GRUBER, S. and HAEBERLI, W., 2007: Permafrost in steep bedrock slopes and its temperature-related destabilization following climate change. Journal of Geophysical Research, 112(F02S18), doi:10.1029/2006JF000547.

HAEBERLI, W., 1983: Frequency and characteristics of glacier floods in the Swiss Alps. Annals of Glaciology, 4:85-90.

HAEBERLI, W., KÄÄB, A., VONDER MÜHLL, D. and TEYSSEIRE, P., 2001: Prevention of outburst floods from periglacial lakes at Grubengletscher, Valais, Swiss Alps. Journal of Glaciology, 47(156):111-122.

HAEBERLI, W. and HOHMANN, R., 2008: Climate, glaciers and permafrost in the Swiss Alps 2050: Scenarios, consequences and recommendation. Proceedings of the 9th International Conference on Permafrost 2008, Fairbanks, Alaska, USA.

HARDY, C.C. and BURGAN, R.E., 1999: Evaluation of NDVI for monitoring moisture in three vegetation types of the Western U.S.. Photogrammetric Engineering and Remote Sensing, 65:603-610.

HUGGEL, C., KÄÄB, A., HAEBERLI, W., TEYSSEIRE, P. and PAUL, F., 2002: Remote sensing based assessment of hazards from glacier lake outbursts: a case study in the Swiss Alps. Canadian Geotechnical Journal, 39:316-330.

HUGGEL, C., KÄÄB, A., HAEBERLI, W., AND KRUMMENACHER, B., 2003: Regional-scale GIS-models for assessment of hazards from glacier lake outbursts: evaluation and application in the Swiss Alps. Natural Hazards and Earth System Science, 3:647-662.

HUGGEL, C., HAEBERLI, W., KÄÄB, A., BIERI, D. and RICHARDSON, F., 2004a: An assessment procedure for glacial hazards in the Swiss Alps. Canadian Geotechnical Journal, 41:1068-1083.

HUGGEL, C., KÄÄB, A. and SALZMANN, N., 2004b: GIS-

based modelling of glacial hazards and their interactions using Landsat-TM and IKONOS imagery. Norsk Geografisk Tidskrift - Norwegian Journal of Geography, 58(2):61-73.

KÄÄB, A., WESSELS, R., HAEBERLI, W., HUGGEL, C., KARGEL, J., AND KHALSA, S., 2003: Rapid ASTER imaging facilitates timely assessment of glacier hazards and disasters. EOS, Transactions, American Geophysical Union, 84(13):117-124.

KÄÄB, A., HUGGEL, C., FISCHER, L., GUEX, S., PAUL, F., ROER, I., SALZMANN, N., SCHMUTZ, K., SCHNEIDER, D., STROZZI, T. and WEIDMAN, Y., 2005: Remote sensing of glacier- and permafrost-related hazards in high mountains: an overview. Natural Hazards and Earth System Science, 5:527-554.

KORUP, O. and TWEED, F., 2007: Ice, moraine, and landslide dams in mountainous terrain. Quaternary Science Reviews, 26:3406-3422.

MAISCH, M., HAEBERLI, W., HOELZLE, M. AND WENZEL, J., 1999: Occurrence of rocky and sedimentary glacier beds in the Swiss Alps as estimated from glacier-inventory data. Annals of Glaciology, 28:231-235.

MATTHEWS, J.A. and SHAKESBY, R.A., 2004: A twentieth-century neoparaglacial rock topple on a glacier foreland, Ötztal Alps, Austria. The Holocene, 14(3):454-458.

O'CALLAGHAN, J.F. and MARK, D.M., 1984: The extraction of drainage networks from digital elevation data. Computer Vision Graphics and Image Proceedings, 28:323-344.

PAUL, F., KÄÄB, A., MAISCH, M., KELLENBERGER, T. and HAEBERLI, W., 2002: The new remote-sensing-derived Swiss glacier inventory: I. Methods. Annals of Glaciology, 34:355-361.

PAUL, F., HUGGEL, C. and KÄÄB, A., 2004: Combining satellite multispectral image data and a digital elevation model for mapping of debris-covered glaciers. Remote Sensing of Environment, 89(4):510-518.

PAUL, F., 2007: The New Swiss Glacier Inventory 2000 – Application of Remote Sensing and GIS. Schriftenreihe Physische Geographie, University Zurich, 52, 210 pp.

RABUS, B., EINEDER, M., ROTH, A. and BAMLER, R., 2003: The shuttle radar topography mission – a new class of digital elevation models acquired by spaceborne radar. ISPRS Journal for Photogrammetry and Remote Sensing, 57:241-262.

RACOVITEANU, A., MANLEY, W., ARNAUD, Y. and WILLIAMS, M., 2007: Evaluating digital elevation models for glaciologic applications: An example from Nevado Coropuna, Peruvian Andes. Global and Planetary Change, 59(1-4):110-125.

REYNOLDS, J., 1998: High-altitude glacial lake hazard assessment and mitigation: A Himalayan perspective. Maund, J. and Eddleston, M. (eds.), Geohazards in Engineering Geology, Geological Society Engineering Group Special Publication, 15:25–34.

RICHARDSON, S. and REYNOLDS, J., 2000: An overview of glacial hazards in the Himalayas. Quaternary International, 65-66:31-47.

RICKENBACHER, M., 1998: Die digitale Modellierung des Hochgebirges im DHM25 des Bundesamtes für Landestopographie. Kriz, K. (ed.): Hochgebirgskartographie – Silvretta '98. Inst. für Geographie der Universität Wien. (= Wiener Schriften zur Geographie und Kartographie) 11:49-55.

SALZMANN, N., KÄÄB, A., HUGGEL, C., ALLGÖWER, B. and HAEBERLI, W., 2004: Assessment of the hazard potential of ice avalanches using remote sensing and GIS-modelling. Norsk Geografisk Tidskrift - Norwegian Journal of Geography, 58(2):74-84.

SWISSTOPO, 2004: DHM25 - The digital height model of Switzerland. Product Information, 15p.

TOUTIN, 2008: ASTER DEMs for geomatic and geoscientific applications: a review. International Journal of Remote Sensing, 29(7):1855-1875.

VAN ZYL, J.J., 2001: The Shuttle Radar Topography Mission (SRTM): a breakthrough in remote sensing of topography. Acta Astronautica, 48(5-12):559-565.

WESSELS, R., KARGEL, J. and KIEFFER, H., 2002: ASTER measurement of supraglacial lakes in the Mount Everest region of the Himalaya. Annals of Glaciology, 34:399-408.

Correspondence to:

Holger Frey

Glaciology, Geomorphodynamics & Geochronology; Department of Geography

University of Zurich; Switzerland

e-mail: holger.frey@geo.uzh.ch

Paper IV

Frey, H., Haeberli, W., Linsbauer, A., Huggel, C., and Paul, F. (2010a). A multi-level strategy for anticipating future glacier lake formation and associated hazard potentials. *Natural Hazards and Earth System Sciences*, 10: 339–352

Nat. Hazards Earth Syst. Sci., 10, 339–352, 2010
www.nat-hazards-earth-syst-sci.net/10/339/2010/

Natural Hazards and Earth System Sciences

A multi-level strategy for anticipating future glacier lake formation and associated hazard potentials

H. Frey, W. Haeberli, A. Linsbauer, C. Huggel, and F. Paul

Department of Geography, Universtity of Zurich, Switzerland

Received: 30 October 2009 – Revised: 10 February 2010 – Accepted: 12 February 2010 – Published: 22 February 2010

Abstract. In the course of glacier retreat, new glacier lakes can develop. As such lakes can be a source of natural hazards, strategies for predicting future glacier lake formation are important for an early planning of safety measures. In this article, a multi-level strategy for the identification of overdeepened parts of the glacier beds and, hence, sites with potential future lake formation, is presented. At the first two of the four levels of this strategy, glacier bed overdeepenings are estimated qualitatively and over large regions based on a digital elevation model (DEM) and digital glacier outlines. On level 3, more detailed and laborious models are applied for modeling the glacier bed topography over smaller regions; and on level 4, special situations must be investigated in-situ with detailed measurements such as geophysical soundings. The approaches of the strategy are validated using historical data from Trift Glacier, where a lake formed over the past decade. Scenarios of future glacier lakes are shown for the two test regions Aletsch and Bernina in the Swiss Alps. In the Bernina region, potential future lake outbursts are modeled, using a GIS-based hydrological flow routing model. As shown by a corresponding test, the ASTER GDEM and the SRTM DEM are both suitable to be used within the proposed strategy. Application of this strategy in other mountain regions of the world is therefore possible as well.

1 Introduction

In proximity to melting conditions, snow and ice react sensitively to climate change (Haeberli and Beniston, 1998). As a consequence, high-mountain landscapes that are dominated by glacial and periglacial processes are influenced by the governing climatic conditions and their changes. The continuous rapid retreat of glaciers in mountain ranges all over the world is one of the most obvious and reliable indicators of global warming (GCOS, 2004; Lemke et al., 2007); it is well visible and easily understandable for a wider public. Glaciers are also symbols of an intact environment, thus glacier retreat also has a strong impact on the perception of the landscape (WGMS, 2008; Haeberli, 2005).

Fast changes of the high-mountain cryosphere affect various phenomena, processes and process interactions and can lead to hazard situations beyond historically known conditions. Associated with glacier retreat, pro-glacial lakes can form behind moraine dams or in overdeepened parts of the exposed glacier bed. Such new lakes are attractive elements in a landscape and compensate to a certain degree the loss of attractiveness from glacier disappearance (Haeberli and Hohmann, 2008). They also constitute interesting potentials for hydropower production. However, glacier lakes can pose a potential threat to the population and infrastructure in the valleys below as they are forming in an environment dominated by interacting, rapidly changing and highly dynamic processes.

The most severe glacier catastrophes often result from a combination and chain reaction of different processes (Huggel et al., 2004; Kääb et al., 2005; Reynolds GeoScience Ltd, 2003). In glaciated environments, the following changes affect the hazard situation of glacier lakes:

- Glacier retreat can lead to the development of new potential ice avalanche starting zones (Clague and Evans, 2000; Kääb et al., 2005; Richardson and Reynolds, 2000a; Kershaw et al., 2005).
- Transitions in the thermal regime of hanging glaciers, from cold to polythermal or temperate, can destabilize them due to reduced basal friction (Alean, 1985; Fischer et al., 2006; Huggel, 2009).

Correspondence to: H. Frey
(holger.frey@geo.uzh.ch)

Published by Copernicus Publications on behalf of the European Geosciences Union.

- The retreat and thinning of glaciers since the Little Ice Age has a destabilizing effect on steep adjacent rockwalls due to the related debuttressing effect (Augustinus, 1995; Ballantyne, 2002). Such rock walls can be situated close to newly forming glacier lakes (e.g. the Schlossplatten rock fall and -toppling at the tongue of the Lower Grindelwald Glacier) (Oppikofer et al., 2008).
- Glacier retreat often exposes morainic and unconsolidated material (Evans and Clague, 1994) that, if situated in steep terrain, is prone to be the starting zone for landslides and debris flows (Huggel et al., 2004; Haeberli et al., 1991; Hubbard et al., 2005).
- The formation of new glacier lakes itself is a potential threat because an outburst of such a new lake can initiate a cascade-like chain reaction involving other lakes located further downstream (cf. Gruben Glacier, Haeberli et al., 2001).
- Regions with warm permafrost conditions are expected to show the most critical stability conditions of frozen rock walls (e.g., Gruber and Haeberli, 2007). With increasing air temperatures, permafrost degradation and thus deep long-term warming of such rock walls will increase the probability of rock falls. Glacier lake outbursts triggered by rock fall will thus be a scenario of increasing probability in the future.
- Permafrost degradation also reduces the stability of moraine dams that contain dead ice or other subsurface ice (Richardson and Reynolds, 2000b).

Detecting and monitoring of existing glacier lakes by remote sensing methods (Allen et al., 2009; Frey et al., 2010; Huggel et al., 2002; Kääb et al., 2005) as well as field investigations with geophysical methods (Haeberli et al., 2001; Richardson and Reynolds, 2000a) are a research focus in various mountain regions.

Knowledge about sites with potential future lake formation would thus be a useful basis for decision-making by the responsible authorities. So far, only little research has been done in the field of detecting sites with potential future lake formation. Reynolds (2000) found a slope gradient of 2° to be the critical threshold for supraglacial lake formation on debris-covered glaciers in the Himalayas. Quincey et al. (2007) confirmed this finding and concluded that debris-covered glacier parts with low flow velocities are most likely sites with a potential for supraglacial lake formation.

In this study, we present a multi-level strategy to anticipate the formation of future glacier lakes at different scale levels. At all levels, local overdeepenings in the glacier bed are estimated by analyzing the current glacier surface characteristics based on digital elevation models (DEMs), digital glacier outlines and satellite imagery. Such input information is widely available, enabling the methods to be applied to other mountain ranges in the world. The focus of this study is on the quick and qualitative assessment of potential future lake formation in regions, where only sparse data are available. Therefore, the first two larger-scale levels of the strategy are the main focus of this paper; the third and the fourth level relate to existing, but more laborious approaches and are not discussed in detail.

The paper first describes the test sites and the used data before the methods of the four strategy-levels for future lake detection and hazard assessment are presented. In view of the obvious difficulty of verifying predictions of future conditions, the approaches are validated using historic data at a test site in the Bernese Alps (Trift Glacier), where a proglacial lake formed recently. Scenarios of future lake formation are then derived for the two regions Bernina and Aletsch. In addition, the likely runout path of a flood from potential outbursts of expected future lakes are modeled in the Bernina region. In view of applying the approach to other regions in the world, the influence of different DEMs on the results is tested as well.

2 Test sites and data

2.1 Test sites

Although the presented approach is intended to be globally applicable, we chose test sites in the Swiss Alps for this study due to the good data availability, including a high-quality DEM and various historical maps since the middle of the 19th century. The methods for the detection of overdeepenings in the glacier bed are verified at Trift Glacier in the Bernese Alps (Fig. 1). Since the mid 1980's, the tongue of this glacier experienced strong down-wasting (Paul and Haeberli, 2008) and finally collapsed between 2000 and 2005. A new lake (length 1 km, max. width 450 m) formed, which contributed to the rapid disintegration of the glacier tongue. The location is easily accessible and a suspension bridge over the gorge at the end of the lake attracts many tourists in summertime. We applied the assessment strategy on data from before the start of the lake formation (i.e., before 2000), to analyze whether the formation of this lake could have been anticipated with this approach.

For the Aletsch and Bernina regions (Fig. 1), scenarios of potential future lakes are presented. The testing of the different DEMs and the preliminary hazard assessment are performed in the Bernina region. In both regions, glaciers are prominent elements of the landscape (the Aletsch Glacier is the largest glacier of the Alps and part of the UNESCO world heritage Swiss Alps Jungfrau-Aletsch) and of high economic importance for tourism.

2.2 Input data

The used DEM was produced by the Swiss Federal Office of Topography (swisstopo) and has a cell size of 25 m. This

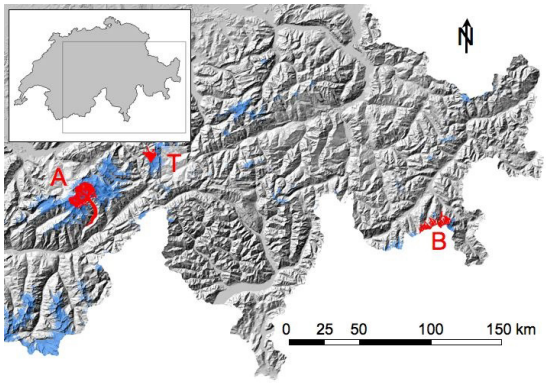

Fig. 1. Overview of the study regions. Aletsch Glacier (A), Trift Glacier (T) and the Bernina region (B) are shown in red, other glaciers are shown in light blue. The relief is depicted as a hillshade view of the DHM25L2.

dataset is based on the interpolation of contour lines from the Swiss National Map (1:25 000) and includes digitized lake perimeters, main break lines and spot heights. Two editions of this data set are available: a Level 1 (DHM25L1) and a Level 2 (DHM25L2) version, which primarily vary regarding the algorithms for the contour line interpolation and the acquisition date (Swisstopo, 2004). The DHM25L1 was acquired around 1985, whereas in the DHM25L2 the contour lines of glaciers were updated to the state of around 1995, except for the Bernina region. In view of applying the here presented approaches to other regions in the world, the influence of the DEM quality on the result is tested in the Bernina region for different DEMs, including the global DEM compiled from ASTER data (ASTER GDEM, Hayakawa et al., 2008) and the DEM from the Shuttle Radar Topography Mission (SRTM, Farr et al., 2007) in addition to the DHM25L2.

To determine the glacier extent, we used glacier outlines from the Swiss Glacier Inventory (SGI, described in Paul, 2007). Regarding applications to other regions, digital glacier outlines can be found for example in the Global Land Ice Measurement from Space (GLIMS) glacier database (Raup et al., 2007). To study the crevasse pattern of glaciers, the panchromatic channel with a resampled spatial resolution of 10 m from two scenes of the Indian Remote Sensing satellite (IRS-1C) from September 1997 were used.

For the validation at Trift Glacier, the corresponding map sheet of the Siegfriedkarte is used, a precursor of the actual topographic map of Switzerland. For the Alps, the Siegfriedmap has a 1:50 000 scale and we used the 1932 edition of sheet number 392 “Meiringen”.

3 Methods

3.1 Strategy to detect glacier bed overdeepenings

Glaciers have a considerable erosive power, which – unlike fluvial erosion – can result in large depressions in the bed. When such overdeepened parts of the glacier bed are exposed after glacier disappearance and filled with (melt-) water rather than with sediments, new proglacial lakes appear (Clague and Evans, 1994; Costa and Schuster, 1988). In other words, sites with potential future lake formation can be identified by detecting overdeepenings in the glacier bed. Roughness and irregularities of the glacier bed induce stresses to the glacier ice, which are compensated to a certain degree by deformation. But due to the non-perfect plasticity of ice, bed irregularities are only partly compensated. Hence, the glacier surface topography is in principle a smoothed image of the underlying bed, and the current glacier surface can serve as a key to identify overdeepened parts of the glacier bed (Oerlemanns, 2001).

A multi-scale approach for identifying such overdeepenings allows to cover large regions on the one hand (level 1 and level 2), and to analyze selected situations in more detail (level 3 and level 4) on the other hand.

The assessment strategy integrates the following four levels (Fig. 2):

- Level 1: selection of parts of the glacier surfaces below a slope threshold. Application to regions of 10^4 km^2 to 10^5 km^2 to quickly obtain an overview over large regions.
- Level 2: manual application of three criteria (distinct slope increase, reduction of glacier width, and crevasse-free part followed by heavily crevassed part), to detect potential overdeepenings in the glacier bed. Application to regions of 10^3 km^2 to 10^4 km^2 to detect regions and situations of special interest.
- Level 3: use of more detailed tools, which require more input data (e.g. digitized central flow lines) to model the ice thickness distribution (e.g., Farinotti et al., 2009; Linsbauer et al., 2009). The region of application ranges from individual glaciers up to several 10^4 km^2, depending on the model and the availability of required input data.
- Level 4: in-situ geophysical investigations (e.g., radio-echo sounding) or drilling in the field for detailed information about the bed topography and bed properties at individual points or transects. Local application for situations that are considered to be critical. This level 4 is not further discussed in this article.

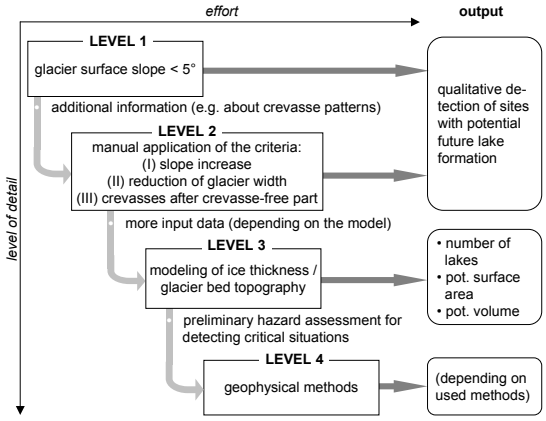

Fig. 2. Illustration of the different levels of the strategy for detecting sites with potential future lake formation.

3.1.1 Level 1

Rothenbühler (2006) selected sites with a glacier surface gradient below 5° and a minimum area of 6250 m^2 (ten 25 m-cells) to define sites with potential lake formation on glaciers in the Bernina region. Instead of selecting only parts that consist of 10 connected cells as proposed originally, we here used a median filter that was applied on a 5 by 5 cells moving window (low pass filtering). That way, isolated pixels are eliminated, small holes are filled and the result is smoothed. This threshold algorithm can be easily implemented in a Geographic Information System (GIS) and a first overview of potential overdeepenings can be quickly gained for a large region. The 5° threshold also includes the critical slope gradient of 2° for supraglacial lake formation on debris-covered glaciers (Reynolds, 2000).

3.1.2 Level 2

Based on simple ice mechanical considerations, we defined three additional criteria for level 2: (I) a distinct break in slope, (II) a reduction in glacier width, and (III) a heavily crevassed glacier part below a crevasse-free part. The explanations for these criteria are as follows:

(I) According to the shallow ice approximation (SIA) and the assumption of perfect plasticity (Paterson, 1994) and thus constant basal shear stress (τ), the ice thickness (h) only depends on the surface slope (α), averaged over a distance longer than the thickness:

$$h = \frac{\tau}{F\rho g \sin\alpha}$$

with F = shape factor, ρ = density of ice, and g = the gravitational acceleration It follows that steep parts of a glacier have thinner ice than flat parts. Thus, depressions in the bed can be expected at places that are above a distinctive break in the surface slope along the flow direction, where a glacier moves from a flat part with thick ice into a steeper section with thinner ice. This is qualitatively correct, although valley glaciers support a considerable amount of the driving stress by lateral drag. The influence of the shape factor (F) (Paterson, 1994), as well as the variability of the basal shear stress (τ) with different slopes (Haeberli and Schweizer, 1988) are neglected here.

(II) Assuming that cross sections of valley glaciers are uniform, there is an empirical relation between width (w) and ice thickness (h) in the form of

$$h \sim \frac{w}{c}$$

with values for the constant c in valley glaciers ranging from 3 for steep slopes to 8 for less pronounced valleys (Benz, 2003; Haeberli and Schweizer, 1988). Accordingly, wide glacier parts have a larger ice thickness than narrow parts and an overdeepening can be expected above a distinct glacier narrowing.

(III) If the glacier has to overcome a negative bed slope at the end of an overdeepened basin, the ice will undergo longitudinal compression and thus has no crevasses (compressive flow), but showing a crevassed surface (extending flow) when overflowing a threshold in the bed (Paterson, 1994). A part without crevasses followed by a heavily crevassed region, mainly with transversal crevasses, can thus indicate an overdeepening. This criterion is often coexistent with criterion (I) and (II), because a distinct increase in slope is often related to a narrowing of the valley and accelerating flow and, thus, a crevassed surface (e.g., Hooke, 1991).

These three criteria are schematically illustrated in Fig. 3. There is no need that all three criteria are fulfilled simultaneously, but often they occur combined. Criteria (I) and (II) can be estimated with terrain information (DEM) whereas for criterion (III) a satellite image of at least 30 m resolution (e.g. Landsat TM) or better or an aerial photograph can be used. Tools like Google Earth™ might also be suitable if high-resolution imagery is at hand in those services. If available, also a high resolution DEM – e.g. from airborne LIDAR – can help to identify the crevasse pattern at the surface. In general, large flat glacier parts as used in level 1 are closely related to all the three criteria of level 2, as often a steeper scarp is following (I), narrow glacier parts normally are steeper than the wide parts (II), and flat parts tend to show no or only few crevasses (III). Therefore, the results of level 1 can be used as a guideline for the manual analysis of level 2.

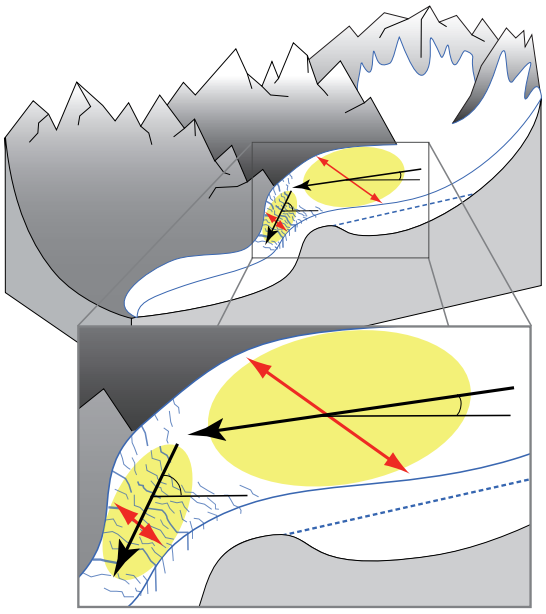

Fig. 3. Simplified schematic sketch of the three criteria that are applied manually on level 2. The black arrows indicate a distinct break in slope (criterion I), the red arrows show a narrowing of the glacier width (criterion II) and the yellow areas cover a flat and crevasse-free region followed by a heavily crevassed area (criterion III). The dashed line in the overdeepening represents the potential future lake level.

3.1.3 Level 3

Models like the ones presented by Farinotti et al. (2009) or Linsbauer et al. (2009) estimate the ice thickness distribution or the glacier bed topography, respectively. They proved to be in good agreement with ice thicknesses measured in the field and provide thus helpful tools for the detection of overdeepened parts of the glacier bed. Compared to the results of level 1 and level 2, quantitative information can be gained at this level. Of course, in an absolute sense the modeled glacier beds might have large uncertainties. However, the potential maximum area and volume of a lake as well as topography of the lake bottom and the surrounding terrain after glacier disappearance can be realistically estimated. Compared to the methods for assessments on level 1 and level 2, such models require additional input data (e.g. digitized center lines for major glacier branches and parameters describing the mass balance distribution and the ice flow). Depending on the model, the size of the region that can be processed may be restricted due to limited computational power or the availability of input data. In this study, we used the model of Linsbauer et al. (2009) for comparison and validation purposes, and the modeled glacier bed topography with its overdeepenings was used as input for the modeling of potential future lake outbursts (see Sect. 5). The main workload for this model is given by the manual digitization of flow lines for each glacier and all its main tributaries.

3.1.4 Level 4

For more detailed investigations of a specific site, e.g., accurate assessment of potential future lake volume, geophysical measurements like ground penetrating radar (GPR) (e.g., Binder et al., 2009) or even drilling (e.g., Truffer et al., 1999) have to be performed. However, as mentioned before, these methods are not further discussed in this study.

3.2 Validation

To validate the methods of the different levels, they were applied to historical data to allow a comparison with the present situation (Fig. 4). For Trift Glacier in the Bernese Alps, where a lake formed after the year 2000, the topographic map (Siegfriedkarte) from 1932 and a photograph from 1948 provide the information for the qualitative assessments. For the quantitative analyses the DHM25L1, representing the surface of 1985, was used.

Analyses on level 1 and 2 based on the historical map are shown in Fig. 4a. The contour lines indicate a surface slope slightly below 5° (level 1) in the region of the present-day lake, and the criteria of level 2 apply as well. In the photograph from 1948 (Fig. 4b), these criteria are illustrated as well, to demonstrate that they can also be applied visually in the field for a rough assessment. Based on the DHM25L1 (dating to 1985) and the digital glacier outlines from 1973 (Paul, 2007), the model from Linsbauer et al. (2009) was used to estimate the glacier bed topography at level 3 (Fig. 4c). The results indicate a distinct depression in the glacier bed with a depth of about 100 m at the location of the new lake. The surface slope of the glacier in 1985 (calculated from DHM25L1) is slightly larger than in 1932 (measured in the Siegfriedkarte), but the surface gradient near the tongue is still below 5°. Qualitative tests of the strategy on level 1 and level 2 with historical maps were also performed at Rhone Glacier and Gauli Glacier, two other sites with recent lake formation. In both examples, the former glacier surface was flat and all three criteria of level 2 applied as well. Concluding, it can be stated that these lakes could clearly be anticipated from the historic data by the manual application of the three criteria of level 2 and the model used on level 3. The application of the slope threshold on level 1, although being less reliable, also proved to give a quick and sufficiently accurate overview.

3.3 Modeling potential future lake outbursts

In order to detect critical situations and cases, which require in-situ investigations on level 4, a hazard assessment concerning the expected lakes is performed based on the results

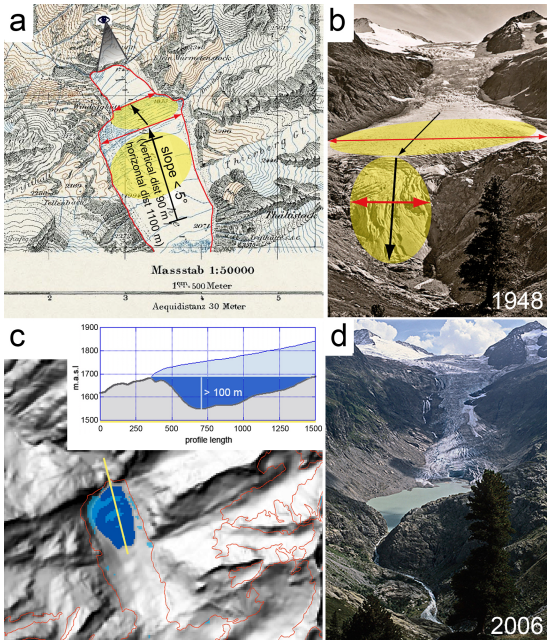

Fig. 4. Application of the strategy to Trift Glacier, using historical data. **(a)** Level 1 (slope<5°) and level 2 (three criteria, same symbols as in Fig. 2) applied to the Siegfried map from 1932. The eye and the triangle indicate viewing directions of photographs shown in **(b)** and **(d)**. (b) Photograph from 1948, level 2 criteria are indicated again. **(c)** Modeled bed topography based on DHM25L1 from 1985 and glacier outlines from 1973 (red lines). The modeled overdeepening (blue) is more than 100 m deep. Light and transparent blue areas are parts with surface gradient below 5° (level 1) for comparison. (d) Photograph from 2006, taken from the same location as (b). Photographs (b) and (d) © Gesellschaft für ökologische Forschung (www.gletscherarchiv.de).

of level 3. Because these future scenarios have large uncertainties about the exact location, lake volume and properties of the environment surrounding the lakes, such an assessment can only be of preliminary nature. Relationships gained from the analyses of past events showed that for the formation of debris flows, firstly loose sediments must be available for entrainment, and secondly, a minimum channel slope of 8° is required to mobilize the material (Hungr et al., 1984; O'Connor et al., 2001). So far, the maximum runout distances of coarse debris flows originating from outbursts of ice and moraine dammed lakes in the European Alps have not been documented to fall below 11° ($\tan\alpha = 0.19$) (Haeberli, 1983; Huggel et al., 2002). This value can thus be used as a limit for worst-case scenarios of debris flow type outburst floods. If no loose sediment is available or slopes are too flat for sediment entrainment and the water volume by far exceeds the sediment volume, flood waves with much longer potential runout distances can form. For such a case, Haeberli (1983) found in an empirical study in the Swiss Alps an overall slope of 2° to 3° as maximum distance of the destructive reach of flood waves.

Huggel et al. (2003) presented a simple but robust debris flow model that includes these empirical runout distances and slope thresholds, and that can be applied with reasonable assumptions for the required input data. The so-called modified single flow model (MSF) is a hydrological flow routing model that calculates for each cell of a DEM a probability of affection by a flooding event. It is based on a hydrological algorithm that calculates the flow direction from one DEM cell to another according to the steepest downward gradient between one cell and its eight neighbours. In addition, it allows also a flow spreading of up to 45° from the main flow direction. The input data are starting cells and a DEM. In this study we used the modeled potential future lake areas as starting zones and the DEM without glaciers obtained on level 3 for flow path modeling. The MSF model can be applied to larger regions, i.e. several lake outbursts can be modeled within one model run. The somewhat speculative and uncertain assumptions about the volume and the sediment concentration of outburst floods are not considered in the model.

4 Results

4.1 Future lake scenarios

For the Aletsch and for the Bernina test regions, locations with potential future lake formation were delineated based on the results of levels 1 and 2 (Figs. 5 and 6). The DHM25L2 was used for an automated selection of glacier parts with surface slopes below 5° (level 1, blue areas). For the manual application of the three criteria on level 2, a slope map derived from the DHM25L2, the digital glacier outlines from the SGI, and the IRS-1 C scenes were used.

In Fig. 5 the results for the Aletsch Glacier are shown. Large parts of the glacier surface have a slope gradient below 5° (blue areas in the figure) and are selected on level 1. This is not surprising, as large glaciers tend to have low mean slope values (Paul, 2007). However, it is unlikely that all these parts with a flat surface are overdeepened. On level 2, the overdeepenings can be located already from the information from level 1, although estimations of the exact positions and sizes of the overdeepenings 2, 3, 5, 9, 10 and 11 are uncertain. On the one hand, it is possible that some of them are connected (e.g. overdeepenings 2 and 3), on the other hand, some of them are likely to be much smaller than indicated. The other overdeepenings were identified according to the following criteria of level 2: at locations 8 and 9, a distinct break in slope (criterion I) applies, at number 1, 6 and 7, a reduction in glacier width further downstream (criterion II), can be observed. Overdeepenings number 4 and 6 are located

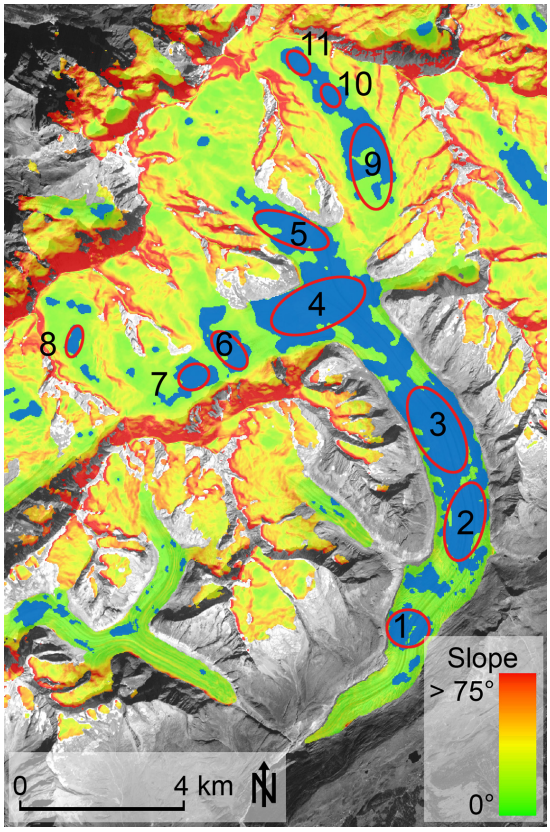

Fig. 5. Potential overdeepenings in the bed of Aletsch Glacier; IRS-1C scene (10 m resolution) in the background. Surface gradient of glaciers is shown in green (flat) to red (steep): results of level 1 are shown in blue (glacier surface parts with slope <5°); and the overdeepenings estimated on level 2 are indicated with red circles. Further explanations are given in the text.

at confluences with tributary glaciers, a factor that favors the erosive power of a glacier (MacGregor et al., 2000).

The application of the methods to the Bernina region is shown in Fig. 6. On level 1, the overdeepenings number 2, 4, 6, 7 and 10 can be identified, while locations 1, 3 and 5 are somewhat unclear because only small flat areas are detected. On level 2, numbers 3 and 5 are detected more clearly: all criteria apply at site 3 and criterion (I) and (III) apply for location 5. Site 7 is considered to be overdeepened as well, because the confluence of the two glacier branches favors erosion. Sites 8 and 9 are identified clearly on this second level, also here all three criteria apply, at site 9 even more clear than at site 8. However, the surface gradients are slightly steeper than 5° at both locations.

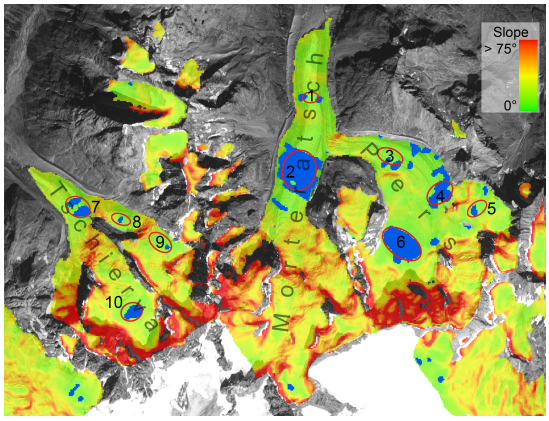

Fig. 6. Potential overdeepenings in the Bernina region; IRS-1C scene (10 m resolution) in the background. Surface gradient of glaciers is shown in green (flat) to red (steep): results of level 1 are shown in blue (glacier surface parts with slope <5°); and the overdeepenings estimated on level 2 are indicated with red circles. Further explanations are given in the text.

4.2 Comparison of qualitative assessment (levels 1 and 2) with modeled overdeepenings (level 3)

With regard to applications of this strategy to other mountainous regions, we applied only the first two levels on both regions, as it would be the case for remote and unexplored regions, where input data for more detailed investigations are missing. A comparison of the results of these qualitative assessments to the modeled overdeepenings from the estimated bed topography (level 3) is shown in Fig. 7 to reveal the strengths and weaknesses of these first two levels.

According to the interpolated bed topography from level 3 by the model from Linsbauer et al. (2009), there are seven sites in the Bernina region with a potential for the formation of a larger lake in the region of Morteratsch Glacier and Pers Glacier (Fig. 7 A and 1 to 6). Three of these seven sites, 2, 4 and 6, are detected on level 1 due to their surface slopes below 5°. The modeled overdeepening at site 3 is only weakly indicated on level 1 by the patchy distribution of areas with flat surfaces, but is detected on level 2. At the site 1, two small patches of flat areas are indicated on level 1, and on level 2 a slight increase in slope (criterion I), however it was still unclear if there is an overdeepening in the bed. At site 5, a small flat part and a distinct increase in slope indicate an overdeepening. The model applied on level 3 shows an overdeepening, however, it is a small depression and it is even possible that the depression is only an artifact of the model and the bed is not overdeepened at all at this location. To assess this in more detail, geophysical measurements must be performed (level 4). Finally, the modeled

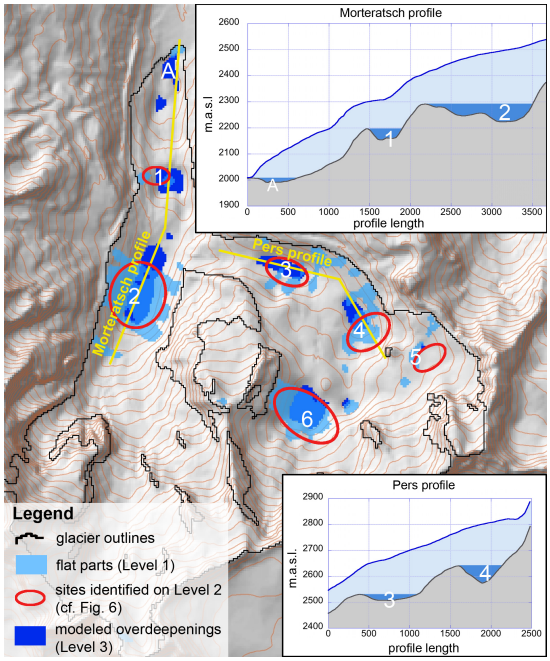

Fig. 7. Comparison of the results from level 1 and 2 with the modeled bed topography (level 3, overdeepenings shown in dark blue, A–G) on Morteratsch- and Pers Glacier (Bernina region), including two profiles. Results from level1 are shown in transparent light blue, results from level 2 are indicated by red circles (compare to Fig. 6).

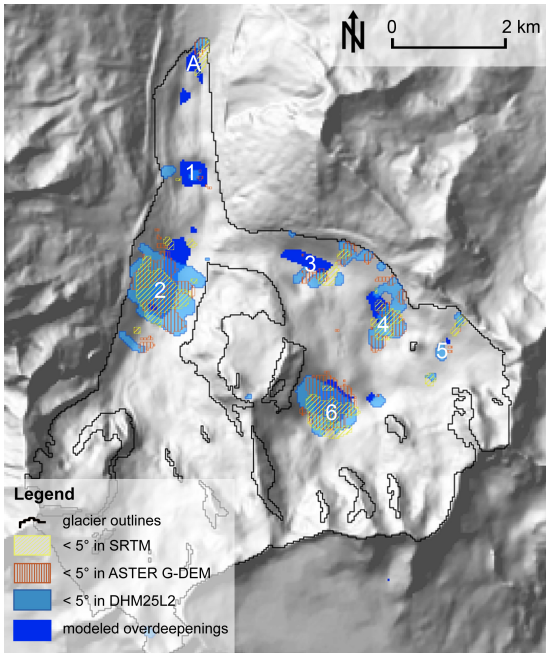

Fig. 8. Glacier surface areas with slope <5° (level 1) on Morteratsch- and Pers Glacier derived from the ASTER GDEM (yellow) and SRTM (orange). For comparison, flat parts derived from the DHM25L2 (light blue) and overdeepenings in the modeled glacier bed (blue) are shown as well. The background is a hillshade view of the modeled bed topography and the DHM25L2 outside the glacier margins.

overdeepening at site A near the terminus may be an artifact of the model due to the interpolation of a concave shaped bed between the last interpolation point and the glacier outline (Linsbauer et al., 2009). Regarding the formation of lakes at these overdeepenings, the temporal component of glacier retreat is important. Generally, lakes form earlier in lower overdeepenings. Transient glacier retreat models could help to estimate the point in time when the formation of a lake will start.

4.3 Potential for application in other regions

According to the verification at Trift Glacier and the comparison with the modeled bed topography, the first two levels of the assessment strategy are sufficient for a preliminary and qualitative identification of sites with potential future lake formation in a larger region. In view of applying these methods to other mountain regions of the world, it was tested whether the SRTM DEM and ASTER GDEM can be used within this strategy. Therefore, for both DEMs the Morteratsch region was clipped, reprojected to the Swiss coordinate system, horizontally adjusted to the DHM25L2 (Paul and Haeberli, 2008) and resampled to 25 m by bilinear interpolation. In contrast to the processing of the DHM25L2 on level 1 (see Sect. 3.1.1), no filter was applied to the flat regions derived from the SRTM and the ASTER GDEM. They were smoothed already during the resampling process. The selection of flat glacier parts with surface slopes below 5° (level 1) is shown in Fig. 8. Flat parts from the high-quality DHM25L2 and the overdeepenings in the modeled bed topography are also shown. The larger overdeepenings at sites 2, 4 and 6 can be identified in both other DEMs clearly; 3 and 5 remain unclear on level 1. Flat parts derived from both DEMs are smaller compared to the DHM25L2 and small flat parts in the latter are not represented in the other DEMs. This is due to the coarser resolution of the original datasets. In general, the results from SRTM correspond slightly better to the results from the DHM25L2 than the results derived from the ASTER GDEM.

For the second level, slope masks (not shown here) were derived from the two additional DEMs. Again, compared to the DHM25L2 both slope masks are less detailed and show more artifacts. Also, the larger overdeepenings can be identified again; but smaller ones remain unclear or cannot be

resolved. However, because the information extracted from the DEMs is only used for a qualitative assessment on level 1 and 2, they are both considered to be suitable for being used within this strategy, at least on the first two levels. Assuming that the quality of these datasets is similar in other mountain regions, these DEMs allow an application of the presented strategy also beyond the European Alps.

5 Assessing potential future glacier lake outburst

In this study, the temporal evolution of glacier retreat and thus also the temporal evolution of lake formation is not considered. Instead, runout paths for worst-case scenarios of glacier lake outburst are modeled: all glaciers have retreated strongly, most parts of the beds are exposed, and all overdeepenings modeled on level 3 are completely filled with water. Based on this setup, potential future lake outbursts are modeled for the Morteratsch- and Pers Glaciers, also to demonstrate the potential of simple flow-routing models like the MSF model (Huggel et al., 2003) that can be used in such cases with highly uncertain conditions. Based on the results of such a preliminary assessment, sites that require more detailed investigations on level 4 can be selected. Nevertheless, the temporal evolution of glacier retreat and lake formation has a direct influence on the hazard situation. For example, after the formation of a lake at overdeepening 3 in Fig. 7, Pers Glacier will terminate in a steeper part of the bed and thus favor the formation of ice avalanches. The new lake in front of this tongue might be in the runout distance of such ice avalanches. After continued retreat of Pers Glacier, the situation might become less critical.

5.1 Potential future lake outbursts at Morteratsch Glacier and Pers Glacier

The results of the MSF modeling are shown in Fig. 9. According to the modeled bed topography, the lakes are all hydrologically connected, in other words, many of the outburst floods reach other lakes located further downstream. This is inherent to the applied model approach, because the largest depths are modeled along the central flow line. However, this is also realistic from a glaciological point of view, because the depressions were shaped by the same glacier. The slope values from the modeled glacier bed exceed 8° in the surrounding of most future lakes, hence, loose material could be entrained by outburst floods from these lakes. The average slope values of the glacier beds are around 25°, but below the glacier tongues the terrain levels out. Even in worst-case scenarios with runout distances for debris flows according to an 11° average slope threshold (Haeberli, 1983; Huggel et al., 2002), debris flows from future glacier lakes could reach lakes situated below, but in most cases the affected areas are confined to regions close to the lakes; they do not reach presently existing buildings, settlements or other expensive infrastructure (Fig. 9a).

Because it is highly uncertain how much loose sediment will be available in the future, we also modeled potential flood waves, which, compared to debris flows, have a much lower sediment concentration (Fig. 9b). For the maximum runout distance we chose again a worst-case approach and used a maximum average slope of 3° (see Sect. 3.3).

In the combined modeling of the whole region in a single model run, the MSF model calculates the average slope always from the lowest starting zone. In other words, if a lake outburst flood reaches a lower lake, the modeling of the flood from the upper lake is aborted and only the flow path from the lower lake is calculated. This is reasonable because a debris flow or flood wave from an upstream lake can trigger an outburst of a lower lake, but the kinetic energy of the incoming flow mass will be used to displace the water from the lower lake. However, in the case of modeling outbursts from potential future lakes, it is uncertain which lakes will form at all and when. It is possible that a lower lake is filled with sediments, drained already earlier, or did never form at all. For this reason, we modeled flood waves for all potential future lakes individually to avoid undesirable interactions.

The maximum runout paths of the individual flood waves are shown in Fig. 9c. According to the model, the floods could reach existing settlements and infrastructure. Flood waves from all these potential future lakes could affect the roads and the railroad in the Bernina Valley. Floods originating from the bed of Morteratsch Glacier would not reach Pontresina (P), but all expected future lakes of Pers Glacier have the potential to cause flood waves that could reach the village of Samedan (S).

The influence of lakes located in the runout of an upstream lake can be shown with the example of the lowest lake on Morteratsch Glacier (M1). If this depression is empty of water during an outburst of P1, P2 or P3, the potential destructive reach of such a flood wave could reach the flood plain of Samedan, where a regional airport is located. But if there is a full lake at M1, it could absorb the energy from an outburst of a smaller lake upstream. Of course this depends strongly on the volume and geometry of the retention basin at M1 and the magnitude of the outburst flood from P1, P2 and P3. From these finding the hypothesis arises, that a lake of a sufficient size, located at the transition from steep terrain to a flat valley bottom reduces the hazard potential of other lakes located higher up in steep terrain. This is only the case, if the lower lake is large enough and has a sufficiently stable dam to absorb the kinetic energy of an incoming flood wave from an upstream lake outburst.

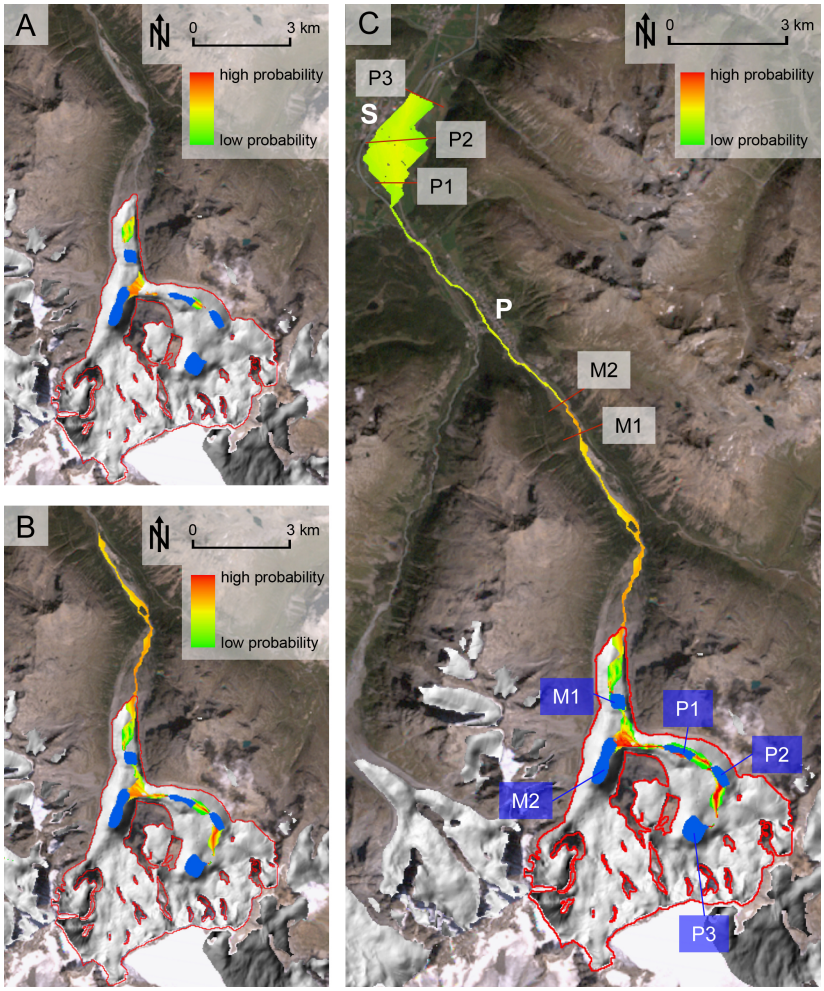

Fig. 9. Flow routes of outbursts from potential future glacier lakes of Morteratsch (M1, M2) and Pers Glacier (P1–P3) modeled with the MSF algorithm. Background image is a Landsat 5 TM scene from 1999; glaciers were replaced by hillshade views of the modeled glacier beds. **(A)** debris flows; **(B)** flood waves modeled in one model run (runout path is interrupted as soon as another lake is reached); **(C)** flood wave paths modeled for each glacier individually. The starting points are indicated by blue boxes; respective maximum destructive runout distances are shown in grey boxes. Indicated settlements are Pontresina (P) and Samedan (S).

6 Discussion and perspectives

The presented strategy to detect sites with potential future lake formation on four different levels proved to be feasible and the results of the different levels are consistent. In the Bernina region all the overdeepenings in the modeled bed topography at level 3 could be identified on the previous levels already. Regarding an application to other mountain regions of the world, where only sparse input data may be available, the methods of these first two levels can quickly provide qualitative information without much computational effort.

For such an approach, designed to anticipate future scenarios, it is essential that all overdeepenings are identified, even though not all of them may cause lake formation. In statistical terminology type II errors (false negatives; in this case a real overdeepening that is not detected by the strategy) must be minimized. It is therefore accepted that too large areas are selected at level 1. But because the real glacier bed topography and its properties are not known before glacier disappearance, the value of this type II error cannot be quantified precisely.

So far, glacier sedimentation was not considered in this study. The sedimentary properties of the glacier beds that will be uncovered in the future have a twofold impact on potential lake formation: on the one hand, continued sedimentation can fill overdeepenings in the bedrock and thus reduce the lake volume or prevent lake formation at all. On the other hand, sedimentary glacier beds can provide loose material for debris flow formation and lead to moraine dammed lakes with a potential for mechanical dam failures and related extreme discharges. Maisch et al. (1999) presented an index to discriminate sedimentary and rocky glacier beds, based on the heights of surroundig rock walls and a number of glacier characterisitcs. Zemp et al. (2005) implemented this index into a GIS, which allows including it in the suggested assessment strategy at level 3, e.g. supplementary to the modeling of potential outburst floods.

The methods of this study were developed and tested for glaciers without extensive debris cover. However, supraglacial lakes can also develop on debris-covered glaciers of the Alps, e.g. on the Belvedere Glacier in Italy or on the tongue of the Lower Grindelwald Glacier in Switzerland. Reynolds (2000) anticipated sites with potential supraglacial lake formation on heavily debris-covered glaciers in the Himalayas (Bhutan) by identifying stagnant parts of the glacier tongue with average surface slopes below 2°. This approach was later confirmed by a study of Quincey et al. (2007) who investigated the flow velocities of debris-covered tongues in Nepal and Tibet (China) by using synthetic aperture radar (SAR)-interferometry. In principle, this procedure corresponds to our approach at level 1 and level 2, respectively. The different lake formation processes explain the differences of the slope values for level 1: on debris-covered tongues, lake formation normally starts with the occurrence of small individual supraglacial ponds that coalesce later to a single lake, which finally grows constantly by melting the adjacent ice in all directions (mainly upstream). This process can take the whole valley width and finally even replace a large part of the tongue (Bolch et al., 2008; Komori, 2008; Reynolds, 2000; Watanabe et al., 1994). Our approach is related to proglacial lake formation at (nearly) debris-free glaciers where lake formation starts at the (retreating) glacier front. Thus, the threshold slope value for the detection of glacier-bed overdeepenings is greater than for supraglacial lake formation on debris-covered tongues (5° instead of 2°).

The formation of a lake that is in contact with a glacier can have a strong impact on glacier dynamics. In general, a lake at the front of a glacier will accelerate glacier retreat due to increased ablation by calving and thermokarst effects (Kääb and Haeberli, 2001). For this reason, length changes of glaciers that terminate into a lake, are to a certain degree decoupled from the direct forcing of climate change and should thus not be used as indicators of climatic changes. Chinn et al. (2008) estimated an increase in the rate of ice loss by about one order of magnitude for glaciers terminating in a lake compared to other glaciers with ice loss only due to surface melt. These authors also state, that the inclined glacier surfaces are replaced by horizontal water surfaces which results in steeper upslope glacier surfaces and, hence, in faster ice flow. Such impacts of glacier lake formation on glacier dynamics are not commonly taken into account for physically based, dynamic modeling of future glacier development (e.g., like in the studies from Jouvet et al., 2009 or Le Meur et al., 2007). In combination with such models of transient glacier evolution, the temporal component could be included in the assessment of future lake formation. So far, only relative predictions of sequence of lake formation for individual glacier branches are possible by locating the bed-overdeepenings (first, the lake at the lowest overdeepening will form). As soon as multi-tributary glaciers start to separate into individual glaciers, the order of formation may change. For example, Morteratsch and Pers Glacier will separate in the near future and it is possible, that a lake at overdeepening 3 (Fig. 7) will form earlier than the lower lake at overdeepening 2 due to different retreat rates caused by different ice thicknesses of the individual glacier branches.

In this study outburst floods were modeled, but other important components for the determination of the hazard potential of future lakes were not considered. Dam characteristics for example strongly influence the risk of failure, and external factors like impact waves from mass movements can trigger catastrophic lake outbursts. To allow a more detailed and integrated hazard assessment of lakes expected to form in the future, such components must be anticipated as well. More detailed assumptions about the lake size, dam properties and lake surrounding would allow a more sophisticated modeling of potential lake outbursts.

7 Conclusions

The presented integrated four-level strategy for the detection of sites with potential glacier lake formation is a suitable approach to anticipate future situations in high-mountain environments. Starting with the first level to gain a rough overview over a large region, the strategy subsequently focuses on smaller regions in more detail, down to in-situ geophysical measurements in the field. This multiscale procedure allows to rapidly identifying the most critical sites in a large region. Applications of the strategy to two test regions showed, that the newly presented, qualitative approaches (levels 1 and 2) proved to be consistent with the results from more detailed/laborious models that are applied on the third level. In both test regions, ten or more overdeepenings were detected and the formation of several glacier lakes has to be expected in the future. Due to the irregular longitudinal bed profiles caused by glacier erosion (Hooke, 1991), glacier lakes will form in the course of continued glacier retreat in cold mountain regions. Tests of the presented strategy with the nearly globally available SRTM and ASTER DEMs revealed satisfying results. This indicates that the approach

can be applied worldwide, even in remote regions with less detailed data coverage.

The hazard situation of such glacier lakes needs to be (re-)assessed regularly and at short time intervals, because these lakes form in a rapidly changing environment and their hazard potential is determined by factors that are themselves subject to changes. Modeling of potential glacier lake outbursts is an important part of such a hazard assessment and can also be performed for glacier lakes that are expected to form in the future. The modeling of potential debris flows and flood waves originating from anticipated future lakes of the Morteratsch- and Pers glaciers indicated that a growing number of lakes may not in all cases imply a higher regional hazard potential.

To predict the time of lake formation, the here-presented strategy needs to be coupled with simple but transient models that determine glacier retreat over large regions. Such a combination is in the focus of future research and will further increase the benefit of the presented approaches.

Acknowledgements. We are grateful to J. Bordonau and an anonymous reviewer whose comments helped to improve the quality of this paper. In Figs. 4c, 5, 6, 7, 8 and 9 the DHM25 is reproduced by permission of swisstopo (BA100064). Funding of this study was partly provided by the ESA project GlobGlacier (21088/07/I-EC).

Edited by: J. M. Vilaplana
Reviewed by: J. Bordonau and another anonymous referee

References

Alean, J.: Ice avalanches: some empirical information about their formation and reach, J. Glaciol., 31, 324–333, 1985.

Allen, S. K., Schneider, D., and Owens, I. F.: First approaches towards modelling glacial hazards in the Mount Cook region of New Zealand's Southern Alps, Nat. Hazards Earth Syst. Sci., 9, 481–499, 2009, http://www.nat-hazards-earth-syst-sci.net/9/481/2009/.

Augustinus, P.: Glacial valley cross-profile development: the influence of in situ rock stress and rock mass strength, with examples from the Southern Alps, New Zealand, Geomorphology, 14, 87–97, 1995.

Ballantyne, C.: Paraglacial geomorphology, Quaternary Sci. Rev., 21, 1935–2017, 2002.

Benz, C.: Der würmeiszeitliche Rheingletscher-Maximalstand: Digitale Rekonstruktion, Modellierung und Analyse mit einem Geographischen Informationssystem, Ph.D. thesis, University of Zurich, 2003.

Binder, D., Brückl, E., Roch, K., Behm, M., Schöner, W., and Hynek, B.: Determination of total ice volume and ice-thickness distribution of two glaciers in the Hohe Tauern region, Eastern Alps, from GPR data, Ann. Glaciol., 50, 71–79, 2009.

Bolch, T., Buchroithner, M. F., Peters, J., Baessler, M., and Bajracharya, S.: Identification of glacier motion and potentially dangerous glacial lakes in the Mt. Everest region/Nepal using spaceborne imagery, Nat. Hazards Earth Syst. Sci., 8, 1329–1340, 2008, http://www.nat-hazards-earth-syst-sci.net/8/1329/2008/.

Chinn, T., Salinger, J., Fitzharris, B., and Willsman, A.: Glaciers and climate, Bulletin of the Federated Mountain Clubs of NZ, 171, 1–15, 2008.

Clague, J. and Evans, S.: Formation and failure of natural dams in the Canadian Cordillera, Geological Survey of Canada Bulletin, 464, 35 pp., 1994.

Clague, J. and Evans, S.: A review of catastrophic drainage of moraine-dammed lakes in British Columbia, Quarternary Sci. Rev., 19, 1763–1783, 2000.

Costa, J. and Schuster, R.: The formation and failure of natural dams, Geol. Soc. Am. Bull., 7, 1054–1068, 1988.

Evans, S. and Clague, J.: Recent climatic change and catastrophic geomorphic processes in moutnain environments, Geomorphology, 10, 107–128, 1994.

Farinotti, D., Huss, M., Bauder, A., Funk, M., and Truffer, M.: A method to estimate the ice volume and ice-thickness distribution of alpine glaciers, J. Glaciol., 55, 1–9, 2009.

Farr, T. G., Rosen, P. A., Caro, E., Crippen, R., Duren, R., Hensley, S., Kobrick, M., Paller, M., Rodriguez, E., Roth, L., Seal, D., Shaffer, S., Shimada, J., Umland, J., Werner, M., Oskin, M., Burbank, D., and Alsdorf, D.: The Shuttle Radar Topography Mission, Rev. Geophys., 45, 1–33, 2007.

Fischer, L., Kääb, A., Huggel, C., and Noetzli, J.: Geology, glacier retreat and permafrost degradation as controlling factors of slope instabilities in a high-mountain rock wall: the Monte Rosa east face, Nat. Hazards Earth Syst. Sci., 6, 761–772, 2006, http://www.nat-hazards-earth-syst-sci.net/6/761/2006/.

Frey, H., Huggel, C., Paul, F., and Haeberli, W.: Automated detection of glacier lakes based on remote sensing in view of assessing associated hazard potentials, in: Proceedings of the 10th International Symposium on High Mountain Remote Sensing Cartography. Grazer Schriften der Geographie und Raumforschung, edited by: Kaufmann, V. and Sulzer, W., vol. 45, in press, 2010.

GCOS: Implementation plan for the Global Observing System for Climate in support of the UNFCCC, GCOS – 92, WMO, Geneva, 2004.

Gruber, S. and Haeberli, W.: Permafrost in steep bedrock slopes and its temperature-related destabilization following climate change, J. Geophys. Res., 112, F02S18, doi:10.1029/2006JF000547, 2007.

Haeberli, W.: Frequency and characteristics of glacier floods in the Swiss Alps, Ann. Glaciol., 4, 85–90, 1983.

Haeberli, W.: Changing views on changing glaciers, in: The Darkening Peaks: Glacial Retreat in Scientific and Social Context, edited by: Orlove, B., Wiegandt, E., and Luckman, B., Berkeley: University of California Press, 2005.

Haeberli, W. and Beniston, M.: Climate change and its impacts on glaciers and permafrost in the Alps, Ambio, 27, 258–265, 1998.

Haeberli, W. and Hohmann, R.: Climate, Glaciers and Permafrost in the Swiss Alps 2050: Scenarios, Consequences and Recommendations, Proceedings of the 9th International Conference on Permafrost 2008, Fairbanks, Alaska, USA, 2008.

Haeberli, W. and Schweizer, J.: Rhonegletscher 1850: Eismechanische Überlegungen zu einem historischen Gletscherstand, Mitteilungen VAW/ETHZ, 94, 59–70, 1988.

Haeberli, W., Rickenmann, D., Zimmermann, M., and Rösli, U.: Murgänge, in: Ursachenanalyse der Hochwasser 1987, Ergebisse der Untersuchungen, vol. 4, Mitteilungen des Bundesamtes für Wasserwirtschaft, 77–88, 1991.

Haeberli, W., Kääb, A., Mühll, D. V., and Teysseire, P.: Prevention of outburst floods from periglacial lakes at Grubengletscher, Valais, Swiss Alps, J. Glaciol., 47, 111–122, 2001.

Hayakawa, Y. S., Oguchi, T., and Lin, Z.: Comparison of new and existing global digital elevation models: ASTER G-DEM and SRTM-3, Geophys. Res. Lett., 35, L17404, doi:10.1029/2008GL035036, 2008.

Hooke, R.: Positive feedbacks associated with erosion of glacial cirques and overdeepenings, Geol. Soc. Am. Bull., 103, 1104–1108, 1991.

Hubbard, B., Heald, A., Reynolds, J., Quincey, D., Richardson, S., Luyo, M., Portilla, N., and Hambrey, M.: Impact of a rock avalanche on a moraine-dammed proglacial lake: Laguna Safuna Alta, Cordillera Blanca, Peru, Earth Surface Processes and Landforms, 30, 1251–1264, 2005.

Huggel, C.: Recent extreme slope failures in glacial environments: effects of thermal perturbation, Quaternary Sci. Rev., 28, 1119–1130, doi:10.1016/j.quascirev.2008.06.007, 2009.

Huggel, C., Kääb, A., Haeberli, W., Teysseire, P., and Paul, F.: Remote sensing based assessment of hazards from glacier lake outbursts: a case study in the Swiss Alps, Can. Geotech. J., 39, 316–330, 2002.

Huggel, C., Kääb, A., Haeberli, W., and Krummenacher, B.: Regional-scale GIS-models for assessment of hazards from glacier lake outbursts: evaluation and application in the Swiss Alps, Nat. Hazards Earth Syst. Sci., 3, 647–662, 2003, http://www.nat-hazards-earth-syst-sci.net/3/647/2003/.

Huggel, C., Haeberli, W., Kääb, A., Bieri, D., and Richardson, F.: An assessment procedure for glacial hazards in the Swiss Alps, Can. Geotech. J., 41, 1068–1083, 2004.

Hungr, O., Morgan, G. C., and Kellerhals, P.: Quantitative analysis of debris hazards for design of remedial measures, Can. Geotech. J., 21, 663–677, 1984.

Jouvet, G., Huss, M., Blatter, H., Picasso, M., and Rappaz, J.: Numerical simulation of Rhonegletscher from 1874 to 2100, J. Comput. Phys., 228, 6426–6439, 2009.

Kääb, A. and Haeberli, W.: Evolution of a high-mountain thermokarst lake in the Swiss Alps, Arctic, Antarctic, and Alpine Research, 33, 385–390, 2001.

Kääb, A., Huggel, C., Fischer, L., Guex, S., Paul, F., Roer, I., Salzmann, N., Schlaefli, S., Schmutz, K., Schneider, D., Strozzi, T., and Weidmann, Y.: Remote sensing of glacier- and permafrost-related hazards in high mountains: an overview, Nat. Hazards Earth Syst. Sci., 5, 527–554, 2005, http://www.nat-hazards-earth-syst-sci.net/5/527/2005/.

Kershaw, J., Clague, J., and Evans, S.: Geomorphic and sedimentological signature of a two-phase outburst flood from moraine-dammed Queen Bess Lake, British Columbia, Canada, Earth Surface Processes and Landforms, 30, 1–25, 2005.

Komori, J.: Recent expansions of glacial lakes in the Bhutan Himalayas, Quaternary International, 184, 177–186, 2008.

Le Meur, E., Gerbaux, M., Schäfer, M., and Vincent, C.: Disappearance of an Alpine glacier over the 21st Century simulated from modeling its future surface mass balance, Earth Planet. Sci. Lett., 261, 367–374, 2007.

Lemke, P., Ren, J., Alley, R., Allison, I., Carrasco, J., Flato, G., Fujii, Y., Kaser, G., Mote, P., Thomas, R., and Zhang, T.: Observations: Changes in Snow, Ice and Frozen Ground, in: Climate Change 2007: The Physical Science Basis. Contribution of Working Group I to the Fourth Assessment Report of the Intergovernmental Panel on Climate Change, edited by: Solomon, S., Qin, D., Manning, M., Chen, Z., Marquis, M., Averyt, K., Tignor, M., and Miller, H., Cambridge University Press, Cambridge, United Kingdom and New York, NY, USA 2007.

Linsbauer, A., Paul, F., Hoelzle, M., Frey, H., and Haeberli, W.: The Swiss Alps Without Glaciers – A GIS-based Modelling Approach for Reconstruction of Glacier Beds, in: Geomorphometry 2009 Conference Proceedings, edited by: Purves, R., Gruber, S., Straumann, R., and Hengl, T., University of Zurich, Zurich, 243–247, www.geomorphometry.org, 2009.

MacGregor, K., Anderson, R., Anderson, S., and Waddington, E.: Numerical simulations of glacial-valley longitudinal profile evolution, Geology, 28, 1031–1034, 2000.

Maisch, M., Haeberli, W., Hoelzle, M., and Wenzel, J.: Occurrence of rocky and sedimentary glacier beds in the Swiss Alps as estimated from glacier-inventory data, Ann. Glaciol., 28, 231–235, 1999.

O'Connor, J. E., Hardison, J. H., and Costa, J. E.: Debris flows from failures of neoglacial-age moraine dams in the Three Sisters and Mount Jefferson wilderness areas, Oregon, USGS professional paper, 1606, 2001.

Oerlemanns, J.: Glaciers and Climate Change, A.A. Balkema Publishers, ISBN 9026518137, 2001.

Oppikofer, T., Jaboyedoff, M., and Keusen, H.-R.: Collapse at the eastern Eiger flank in the Swiss Alps, Nature Geosci., 1, 531–535, 2008.

Paterson, W.: The physics of glaciers, Pergamon Press, Oxford, 3rd edn., 1994.

Paul, F.: The New Swiss Glacier Inventory 2000 - Application of Remote Sensing and GIS. Schriftenreihe Physische Geographie, 52, Ph.D. thesis, University of Zurich, 2007.

Paul, F. and Haeberli, W.: Spatial variability of glacier elevation changes in the Swiss Alps obtained from two digital elevation models, Geophys. Res. Lett., 35, L21502, doi:10.1029/2008GL034718, 2008.

Quincey, D., Richardson, S., Luckman, A., Lucas, R., Reynolds, J., Hambrey, M., and Glasser, N.: Early recognition of glacial lake hazards in the Himalaya using remote sensing datasets, Global Planet. Change, 56, 137–152, 2007.

Raup, B., Racoviteanu, A., Khalsa, S., Helm, C., Armstrong, R., and Arnaud, Y.: The GLIMS geospatial glacier database: A new tool for studying glacier change, Global Planet. Change, 56, 101–110, 2007.

Reynolds, J. M.: On the formation of supraglacial lakes on debris-covered glaciers, in: Debris-Covered Glaciers. Proceedings of a workshop held at Seattle, Washington, USA, September 2000, edited by: Nakawo, M., Raymond, C., and Fountain, A., 153–161, IAHS Publication, 2000.

Reynolds Geo-Science Ltd: Guidelines for the management of glacial hazards and risks, Reynolds Geo-Science Ltd, Mold, UK, 2003.

Richardson, S. and Reynolds, J.: An overview of glacial hazards in the Himalayas, Quaternary Int., 65–66, 31–47, 2000a.

Richardson, S. D. and Reynolds, J. M.: Degradation of ice-cored moraine dams: implications for hazard development, in: Debris-Covered Glaciers, edited by: Nakawo, M., Raymond, C. F., and Fountain, A., Proceedings of a workshop held at Seattle, Washington, USA, September 2000, Oxford, IAHS Publication,

2000b.

Rothenbühler, C.: GISALP: Räumlich-zeitliche Modellierung der klimasensitiven Hochgebirgslandschaft des Oberengadins, Ph.D. thesis, University of Zurich, 2006.

Swisstopo: DHM25 – The digital height model of Switzerland. Product information, http://www.swisstopo.admin.ch/internet/swisstopo/en/home/products/height/dhm25.html, 2004.

Truffer, M., Motyka, R., Harrison, W., Echelmeyer, K., Fisk, B., and Tulaczyk, S.: Subglacial drilling at Black Rapids Glacier, Alaska, USA: drilling method and sample descriptions, J. Glaciol., 45, 495–505, 1999.

Watanabe, T., Ives, J., and Hammond, J.: Rapid growth of a glacial lake in Khumbu Himal, Himalaya: Prospects for a catastrophic flood, Mountain Research and Development, 14, 329–340, 1994.

WGMS: Global Glacier Changes: facts and figures, edited by: Zemp, M., Roer, I., Kääb, A., Hoelzle, M., Paul, F., and Haeberli, W., UNEP, World Glacier Monitoring Service, Zurich, Switzerland, 2008.

Zemp, M., Kääb, A., Hoelzle, M., and Haeberli, W.: GIS-Based modelling of glacial sediment balance, Zeitschrift für Geomorphologie N.F., 138, 113–129, 2005.

Part III

Appendix

Personal bibliography

Frey, H., Huggel, C., Paul, F., and Haeberli, W. (2010b). Automated detection of glacier lakes based on remote sensing in view of assessing associated hazard potentials. In: *Grazer Schriften der Geographie und Raumfoschung 45: Proceedings of the 10th Internatinal Symposium on High Mountain Remote Sensing Cartography, 8.-11.9.2008, Kathmandu, Nepal.*, (edited by Kaufmann, V. and Sulzer, W.), pp. 261–272.

Frey, H., Haeberli, W., Linsbauer, A., Huggel, C., and Paul, F. (2010a). A multilevel strategy for anticipating future glacier lake formation and associated hazard potentials. *Natural Hazards and Earth System Sciences*, 10: 339–352.

Frey, H. and Paul, F. (in press). On the suitability of the SRTM DEM and ASTER GDEM for the compilation of topographic parameters in glacier inventories. *International Journal of Applied Earth Observation and Geoinformation*. doi: 10.1016/j.jag.2011.09.020.

Frey, H., Paul, F., and Strozzi, T. (in rev.). Compilation of a glacier inventory for the western Himalayas from satellite data: Methods, challenges and results. *Remote Sensing of Environment*.

Bolch, T., Kulkarni, A., Kääb, A., Huggel, C., Paul, F., Cogley, J. G., Frey, H., Kargel, J. S., Fujita, K., Scheel, M., Stoffel, M., and Bajracharya, S. (subm.). The state and fate of Himalayan glaciers. *Science*.

Le Bris, R., Paul, F., Frey, H., and Bolch, T. (2011). A new satellite-derived glacier inventory for Western Alaska. *Annals of Glaciology*, 52 (59): 135–143.

Linsbauer, A., Paul, F., Hoelzle, M., Frey, H., and Haeberli, W. (2009). The Swiss Alps without glaciers – A GIS-based modelling approach for reconstruction of glacier beds. In: *Geomorphometry 2009 Conference Proceedings*, (edited by Purves, R., Gruber, S., Straumann, R., and Hengl, T.), pp. 243–247. University of Zurich, Zurich.

Paul, F., Barry, R. G., Cogley, J. G., Frey, H., Haeberli, W., Ohmura, A., Ommanney, C. S. L., Raup, B., Rivera, A., and Zemp, M. (2009a). Recommendations for the compilation of glacier inventory data from digital sources. *Annals of Glaciology*, 50 (53): 119–126.

Paul, F., Frey, H., and Le Bris, R. (in press). A new glacier inventory for the European Alps from Landsat TM scenes of 2003: Challenges and results. *Annals of Glaciology*.

Curriculum Vitae (short version)

Personal details

First names:	Holger Rudolf
Last name:	Frey
Date of birth:	8 December, 1981
Place of birth:	Richterswil, Switzerland
Citizenship:	Swiss

Education

08/1996–02/2001	Grammar School at the Mathematisch-Naturwissenschaftliches Gymnasium Rämibühl Zürich, Switzerland
02/2001	Matura Typus C
10/2001–06/2007	Studies in Geography at the University of Zürich Specialization: Physical Geography, Glaciology, Remote Sensing and GIS Thesis: *Identification and analysis of glacial lakes based on remote sensing and GIS* (in german)
07/2007	Master of Science in Geography, University of Zurich
10/2007–09/2011	PhD student at the Department of Geography, University of Zurich

Acknowledgements

On the way to obtaining my PhD, I had the opportunity to visit exciting places like the Nepalese and Indian Himalayas and the arctic world of Svalbard, while also traversing a few deep valleys en route to the higher peaks. On this journey I have been supported and accompanied by numerous people, and I would now like to express my deep gratitude to each and all of them. In the following, while some are mentioned explicitly; my sincere thanks go also to all those persons who are not listed individually; their help is nevertheless remembered and very much appreciated.

First of all, I'd like to extend my sincere gratitude to Frank Paul, supervisor of this thesis. Already during the time of my Diploma thesis he introduced me to the world of glaciers, pixels, satellite images, academic papers, and other aspects of science. Thanks to him, I had the opportunity to earn my PhD in the framework of ESA's *GlobGlacier* project that funded this thesis (21088/07/I-EC). Although Frank was often buried under work and pursuing several deadlines, he always found time and had an open ear for my worries and problems, always with a solution at hand. Many skills I needed for this work I learned from him, not least that a day has twenty-four hours (and maybe a little bit more if you hurry…). Thank you very much, Frank!

Particular thanks go to Wilfried Haeberli. During my studies in physical geography and glaciology he aroused my interest in glacierized high-mountain environments, encouraging me to embark on a PhD. His enthusiasm and sanguinity have been very motivating during all phases of this journey. When I had doubts about the meaning of it all or when lost somewhere in a tiny detail, he could always look above the fog, keep the broader picture in view, and help me to get back on the right track again.

My gratitude also goes to Christian Huggel, who anticipated any potential threats and traps. I learned a lot from Christian related to hazards and catastrophes, but – maybe even more important – also about measures to avoid them. His relaxed manner was often a calming pole in stressful times. Besides academic adventures, I enjoyed also many shared kilometers on cross-county ski trails.

The period of my doctoral studies would not have been the same without Raymond Le Bris, also working in the GlobGlacier project as a PhD student. Besides countless fruitful discussions and mutual assistance with strangely behaving software, I enjoyed with him many high-level debates about football and other important things in life, countless invaluable French lessons, and some hilarious encounters with 'Regis'. And I will always remember our amazing trip to the arctic winter and spring in Svalbard. Merci, Raymond!

A very warm thank you is extended to the 3G group for the enjoyable ambiance in our department. One element was the stimulating and enthusiastic work atmosphere and scientific discussions during seminars and meetings, but equally important were the inspiring non-scientific chats during coffee breaks as well as fieldwork adventures and leisure time in the mountains. A toast to all of you! Particular thanks go also to my office-mates Andi, Isa, Raymond, and Stefi, as well as to Andreas Linsbauer for providing me with ice-thickness estimations and glacier bed topographies calculated using his *Glabtop* model.

Furthermore I would like to thank Markus Stoffel from the Universities of Berne and Geneva for offering me the opportunity to participate in the EU FP7 project *HighNoon* and therefore to continue to work on Himalayan glaciers. Special thanks also to Raphael Worni for taking me on an unforgettable field trip to India.

Many other people eased my everyday life by their help and support: Lisbeth Nietlispach and Helene Grüter solved administrative issues, the GIUZ IT group offered and maintained a very good and (almost always) well-functioning IT infrastructure, Ronald Schmidt solved many GIS problems, and Susan Braun-Clarke helped me to improve the English of this thesis. Many thanks to all of you!

Finally, I am greatly indebted to my parents for offering me the opportunity to receive a good education, a process that lasted, in the end, almost a quarter of a century. Thank you very much for your wonderful support! And last but not least, I thank Nati for her persistent support; her share of the success of this thesis is greater than she might think.